Characterisation of Flax Fibres and Flax Fibre Composites. Being cellulose based sources of materials

Aslan, Mustafa; Sørensen, Bent F.; Madsen, Bo

Publication date:
2012

Document Version
Publisher's PDF, also known as Version of record

Technical University
of Denmark

DTU

Characterisation of Flax Fibres and Flax Fibre Composites

Being cellulose based sources of materials

Mustafa Aslan

DTU Wind Energy Report E-0005(EN)
July 2012

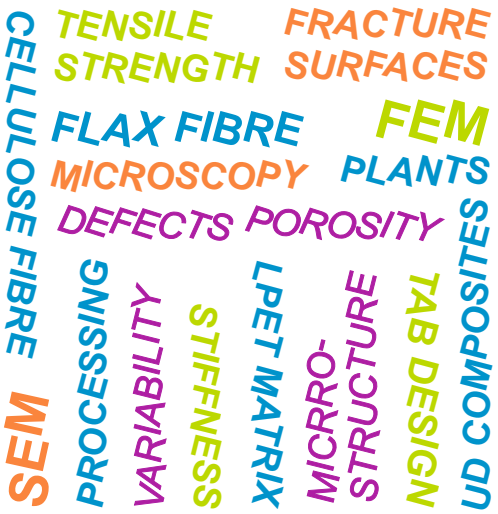

DTU Wind Energy
Department of Wind Energy

Author: Mustafa Aslan

Titel: Characterisation of Flax Fibres and Flax Fibre Composite Being cellulose based sources of materials

Department: Department of Wind Energy
Section of Composites and Material Mechanics

Supervisors: Senior Scientist, Bent F. Sørensen
Senior Scientist, Bo Madsen

Report number:
DTU Wind Energy PhD-0005 (EN)

Submission date: July 2012

ISBN: 978-87-92896-07-0

Contract no.: 1615115-00

Project no.: 274-07-0300

Sponsorship: Danish Agency for Science, Technology and Innovation

Cover picture:
Microscopic image showing fracture surface of flax/LPET composite

Technical University of Denmark
DTU Wind energy
Risø Campus, Frederiksbergvej 399
Building 228
DK 4000 Roskilde
Denmark
Telefon 46775800
muas@risoe.dtu.dk
www.vindenergi.dtu.dk

PREFACE

This PhD thesis is based on research done for a project "WoodFibre3D" undertaken between 2008 and 2012 at the Section of Composites and Materials Mechanics, Department of Wind Energy (former Risø National Laboratory for Sustainable Energy), Technical University of Denmark.

The PhD study has been supervised by:

Main supervisor; Professor, PhD, Bent F. Sørensen (DTU Wind Energy)

Co-supervisor; Senior Scientist, PhD, Bo Madsen (DTU Wind Energy)

The "WoodFibre3D" project was financially supported by Danish Agency for Science, Technology and Innovation project (grant no 274-07-0300). The research has also been partly funded under "NATEX" project at the European Community's Seventh Framework Programme (grant no 214467). Their supports are gratefully acknowledged.

As part of my PhD project, I have conducted laboratory experiments, participated in two international and two national conferences, visited universities in Europe, participated in several project meetings as a member of a European project group "WoodFibre3D", and contributed to international scientific journals.

Presentations at project meetings and conferences:

Aslan M., "Tensile strength of single wood fibres", WoodFibre3D meeting, 18 February 2009. Uppsala, Sweden.

Aslan, M., Characterization and micromechanical modelling of wood fibres and composites. 12th Internal Symposium at Danish Centre for Applied Mathematics and Mechanics (DCAMM), 23-25 March 2009 Ringsted, Denmark.

Aslan M., Madsen B., "Characterization of single flax fibres and flax fibre composites", Natex project meeting, 4 May 2010, Roskilde, Denmark.

Aslan M., "Characterization of wood fibres and wood fibre composites". Experimental and computational methods in wood mechanics. Cost Action FP0802 Workshop, May 2009. Vienna, Austria.

Madsen B., Mehmood S., Aslan M., "Variability in properties of natural fibres", Natural aligned fibres and textiles for use in structural composites, Natex Workshop, 18 April 2012, Chesterfield, UK.

Conference papers

[A1] Aslan, M., Mehmood, S., Madsen, B., Goutianos, S. The effect of processing on defects and tensile strength of single flax fibres, Proceedings of the 14th European Conference on Composite Materials (ECCM-14), 7-10 June 2010, Budapest, Hungary.

Aslan, M., Modelling of stress singularity in bimaterial wedge by finite element modelling. 13th Internal symposium at Danish Centre for Applied Mathematics and Mechanics (DCAMM), 14 March 2011, Vejle, Denmark (Short paper).

Journal papers

[A2] Aslan, M., Chinga-Carrasco, G., Sørensen, B.F. Madsen, B., (2011) Strength variability of single flax fibres, Journal of Materials Science 46:6344-6354 (ISSN: 0022-2461) (DOI: 10.1007/s10853-011-5581-x).

[A3] Aslan M., Mehmood S., Madsen B., Effect of consolidation pressure on volumetric composition and stiffness of unidirectional flax fibre composites. (to be submitted to Composites Part A).

[A4] Aslan, M., Sørensen, B.F., Tab design for uniaxial tensile test specimens of composite materials. (Submitted to Composites Part A).

In the text, the papers are referred to by the names of the authors and their appendix number.

ACKNOWLEDGEMENTS

I sincerely thank my supervisor Bent F. Sørensen and my co-supervisor Bo Madsen who nominated me for the DTU PhD scholarship. I am very grateful to Bent to provide patiently the vision and encouragement. He has advised me with creative ideas in the simplest and logical way to precede the program. And I am also thankful to Bo for sharing with me his knowledge and also for high motivation by pushing things further.

I would like to thank my office mates Karolina Martyniuk and Morten Rask for their valuable help at Risø and special thanks go to my colleagues Shahid Mehmood, Mohammad Hussein and Durai Prabhakaran for their brotherhood.

Special thanks go to my colleagues Malcolm McGugan, Eric Vogeley and Frank Adrian in the test laboratory; Tom Løgstrup Andersen, Christian H. Madsen, Jonas Heininge Kreutzfeldt and Jacob Christensen in the fibre laboratory to teach me the preparation of the samples and to use of the machines with high discipline.

Special thanks to the other scientists Hans Lilholt, Lars Pilgaard Mikkelsen and Helmuth Langmaack Toftegaard, Brian Ralph for guidance and inspiring discussions. Also special thanks go to Preben Olesen, Niels Jørgen Pedersen, Gitte Christiansen, Ann Gaust Thomsen, Lene Danielsen Kamilla Fugleberg and Heidi Thomsen for helping me on technical procedures and thanks to the entire Composite group which have been a great part of my life at Risø DTU, as good colleagues and great friends.

Special thanks to my friends in Denmark; Ali Yilmaz, Ali Kutlu, Emrah Turan, Faruk Kılıç, Lütfi Peker, Haydar Metin and Torsten Freltoft to make me feel at home. Special thanks to my colleagues in Turkey; Cenk Demirkir, Şükrü Özşahin, Ali Temiz, my previous supervisor Hülya Kalaycıoğlu and friends from other parts of the World that gave me inspiration, moral support and good wishes.

I thank my parents Emine Aslan, Ahmet Aslan and my brother Bünyamin Aslan. I always feel their good wishes in my heart. Finally, I would like to dedicate this work to my wife Aysegül Aslan and my new born son Kerem Aslan that are the most beautiful presents in my life.

SUMMARY

Cellulosic fibres, like wood and plant fibres, have the potential for use as load-bearing constituents in composite materials due to their attractive properties such as high stiffness-to-weight ratio that makes cellulosic fibre composites ideal for many structural applications. There is thus a growing interest among composite manufacturers for such low-cost and low-weight cellulosic fibre composites. In addition, wood and plant fibre based composites with thermoplastic polymeric matrices are recyclable, and they are cost attractive alternatives to oil based fibre reinforced polymer composites that currently have the largest market share for composite applications. However, the most critical limitation in the use of cellulosic fibre composites for structural applications is the lack of well described fibre properties, in particular, the tensile strength. This is due to variations in fibre morphology, fibre processing conditions, and applied test methods. Other limitations such as dimensional instability and low fibre-matrix adhesion have already been intensively investigated, and solutions have been found for many commercial applications. Therefore, a better understanding of the mechanical performance of these fibres, and with a focus on increasing their strength will make it possible for them to reach their full potential as reinforcement in composites. The present PhD study deals with several important subjects related to the use of flax fibres in composites. The emphasis is on the relationship between the complex microstructure and the tensile properties of flax fibres and their composites, based on textile flax yarn and a thermoplastic polymeric matrix.

Single flax fibres were isolated from flax fibre bundles which have been processed in two different steps of natural treatments (retting) and mechanical treatments (scutching and hackling). Microscopic observations of the defects formed in the fibres and their fracture surfaces after tensile testing show that large fracture areas are formed in a complex way due to defects in the fibre cell wall, and due to anisotropy of the internal cell wall structures. This is in contrast to the crack growth in brittle ceramic and glass fibres. Moreover, two typical stress-strain curves (linear and non-linear) measured for the flax fibres were found to be correlated with the amount of defected region in the fibres. The defects are induced in larger numbers and larger sizes during processing of the fibres, and this is found to be correlated with a decrease in tensile strength of the fibres. It is found that processing reduces the tensile strength from average values of 1450 MPa for naturally processed single fibres to 810 MPa for mechanically processed single fibres.

The large variation in tensile properties of flax fibres leads to an examination of the effect of defects and applied test methods. The fibres show a large coefficient of variation (CV) in the range 20-60% in general for all measured tensile properties. One reason for these relative large variations can be attributed to the assumption of a circular cross sectional area of the fibres. On average, these results in a 39% lower tensile strength than when the true fibre cross sectional area is used, and moreover, the variable aspect ratio of the cross section of fibres significantly affects the variation of the results. Also, the large variation in properties is likely to be attributed to the distribution of

defects along the fibres since the large defects lead to low mechanical properties, whereas smaller defects result in less reduced mechanical properties.

On the level of composites, the effect of consolidation pressure on the tensile properties of flax fibre composites was investigated. A porosity corrected rule of mixtures model, and a volumetric composition model for composites were used to model the experimental data. Flax fibre yarns and thermoplastic low-melting temperature polyethylene terephthalate (LPET) filaments were aligned in assemblies of different fibre weight fractions in the range 0.24 to 0.83 to manufacture unidirectional composites using two different consolidation pressures of 1.67 and 4.10 MPa. The maximum attainable fibre volume fraction is found to be 47% for the low pressure composites, whereas it is found to be 60% for the high pressure composites. The stiffness of the flax fibre/LPET composites is measured to be in the range 16 to 33 GPa depending on the volumetric composition of the composites. The high pressure composites are found to have superior tensile properties in comparison with the low pressure composites. The tensile strength (mean ± std. dev.) of the low pressure composites was found to be 183±7 MPa while that of the high pressure composites was found to be 209±6 MPa at a fibre volume fraction of 22%. The effect of fibre correlated porosity and structural porosity in the composites is found to be highly important for the volumetric composition and tensile behaviour of the composites. The total porosity is measured in the range 2.4 to 32%, and it is found to be increased dramatically when the fibre weight fraction is increased above a transition value, as predicted by the volumetric composition model. This leads furthermore to a scatter in the experimental data of stiffness at high fibre weight fractions. The qualitative analysis of the composite cross sections by microscopy also shows that the low and high pressure composites have a similar microstructure at low fibre weight fractions. However, when the fibre content is increased, a difference in porosity content can be observed from the composite cross sections.

The nominal tensile strength of the unidirectional flax fibre/LPET composites is measured in the range 180 to 340 MPa. However, in many cases, the tensile strength determined of unidirectional composites is not valid due to the fact that failure does not occur in the gauge section. It is actually common that unidirectional composites fail close to the grips, and they then split along the specimen in the tensile direction. Traditionally, the problem has been approached by the use of local reinforcement of the specimen in the gripping areas, the so-called tabs, but the problem has not been efficiently solved in practice. A key problem is that the stress state at the end of the tab can be singular, leading to premature failure of the tensile specimen. In the present study, the dependence of the order of the stress singularity at the vertex of dissimilar isotropic and orthotropic materials is investigated in terms of the elastic mismatches between the specimen and the tab materials, and the tab angle. Finite element modelling is performed to analyse the situation of a stress singularity. The results are aimed at creating a better specimen/tab design to accomplish failure in the gauge section of the tensile specimens, and thereby determine the true tensile strength of the materials. It is found that the stress singularity in the tab wedge is reduced with a decreased

tab angle and with a decreased stiffness of the tab material. A simple criterion is proposed for the assessment of the severity of the stress singularity. In practice, gauge section failures should be achievable by selecting a test specimen design based on combinations of a stiff material in the tab section combined with a soft material (eg. epoxy adhesive) at the wedge end of the tab, forming a wedge. The wedge tip should have a small wedge angle in the range 5° and 10° depending on the stiffness ratio.

The conclusion of the PhD study is that flax fibres are an important source of cellulosic fibres. When the appropriate composite processing methods and the accurate test methods are used, flax fibre composites are demonstrated to be promising material candidates for structural applications as an attractive alternative to synthetic fibre composites.

RESUME

Cellulose fibre, såsom træ- og plantefibre, har potentiale til anvendelse som forstærkning i kompositmaterialer til strukturelle komponenter på grund af fibrenes fordelagtige egenskaber, såsom et højt stivheds-vægtforhold. Der er således en stigende interesse blandt producenter af kompositmaterialer for sådanne billige og lette cellulose fiberkompositter. Hertil kommer at træ- og plantefiber baserede kompositter med termoplastiske polymer matricer kan genbruges, og de er derfor attraktive alternativer til de oliebaserede fiberkompositter, der i øjeblikket har den største markedsandel inden for kompositmaterialer. Imidlertid er den mest kritiske begrænsning for brugen af cellulose-baserede fiberkompositter til strukturelle anvendelser, manglen på velbeskrevne fiberegenskaber, navnlig trækstyrken. Dette skyldes variationer i fibermorfologi, fiber-forarbejdning, og anvendte testmetoder. Andre begrænsninger såsom dimensional ustabilitet og lav fiber-matrix binding er allerede blevet undersøgt intensivt, og løsninger for disse begrænsninger er blevet fundet for mange kommercielle anvendelser. Derfor vil en bedre forståelse af den mekaniske opførelse af disse fibre, med fokus på at øge deres styrke, gøre det muligt at udnytter fibrenes fulde potentiale som forstærkning af kompositter. Ph.d.-studiet omhandler en række vigtige emner relateret til brugen af hørfibre i kompositmaterialer. Der lægges vægt på relationen mellem den komplekse mikrostruktur og de mekaniske trækegenskaber af hørfibre og deres kompositter, som er baseret på hørgarn og en termoplastisk polymer matrix.

Enkeltfibre er isoleret fra hørfiber-bundter, som er blevet forarbejdet i to forskellige trin bestående af naturlige behandlinger (rødning) og mekaniske behandlinger (scutching og hackling). Mikroskopiske observationer af de dannede defekter i fibrene og fibrenes brudflader efter trækprøvning, viser at de store brudzoner bliver dannet på en kompleks måde på grund af defekter i fibrenes cellevægge, og på grund af anisotropien af cellevæggenes mikrostruktur. Denne brudmåde er forskellig fra brud i sprøde keramik- og glasfibre. Desuden kan det vises at de to typiske spændings-tøjningskurver (lineære og ikke-lineære) som blev målt for hørfibre er korreleret med mængden af defekter i fibrene. Det viser sig at defekterne induceres i stigende antal og størrelser under forarbejdning af fibrene, og dette viser sig at være korreleret med et fald i trækstyrken af fibrene. Det er fundet, at forarbejdning reducerer middelværdi trækstyrken på 1450 MPa for naturligt behandlede enkeltfibre til en middelværdi trækstyrke på 810 MPa for mekanisk behandlede enkeltfibre.

Den store variation i trækegenskaberne af hørfibre førte til en undersøgelse af effekten af defekter og anvendte testmetoder. Hørfibrene udviser en stor variationskoefficient i området 20-60 %, generelt for alle målte trækegenskaber. En af årsagerne til disse relativt store variationer i egenskaberne kan tilskrives den typiske antagelse om at fibrene har et cirkulært tværsnit. I gennemsnit medfører denne antagelse en lavere trækstyrke (39%) end hvis det korrekte tværsnitsareal af fibrene blev brugt, og derudover medfører det variable bredde-højdeforhold for fibrenes tværsnit at de målte egenskaber udviser stor variation. Den store variation i egenskaber kan sandsynligvis også tilskrives fordelingen af defekter langs fibrene, idet de store defekter fører til

lave mekaniske egenskaber, hvorimod de mindre defekter resulterer i en mindre reduktion af de mekaniske egenskaber.

På komposit-niveau er det blevet undersøgt hvordan et varierende konsolideringstryk anvendt under fremstilling af hørfiberkompositter, påvirker trækegenskaberne af kompositterne. En porøsitetsmodificeret rule-of-mixtures model bliver brugt til at modellere de eksperimentelle data. Ensrettede kompositter af hørgarn og en termoplastisk matrix af polyethylen terephthalat, med lavt smeltepunkt (LPET), blev fremstillet med fibervægtfraktioner i intervallet 0.24 til 0.83, og med to forskellige konsolideringstryk på 1.67 og 4.10 MPa. Den maksimalt opnåelige fibervolumenfraktion er fundet til at være 47 % for lavt-tryk kompositterne, mens det er 60% for højt-tryk kompositterne. Stivheden af hørfiber/LPET-kompositterne er målt i området fra 16 til 33 GPa afhængigt af den volumetriske sammensætning af kompositterne. Kompositterne fremstillet med højt tryk har overlegne trækegenskaber sammenlignet med kompositterne fremstillet med lavt tryk. Trækstyrken (middelværdi ± standard afvigelse) for lavt-tryk kompositterne blev fundet til at være 183±7 MPa, medens den for højt-tryk kompositterne blev fundet til at være 209±6 MPa, for kompositter med en fibervolumenfraktion på 22 %. Effekten af fiber-korreleret porøsitet og strukturel porøsitet i kompositterne er påvist til at være meget vigtig for den volumetriske sammensætning og trækegenskaber af kompositterne. Den totale porøsitet er målt til at være i intervallet fra 2,4 til 32 %, og det konstateres at porøsiteten øges dramatisk når fibervægtfraktionen øges til en værdi over en given overgangsværdi, som forudsagt af en model for den volumetriske sammensætning af kompositter. Kompositter der har en fibervægtfraktion højere end overgangsværdien viser sig at have en større spredning i de eksperimentelle data for stivhed. Den kvalitative analyse af kompositternes tværsnit, bestemt ved hjælp af mikroskopi, viser at lavt-tryk og højt-tryk kompositterne har samme mikrostruktur ved de lave fibervægtfraktioner, mens forskellen i porøsitetsindhold kan identificeres når fiberindholdet øges i kompositterne.

Den nominelle brudstyrke for de ensrettede hørfiber/LPET-kompositter er målt til at være i intervallet fra 180 til 340 MPa. Imidlertid sker bruddet ikke som ønsket i gauge-sektionen, men tæt på kæberne og fører til splitrevner langs fibrene i trækretningen. Derfor er den målte trækstyrke for ensrettede kompositter ikke korrekt. Dette er et velkendt problem for ensrettede fiberkompositter. Traditionelt er dette problem søgt afhjulpet ved brug af lokale forstærkninger af trækemnerne i kæbeområdet, de såkaldte tabs, men problemet er ikke endnu ikke blevet løst i praksis. Det centrale problem er at spændingstilstanden ved overgangen mellem tab'en og testmateriale kan være singular, og det fører til et for tidligt brud af trækemnet. I nærværende undersøgelse er spændingstilstanden ved en kileformet tab på et testmaterialer studeret ved hjælp af finite element modellering. Resultaterne har til formål at skabe en bedre tab udformning således der opnås svigt i gauge-sektionen (den lige del af prøveemnet). Det vises at der altid er en singulær spændingstilstand ved kilens spids. Men singularitetens styrke afhænger af kilens vinkel, stivhedsforhold mellem tabmateriale og testmateriale samt deres elastiske anisotropi. Styrken af spændings singulariteten kan reduceres ved at reducere kilenvinklen og ved at reducere stivheden af

tab materialet i forhold til test materialet. Et nyt kriterium er opstillet for at vurdere om der sker brud i tabs eller brud i gauge-sektionen. I praktisk bør brud i gauge-sektionen kunne opnås ved at vælge en tabudforming baseret en kombination af to materialer: et stift og stærkt tabmateriale (der overfører kræfter fra kæberne til emne) og et blødt ”kilemateriale” med lave kilevinkler (i området fra 5° til 10° afhængigt af stivhedsforholdet mellem kilematerialet og testmaterialet) for at sikre lav styrke af spændingssingulariten.

Konklusionen for dette ph.d.-studium er at hørfibre er en vigtig kilde til cellulose-baserede fibre. Når de relevante kompositfremstillingsmetoder og de præcise testmetoder anvendes, er det påvist at hørfiberkompositter er lovende materialekandidater til strukturelle komponenter, og de er således attraktive alternativer til de nuværende syntetiske fiberkompositter.

CONTENT

1. INTRODUCTION

Cellulose fibres are natural materials that are building blocks of plants and trees. They have been used by humans for many centuries for making sailing ships, ropes, tools, textiles, and shelters, etc. Nowadays cellulose based materials are the focus among consumers and engineers due to their sustainable nature.

The abundant availability of cellulosic fibres especially wood and plant fibres, their low cost as a raw material, their lightweight and their comparable stiffness properties to synthetic fibres especially glass fibres, has provided the opportunity to find alternative applications other than energy, textiles, paper, and wood based products. The use of cellulosic fibres in composites has grown recently due to the fact that cellulose is renewable and recyclable when combined with thermoplastic polymers (Oksman et al., 2003; Wolcott and Englund, 1999; Wool and Sun, 2005). According to the end of life directive in Europe for cars, at least 85% of a vehicle (by weight) must be recyclable by 2015 (Commission, 2010). Due to continuously growing prices of petroleum and fear of depletion of oil reserves in the near future, cellulosic fibres have become important. The low density cellulosic fibres reduce the weight of composites, provide fuel efficiency in the automotive industry and less energy is needed for their production.

Most varieties of cellulosic wood fibre sources have been used with thermoplastic polymer matrices as a non-reinforcing filler due to the short length (0.5-4 mm), low cost and low weight of these fibres (Bledzki et al., 2002; Kim and Pal, 2010; Wolcott and Englund, 1999). When these fibres are used in injection moulding and extrusion methods, the aspect ratio (fibre length to diameter ratio) of the fibres is decreased even further resulting in deterioration of the composites mechanical properties (Nygard et al., 2008) and therefore, in these cases, cellulosic fibres are only used to reduce the weight and cost of thermoplastic composites.

On the other hand, the continuous textile yarns of spun plant fibres can be combined with thermoplastic polymers to produce unidirectional composites which can be used in load-bearing applications such as construction and transportation elements. From a commercial viewpoint, the most viable structural fibres come from commercially grown textile plants such as flax, hemp, and jute. The long plant fibres (10-90 mm) can be used to produce textile yarn reinforcement with a low twisting angle. (Goutianos et al., 2006). In recent years, bast fibres like hemp, jute and especially flax fibres, which are grown in the largest quantity in Europe (115000 tonnes per year) (Commission, 2009), have been used to produce continuous textile yarn with excellent properties for unidirectional composites (Madsen et al., 2007b).

The quality of composites is governed by the content of the three constituent phases: fibre, matrix and porosity. The optimum quality level is obtained by a combination of high fibre volume content and low porosity content. The variability in mechanical properties of plant fibres is seen as an

important drawback to produce unidirectional composites. The structural variability of flax fibres and the deformation induced during fibre processing result in variable tensile behaviour of the fibres. Moreover, fibre related porosity, such as the porosity in the centre (the lumen) of the fibres, and impregnation porosity, which might be induced at a low consolidation pressure, are important to control in order to obtain good mechanical properties of the composites (Madsen et al., 2009).

The fibre content in composites is constrained by a maximum obtainable fibre volume fraction (Madsen, 2004). It is expected that the fibre content should be as high as possible to be able to compete with glass-fibre-reinforced composites. The glass fibre composites can be produced with fibre volume fractions up to 50-60 %. However, the obtainable maximum fibre volume fractions of plant fibre composites can only reach 40-50 % due to the low packing ability of plant fibres (Madsen and Lilholt, 2002). For this reason, understanding the effect of the fibre structure such as, cross sectional shape and processing parameters such as consolidation pressure must be taken into consideration during composite production since they affect impregnation of fibre yarns with thematrix, and thereby induce an increased porosity content in composites (Saheb and Jog, 1999).

In particular, with the increasing use of cellulosic fibre composites, the demand for stiffness and strength evaluation has also increased. However, test methods that have worked well with non-woven cellulose fibre composites are often found inadequate for unidirectional cellulose fibre composites having increased strength and stiffness. Various attempts have been made to improve the reliability of the existing test methods, and to develop new test specimens and test techniques for unidirectional composites (Hojo et al., 1994; Joyce et al., 2002). While the stiffness of the composites can be obtained by available test methods, the uniaxial tensile strength is still a challenge due to grip section failure. The singular stress peaks near the end of the tabbed grip sections are the reason for early failure of the specimens.

1.1. Objectives

The overall objectives of this study are:

- To promote an increasing use of cellulosic fibre composites being a green product compared with synthetic fibre composites
- To optimize production and to develop the load-bearing capacity of unidirectional flax fibre thermoplastic composites for structural applications using continuous textile yarns.

The work conducted is of both an experimental and theoretical nature, and has been divided into two basic areas (flax fibres, and flax fibre composites), and the specific objectives are:

Flax fibres

- To investigate the tensile behaviour of single flax fibres in terms of the microstructure, processing and testing methods.
- To investigate the effect of cross section measurements on the accuracy determined of the ultimate tensile strength of flax fibres.

Flax fibre composites

- To study the effect of the applied consolidation pressure on the physical and mechanical properties of unidirectional flax fibre reinforced thermoplastic composites.
- To study the effect of porosity on the mechanical properties of unidirectional flax fibre composites.
- To develop a tensile test specimen geometry that creates valid failures within the gauge section of the test material by minimising the stress singularity at the vertex of the tab wedge.

The scope and limitation of the work

The present study concerns mechanical characterisation of flax fibres, being a representative type of cellulose fibres. Flax fibres were selected as a cellulosic fibre source due to their relatively high length to study in the experimental part of the study and high availability in Europe. On the other hand, the selection of the polymer matrix for the composites is generally limited to thermoplastic polymers such as polypropylene and polyethylene with a low melting point to prevent degradation of the cellulose fibres. A low melting point PET thermoplastic matrix which has higher tensile properties than PP and PE matrices was selected for the flax fibre composites.

The flax fibre/LPET composites were characterised by tensile properties only in the axial direction to make it easier to interpret the complex failure behaviour of the cellulosic fibres. Although the flax fibres are supplied in the form of fibre bundles from the same batch in order to decrease the variability of the properties of the fibres, a constant fibre quality cannot be guaranteed. The single fibres were carefully prepared by hand for testing of fibre properties, but the effect of hand preparation on the formation the fibre defects has not been fully examined.

Furthermore, the moisture sensitivity of the fibres needs to be taken into consideration by keeping the single fibres and the fibre composites at controlled ambient humidity conditions before and during testing. The moisture behaviour of the fibres was however not fully controlled during single fibre testing. Textile flax yarns with twisting angles in the range of 10-15° were used for composite production, since yarns with higher angles might affect adversely the stiffness of the composites (Goutianos et al., 2006). The other difficulty of using cellulosic fibres in composites is the lack of strong adhesion with most thermoplastic polymeric matrices (Saheb and Jog, 1999). The hydrophilic fibres are generally treated with coupling agents to promote the fibre adhesion with the

hydrophobic matrix (Zafeiropoulos et al., 2007). In this study, the flax fibres are, however not impregnated with any coupling agent to increase adhesion between the flax fibres and the low melting PET filaments since the fibre-matrix adhesion has not been investigated.

1.2. Outline

The thesis consists of four chapters together with four attached scientific journal and conference papers dealing with different aspects of the mechanical characterisation of flax fibres and flax fibre composites. The experimental and modelling work address the microstructural and processing parameters and their effects on the macro-mechanical properties of flax fibres and flax fibre composites. The first chapter, the introduction, provides a general perspective of the thesis and shows overall and specific objectives of the work.

Chapter 2 is an introductory survey which is indended to give background information about cellulosic fibres and their composites. The two types of cellulosic fibres, wood and plant fibres are comparatively summarised in terms of chemistry, structure, processing and mechanical properties. The applied microscopic observations of softwood fibres and flax fibres are presented indicating the process-related defects such as nodes and pits. Afterwards, the applications of plant fibre composites are presented in this chapter.

Chapter 3 (Paper A1 and A2) presents firstly a literature review of the single flax fibres in terms of morphology and mechanical properties. Next, the experimental results of single flax fibres are presented in terms of the isolation procedure of the fibres. The results explain how the cross sectional area and defects of the fibres, which are characterised by microscopic methods, affect the tensile properties of the single flax fibres. The stress-strain and fracture behaviour are analysed for differently processed flax fibres.

Chapter 4 (Paper A3 and A4) covers the processing and characterisation of flax fibre composites. A literature review is presented to give an overview of relevant previous studies. The main topics are microscopic observations of composite cross sections, and composite production methods. The results for volumetric composition, density and tensile stiffness of the composites consolidated with different pressures are presented as a function of the fibre weight fraction. The results are modelled with a modified rule of mixtures model that includes the effect of porosity on composite properties. The fracture and stress-strain behaviour of the composites are presented for different fibre weight fractions. The maximum failure load of the unidirectional composites is not achieved due to grip section failure of the specimens. For this reason, the unidirectional tensile test specimens are investigated by finite element modelling in order to set a criterion for test specimen geometry so that it becomes possible to obtain gauge section failure to obtain the correct tensile strength.

Chapter 5 summarizes the key results and conclusions of thesis. Chapter 6 contains ideas related to future developments.

2. BACKGROUND

Composite materials manufactured using cellulosic fibres and thermoplastic matrices have gained increasing attention today due to their specific characteristics compared with synthetic fibres such as environmental awareness, economical feasibility and long term sustainability (Eichhorn et al., 2001). Cellulose fibres are renewable, recyclable, biodegradable and they have low densities, comparable mechanical properties especially stiffness with glass fibres (Mohanty et al., 2000). There are many varieties of cellulosic fibres in nature and cellulose fibres can be classified based on their origin. The biomasses such as annual crops; forest resources; municipal wastes are the important sources of the cellulose fibres. Cellulose fibres used to manufacture composites mostly come from annual plants and wood fibre resources (Müssig and Stevens, 2010) as shown in Fig. 2.1

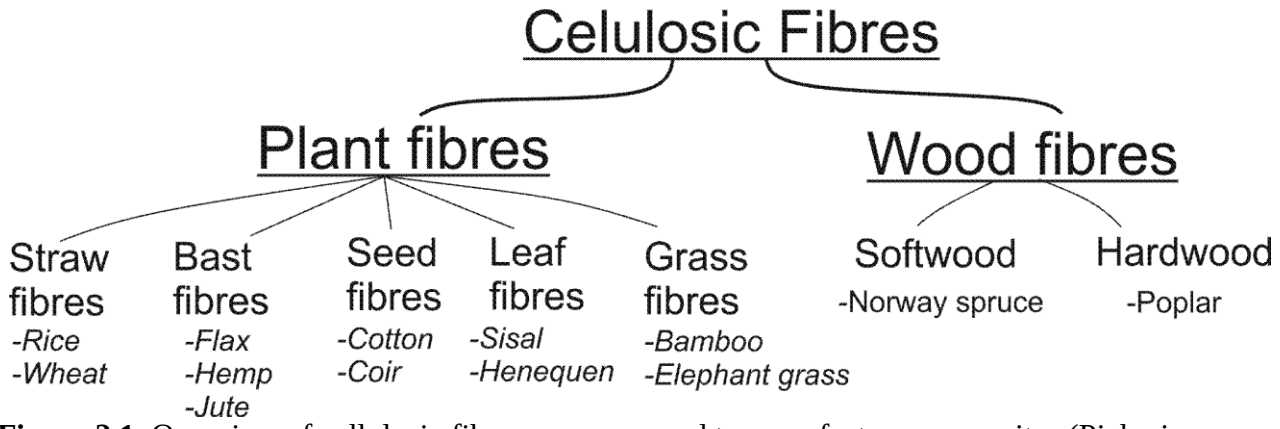

Figure 2.1. Overview of cellulosic fibre resources used to manufacture composites (Pickering, 2008).

Wood has been used as a construction material for many centuries. The wood and wood-based industry mainly produces flat sheet products such as fibreboard, particleboard, and plywood. They are relatively cheap and used for traditional applications such as furniture and construction industries. These products are basically designed for low strength and high deflection (low stiffness) properties. They contain a low amount of phenol-based adhesives (3-12% by weight) and a high void content (20-56% by volume) (Rowell, 2005). Wood is an abundant source of short fibre (below 5 mm). Wood fibre plastic composites (WPCs) are a new class of materials which are produced from very short wood fibres (less than 1 mm) and thermoplastic matrices and moulded into complex components using extrusion and injection methods (Wolcott and Englund, 1999).

The plant fibres such as flax, hemp, jute and sisal have been used as reinforcement in fibre composites. The long plant fibres (5-50 mm) have a higher aspect ratio (length to diameter ratio) and higher stiffness and strength properties, than those of traditional wood fibres (Bledzki et al., 2002). They can be tailored to produce complex shapes of composites. They have been mostly used in nonwoven forms for semi-structural applications such as interior automotive applications as a substitute reinforcement for glass fibres when weight saving is important. Plant fibres have a

sustainable nature and show comparable specific stiffness and strength properties with glass fibres (Müssig and Stevens, 2010). On the other hand, plant fibres are prone to moisture absorption due to their hydrophilic nature and this leads to a weak interface when combined with hydrophobic polymers. Plant fibre composites show inferior composite properties to glass fibre composites which are widely used for structural load-bearing applications.

This chapter aims to show general properties of wood fibres and plant fibres comparatively. Some of the important properties are chemical properties, morphology, and mechanical properties. These two fibre groups have many subgroups (Figure 2.1). However, the bast type flax fibres have generally attracted attention due to their large availability in Europe and good quality properties among other natural fibres for composite manufacturing.

2.1. Cellulose fibres

2.1.1 Cellulose fibre chemistry

The chemical composition of plant and wood fibres is given in the Table 2.1. The chemical composition of the fibres varies to a great extent between and within the plant species due to variable growth conditions (weather, soil) and the fibre processing method (Mohanty et al., 2000). The physical properties of cellulosic fibres are mainly influenced by their degree of polymerization, cellulose content, microfibril orientation, and crystallinity (Nevell and Zeronian, 1985). Therefore, the mechanical properties of plant fibres among the same plant stem vary significantly while synthetic fibres have consist properties. The fibres have a composite-like structure and consist of stiff crystalline cellulosic microfibrils as reinforcement held together through lignin, hemicelluloses, waxes and some water-soluble extractives (Fengel and Wegener, 1989).

Table 2.1: Chemical composition of wood and plant fibres (Bledzki et al., 2002; Hamad, 2002; Rowell, 2005; Wallenberger and Weston, 2004).

Component	**Unit**	**Wood fibre (Softwood)**	**Plant fibre (Flax)**	**Role**
Cellulose	wt%	44-50	45-76	Reinforcement
Hemicelluloses	wt%	20-30	13-22	Bonding
Lignin	wt%	20-35	0.6-13	Stiffness
Pectin	wt%	-	0.9-5	Bonding
Waxes	wt%	-	0.2-1.7	Coating
Extractives	wt%	0-10	0.3-1.7	Encrusting
Ash	wt%	<1	0.8-5	Root growth
Microfibril angle	deg.	30-60	5-10	-
Crystallinity	wt%	60-70	90–100	-

Cellulose is the main structural component that provides strength and stability to the plant cell walls and it is one of the most abundant organic compounds on earth. Cellulose exists in nature as a semi-crystalline macromolecule which shows non homogeneity molecular weight in the body. It has a high degree of polymerization which is typically between 10000 and 15000 glucose residues depending upon the source of the cellulose (Rowell, 2005). Wood celluloses have a particularly lower molecular weight compared with the cellulose derived from plant fibre sources such as flax and cotton. Moreover, a flax fibre is highly crystalline and contains mainly homogeneous cellulose of a high molecular weight, whereas wood cellulose tends to be less crystalline with amorphous cellulose parts (Nevell and Zeronian, 1985). Moreover, the cellulose content in plant fibres of 63 wt% is higher than the cellulose content in wood fibre of 49 wt% (Thygesen et al., 2005a).

The cellulose microfibrils are composed of amorphous cellulose regions where cellulose chains are not oriented parallel to one another, in addition to well-ordered crystalline regions. The basic unit of cellulose is d-glucose monomers which are connected to each other by anhydro-β-1, 4-glucopyranose linkages and are known as cellobiose (Figure 2.2). Adjacent molecules are stabilized laterally by hydrogen bonding between hydroxyl groups, resulting in three dimensional structures called microfibrils, each of which oriented at a specific angle with regards to the fibre axis (Atalla, 1982). The hydroxyl groups are responsible for moisture adsorption which ranges from 7-12% for plant fibres and 25-30% for wood fibres (Nevell and Zeronian, 1985). Lignin is a hydrocarbon polymer with an amorphous structure and consists of both aliphatic and aromatic constituents. It acts as a bonding glue for cellulose microfibrils and resists microbial and ultraviolet degradation. Hemicellulose contains several type sugar units and has a low degree of short chains. It serves as a connecting agent and is responsible for temperature degradation and moisture adsorption (Saheb and Jog, 1999).

2.1.2. Cellulose fibre morphology and structure

Cellulose fibres are composed of bundles of elongated thick walled tubular cells (Mohanty et al., 2000). The long fibre bundles (technical fibres) that consist of single (elementary) fibres are located on the outer part of the plant (flax) stem cross section (Figure 2.2).

The single fibres are bonded together by a pectin interface. A single flax fibre is typically of length of 1 to 50 mm and diameter in the range 10-30 μm (Wallenberger and Weston 2004). Individual long fibres (elementary fibres) or long fibre bundles can be obtained from many agricultural fibre crops at relative low cost. However, plant fibres have a heterogeneous cell structure in terms of the shape of cross section and length. Cross section analysis of wood fibres shows that they are similar to that of plant fibres, consisting of a primary cell wall, secondary cell wall and middle lamella with lumen. Softwood fibres, which are oriented longitudinally in the tree, are known as tracheids and have a length of 0.5-5 mm and 25-50 μm in diameter (Sedighi-Gilani and Navi, 2007).

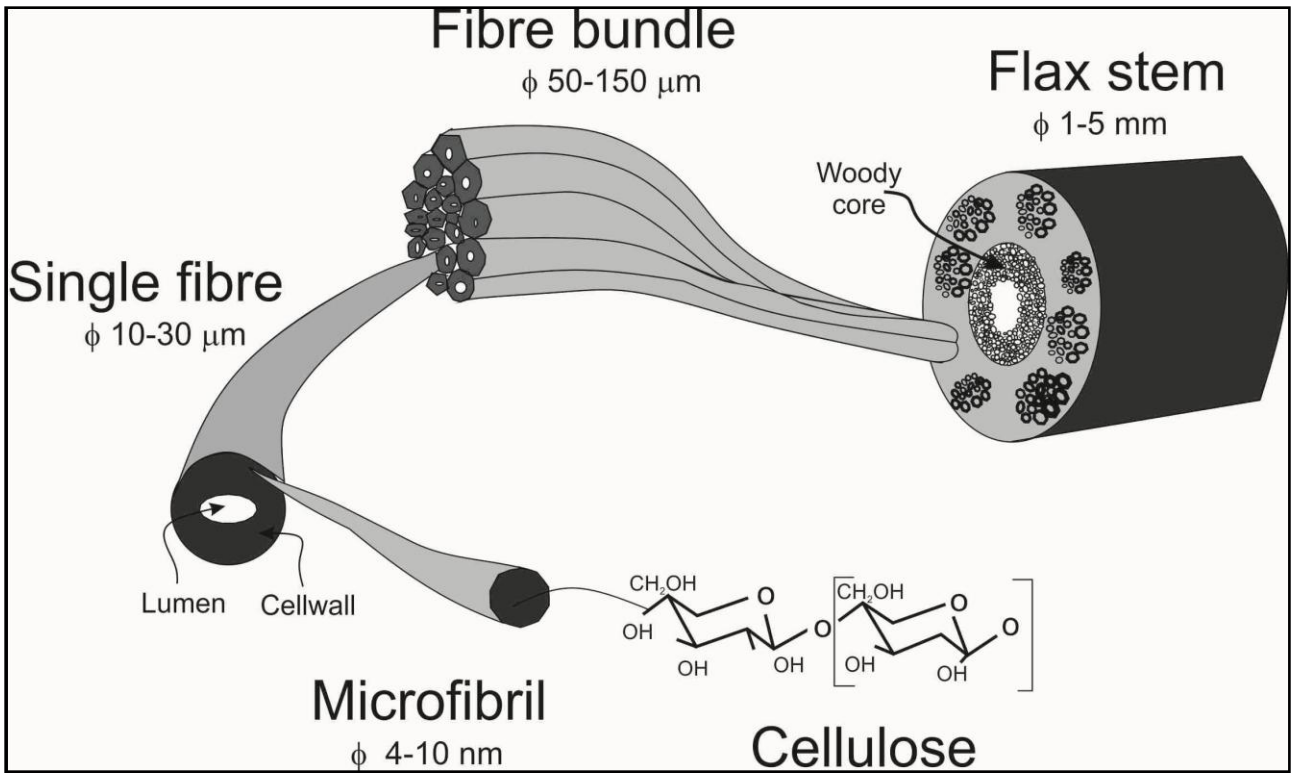

Figure 2.2. Schematic of plant fibre from stem to cellulose.

The cell wall of a single wood and plant fibre is shown in Figure 2.3. The two fibre types have similar cell wall structures and appear like inter-connected tubular structures. The cell wall is a combination of many microfibrils, which are bonded with pectin and/or lignin (Mohanty, Misra et al. 2000). The fibre cell wall consists of a primary cell wall, secondary cell wall and lumen, which is a void in the centre of the fibre. The ratio of the lumen area to the cell wall is in the range 1.5-5% for flax fibres while the lumen area is 20-70% of the fibre cross section area for wood fibres. The primary cell wall is the first layer formed during cell wall growth and it is relatively thin. The secondary cell wall is comprised of three layers (S1, S2, and S3), which have different microfibril orientations. The characteristic value for this structural parameter varies from one plant fibre to another and lies in the range 5 to 10 degree for bast fibres, while the microfibril angle in wood fibres vary from 10 to 60 degree (Astley and Donald, 2001; Page, 1969). The secondary cell wall makes up most of the cell wall thickness and is composed of cellulose and hemicelluloses.

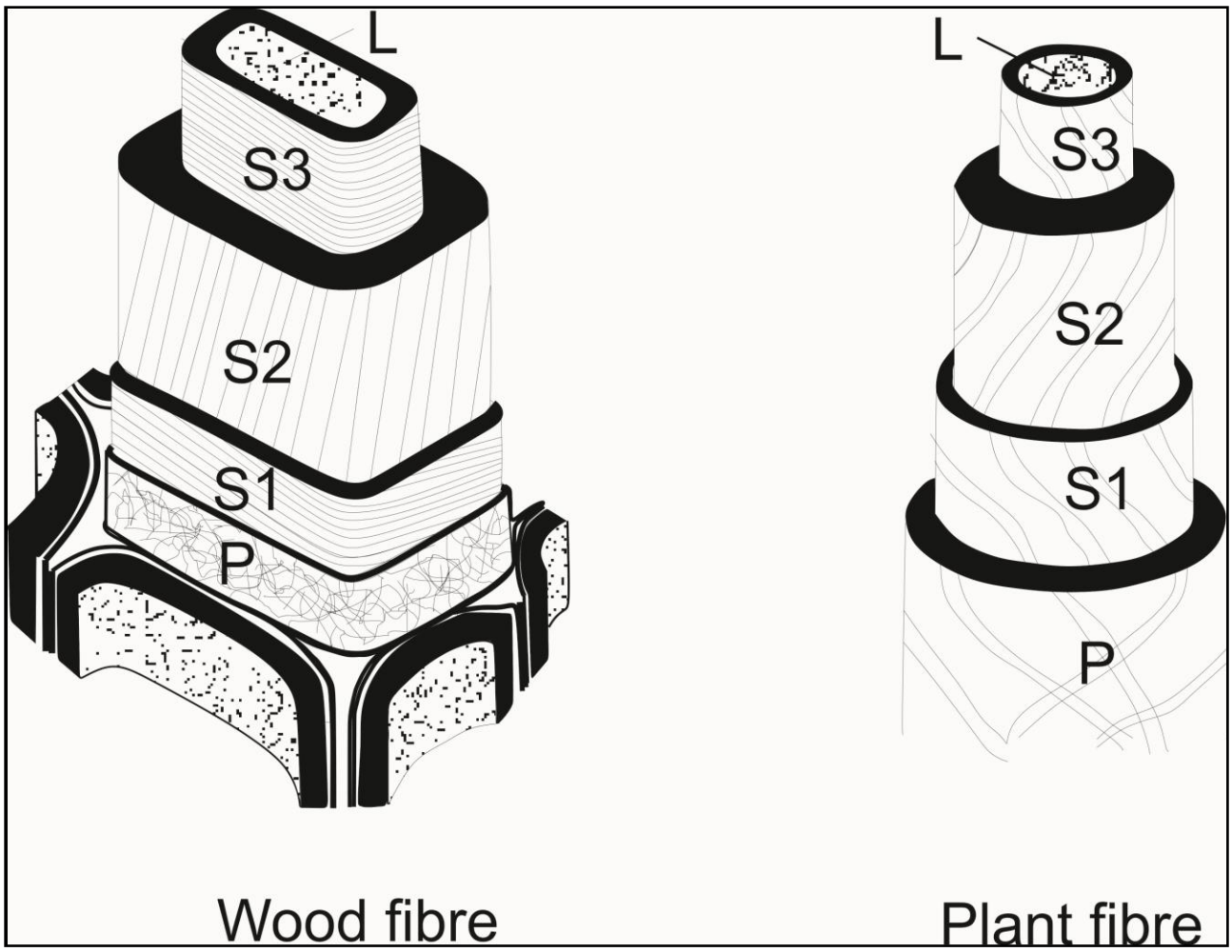

Figure 2.3. Schematics of the cell wall in wood fibres (Fengel and Wegener, 1989) and in plant fibres (Rong et al., 2001).

2.1.3. Processing of cellulosic fibres from plant to fibre bundles

Processing of cellulose fibres varies with the fibre source and final application of the fibres. For example, short wood fibres are used to produce pulp for paper-based products while the long plant fibre bundles are used in fibre composites due to their high aspect ratio (= length/diameter). These fibre bundles have inferior mechanical properties in comparison with single fibres (Pickering, 2008). The plant stem is not separated into single fibres but into fibre bundles (Thomas and Pothan, 2009); in contrast, wood is usually separated into single fibres or very small fibre bundles suiting the particular needs of the pulp, paper or board industries (Biermann, 1996).

Separation of plant fibres starts with the harvesting of fibre crops (Fig. 2.4). First, fibres are extracted from the woody section of the fibre crops. This separation process that causes the isolation of the technical fibre bundles from the central stem is known as retting. This process basically relies on

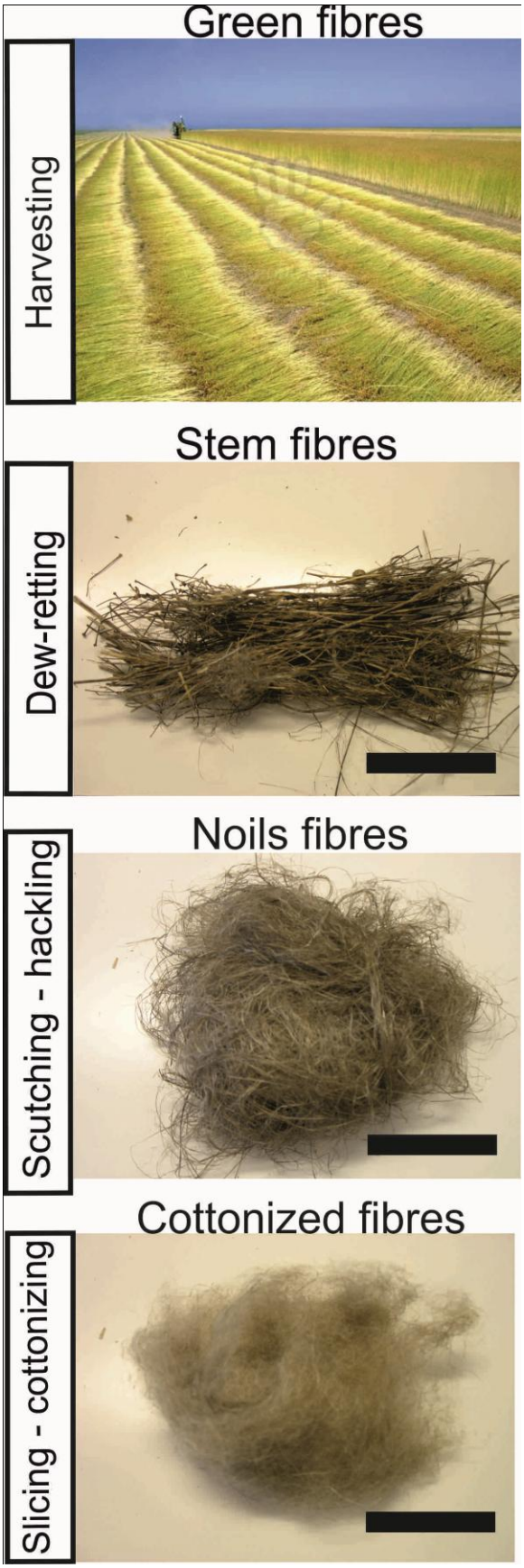

Figure 2.4. Images of differently processed flax fibres according to processing flow from green flax stems to cottonized fibre bundles (top-down). The scale bar is 50 mm.

the biological activity of micro-organisms to degrade the pectin (non-fibre section) and thereby separate the fibre bundles. Retting of fibres can be done with many different methods such as field retting, hot and cold water retting (Müssig and Stevens, 2010).

After the fibres have been loosened from the stem, the stem is broken between rollers. The broken stem parts are then removed from the fibre bundles in a scutching turbine, which basically scrapes the fibres, thereby removing the broken woody stem parts (the so-called shives). The scutched fibres are called fibre bundles, and are still relatively coarse and thick, ribbon-shaped, like their morphology in the plant. The coarse fibre bundles are then combed in a hackling process to get more homogeneous fibre bundle structures. In some applications, fibre bundles are chopped to uniform the length. The fibre bundles are further refined and cleaned to produce cottonized flax. Images of differently processed fibres are shown in Figure 2.4.

During processing of fibres using mechanical treatments, the fibres experience local bending and compressions which leads to the formation of defects such as kink bands. They might also be formed due to environmental forces during growth. The kink bands, also called "nodes" and "dislocations", are regions of the cell wall with a disordered organisation of the cellulose microfibrils in the matrix of hemicellulose and lignin. They are oriented perpendicular to the fibre axis as horizontal bands (Bos et al., 2002).

Wood fibres, however, are more difficult to process than plant fibres and their properties vary with the fibre extraction methods. Fibre extraction methods can be classified as mechanical, thermal and chemical methods (Bledzki et al., 2002) for cellulosic fibres. These treatments can be applied in combination or individually to produce the desired fibre quality. In wood fibres, an important step is the disruption of the middle lamella which is the main lignin source. After the lignin is broken down and dissolved, individual fibres are separated from each other (Biermann, 1996).

2.1.4. Structural and processing defects

It is noted that processing of cellulose fibres causes serious fibre damage (Baley, 2004; Hornsby et al., 1997). Fibres originally also contain defects such as bordered pits and kink bands for wood and plant fibres, respectively (Mott et al., 1996; Thygesen and Asgharipour, 2008). Figure 2.5 shows fibre damages on single flax fibres and spruce pulp fibres after extraction using industrial mechanical treatments. Plant fibres and wood fibres are strongly affected by processing. Single flax fibres have visible defects as kink band regions and single wood fibres have bordered pit regions. The effect of defects on the mechanical properties has been investigated by the present study using qualitative methods (microscopy), and the results are compared with previous investigations (Davies and Bruce, 1998; Thygesen et al., 2005b).

2.1.5. Mechanical properties of single fibres

As mentioned earlier, the mechanical properties of plant fibres are influenced by several microstructural and processing parameters. The chemical composition such as cellulose content, microfibril angle, fibre microstructure such as cross sectional shape, aspect ratio, cell dimensions besides defects during processing are the most important variables that determine the mechanical properties of fibres, (Madsen, 2004; Mehmood, 2009; Thygesen, 2006). However, the cellulosic fibres show different mechanical properties with regards to the structural hierarchy level from fibre bundle to the cellulose microfibril. The cellulose microfibrils possess a very high theoretical modulus of 120-150 GPa (Lilholt and Lawther, 2000)

In order to employ cellulosic fibres as the reinforcement in composites, measuring the fibre properties is essential to predict the mechanical performance of the composites. The stiffness and strength properties of plant fibres are lower than those of glass and carbon fibres. However, since plant fibres have a low density, the specific stiffness of plant fibres is comparable to glass fibres (Bledzki and Gassan, 1999). The properties of typical synthetic and cellulosic fibres are summarised in Table 2.2. One can see that the flax fibres are comparable with glass fibres due to a lower density but they are not as strong as glass and carbon fibres.

Table 2.2. Density and tensile properties of different natural and synthetic fibres.

Fibre types	**Density gcm^{-3}**	**Tensile strength GPa**	**Young's Modulus GPa**	**Specific Strength GPa/g cm^{-3}**	**Specific Stiffness GPa/g cm^{-3}**	**References**
Carbon fibre	1.8	4	230	2.2	128	(Barbero, 1999)
Glass fibres	2.54	2.4	70	0.9	28	(Barbero, 1999)
Flax fibres	1.54	0.4-1.5	30-60	0.3-1	20-39	(Bledzki 2002)
Softwood fibres	1.5	0.2-1	15-30	0.1-0.7	10-20	(Bledzki 2002)

Wood fibres show a much lower tensile strength than plant fibres which have a similar relation with the microfibril angles. It has been found that the tensile strength of fibres basically depends on the microfibril angle (Neagu et al., 2006; Page, 1969). In general, the tensile strength and Young's modulus of plant fibres and wood fibres increase by increasing the cellulose content of the fibres (Nevell and Zeronian, 1985; Thygesen et al., 2005a). Furthermore, the wood fibres possess lower mechanical properties in composites since they act more as a filler other than as a reinforcement due to their lower aspect ratio of 50-100 (Eichhorn et al., 2001) in comparison with plant fibres with aspect ratios of about 1000-2000 (Mukherjee and Satyanarayana, 1986).

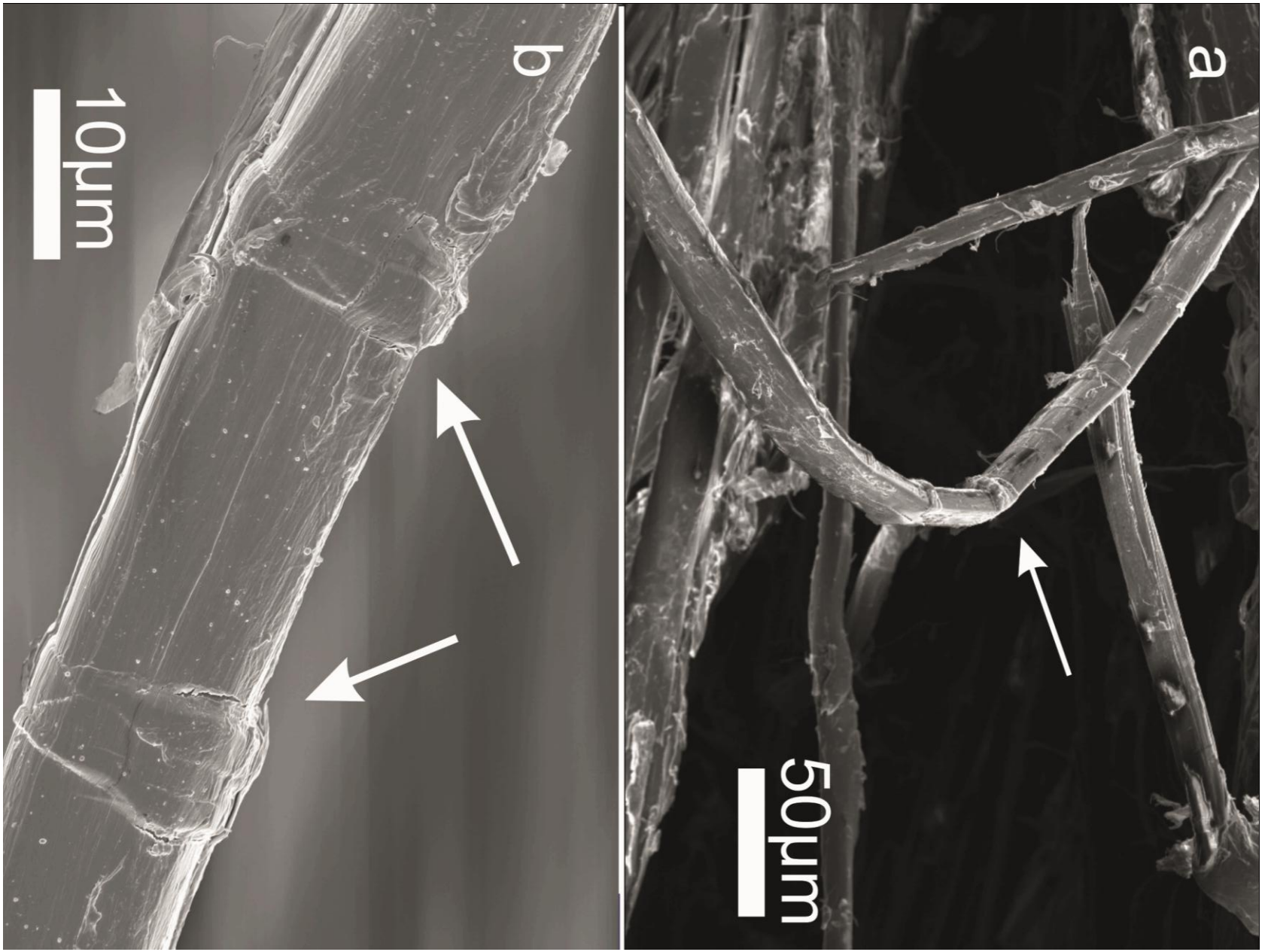

Figure 2.5. SEM micrographs of flax (a,b) fibres with defect regions. Arrows show the kink bands on flax fibre surfaces

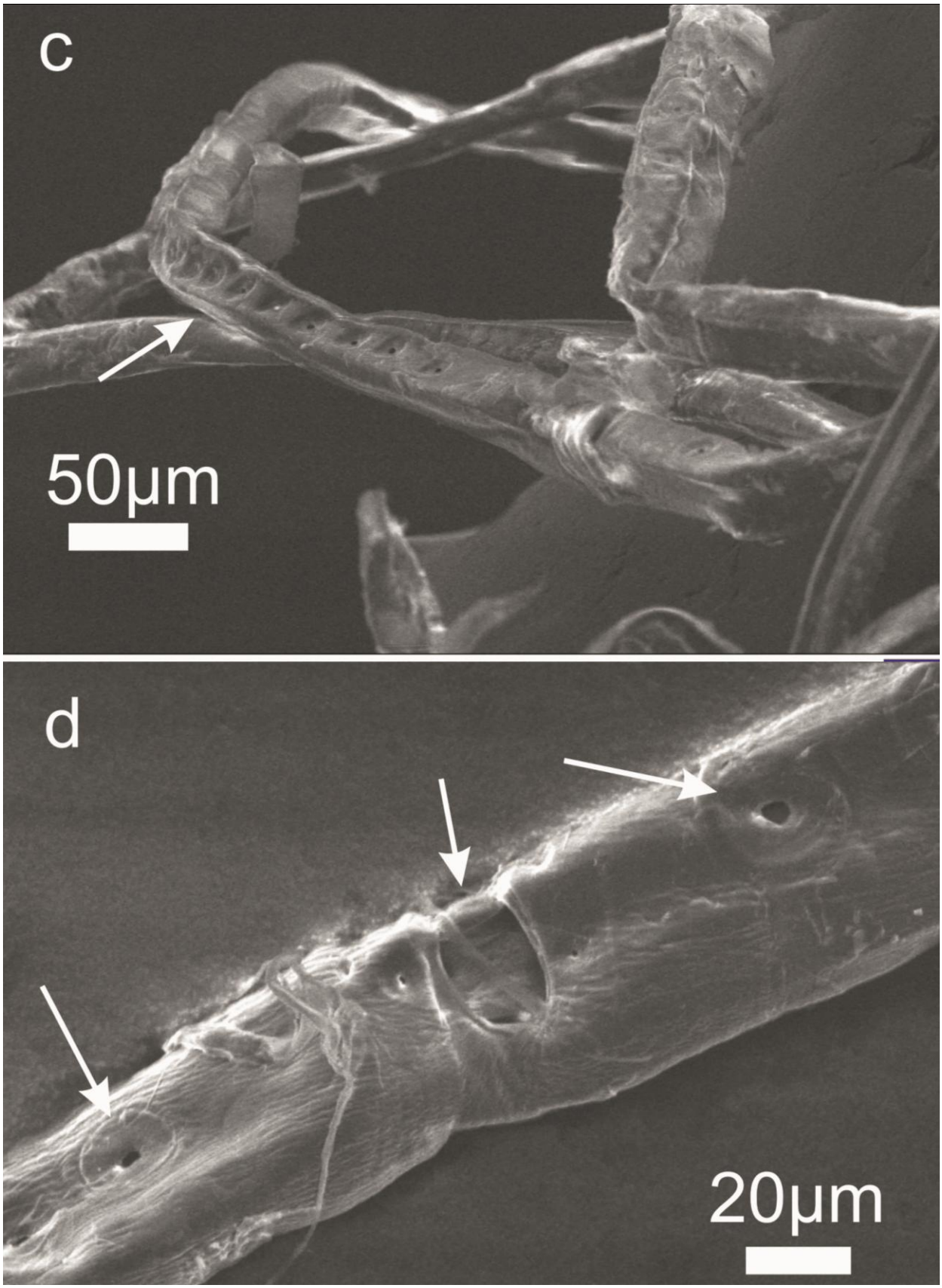

Figure 2.5. SEM micrographs of wood fibres (c,d) with defect regions. Arrows show the bordered pits on wood fibre surfaces

2.2. Cellulose fibre composites

2.2.1. Thermoplastic matrix

Thermoplastics matrix composites are fabricated using a combination of heating, pressing and cooling. This also allows for a high efficiency in recycling of the materials even though recycling causes a decreasing quality due to reducing the length of the polymer chains (Wool and Sun, 2005). Thermoplastic polymers consist of linear and branched molecular chains that do not form a covalently cross linked network (Thomas and Pothan, 2009). The most used thermoplastics are PP (polypropylene), PE (polyethylene), and biodegradable resins such as PLA (polylactic acid) for cellulose fibre based composites (Van de Velde and Kiekens, 2001). Other thermoplastic matrices such as PET (polyethylene terephthalate) are not practical due to their high melting temperatures since cellulosic fibres start to degrade at 200 °C (Thomas and Pothan, 2009). However, low-melting PET matrices are also commercially available to produce cellulose based fibre composites (Niu et al., 2010).

2.2.2. Processing of cellulose fibre composites

The field of cellulosic (natural) fibre composites has an old history and a large application field. The wood based composite industry expands the field from particleboard to new type fibre based boards such as fibreboards, and wood fibre plastics. Phenolics, melamines, polyesters and ureas are some of the thermoset matrix resins which have been commonly used for wood based composites such as fibreboard, particleboard and plywood panels (Pilato, 2010). Although the thermoset matrices have lower water absorption and higher thermal stability in comparison with thermoplastic matrices, the thermoplastics gain increasing interest in order to manufacture recyclable composites with alternative processing techniques, and this is the driving force to produce thermoplastic type cellulosic composites (Pickering, 2008).

The shape of the final product, its performance attributes, cost and ease of manufacturing are the primary drivers for selection of the suitable processing technique to produce thermoplastic fibre composites (Walcott and Englund 1999). Wood and plant fibre composites have common ground between all the manufacturing operations. The short plant fibres and wood fibres are mixed with thermoplastic matrices to produce pellet compounds. The pellets contain randomly distributed short fibres of approximately 1 mm fibre length and have an irregular structure (Nygard et al., 2008). These compounds are processed to complex shaped semi-structural products using extrusion, injection and compression moulding methods (Okamoto, 2003). The longer plant fibres or fibre bundles are brought together as in traditional paper forming and textile methods to produce mats (Pickering, 2008). A homogeneous distribution of the strengthening long flax and hemp fibres is often produced by a carding method for semi-finished products. In carding the fibre material is guided over rotating rollers that are covered with little hooks which separate the fibres and produce

a non-woven fibre mats. (Mieck et al., 1996; Wang et al., 2005). The strength of the mat can be improved by textile interviewing or entanglements (woven and stitching) (Mieck et al., 1996). Furthermore, the long plant fibres can be spun for continuous fibre textile yarn production by well-established spinning methods (Jiang et al., 2011). The twisted or untwisted textile fibre yarns are abundantly available and contain well oriented fibres sources for the production of structural composites using filament winding technique (Madsen and Lilholt, 2003). The composites made with yarns and fabrics or woven performs show higher mechanical properties than composites made with traditional random non-woven forms (Miao and Shan, 2011). However, the yarn and fabric strength is affected by the twisting angle and fabric structure (Goutianos et al., 2006). The processing of the commingled cellulosic fibre/thermoplastic polymer composites using filament winding provides a simpler and uniform matrix distribution than other processing methods such as the film stacking method and it shows better impregnation with the matrix, a lower porosity content and higher mechanical properties (Madsen and Lilholt, 2003).

2.2.3. Composite mechanical properties

Properties of composites not only depend on the properties of their constituents but also on other parameters such as: fibre content, fibre orientation (Van de Velde and Kiekens, 2003). Most of the previous studies show that thermoplastic fibre composites with unmodified cellulosic fibres exhibit a lower tensile strength (Li et al., 2007). For unidirectional fibre composites, axial tensile properties show a significant improvement with increasing fibre volume fraction (Madsen et al., 2007a). However, after an optimum level of fibre volume content, addition of further fibres reduces the tensile properties of the composites. Fibre addition also reduces the failure strain of the cellulosic fibre composites.

Table 2.3: Tensile properties of wood, plant and glass fibre reinforced PP composites

Fibre type	**Fibre direction**	**Volume fraction (%)**	**Strength MPa**	**Stiffness GPa**	**References**
E-glass	aligned	55-60	1020	45	(Gamstedt et al., 1999)
E-glass	random	25-35	60-150	6-9	(Garkhail et al., 2000)
Flax	aligned	30-50	250-300	20-30	(Madsen et al., 2007c)
Flax	random	40	67	7	(Pickering, 2008)
Wood	random	40	19	3	(Pickering, 2008)

The mechanical properties of fibre composites are usually expressed in the form tensile strength and stiffness, and these properties vary with fibre type, fibre content and fibre direction as shown in Table 2.3. The results demonstrate that fibre direction makes a clear difference in the tensile behaviour of flax and glass fibre composites. The aligned and random flax fibre composites show comparable mechanical properties with random glass fibre composite at lower fibre volume fractions.

2.2.4. Applications of cellulose fibre composites

Cellulosic fibres, especially bast type fibres such as flax, hemp, and jute, are very fast growing types of fibres for composite reinforcement, and in particular, they show an increasing trend of production using injection and extrusion moulding techniques (Thomas and Pothan, 2009). Considerable markets are emerging in, furniture, packaging, automotive, transportation, construction and marine applications (Müssig and Stevens, 2010).

The automobile industry needs low weight and high performance materials which can be recycled at the end of life. The non-woven plant fibre based composites produced by compression moulding, and the wood fibre plastic composites produced by extrusion and injection moulding have been used in automobiles for semi-structural applications, such as dashboard parts, door panels, floor panels, seat backs and trunk covering panels (Kim and Pal, 2010). In the building industry, wood based composites are mostly employed as low cost insulation materials, acoustic materials and decking materials.

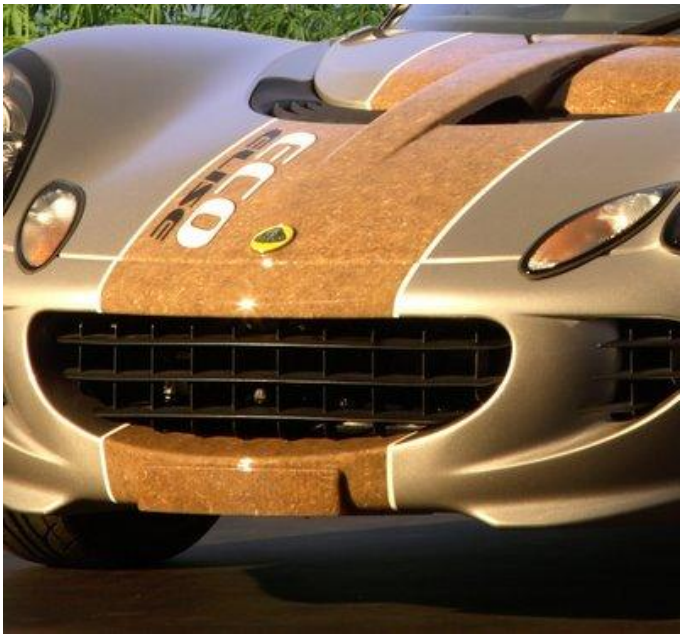

Figure 2.6 A car body (Lotus eco) produced with plant fibre composites (www.lotuscars.com, 2012).

Currently, cellulosic fibres are preferred in composite components in semi-structural and structural applications. These components also have exceptional characteristics such as: green by nature, 100% renewable raw material by biodegradable polymers, sustainable, recyclable, high strength and stiffness, low density, vibration dampening, good thermal and acoustic insulation, low abrasion. These developments have been studied with plant fibres in the form of yarns and slivers by producing composite prepregs (Mussig and Stevens, 2010). The new innovative applications for structural applications are nowadays produced with the concept models (Fig. 2.6) such as transport, marine and sports products, in order to replace synthetic materials with natural materials.

3. FLAX FIBRES

3.1. Literature review of flax fibres

3.1.1. Flax fibre morphology

Flax, one of the bast types of natural fibres with a good mechanical performance, has been widely used to produce composites. Contrary to artificial fibres, flax fibres are not continuous fibres but they have a composite like hierarchically organized structure. Their macroscopic properties emerge from their micro and nano-structural level (Bos and Donald, 1999; Thomas and Pothan, 2009).

Flax is a fast growing annual crop and belongs to the genius of the Linacea family including other bast fibres like hemp, kenaf, and jute. The morphology of the fibres shows similarities and composites produced using them show similar properties. The industrially important flax fibres are placed as fibre bundles in the outer surface of the plant stem as shown in Figure 3.1. The bundles (technical fibres) are between 60 and 140 cm long and their diameter ranges from 40 to 80 µm. The flax stem contains 20-50 bundles in their cross section. Each bundle consists of 10-40 spindle shaped single (elementary) fibres of 1-12 cm length and 15-30 µm diameter (Müssig and Stevens, 2010; Sumere, 1992).

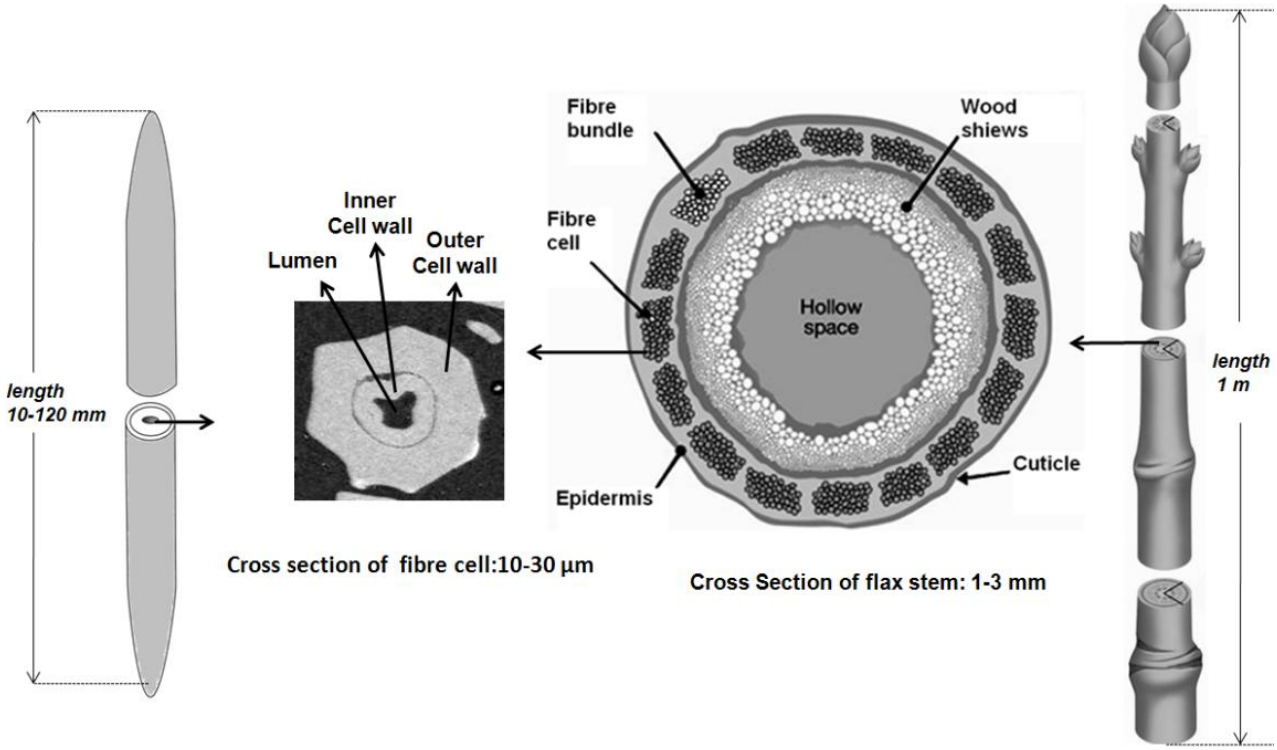

Figure 3.1: A schematic comparison of a single flax fibre and the cross section of a flax stem. After (Winterborne, 2005).

The single fibres have been shown to possess different cross sectional shapes along the fibre axis. Some researchers have approximated fibres possessing hexagonal or pentagonal cross-sections (Baley, 2002). However, the fibres vary in their non-uniform geometrical shapes along the fibre axis. Owing to these irregularities in the thickness of the cell walls, the fibres vary greatly in strength (i.e. failure load, N). A single fibre across the cross section consists of a primary cell wall and secondary cell walls, and a lumen in the centre of the fibre (Bos et al., 2002).

Charlet et al. (2007) basically showed that the fibre diameter can vary two to threefold within a few millimetres of fibre length. They studied the diameter of the elementary fibres isolated from the bottom, the middle and the top part of the flax stems. The mean fibre diameter was found to decrease from the bottom to the top of the stems. The cross sectional area of fibres from each zone was analyzed to measure the fibre cell wall area. They also found that the mechanical properties of the fibres are strongly influenced by their location in the stem.

3.1.2. Flax fibre mechanical properties

Many researchers have investigated flax fibre properties at the levels of elementary fibres and technical fibres, and it can be concluded from the results that there is a large variability in the reported tensile strength and Young's modulus of flax fibres. Table 3.1 represents the tensile properties of elementary and technical flax fibres measured in various studies. The reason for the scattering has been attributed partly to uncertainties in the measurement of the fibre cross sectional area (i.e. due to the irregularity in the cross sectional fibre shape). The tensile strength data has been mostly described using a Weibull distribution function (Wang et al., 2006).

Davies and Bruce (1998) have performed static and dynamic measurements of tensile modulus and strength of elementary flax fibres in order to analyze the effect of damage size under varying environmental conditions. Since processing induces damages to the fibres, the fibre properties depend inevitably on processing methods, fibre type and the extent of damage. They found almost linear stress strain behaviour of the single fibres. The average (± std. dev.) strain to failure was found to be 1.3±0.6. Since strength values showed high variability, they were described by a Weibull distribution.

The scatter in tensile properties of single flax fibres might be related with the diameter variation of fibres. Virk et al. (2010) have focused on the issue of determining an accurate fibre cross sectional area. It is not straightforward to determine the cross sectional area from width (diameter) measurements along the fibre axis for each individual fibre. They found that the coefficient of variation (CoV), which is defined as the ratio of the standard deviation to the mean, is a key parameter to describe the effect of the fibre diameter on the measured strength and failure strain. Hence, the strength of the fibres as a function of fibres diameter shows high variability. However,

the failure strain of the fibres is independent of the fibre diameter and shows a more consistent CoV than that for the fibre strength (Virk et al., 2010).

Charlet et al (2007) have determined the stress strain behaviour of flax fibres. A non-linear region is observed in the early stage of the loading for small deformations. This behaviour has been explained by visco-elastic movements of the microfibril angles along the fibre axis in the large defect zones of the cell wall (Baley, 2004). The microfibril angle of flax fibres has been reported in the literature to be around 10° to the fibre axis (Charlet et al., 2009; Kolln et al., 2005).

Table 3.1. Tensile properties of elementary and technical flax fibres (various references).

Flax fibre type	**Method**	**Gauge Length [mm]**	**Average Strength ± Std. dev. [MPa]**	**Young's Modulus ± Std. dev. [GPa]**	**Failure Strain ± Std. dev. [%]**	**References**
Elementary fibre	Green fibre	5	678 ± 216	-	-	(Zafeiropoulos et al., 2007)
Elementary fibre	Dew retted	5	906 ± 246	-	-	(Zafeiropoulos et al., 2007)
Elementary fibre	Dew retted	8	621 ± 295	52 ± 18	1.3 ± 0.6	(Davies and Bruce, 1998)
Elementary fibre	Enzyme retted	9	591 ± 250	57 ± 22	1.4 ± 0.9	(Hu et al., 2010)
Elementary fibre	Enzyme retted	5	750 ± 650	89 ± 35	-	(Joffe et al., 2003)
Elementary fibre	Scutched	5	732 ± -	-	-	(Van de wejenberg I, 2000)
Elementary fibre	Hackled	3	1522 ± 400	-	-	(Bos et al., 2002)
Elementary fibre	Hackled	10	945 ± 190	57 ± 35	2.0 ± 0.4	(Charlet et al., 2007)
Elementary fibre	-	10	1339 ± 486	54 ± 15	3.3 ± 0.8	(Baley, 2004)
Elementary fibre	-	10	722 ± -	-	-	(Andersons et al., 2009)
Technical fibre	-	-	690 ± 345	28 ± -	2.9 ± 0.3	(Sridhar and Basavarajappa, 1982)
Technical fibre	-	20	613 ± 442	-	-	(Romhany et al., 2003)

Koln et al (2005) have investigated the tensile behaviour of single flax fibres. The fibres were extracted from bundles of bleached industrial flax fibres, and investigated by X-ray diffraction. The strain rate was assumed to be high enough to avoid relaxation. Tensile tests were performed in order to reveal a change of orientation in the cellulose microfibrils while stretching the fibres. They found that the microfibrils rotated during the first percent of tensile strain into a more parallel orientation to the fibre axis. In addition, the irregular spatial distributions of less ordered regions were shown to be much more homogeneous after the visco-elastic stretching (Kolln et al., 2005).

Thygesen et al. (2007) have investigated the changes of the disordered regions, which also are called "kink bands or dislocations", by fibre stretching under a polarized light microscope. They found that these regions disappeared after the tensile failure test. Furthermore, they employed a relaxation time of 20 minutes at a constant force for single fibres in order to understand the dislocation behaviour. They demonstrated that the fibres show a very small extent of visco-elastic behaviour. They also investigated the effect of the relative dislocation area on the failure stress and Young's modulus of the fibres. The results did not show any clear relation between the dislocation area and the mechanical properties. They concluded that the mechanical properties of fibres were decreased for severely damaged fibres (Thygesen et al., 2007).

Bos et al. (2002) performed tensile tests to determine the strength of elementary and technical flax fibres. They found that the elementary flax fibres showed a considerably higher strength than technical fibres of the same length due to a bundle effect. This partially overshadows the fibre damages occurring during fibre extraction. The mechanical treatments were found to induce kink bands in the fibres and thereby reducing their tensile strength (Bos et al., 2002). It has been determined that the fibre strength decreases with increasing fibre gauge length (Bos et al., 2002) (Romhany et al., 2003).

Bos et al. (2002) also showed that tensile strength of the fibres depends on the isolation procedure. Hand isolated fibres are stronger than mechanically isolated fibres. However, they noted that the scatter in strength is much larger for the hand isolated elementary fibres than for the standard mechanically isolated elementary fibres. They claimed that the mechanical fibre processing methods affect the number of large defects, which reduces the scatter in the fibre strength although the fibres show a lower mean strength. Joffe et al. (2003) performed tensile tests on elementary flax fibres. They showed that fibres separated as a result of an enzyme treatment show less damage compared to mechanically processed fibres. This finding is supported by Oksman (2001) who found that the enzyme-treated flax fibres have a stiffness which is higher than for glass fibres, and it was estimated to be in the range 80 to 100 GPa (Oksman, 2001).

Baley (2004) has determined the tensile strength of elementary flax fibres. He suggested that the fibre kink bands and micro compression defects cause a loss of tensile strength of the fibres, and they act as points of fracture initiation during fibre failure. The tensile strength and Young's

modulus of the fibres were found to decrease with increasing fibre diameter. However, there was no clear relation between tensile strength and number and shapes of kink bands. Baley et al. (2005) have determined the influence of absorbed water on the tensile strength of elementary flax fibres. The results showed that the process of drying of the flax fibres influences significantly their tensile strength (Baley et al., 2005).

Zafeiropoulos et al. (2007) have focused on the effect of two chemical surface treatments (acetylation and stearation) on the tensile strength of flax fibres. The results are discussed and analysed in terms of Gaussian statistics, and it was found that the treatments did not significantly change the flax fibre tensile strength. Moreover, the results showed that dew retted flax fibres have a higher tensile strength than green flax fibres (Zafeiropoulos et al., 2007).

3.2. Summary of results in present study

Single flax fibres were characterised in the present study. The results related with the morphology of the single flax fibres and their tensile properties are summarised here.

3.2.1. Isolation of single flax fibres

The flax fibres were supplied by a flax fibre producer (Ekotex) in the form of technical fibre bundles. The series of processing steps of the flax fibre separation, as described in Chapter 2, can be categorised into two main processing steps: natural processing and mechanical processing.

Naturally processed fibres: These fibres are dried after harvested in the field, and they are formed as a result of natural retting in the fields. They are denoted Green fibres and Stem fibres. These fibres are only exposed to some weak mechanical forces during harvesting and drying.

Mechanically processed fibres: After drying and retting, the flax fibres were separated from the woody parts of the stem by a breaking (or scutching) process. Afterwards, the short fibres were separated from the long fibres by a hackling (or combing) process. The mechanically processed fibres are denoted Noils fibres and Kotonina fibres.

The single flax fibres were carefully extracted by hand from the fibre bundles (technical fibres). The technical fibres were conditioned at a temperature of 23 °C and a relative humidity of 55% in a climate chamber before manual handling. The fibres are delicate materials to test, and paper frames were used to hold the single fibres. The single fibres were mounted on the paper frame under a microscope using cyanoacrylate glue. The single fibres are very likely to get twisted during handling, and this should be avoided.

3.2.2. Microstructure of single flax fibres

Single flax fibres, having a composite-like microstructure, consist of multi-structural microfibrils in their cell wall cross sections, as described in the previous section. The microfibrils are hierarchically placed in the cross section of the fibre. In the present study, the characterisation of the fibres in terms of microstructural and processing factors is made by electron and optical microscopy. In addition, the author was partly involved in the characterisation of defects by optical microscopy. While a large type of defects can be observed on the fibre surfaces with electron microscopy, a small type of defects at the inside of the cell wall can only be seen by optical microscopy. This is because the small type of defects formed on the inner side of the cell wall can be seen with polarized light due to changes of the microfibril angle.

3.2.2.1. Defect observation with optical microscopy

The defect quantification of the individual fibres can be done using polarised optical microscopy. The mechanical deformations on crystalline fibre microstructure can be clearly visible under cross polarised lights due to a change in the birefringent properties. The fibre surface is seen with different brightness levels due to changes of the microfibril angles in the defect regions. Hence, the optical microscope image clearly shows different types of defects along the fibre length. Figure 1 in paper [A1] shows different types of defects which appear as bright and dark lines across the fibre. The defects were also quantified for different types of processed fibres, and the results showed that the number of defects increased with increasing the number of processing steps (Mehmood, 2009).

3.2.2.2. Defect observation with SEM

Figure 3.2a and b shows SEM micrographs of the surface morphology of a single fibre (elementary fibre) and a fibre bundle (technical fibre). The marked areas at the fibre surfaces are developed due to mechanical-induced deformations during fibre processing. They are generally called kink bands, and they are distributed along the fibre length as small and large bands. The deformations seem only to take place in the primary (surface) layers. However, the intact microfibrils are expanded outwards in all layers by a micro buckling effect. The microfibrils (50-150 nm in width) can be seen as bridged cross-fibrillar structures inside the longitudinal fracture formations in the defected zone. It can be concluded that the cross linked microfibrils are not fully separated, and may permit a local cell wall expansion.

Figure 3.2a. SEM micrographs of surfaces of single fibres. Kink band (lumpy swelling) formations are shown with white arrows and magnified in the white boxes.

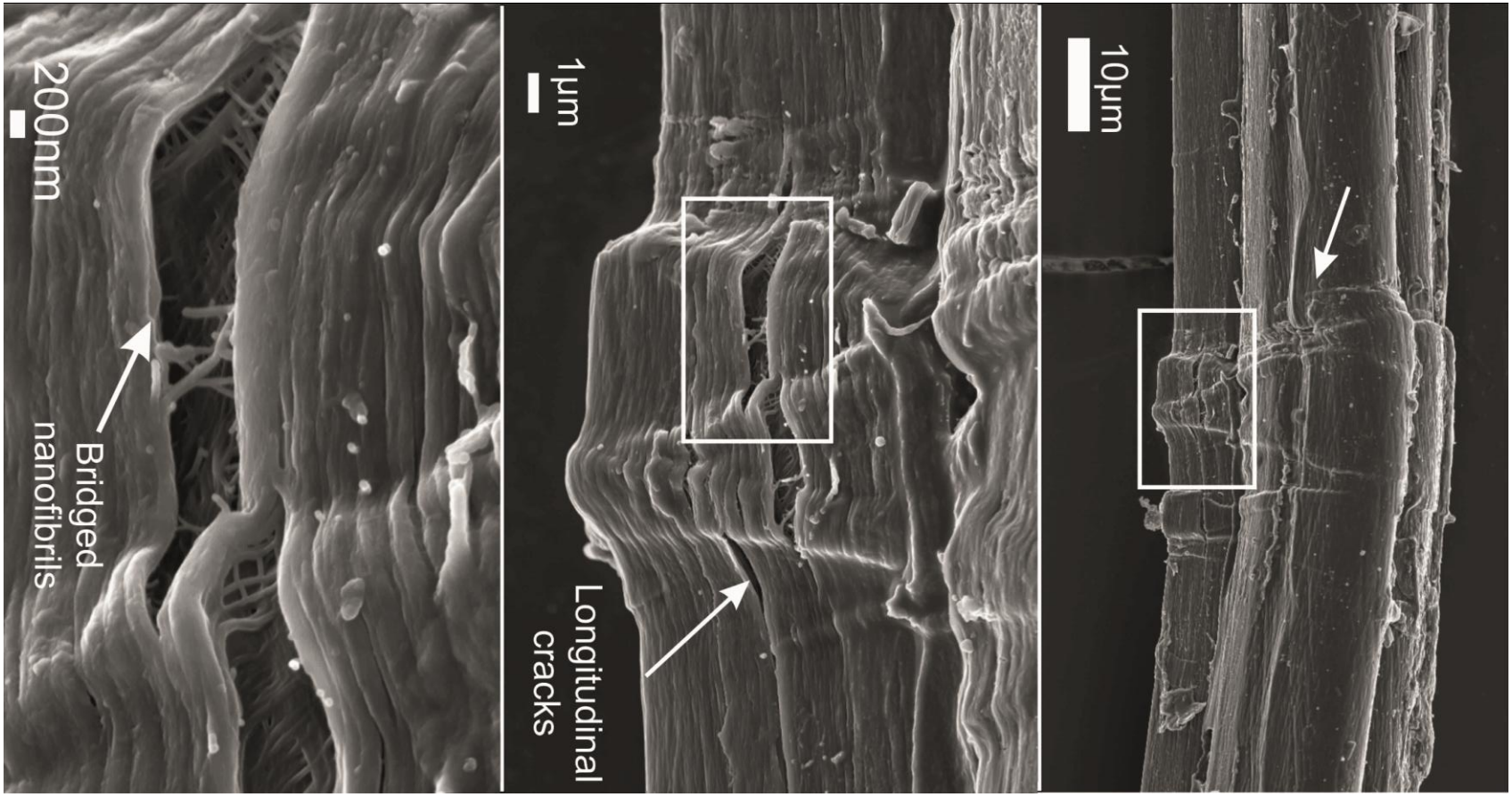

Figure 3.2b. SEM micrographs of surfaces of the fibre bundles. The defect (kink band) zones are magnified in the white boxes and the bridged nanofibril formations are shown through the longitudinal cracks with white arrows.

3.2.2.3. Fibre cross section analyses

An accurate measurement of the cross sectional area is important to calculate correct tensile strength values. The cross sectional area of each fibre is usually calculated from the average of width measurements of the fibres along the fibre length whilst assuming their shape to be perfectly cylindrical (and ignoring the lumen space). However, in practice, the cross section of the fibres show irregular shapes and includes central voids (the lumen spaces). The size of the cross sectional area varies along the fibre length as well. For these reasons, the errors using the circular fibre area assumption will produce incorrect tensile strength values. Figure 3.3 exhibits a schematic view of the two cross sectional areas which are determined according to the circular assumption method (A_{circ}) and the true fibre area method (A_{true}). The area of the lumen (A_{lum}) can only be determined using a fibre cross sectional view (the true fibre area method). The shape of the fibre cross sections can be quantified by the aspect ratio, which is the ratio of the major and the minor axis of a fitted ellipsoidal cross sectional area.

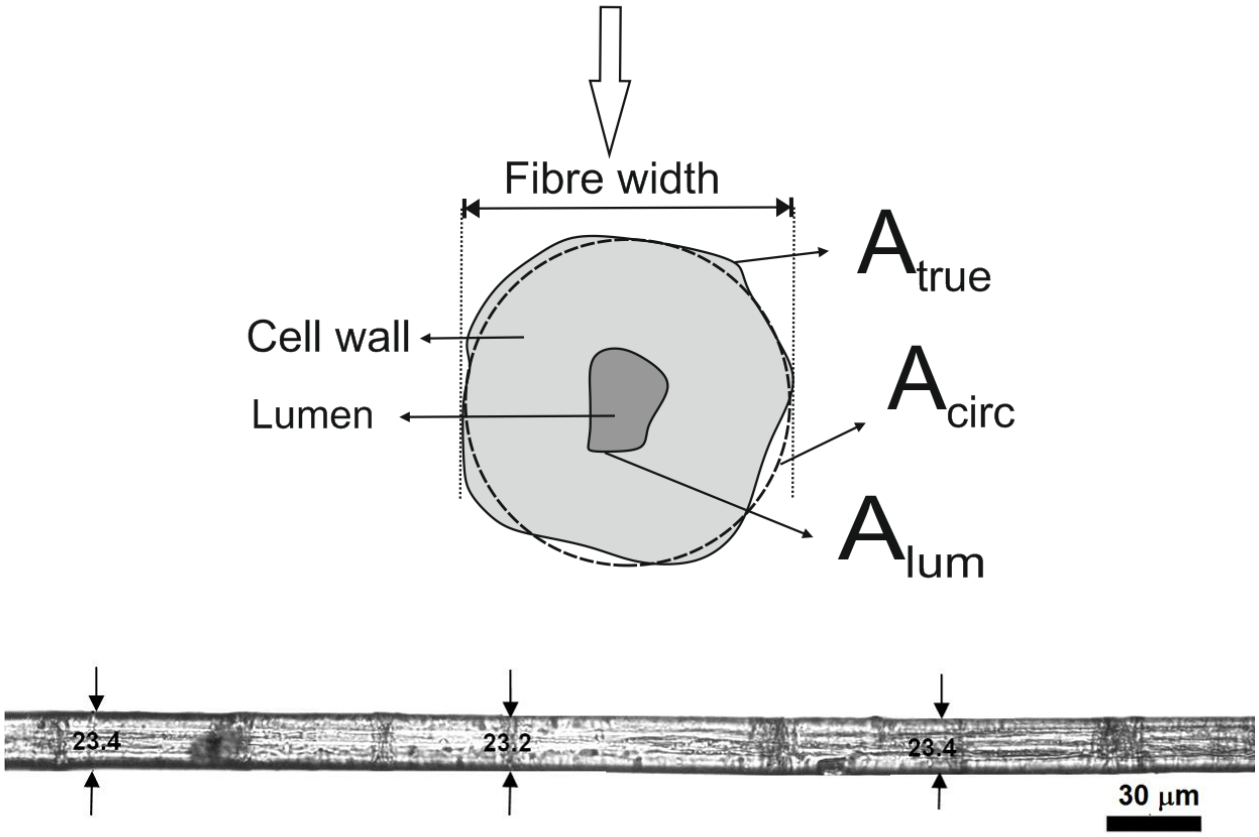

Figure 3.3. A schematic view of cross sectional area measurements based on the actual cross section (top) and the average width of a single flax fibre and their distribution along the fibre to calculate the fibre cross section by the circular assumption method (down).

The frequency distribution of the measured fibre areas using both methods is shown in Figure 3.4. It shows that the determined cross sectional area of fibres using the circular assumption is 39% higher than the area determined from the actual cross section of the fibres. It is also found that the difference in the area measurements is consistently increased when the cross sectional aspect ratio of the fibres is increased. Moreover, the lumen content of the fibres is found to be lower than 1% for 85% of all fibres [A2, Figure 6], and the aspect ratio is not affected by the lumen content of the fibres. It is however shown that the aspect ratio must be taken into account when the fibre diameter measurements are used to calculate the fibre cross sectional area. If this is not done, the fibre areas determined with the circular assumption method are being overestimated for fibres with low aspect ratios under threshold values in the range 1.5-1.8 [A2].

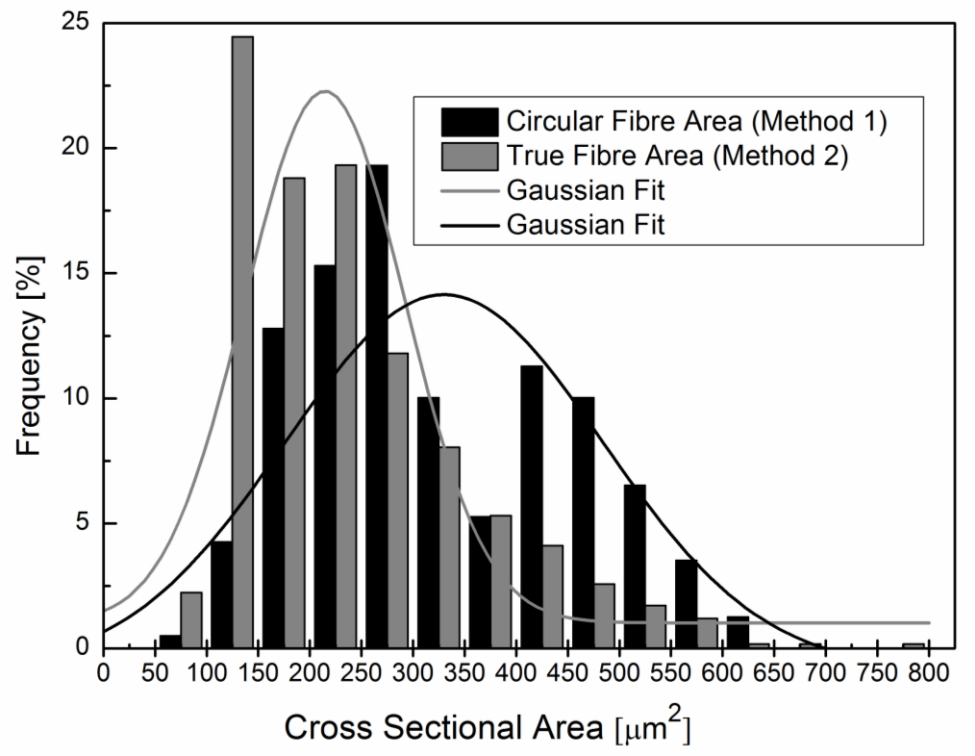

Figure 3.4. Frequency distribution of the cross sectional area of fibres determined by two methods of circular fibre area and true fibre area.

3.2.3. Tensile properties of single flax fibres

The uniaxial tensile behaviour of the different types of single flax fibres are investigated since the tensile behaviour of single fibres is important for the final tensile behaviour of the composites. All testing was conducted at temperature and humidity conditions of about 23 °C and 55% RH, respectively, using a test procedure described in Paper A1.

3.2.3.1. Stress strain behaviour

The stress strain behaviour of the fibres is investigated for differently processed flax fibres. Structural deformations occurring during processing can be interpreted by the two different types of stress strain behaviours observed from the tensile testing results. The first type of stress strain behaviour appears nearly linear and the other is non-linear.

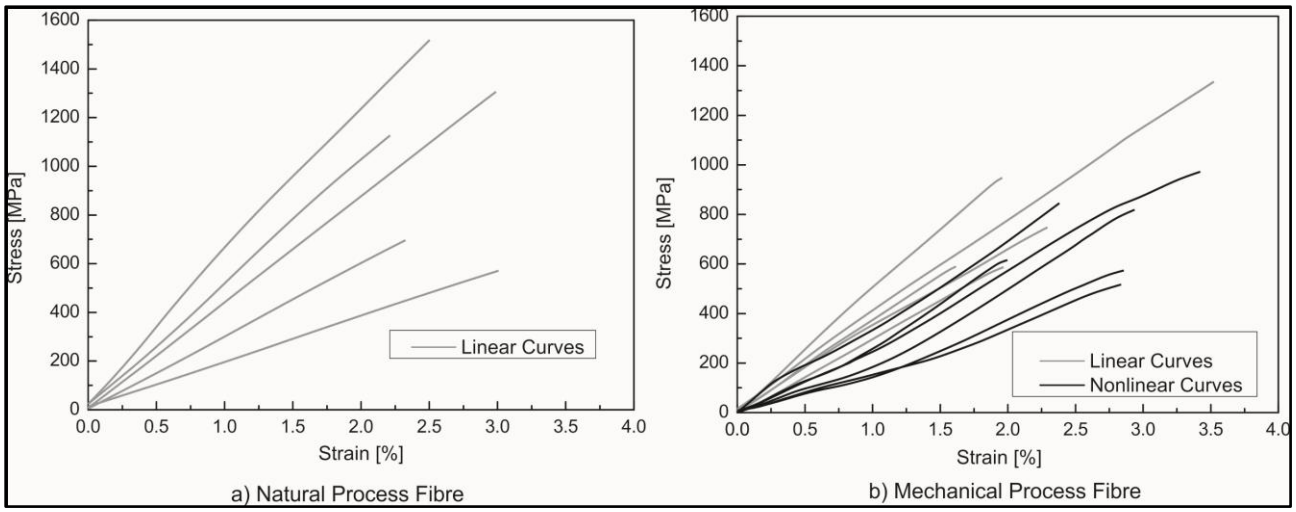

Figure 3.5. Stress strain behaviour of single flax fibres: a) naturally processed fibres, and b) mechanically processed fibres

The naturally processed fibres showed only the nearly linear type of stress strain curves, whereas both the linear and the non-linear types of curves are seen for the mechanically processed fibres (Fig. 3.5). The naturally processed fibres are seen to have a higher stress and higher strain to failure than the mechanically processed fibres [A2]. The non-linear behaviour could be associated with the cross bridged microfibril arrangements at the deformation zones of the fibre cell wall that takes place during loading of the fibre. In other studies (Baley, 2004; Charlet et al., 2009), non-linear curves are also found for single fibres and the non-linear stress strain behaviour is attributed to the microfibril angle variation in the defect zones. This hypothesis is also supported in the present study by the increasing number of non-linear curves for the mechanically processed fibres, which are more likely to have defects compared to the naturally processed fibres.

3.2.3.2. Tensile strength

The mechanical properties of flax fibres do not only depend on the environmental factors such as, growth condition, fibre location on the stem, but it depends also on the fibre process conditions (Charlet et al., 2007)**.** Figure 3.6 shows the mechanical properties of single flax fibres as a function of their cross sectional area determined for differently processed fibres. The results show that the tensile strength of naturally processed fibres is higher than that of mechanically processed fibres.

The strength of the flax fibres decreases when the cross sectional area increases. The cross sectional area of the fibres shows a large variety between about 100-700 μm^2. The large variety in results can be attributed to some extent with the measurement method of the fibres, as previously mentioned: the measurement error is increased when the aspect ratio of the fibre cross section is increased [A2]. Moreover, the large scatter of the tensile strength of the fibres is likely to be related with the distribution of defects along the fibre direction. This is because the defects act as fracture initiation sites and therefore cause a serious reduction of the tensile strength [A1]. The tensile results are comparable with literature data even though they are scattered. The coefficients of variation are found in the range 20-60% [A2].

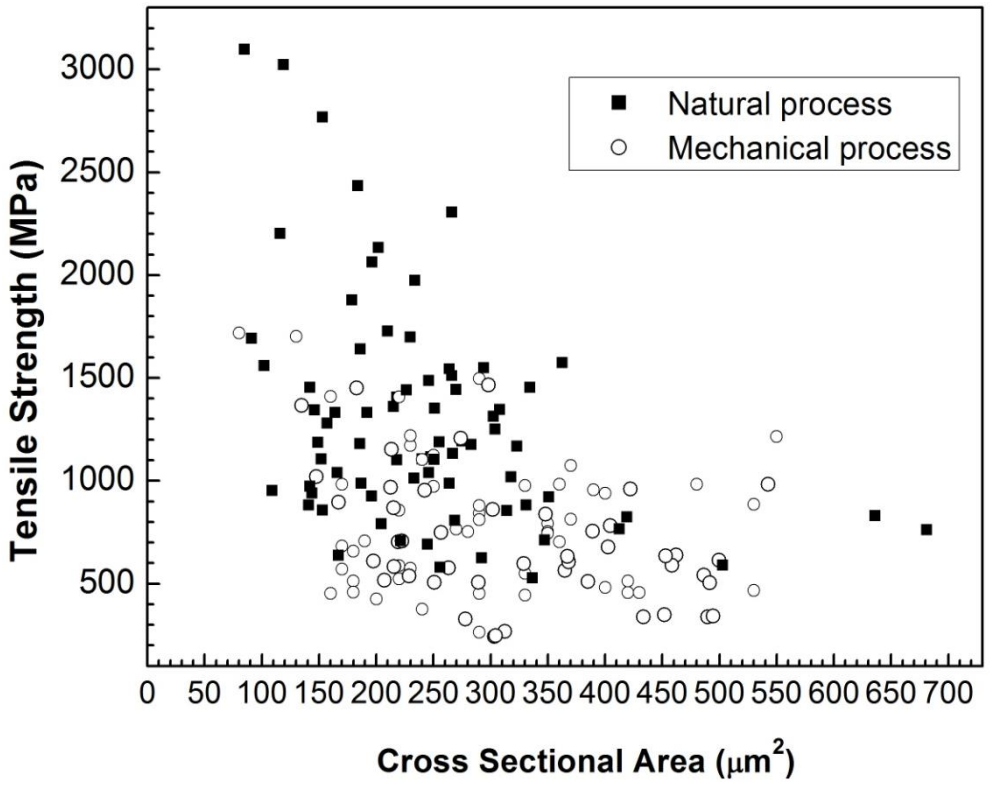

Figure 3.6. Tensile strength of single flax fibres as a function of cross sectional area for naturally and mechanically processed flax fibres.

3.2.4. Fracture behaviour

The microscopic observations of the fibres reveal that the fracture behaviour of a fibre occurs in a complex manner with a large area of longitudinal splitting [A2]. Figure 3.7 shows the fracture behaviour of a single flax fibre which has small and large defects. The fibre can be seen before and after failure, and the fracture formation is illustrated with a schematic view. According to observations during the tensile testing, the fracture was initiated from a large defect zone and grows to split along the fibre length until faced with the next fibre defect zone.

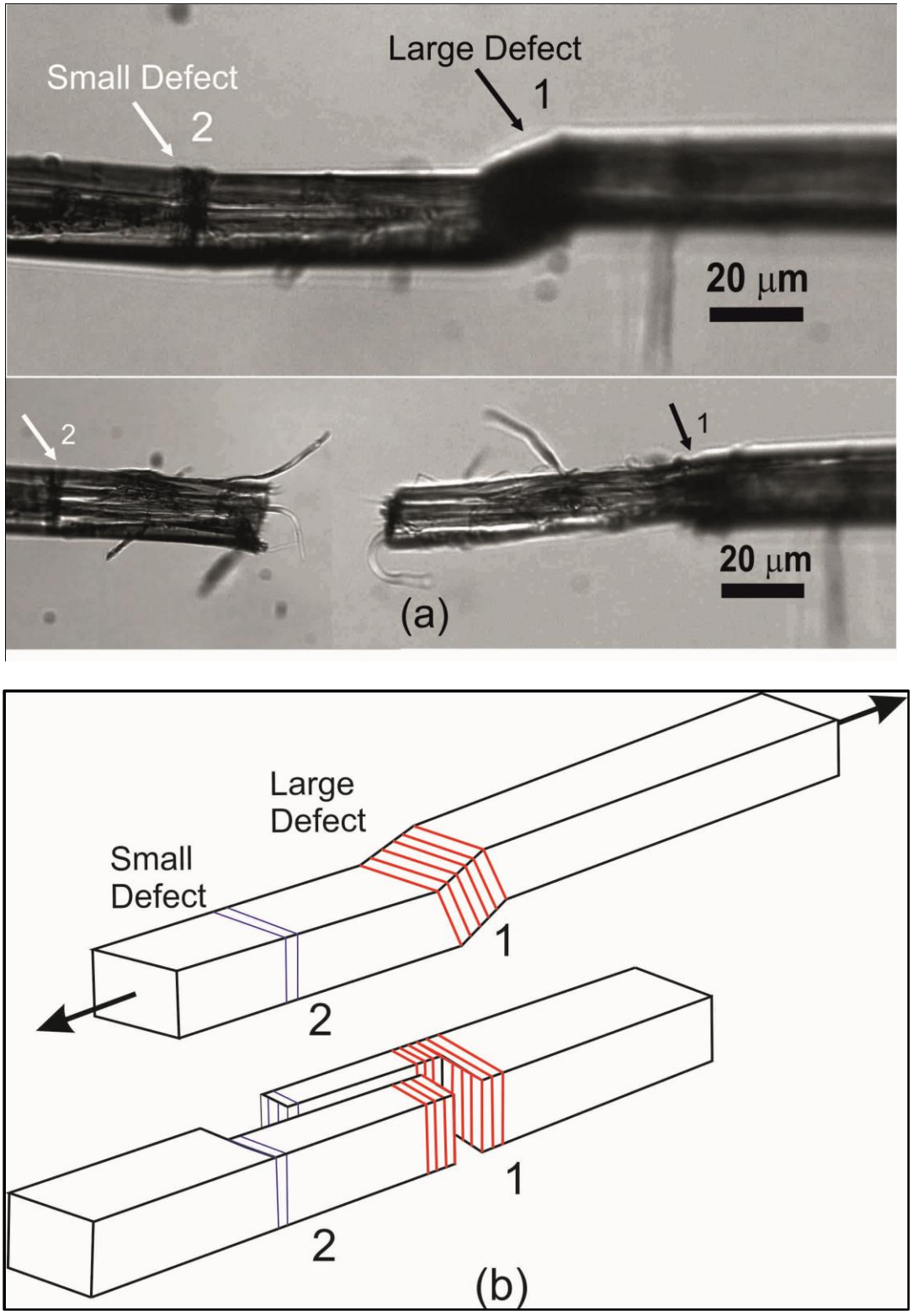

Figure 3.7. Fracture behaviour of single flax fibre shown with (a) optical microscope images and (b) schematic view.

The complex fracture behaviour of single flax fibres includes fibrillation and large fracture surfaces, and this is in contrast to the fracture behaviour of most synthetic fibres. Figure 3.8 shows that flax fibres split in a longitudinal way inside the cell wall between the two fracture ends. The cellulose microfibrils can be seen in the figure at the magnified fractured ends which are apparent in the outer surface in the transverse direction [A1].

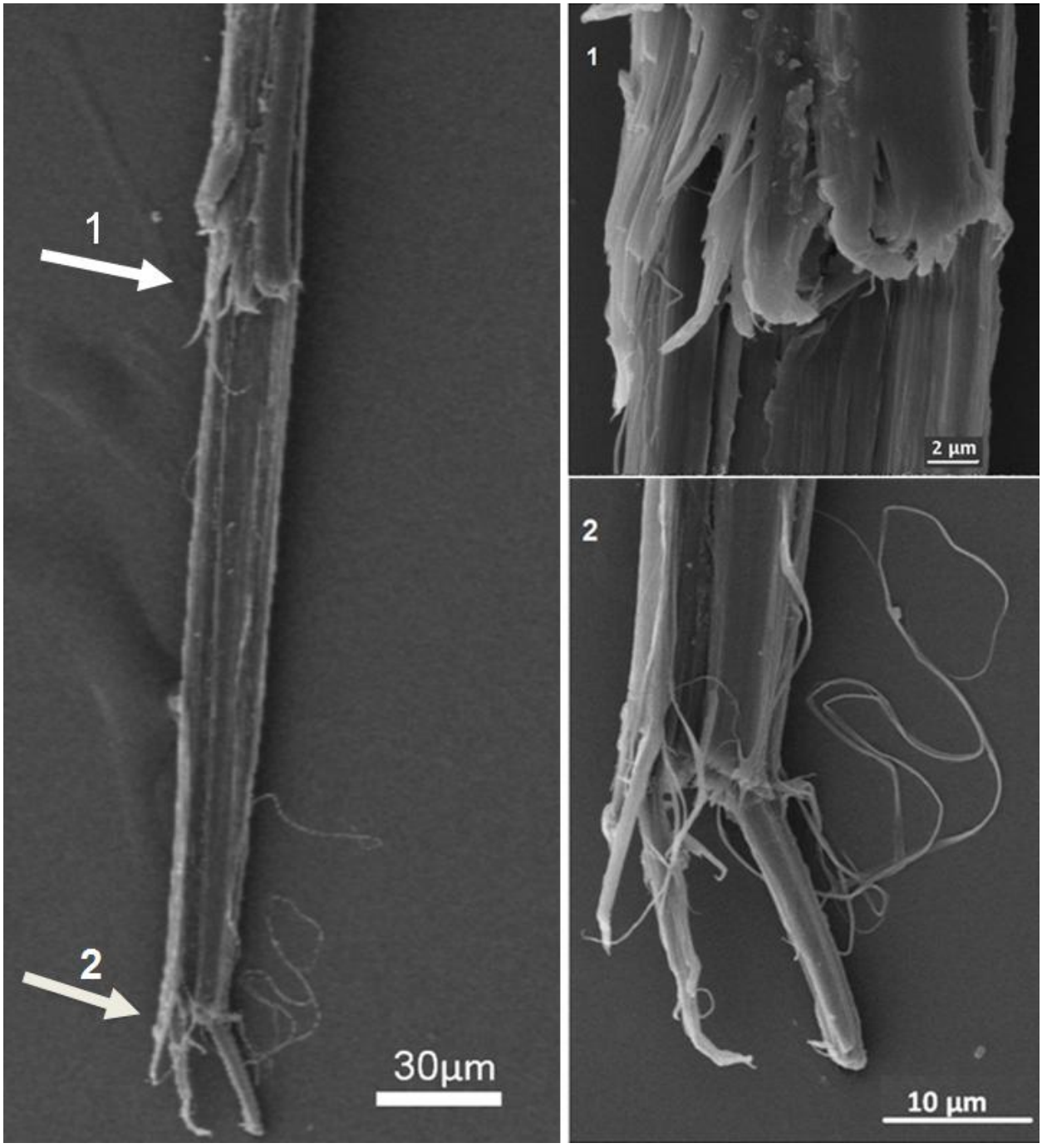

Figure 3.8. Large fracture surfaces of a single flax fibre. The crack initiation site (1) and the point of end failure (2) are carried out in a large zone.

3.2.5. The modelling of tensile strength variation

The fibre tensile strength results show considerable scatter due to the method of cross sectional area measurement, as well as due to a variation in the number of natural and processing defects. The methods used in the cross sectional area measurement of fibres are based on the circular and true cross sectional area, as shown in Figure 3.3. The ratio of maximum and minimum strength values to the true strength values were analytically modelled as a function of the fibre cross sectional aspect ratio in Figure 3.9. The experimental strength results are affected by the aspect ratio of the fibre cross sectional area, and they are well correlated with the predicted strength results. Therefore, a method that includes considerations of the fibre cross sectional aspect ratio is required for correct fibre strength determinations.

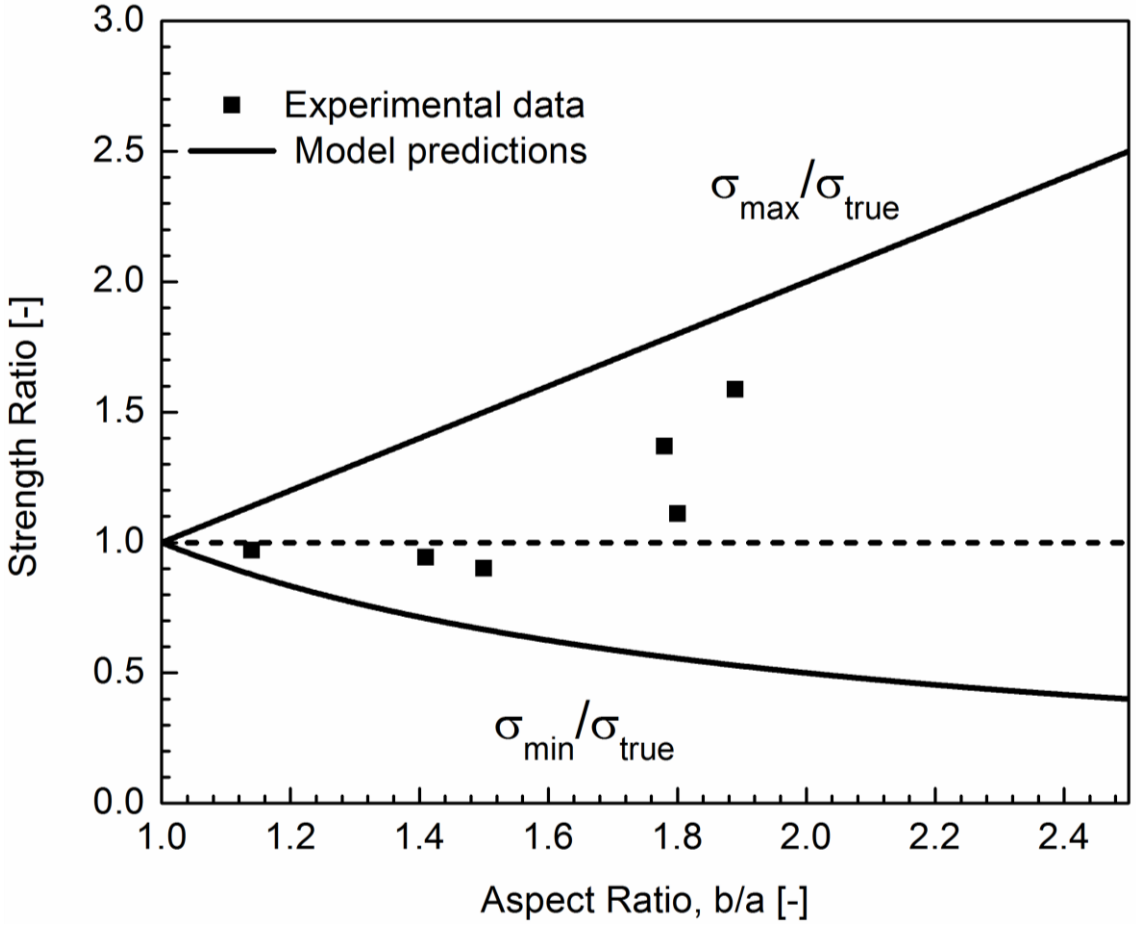

Figure 3.9. Experimental and model predictions of the tensile strength of fibres using the circular assumption method (maximum or minimum cross sectional area) and the true cross sectional method, as a function of the fibre cross sectional aspect ratio.

The tensile strength of brittle synthetic fibres such as glass and carbon are modelled by a two parameter Weibull distribution. The Weibull modulus (m) is an important parameter for characterising the strength variability for a given fibre type. A low Weibull modulus (lower than 10) would introduce much more uncertainty about the strength of a fibre (Hull and Clyne, 1996). The approach of application of Weibull statistics for flax fibres, suggests that the fibre strength of these fibres does not follow a Weibull distribution (Romhany et al., 2003; Van de wejenberg I, 2000; Zafeiropoulos and Baillie, 2007). This can be explained by two basic reasons.

First reason of a low Weibull modulus is due to incorrect cross sectional measurements to a leading large variability in the strength of the flax fibre. The tensile strength results can be suitable to be predicted by a Weibull analysis by applying a correct cross sectional measurement method. For this reason, the model prediction for natural fibres shows a low Weibull modulus representing considerable uncertainty about the stress level of the fibres, which is likely to fail as shown in the literature. (Andersons et al., 2009; Zafeiropoulos and Baillie, 2007).

The second reason is due to the "ductile" fracture behaviour of flax fibres, which is similar to the fracture behaviour of aramid fibres (Hull and Clyne, 1996). The fracture behaviour of flax fibres having large flaws is different for the "brittle" fracture behaviour of most synthetic fibres. Synthetic fibres such as glass and carbon fail by (unstable) growth of a single crack across the cross section initiated from a micro structural defect. For synthetic fibres, it is thus reasonable to expect that a weakest-link mechanism of fibre failure will be followed, which is the basis for the Weibull distribution of fibre strength.

4. FLAX FIBRE COMPOSITES

4.1. Literature review

A large amount of information on mechanical properties of flax fibre composites has been published over the last decades concerning fibre and composite processing topics. The fibre related topics usually consider the spiral angle of the cellulose microfibrils in the cell wall, the fibre moisture, the fibre lumen size, the type and origin of fibres, the length and diameter of fibres, and the defects in the fibres. The composite processing topics are related with the effect of temperature and pressure, the fibre/matrix interfacial adhesion and the surface modification of the fibres, the fibre volume fraction, the fibre orientation in the composite, the matrix type and the properties, and finally, the composite processing methods. It is basically concluded that the major difficulty for cellulosic fibre composites is to achieve high tensile properties, especially high strength, coupled with the achievement of low variability in properties and with a competitive materials costs (Charlet et al., 2009; Kim and Pal, 2010; Pickering, 2008; Thomas and Pothan, 2009; Wool et al., 2005).

Several types of polymers have been used as matrices for cellulosic fibre composites. Thermosetting polymers such as polyesters, epoxies and phenolics have been most commonly used for wood fibre based composites, and for unidirectional plant fibre composites (Bledzki et al., 2002; Pilato, 2010). Thermoplastic polymers such as polypropylene (PP), polyethylene (PE), and polylactic acid (PLA) have been mostly used with plant fibres (Oksman et al., 2003; Saheb and Jog, 1999). In recent years, a number of researchers have been involved in studies investigating the utilization of non-woven natural fibre mats as load bearing constituents in thermoplastic composite materials for many commercial applications (Miao and Shan, 2011; Mieck et al., 1996; Wang et al., 2005). Van de Velde & Kiekens (2003) assessed the most suitable thermoplastic polymers for certain applications, and they pointed out that PP has the most suitable combination of properties as a matrix for cellulosic fibres. They also showed that polyethylene terephthalate (PET) has superior properties in terms of strength and moisture absorption compared with other polyolefins (such as PP and PE).

Flax (*Linum usitatissimum*) fibres have gained the attention of many researchers in the thermoplastic composite industry (Garkhail et al., 2000; Malkapuram et al., 2009). These fibres are attractive as reinforcement due to their ease of handling and good mechanical properties (Müssig and Stevens, 2010). Single flax fibres are extracted from fibre bundles in different lengths and diameters (Bos and Donald, 1999). A single flax fibre has a length in the range 25–30 mm and a diameter in the range 0.012-0.027 mm (Pickering, 2008). The density of the fibres are found to be range 1.45-1.55 g/cm^3 (Müssig and Stevens, 2010).

Conventional flax fibre production allows manufacturing of fibre bundles for the textile industry (Goutianos et al., 2006). The short and long flax fibre bundles are afterwards processed to textile products such as rovings, yarns, non-woven mats and woven fabrics (Mieck et al., 1996). Also, in the composite industry, for the best fibre composite properties, fibres should be aligned (parallel to the principle loading direction) (Hull and Clyne, 1996). While it is easy to align long carbon and glass fibres, it is difficult to control the alignment of the relatively short flax fibres. Therefore, it is useful to make continuous yarns and aligned woven fabrics to create assemblies of aligned short fibres. While the short fibre nonwoven mats can be used for semi-structural applications, the continuous fibre yarns and the aligned woven fabrics can be used for structural applications (Müssig and Stevens, 2010).

A variety of different techniques are used for manufacturing of flax fibre composites (Nattinen et al., 2011; Oksman, 2001). While the thermosetting polymers are mostly used in methods like vacuum infusion, resin transfer moulding (RTM), and pultrusion, the thermoplastic polymers are used in methods like compression moulding, film stacking and filament winding. Oksman (1999) has studied the RTM processing technique with unidirectional high quality flax fibres and epoxy resin. In that study, flax fibre /epoxy composites showed a higher specific stiffness, but lower strength properties than those of glass fibre/epoxy composites. The tensile strength of these flax/epoxy composites was 210 MPa compared with 470 MPa for the glass fibre composites. The specific stiffness was 29 GPa/g cm^{-3} which is superior compared with the value for glass/epoxy composites on 18 GPa/g cm^{-3}.

In order to be able to achieve tensile properties comparable to a glass fibre composite, natural fibre composites should be investigated with respect to the intrinsic properties of the fibre and matrix constituents, the fibre architecture, and the fibre–matrix interface. Many researchers have already shown that a range of physical and chemical treatments can improve the fibre–matrix adhesion (Li et al., 2007; Saheb and Jog, 1999; Van de Weyenberg et al., 2006; Zafeiropoulos et al., 2007). They concluded that strong adhesion between flax fibres and non-polar matrix polymers can be achieved.

The fibre architecture, including the fibre geometry, the fibre orientation, the fibre packing arrangement, and the fibre volume fraction, controls most of the composite properties, particularly the mechanical properties. This can be modelled for unidirectional plant fibre composites by the modified rule-of-mixtures model (Lamy and Baley, 2000; Madsen and Lilholt, 2002; Madsen et al., 2009). The model represents a good tool to predict composite properties (stiffness and strength) from the fibre volume fraction, fibre arrangement, fibre length and porosity. In particular, it is known that most mechanical properties (e.g. stiffness and strength) are increased by increasing the fibre volume fraction up to a certain level. For this reason, the fibre volume fraction should be aimed to be at its maximum level in composite production by promoting a high fibre arrangement and optimal packing behaviour (Madsen, 2004).

Garkhail et al. (2000) have made flax fibre reinforced polypropylene (PP) composites using the film stacking method with random non-woven fibre mats. They reported on the influence of fibre length, fibre content and fibre diameter on the tensile strength of the composites. Toftegard (2002) also reported on the tensile behaviour of flax/PP composites made by the film stacking method, and by using two different pressure levels in order to increase the maximum obtainable fibre volume fraction. Madsen et al. (2002) studied composite volumetric composition as a function of the compaction behaviour of plant fibre assemblies for different fibre types and fibre orientations. They showed that for a given compaction pressure, the highly aligned fibres show a higher packing ability, leading to a higher fibre volume fraction in the composites, than the randomly oriented fibres, and without the formation of a significant amount of porosity in the composites. Moreover, the circular-shaped and equal-sized glass fibres show a higher packing ability than the non-uniformly shaped and sized plant fibres.

Miao et al. (2011) reported on the effect of fibre direction on the mechanical properties of plant fibre composites produced by a press consolidation technique. Non-woven mats with a preferred fibre orientation obtained by a hot rolling method showed higher mechanical properties than non-woven mats with a fully random fibre orientation obtained by a needle punching method. However, the composite made from the aligned non-woven mat showed a lower stiffness than composites made from a unidirectional woven fabric, which is explained by the absence of fibre pre-tensioning introduced during the spinning and weaving operations of the woven fabrics. Jiang et al. (2011) have investigated the effect of fibre twisting on the stiffness of flax/PP composites. They found that the composites made from an untwisted wrap yarn showed a significant improvement in flexural stiffness, compared with those of the twisted yarn composites. They indicated that an improved untwisted fibre orientation of the wrap yarn structure resulted in a better fibre dispersion and fibre packing ability than those in the manufactured twisted composite laminates.

Madsen et al. (2007) have developed a model to predict the volumetric composition (i.e. the volume fractions of fibres, matrix and porosity), the density and the stiffness of composites as a function of the fibre weight fraction. The model particularly uses a modified rule of mixtures model that includes the influence of porosity on composite stiffness and density. The effect of porosity is quantified at different fibre weight fractions in order to find the maximum attainable fibre volume fraction for unidirectional flax and hemp fibre composites. Lamy and Baley (2000) also proposed a modified rule of mixtures model based on the measured fibre diameters in order to achieve the correct stiffness properties of unidirectional flax fibre/epoxy composites. A good correlation was found with the experimental data on composite stiffness. Moreover, it was reported that an increasing diameter of the fibres leads to a decrease in the stiffness of the fibres. A summary of previously reported tensile properties of flax fibre composites is presented in Table 4.1, together with specifications on fibre orientation, fibre volume fraction and composite processing methods.

Table 4.1: Tensile properties of flax fibre composites.

Fibre/Matrix	Vf (%)	Fibre orientation	Strength (MPa)	Stiffness (GPa)	Method	References
Flax/LPET	55	Aligned yarn	343	33	Winding	Present study
Flax/PP	42-55	Aligned yarn	250-321	27-28	Winding	Madsen et al (2003)
Flax/Epoxy	47	Aligned mat	279	39	RTM	Oksman (2001)
Flax/Epoxy	31	Aligned fabric	160	15	Hand lay-up	Goutianos et al. (2006)
Flax/Epoxy	40	Aligned yarns	133	28	Autoclave	Wejenberg (2000)
Flax/Epoxy	21	Aligned fibres	127	17	Compression	Charlet et al. (2007)
Flax/Epoxy	35	Non-woven	53	8	Autoclave	George et al. (1999)
Flax/PP	45	Non-woven	40	10	Film-stacking	Garkhail et al. (2000)
Flax/PP	30	Non-woven	20	2	Extrusion	Contero et al (2003)
Flax/PP	30-40	Non-woven	29	5-8	Extrusion	Oksman et al. (2003)
Flax/PLA	30-40	Non-woven	53-44	8-7	Extrusion	Oksman et al. (2003)

In addition to the issues mentioned above, uniaxial tensile testing of unidirectional composite specimens to measure strength properties presents a well-known challenge (Belingardi et al., 2011; Davis, 2004; Garrell et al., 2003). The challenge is how to minimize the required gripping forces, and thereby measure the accurate tensile strength of the specimens. It is well-known that tensile specimens of unidirectional composites show premature failure due to the presence of a high stresses in the gripping area (Staab, 1999). The most common approach to avoid premature failure of unidirectional composite specimens is to apply tab materials on the gripping area in order to protect the test specimen from damage (Lubin and Peters, 1998; Staab, 1999). However, most of the specimens still show premature failure at the gripping area instead of at the gauge section. Previously, many studies have addressed this problem by applying changing wedge angle (i.e. the angle of the tab), tab thickness, tab length and tab material type, but none of them have been successful in obtaining the correct failure behaviour of the specimens (Hojo et al., 1994; Joyce et al., 2002; Vinson et al., 1985).

The singular stress state for dissimilar isotropic elastic materials has been investigated by linear elastic analysis of two dimensional bonded half planes (Bogy and Wang, 1971; Hein and Erdogan, 1971). These investigations have presented some numerical solutions to show that the stress singularity can be removed as a function of the stiffness ratio of the tab material and the specimen material, and as a function of different wedge angles. Finite element modelling can be used as a tool

for testing different combinations of material types and wedge angles in order to remove the stress singularity conditions during testing of unidirectional fibre composites (Joyce et al., 2002).

4.2. Summary of results in present study

4.2.1. Materials and composite fabrication method

Flax fibres in the form of a fibre yarn, and LPET (polyethylene terephthalate) thermoplastic matrix in the form of a filament, were supplied on bobbins and used for fabrication of unidirectional composites. The densities of the flax yarn and the LPET filament were determined using pycnometry (ASTM D 792) to be 1.55 g/cm^3 and 1.38 g/cm^3, respectively; both densities reflect a dry condition. The fabrication route of the composite laminates is represented in Figure 4.1 by a diagram that consists of two main steps: production of the fibre/matrix assembly (by filament winding) and the consolidation of the composite plate (by vacuum heating and press moulding). The technique has previously been used by Madsen (2004), and will be described in detailed in the following sections.

4.2.1.1. Filament winding

The flax fibre yarn and the thermoplastic LPET filaments are mixed by a winding machine to produce aligned fibre/matrix assemblies. Figure 4.2 shows a schematic view of the winding process. Flax fibre yarns and matrix filaments were wound tightly onto a metal frame after passing through a series of pulleys. The metal frame is fixed between the jaws of the rotating mandrel, and it can be controlled to move horizontally at a constant displacement rate in the range 0.65-1.00 mm/rotation. The commingled yarns of flax and LPET are pulled through a pulleys-path with a controlled tension in the yarns. A computer controls the horizontal displacement rate and the rotation speed of the metal frame. The weight fractions of fibres and matrix, and thereby the volumetric composition of the composite plate can be tailored according to the number, the linear density and the density of the wound fibre yarns and matrix filaments. Based on the wound fibre/matrix assemblies, the linear density of the flax yarn and the LPET filament can be determined by the equation (Thygesen, 2006):

$$Tex_{\ yarn}\left[\frac{g}{1000m}\right] = \frac{w\ [g]}{N_{turn}\ x\ N_{bobbins}\ x\ L_{frame}[mm] x\ 2\ x\ 10^{-6}} \qquad (4.1)$$

where w is weight of the flax or the LPET yarn, N_{turn} is the total number of turns/rotations, and $N_{bobbins}$ is the number of fibre or matrix bobbins. The frame length (L_{frame}) is multiplied by two due to the winding on both sides of the frame for each turn. The linear density (tex) of flax fibre yarn and LPET fibre filaments were measured using Eq. 4.1 to be 92 tex (g/1000m) and 56 tex, respectively, in un-dried conditions.

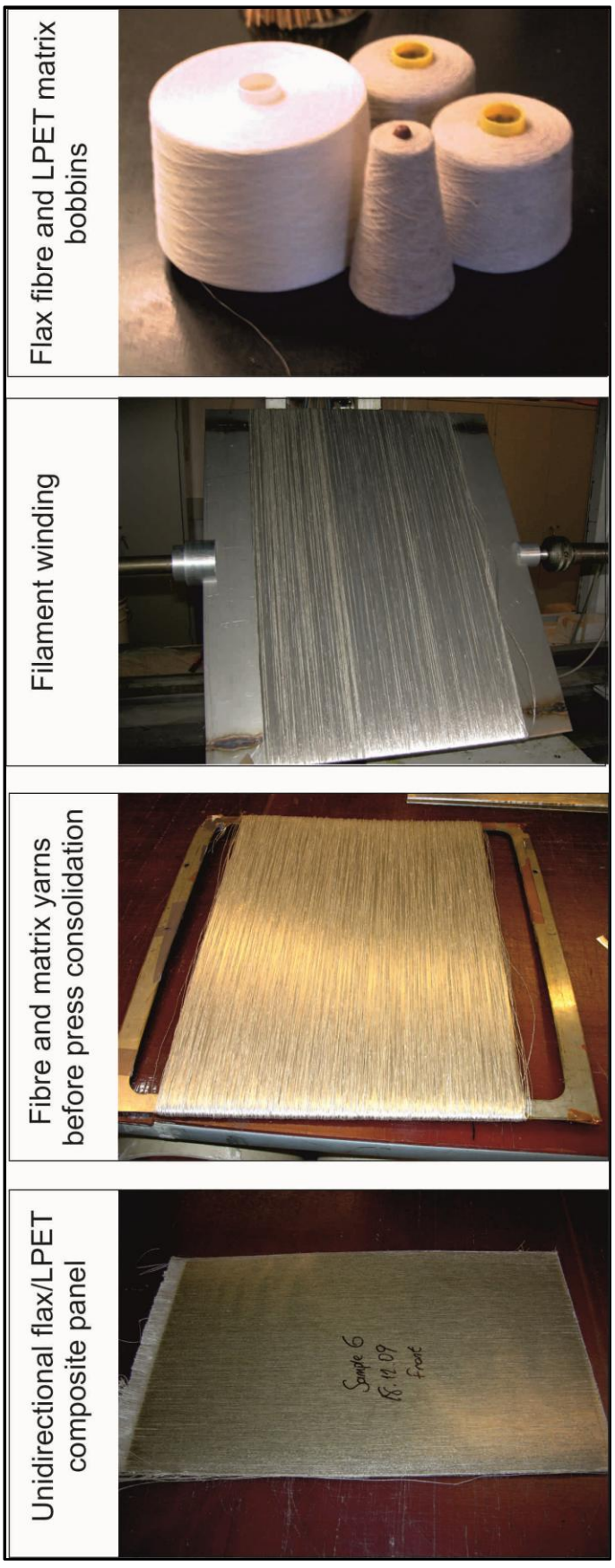

Figure 4.1. The applied fabrication route for unidirectional flax/LPET composites.

The fibre weight fraction (W_f) of the wound fibre/matrix assembly, which is assumed identical to the fibre weight fraction of the composite plate, can be calculated from the measured tex values by using equation 4.2 (Madsen, 2004);

$$W_f = \frac{N_f \text{ x } tex_f}{N_f \text{ x } tex_f + N_m \text{ x } tex_m} \quad (4.2)$$

where N is the number of yarns/bobbins, the subscripts of f and m denote fibre and matrix, respectively. Unidirectional flax/LPET composite laminates were manufactured with fibre weight fractions ranging from 0 to 0.82 [A3]. Based on the desired volume fractions, and the measured fibre and matrix densities, the total composite density can be calculated by using a rule of mixtures relationship. The controlled thicknesses of the composite laminates were between 1.9 to 2.5 mm depending on the fibre weight fraction of the laminates, the horizontal displacement rate, and the number of rotations [A3]. After winding of the flax fibre/LPET matrix assemblies, they were dried in a vacuum chamber (1 mbar, 23°C) for at least 16 hours in order to remove moisture from the flax fibres.

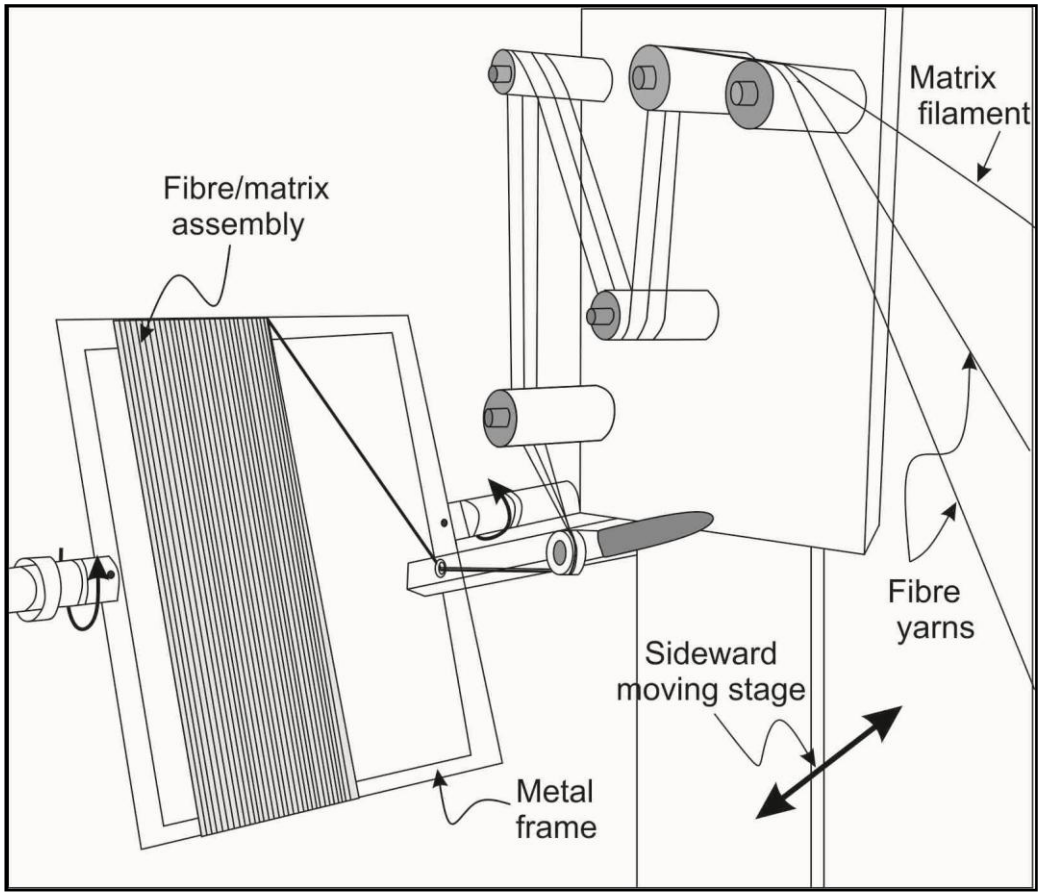

Figure 4.2. Commingled fibre/matrix winding set-up for producing unidirectional flax fibre/LPET assemblies

4.2.1.2. Compression moulding

The dried fibre/matrix assemblies were processed into composite laminates using a vacuum heating, followed by a cold moulding press. The effect of consolidation pressure was studied by using two different sizes of metal frames under the same compression force (200 kN). Small frames (120*400 mm) were consolidated under a maximum panel pressure of 4.1 MPa, henceforth denoted as "high pressure" composites, whereas large frames (300*400 mm) were consolidated under a minimum panel pressure of 1.67 MPa, henceforth denoted as "low pressure" composites [A3]. The applied composite processing technique consists of two main units: a vacuum heating chamber (to melt the matrix polymer) and a cold moulding press (to consolidate the composite laminate). The fibre/matrix assembly is transferred between the two units by a controlled conveyor. Firstly, the assembly is placed on the conveyor after covering it with release Teflon sheets on both sides. The assembly is then transferred to the vacuum heating chamber and stays there for 15 minutes (200°C) under a vacuum condition (4 mbar). After melting of the LPET thermoplastic matrix in the vacuum heating chamber, the flax/LPET assembly is subsequently conveyed to the cold moulding press. The assembly is consolidated with a high compression force (200 kN; 30°C; 1 minute) into a composite laminate. A key feature of the process system is the heating under vacuum. The vacuum condition is thought to provide better impregnation of the fibres with the matrix by removing any possible moisture vapour, and to reduce the tendency of oxidative thermal and hydrolytic degradation of the flax fibres (Madsen, 2004).

4.2.2. Microstructure of composites

The microstructure of the flax fibre reinforced unidirectional composites were observed using a scanning electron microscope and optical microscope with special emphasis on the flax fibre/ LPET interface interactions, the distribution of the flax yarns within the LPET matrix, as well as the shape and the size of the flax fibres. In addition, the composites were also observed to characterise the location and size of porosities (voids), which are one of the most common types of defects in composites. Porosities can be induced due to physical (microstructure) and chemical features of the fibre and matrix components, or due to a non-optimized setting of the composite process parameters such as the pressure and temperature (Madsen et al., 2007c). Figure 4.3 shows the distribution of the flax fibre yarns in composites with different fibre volume fractions as observed by an optical microscope. It can be seen that the increasing fibre content makes higher porosity content in the composites. The porosities appear as a spots of darker colour in the microscope cross sectional images. The relation between fibre content and porosity is also experimentally measured in paper [A3], as shown in the Fig 3. The porosity can be classified into two groups: process related porosity and structural porosity. The process-related porosity is correlated with the fibres (lumen, interface and impregnation porosities), and the matrix (matrix porosity), and this type of porosity is thought to be influenced by the composite process condition. In contrast, structural porosity is thought to be developed after a maximum fibre volume fraction is attained as in section 4.2.3

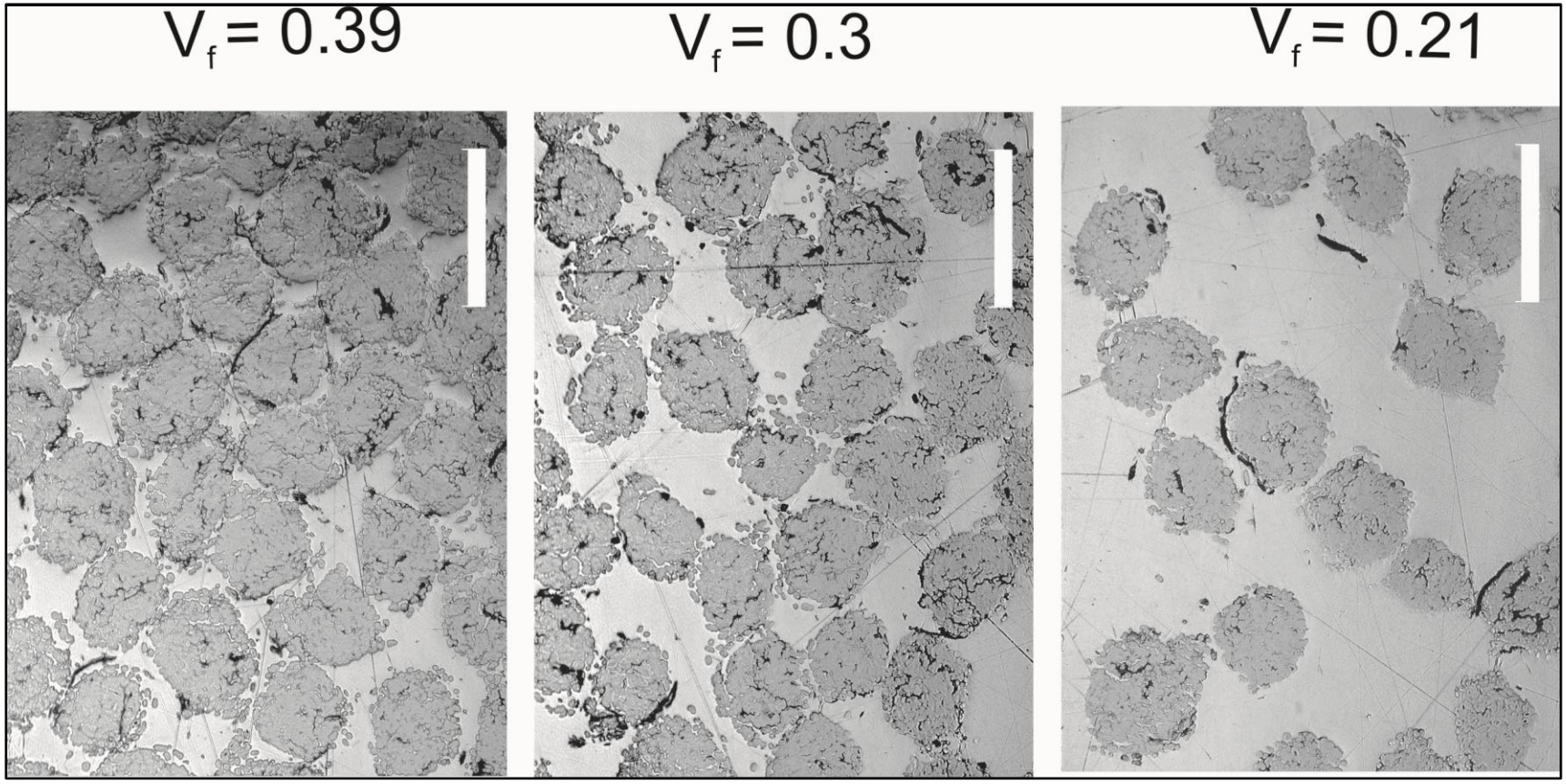

Figure 4.3. Cross-sectional view of unidirectional flax/LPET composites with 6 different fibre volume fractions (V_f= 0.21 - 0.55). The flax fibres, in the form of yarns, the LPET matrix and porosities can be identified. The scale bar is 500 µm.

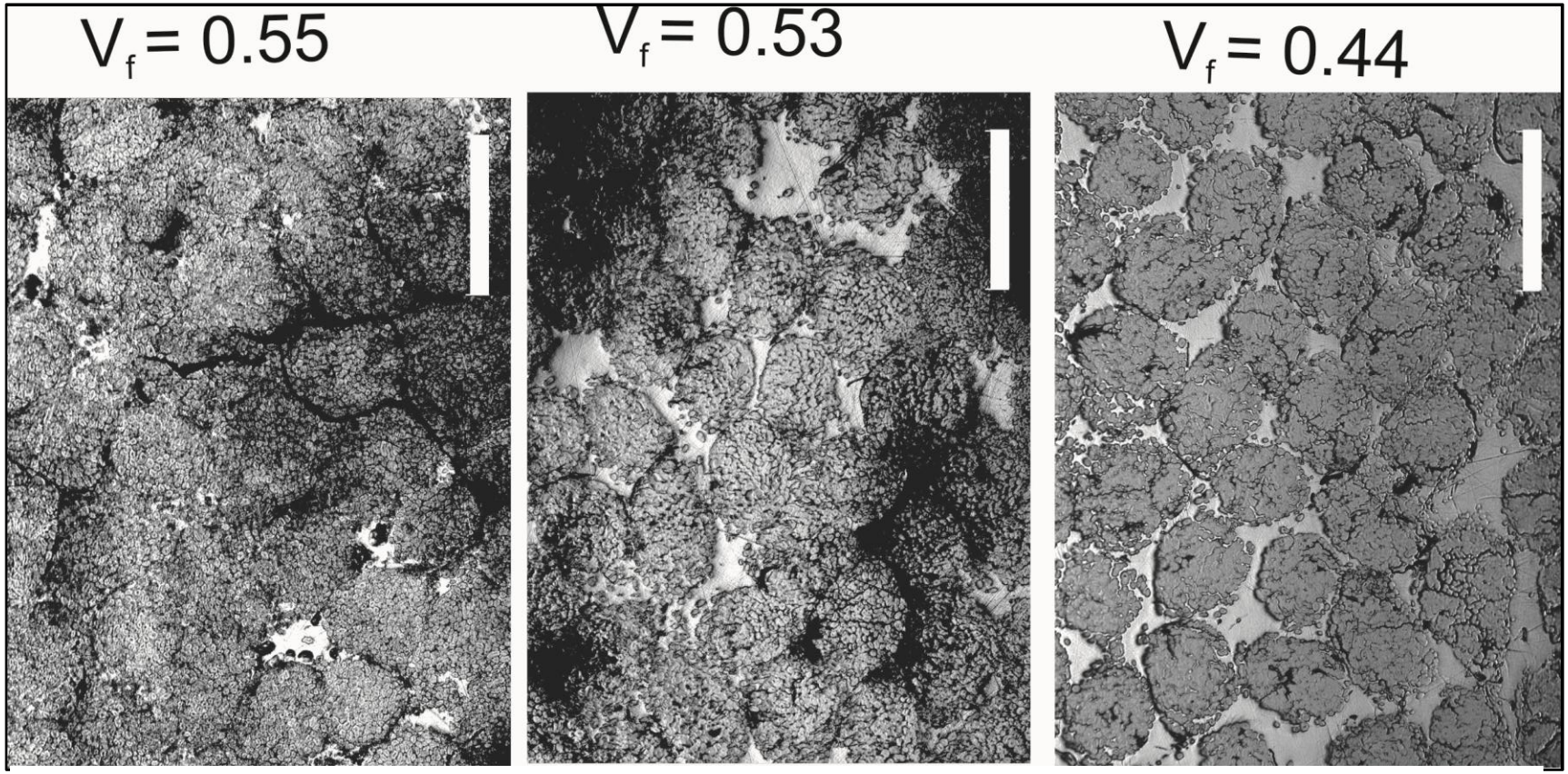

Figure 4.3. Continued. The scale bar is 500 µm.

Structural porosity is caused by that the matrix volume is insufficient to fill out the free volume between the maximum compacted fibres, and this type of porosity is therefore influenced by the packing ability of the fibres.

The following methods were employed to characterize the porosities in the composites (Aslan et al., A3). Based on scanning electron microscopy (SEM) images, the morphology and location of the porosities in composites produced with different fibre weight fractions, and with different consolidation pressures were investigated. The fibre correlated porosities are classified as: lumen porosity (due to the central cavity in natural fibres), interfacial porosity, and impregnation porosity. The fibre lumen porosity and the interfacial porosities can be quantified by image analysis of polished composite cross sections. The impregnation porosity can be determined from the slope of a linear regression line of the relation between experimental values of porosity (V_p) and fibre volume fraction (V_f) of the composites (Madsen et al., 2007c). The matrix correlated porosity can be determined by the ratio of the matrix filament density and the neat matrix panel density. Figure 4.4 shows the different types of porosities in low and high magnification images from cross sections of flax/LPET composites.

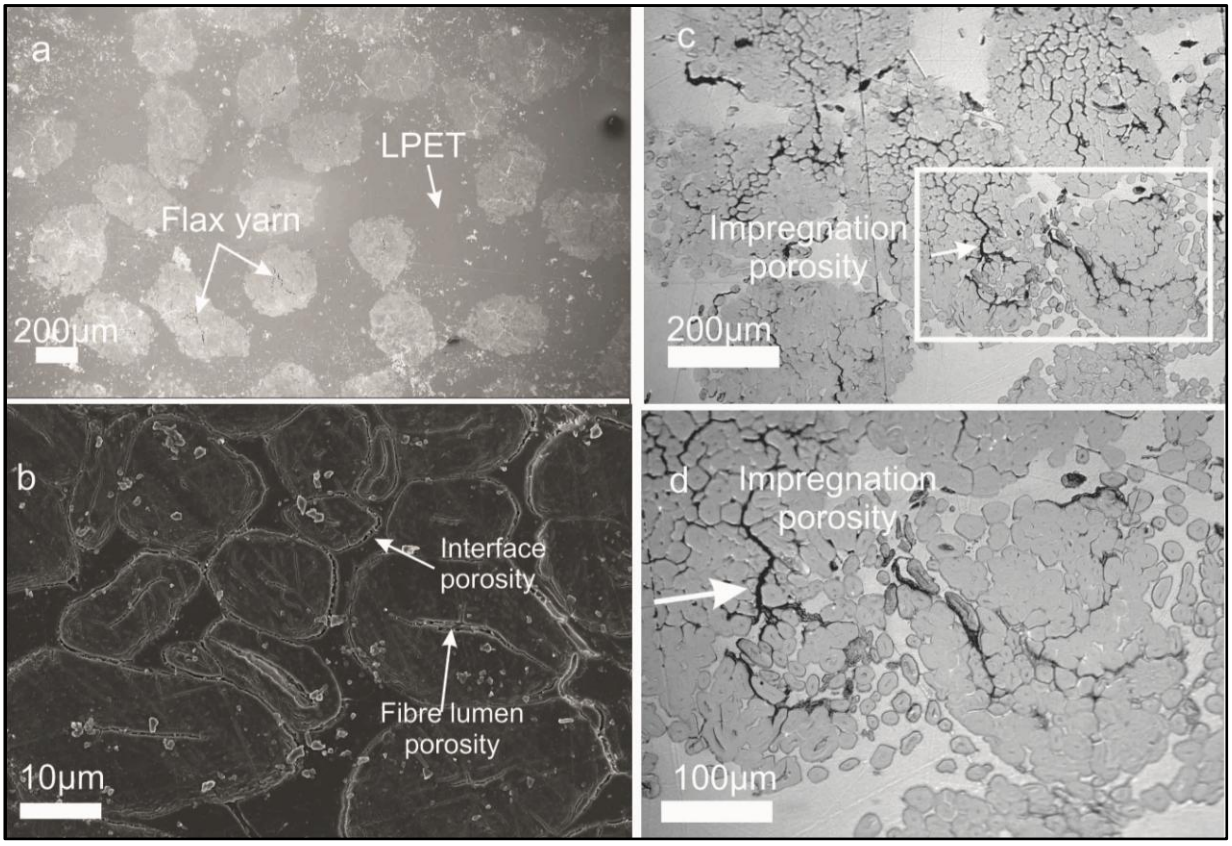

Figure 4.4. SEM micrographs of cross sections of flax/LPET composites: a) flax yarn distribution within the LPET matrix, b) single flax yarn with impregnation porosity, c) interfacial porosity and fibre lumen porosity, d) impregnation porosity at high magnification (white box).

4.2.3. Volumetric composition of composites

The weight fractions of fibres and matrix can be converted to volume fractions of fibres, matrix and porosity using the measured density of composite, fibres and matrix, in addition to the estimated values of the porosity constants, by using the volumetric composition model [A3- Figure 4.3].

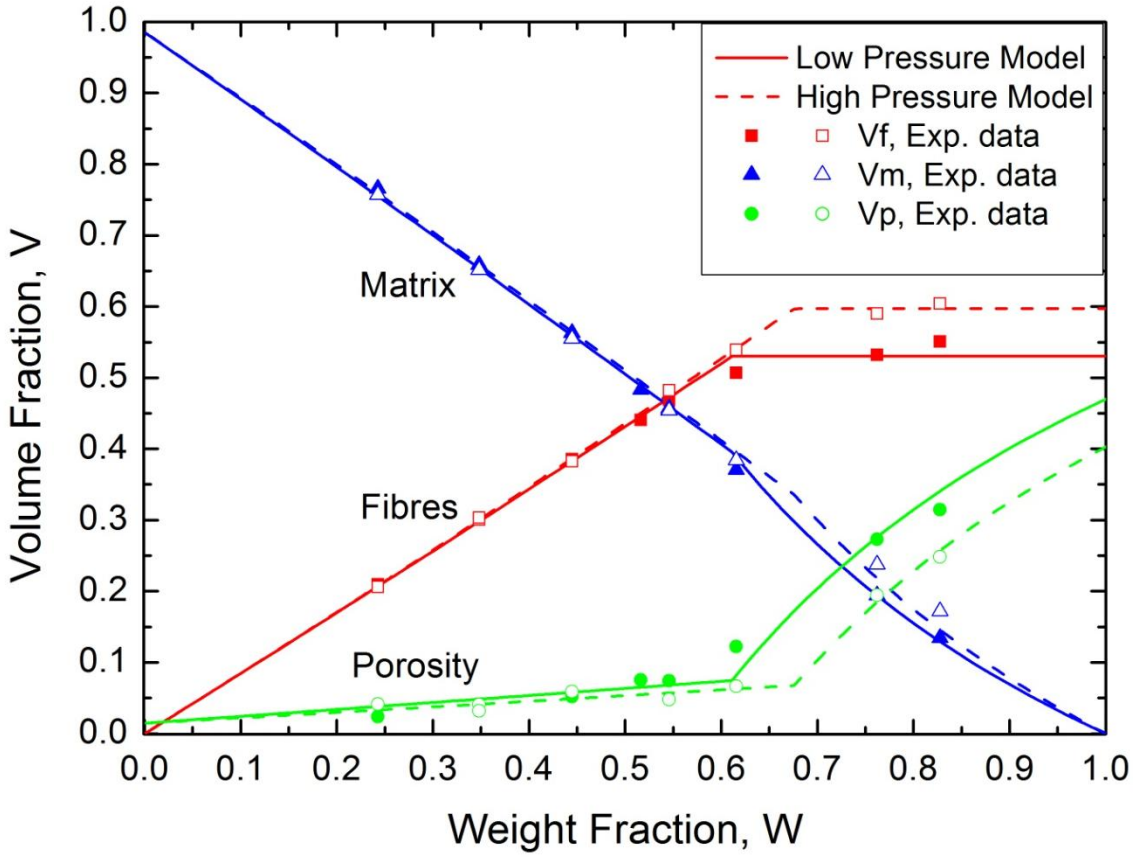

Figure 4.5. Model lines and experimental data points for volume fractions (V_p: porosity, V_f: fibres, V_m: matrix) of flax/LPET composites shown as a function of the fibre weight fraction. Full lines and dotted lines are used for model calculations of low and high pressure composites, respectively.

Figure 4.5. shows model predictions of the volume fractions fibre, matrix and porosity as a function of the fibre weight fraction for unidirectional flax/LPET composites manufactured with two different consolidation pressures. The experimental results, as also presented by Aslan et al. (Fig. 4, A3), verify the expectations that the consolidation pressure affects the volumetric interaction in the composites. For both composites (low and high pressure), it is found that the porosity of the composites is increased by increasing the fibre weight fraction of the composites (Fig. 4, A3). The fibre, matrix and porosity volume fractions show different trends at low and high fibre weight fraction levels. The fibre and porosity volume fractions tend to show a linear increase at low fibre weight fractions. In contrast, at high fibre weight fractions, the fibre volume fraction shows a constant level, and the porosity is increased rapidly and non-linearly (Fig. 4, A3). The maximum

obtainable fibre volume fraction is increased when the consolidation pressure of the composites is increased [Table 2, A3]. This is in agreement with the study of Madsen (2004) on the compacting behaviour of plant fibre assemblies where a maximum attainable volume fraction of unidirectional flax assemblies was found to be 0.60 at a compaction pressure of 4 MPa.

4.2.4 Tensile behaviour of composites

4.2.4.1. Tensile stiffness

Tensile tests were performed on an Instron universal testing machine with a cross head speed of 2 mm/minute and a load cell of 25 kN. The tensile specimens with a thickness in the range 2.0-2.5 mm were tested according to ISO 527 at room temperature.

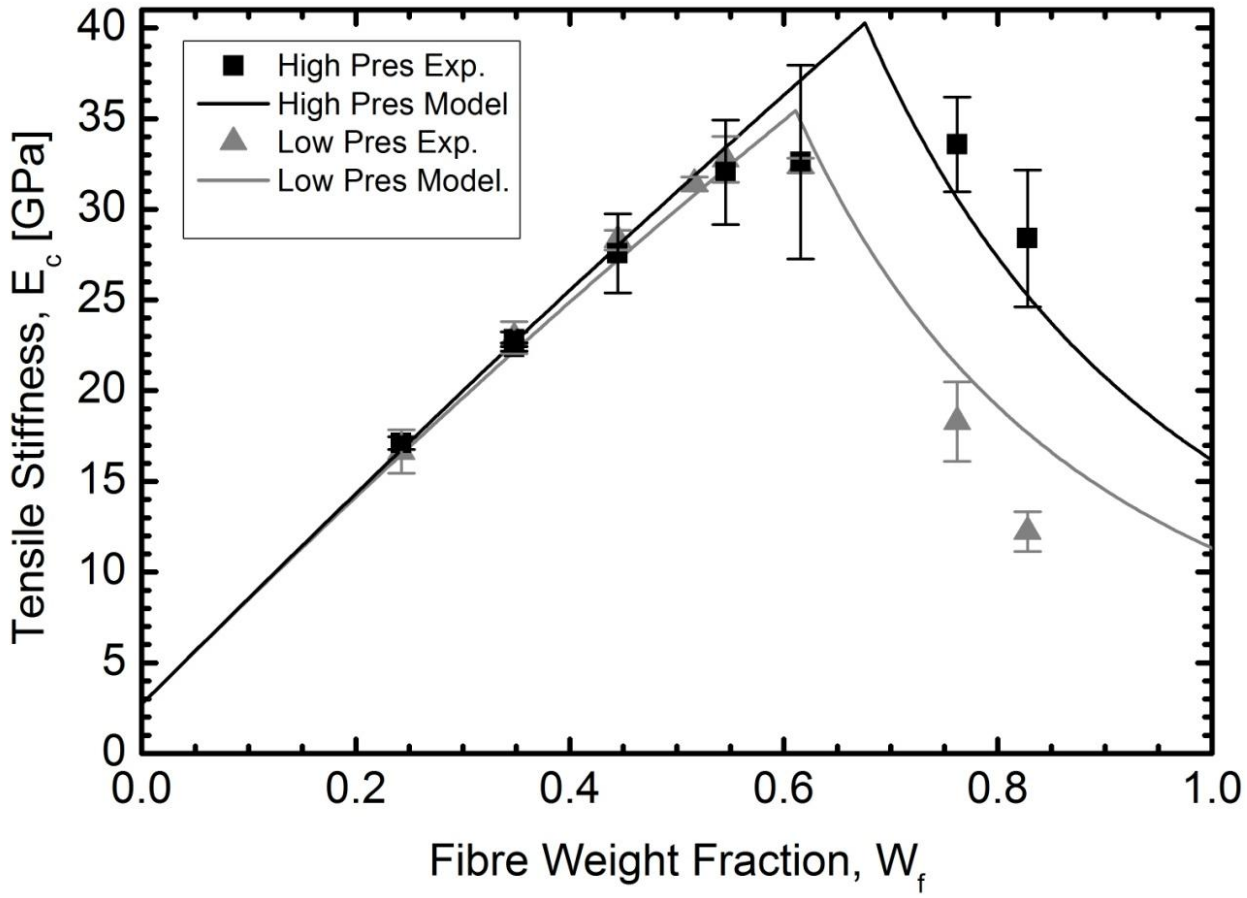

Figure 4.6. Composite stiffness as a function of the fibre weight fraction in unidirectional flax/LPET composites manufactured by a low and a high consolidation pressure.

The stiffness of the unidirectional flax/LPET composites is shown in Figure 4.6 as a function of the fibre weight fraction. The stiffness of the specimens are determined in the strain range 0.01- 0.1%. The results are shown for composites manufactured with the low and high consolidation pressures. The composite stiffness is modelled by a rule of mixtures model using the predicted volume fractions of fibres, matrix and porosity (see Figure 4.5), according to the equations given in [A3-9] (Madsen et al., 2007c). The model predictions are confirmed by the measured stiffness values in the range of fibre weight fractions from 0.24 to 0.82. At low fibre weight fractions ($W_f < 0.60$), the model predictions and the measured values show that the pressure effect is rather low on the stiffness values. At higher fibre weight fractions (above the transition value, $W_f > 0.60$), the pressure has a significant effect in decreasing the stiffness of the composites, and it can also be observed that the experimental values show larger deviations from the model predictions [A3]. The stiffness of the composites is basically controlled by the fibre volume fraction. However, the consolidation pressure cause large difference between stiffness results at the high volume fractions due to a dramatic increase in the porosity fraction of the composites as shown in Figure 4.5.

4.2.4.2. Tensile failure

Typical stress-strain curves are shown in Figure 4.7 for different fibre weight fractions of the unidirectional flax/LPET composites. All composites exhibit similar trends in their stress-strain curves. They show an initial linear slope until a strain range of 0.01-0.1%, and then the curve become non-linear, where after it fails abruptly after a long linear part of the curve.

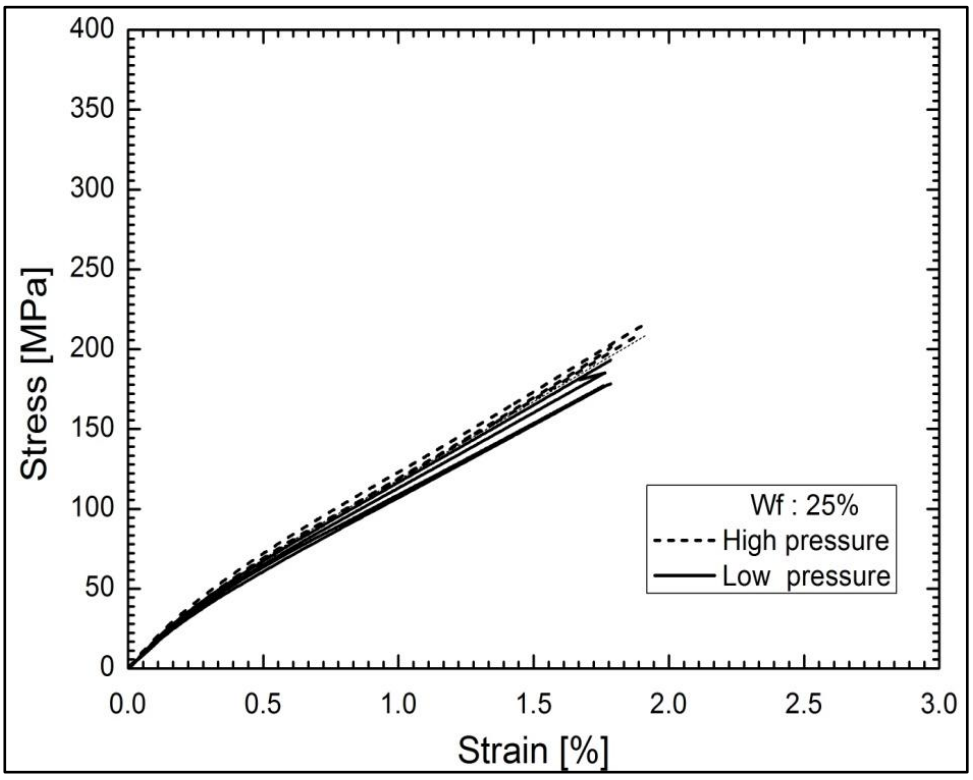

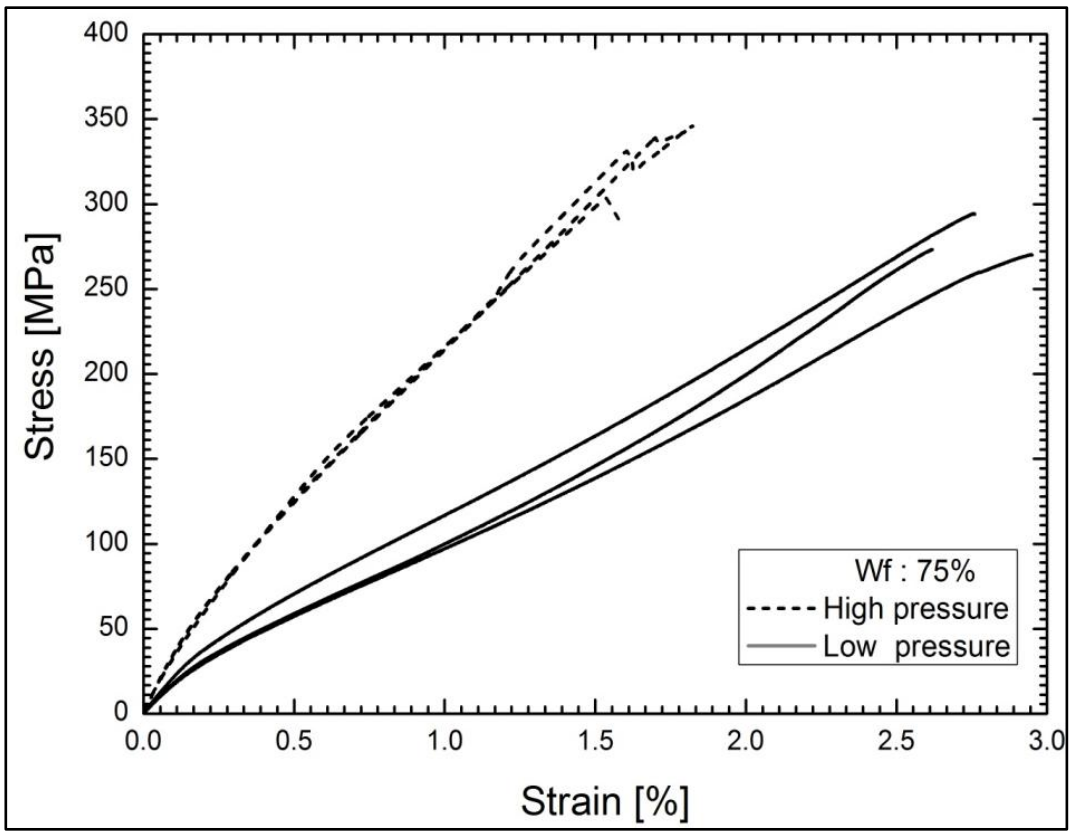

Figure 4.7. Representative stress-strain curves of unidirectional flax/LPET composites with different fibre weight fractions, and manufactured with two different consolidation pressures.

The stress-strain behaviour of the low and high pressure composites is similar at the lower fibre weight fractions ($W_f = 0.25$). However, at the higher fibre weight fractions ($W_f = 0.75$), the stress-strain curves are showing a higher maximum stress for the high pressure composites in comparison with the low pressure composites. This difference is due to the lower porosity content for the low pressure composites (see Figure 4.5). In addition, it can be observed that the stress-strain curves show more non-linearity when the pressure level is decreased, and when the fibre content is increased.

The stress-strain curves obtained can however not be used to determine the true ultimate tensile strength of the unidirectional flax/LPET composites since failure occurred outside the gauge section in the tab region. Square cut tabs were mounted on the specimens according to the specifications given by ISO 527. However, a complicated stress field in the gripping area still caused the specimens to fail prematurely, leading an underestimation of the ultimate tensile strength of the composites. Figure 4.8 shows such typical failures in the gripping area of the composite specimens.

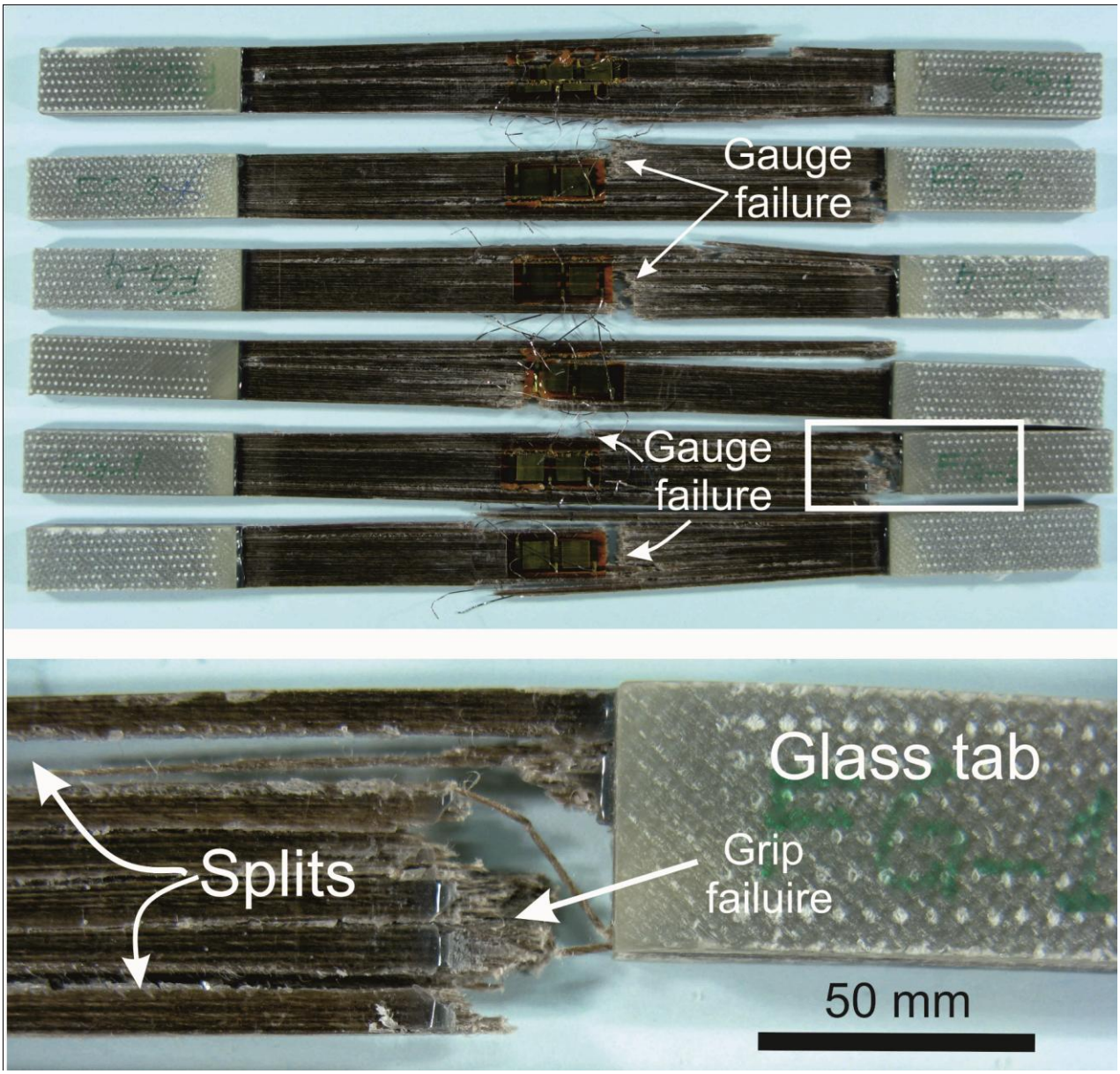

Figure 4.8. Typical specimen-tab edge failure for the unidirectional Flax/LPET composites.

Table 4.2 shows tensile properties of neat LPET matrix, single flax fibre and flax/LPET composites at different weight fractions. The neat LPET panels ($W_f = 0$) show an average (± std. dev.) strain to failure of 1.71%±0.23 is lower than that of a single flax fibre (2.42%±0.6). The flax fibre strength is greater than the breaking strength of the LPET matrix. The strain to failure of the flax fibre is also higher than LPET matrix. The brittle LPET matrix cause to failure of the composite since LPET matrix reaches the strain to failure first.

Table 4.2. Tensile properties of neat LPET, single flax fibres and flax/LPET composites

	Young's modulus [GPa]	Std. Dev	Tensile strength [MPa]	Std. dev	Strain to fail (%)	Std. dev.
Neat LPET	**2.9**	0.4	**43**	2	**1.71**	0.23
Single flax fibre	**28.0**	11.2	**698**	304	**2.42**	0.60
Flax/LPET (W_f: 25%)	**16.6**	1.2	**183**	7	**1.77**	0.01
Flax/LPET (W_f: 55%)	**32.8**	1.3	**343**	8	**1.90**	0.03
Flax/LPET (W_f: 75%)	**18.3**	2.2	**279**	13	**2.77**	0.17

The nominal tensile strength of unidirectional flax fibre composites at different fibre loading are depicted in Fig. 4.9. It is clear that the tensile strength is increased until the fibre weight fraction of 55% for both high and low consolidation pressure composites,. A further increase of the fibre weight fraction leads to a decrease in tensile strength of the composites, which also is observed for the stiffness results in Figure 4.6. The strength results in Figure 4.8 also show that after about 55% fibre weight fraction, the strength show high variability, which assumingly is due to the high porosity content of these composites. The strength results which are more precise at lower weight fractions are consistent with brittle manner fracture surfaces as shown in figure 4.12a,b.

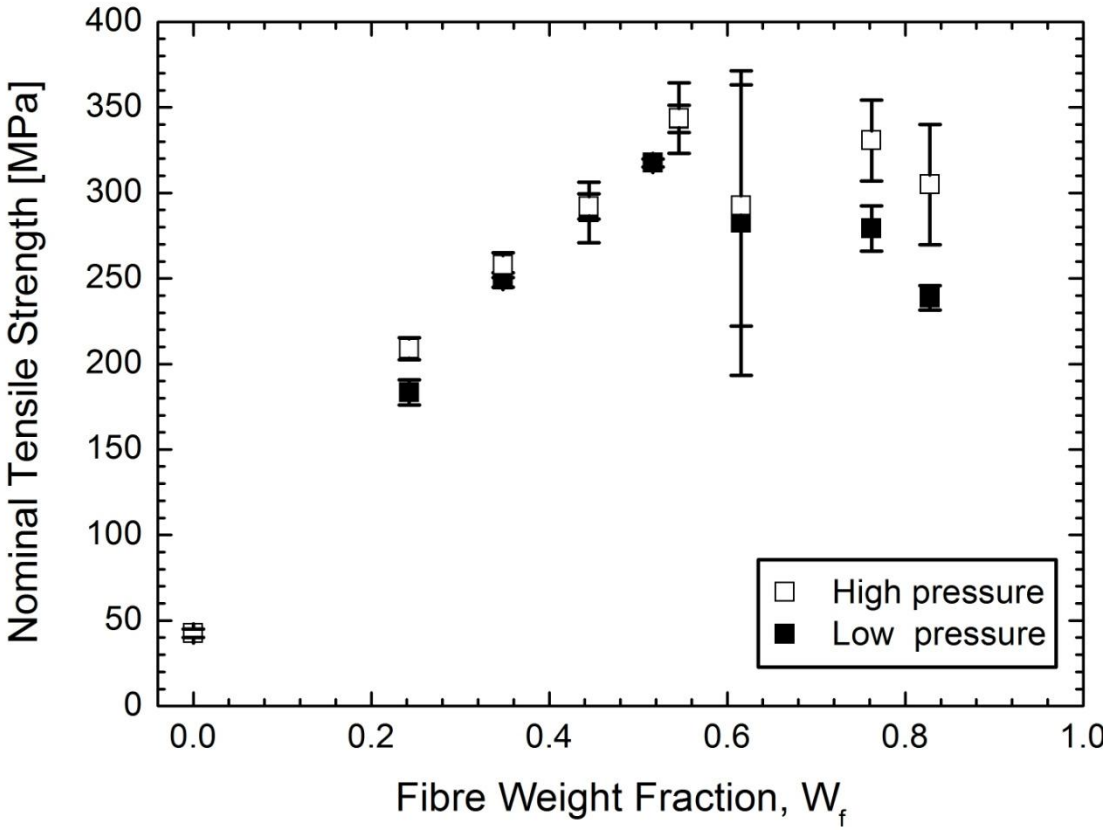

Figure 4.9. Nominal tensile strength of unidirectional flax/LPET composites as a function of fibre weight fraction. The composites were manufactured with two different consolidation pressures.

4.2.4.3. Fracture behaviour

Continuous fibre reinforced composites usually exhibit two types of load transfer mechanisms: the so-called “local load sharing” and “global load sharing” mechanisms (He et al., 1993; Xia and Curtin, 2000). An understanding of the load transfer mechanism is crucial for the understanding of the failure behaviour of the fibre composites.

For the local load sharing mechanism (LLS), as sketched in figure 4.10, that there is no fibre/matrix debonding, so that when a matrix crack reaches a fibre, the fibre ahead of the crack tip experience a very high strain, very locally in front of the crack tip, leading to crack penetration into fibre. The fibres behind the crack tip are all broken at the plane of the matrix crack. The fibres have thus little or not effect on propagation of the matrix crack. Then, once matrix crack growth initiates, the matrix crack can propagate in an unstable manner across the entire width of the specimen. This can be characterised as brittle failure. A major point regarding the fracture surface is that it leads to a fracture surface where all fibres fail at the same plane.

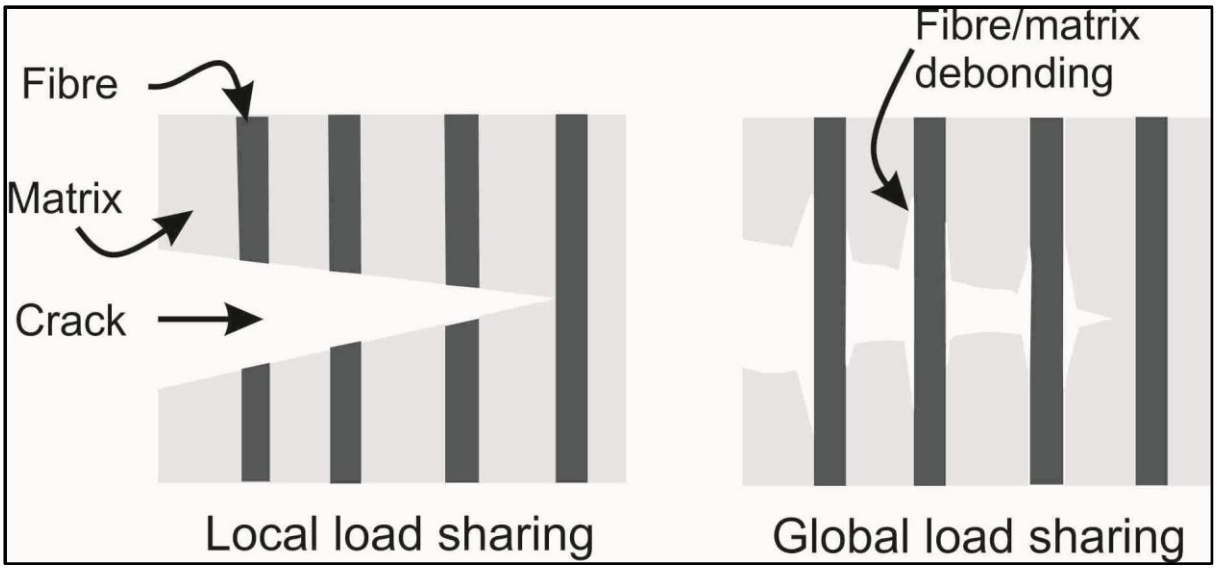

Figure 4.10. A sketch of load transfer mechanisms in fibre composites.

Concerning the global load sharing mechanism (GLS), the key issue is that fibre/matrix debonding occurs. After fibre matrix debonding, the extra stretch of the fibre (due to the crack opening) only results in a relative small strain in the fibre, so that they do not fail near the crack tip. The matrix can then grow across the entire width of the specimen, leaving intact fibres behind, creating a fully bridged matrix crack and thereby causes a significant toughening (Thouless and Evans, 1988). The fibre/matrix debonding and fibre bridging are shown in global load sharing mechanism as sketched in figure 4.10. At higher applied stress level, the fibres fail independently of each other with different fibre pull out length for each fibre (depending on the exact distribution of flaws along the

fibre length). It is the fibre/matrix bonding that dictates whether crack penetration or crack deflection occurs (He and Hutchinson, 1989) and thus controls whether LLS or GLS results. A local load sharing mechanism is usually seen for glass fibre reinforced polymer composites whereas the global load sharing mechanism is observed for metal matrix composites. However, ceramic fibre composites show several examples of a transition between two main mechanisms by increasing interface strength (Curtin et al., 1998).

According to the failure observations of the unidirectional flax/LPET composites, most specimens failed at the end of the gripping section, which is covered with tab material. After initiation of fracture at the tab ends, a long splitting fracture surfaces occurred along the fibre direction until the specimens fully failed at the gauge section. The inspection of the fracture surfaces was made at the gauge section of the failed specimens. On a macroscopic level, the fracture surfaces do not show any clear fracture initiation and growth direction. However, on a microscopic level, the fibre ends and the fibre/matrix interaction zones are clearly visible. A field emission scanning electron microscope (Supra FE-SEM, Zeiss) was used to provide a close inspection of the fracture surfaces of the flax/LPET composites. Images of the fracture surfaces after uniaxial tensile failure of composites with different fibre weight fractions are shown in Figure 4.12.

The fracture surfaces (micrographs) for low and medium fibre weight fraction (low porosity) and high fibre weight fraction (high porosity) can be categorised based on load transfer mechanisms. At low and medium fibre weight fractions ($W_f < 0.6$), the unidirectional flax/LPET composites show evidences of the "local load transfer" mechanism. At failure with this mechanism, the failed fibres at the fracture surfaces show a more brittle failure with increasing fibre matrix interaction at a relatively low porosity condition. It is observed that fibre pull-outs are frequently seen with a similar length, as shown in Figure 4.12a and b. This point towards that the fibre-matrix interface bonding is relatively strong. In addition, the high magnification microscope images in Figure 4.12a and b show that the simultaneously failed fibre bundles are relatively flat in their cross sections and fail in the same plane. This can be considered to be due to local stress concentration where the failure of one single fibre leads to progressing of the crack to the neighbouring fibres, which then leads to failure of the composite.

At high fibre weight fractions ($Wf > 0.6$), it is observed that the fractured surfaces are more uneven, and have large porous regions. Each individual fibre tends to fracture independently at different points along the length of the fibre bundle. Figure 4.12c shows the porosity regions between individual fibres from decreasing the matrix regions at high fibre weight fractions. The insufficient matrix (cavity among fibres) prevents transmitting the load sharing among neighbouring fibres leading to composite failure. For this reason, more individual flax fibres exhibit complex failure modes throughout their cross sections. However, some regions where fibres are covered with matrix indicate the presence of strong interface (Figure 4.12c and 4.13a).

Figure 4.13 shows the microfibrils in the large fracture surfaces of the single fibres. They have longitudinal splitting in the loading direction in a non-brittle manner like a schematic drawing of failure behaviour of the single flax fibre [Fig. 10, A2]. The micro fibril surfaces are fully covered with matrix and the matrix bonds are connected with fibre surfaces.

The microscopic observations showed that the LPET brittle matrix has river line patterns on fracture surfaces. More specifically, river lines (microflow lines) can be observed in the matrix-rich areas between the fibre bundles (white arrows in the Figure 4.12a and 4.14). They are aligned in the general direction of crack propagation. There is close similarity between river lines patterns in the fracture surfaces of the metallurgical materials. The patterns produced by confluence of streams into larger streams into rivers like waves of water flow (Figure 4.11). They consist of serious of closely spaced steps that merge progressively to form larger steps on the fracture surfaces (Hull 1999).

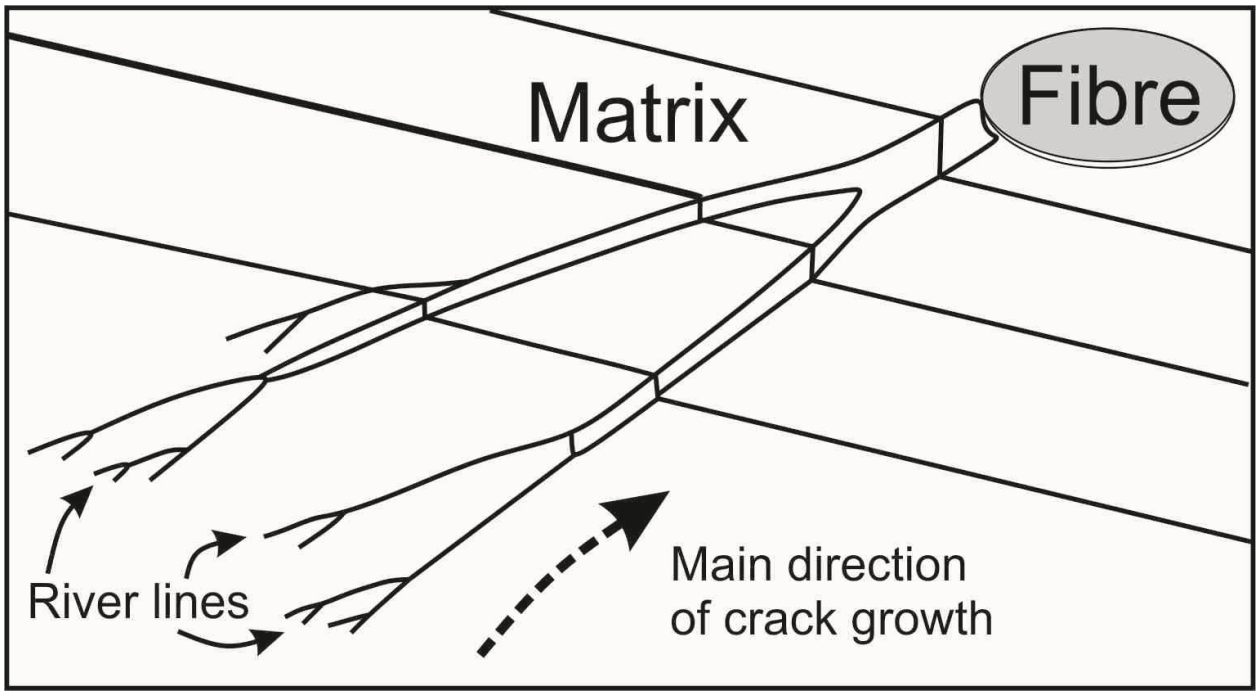

Figure 4.11. Schematic river line patterns showing sequence of steps into larger steps in matrix area after (Hull, 1999).

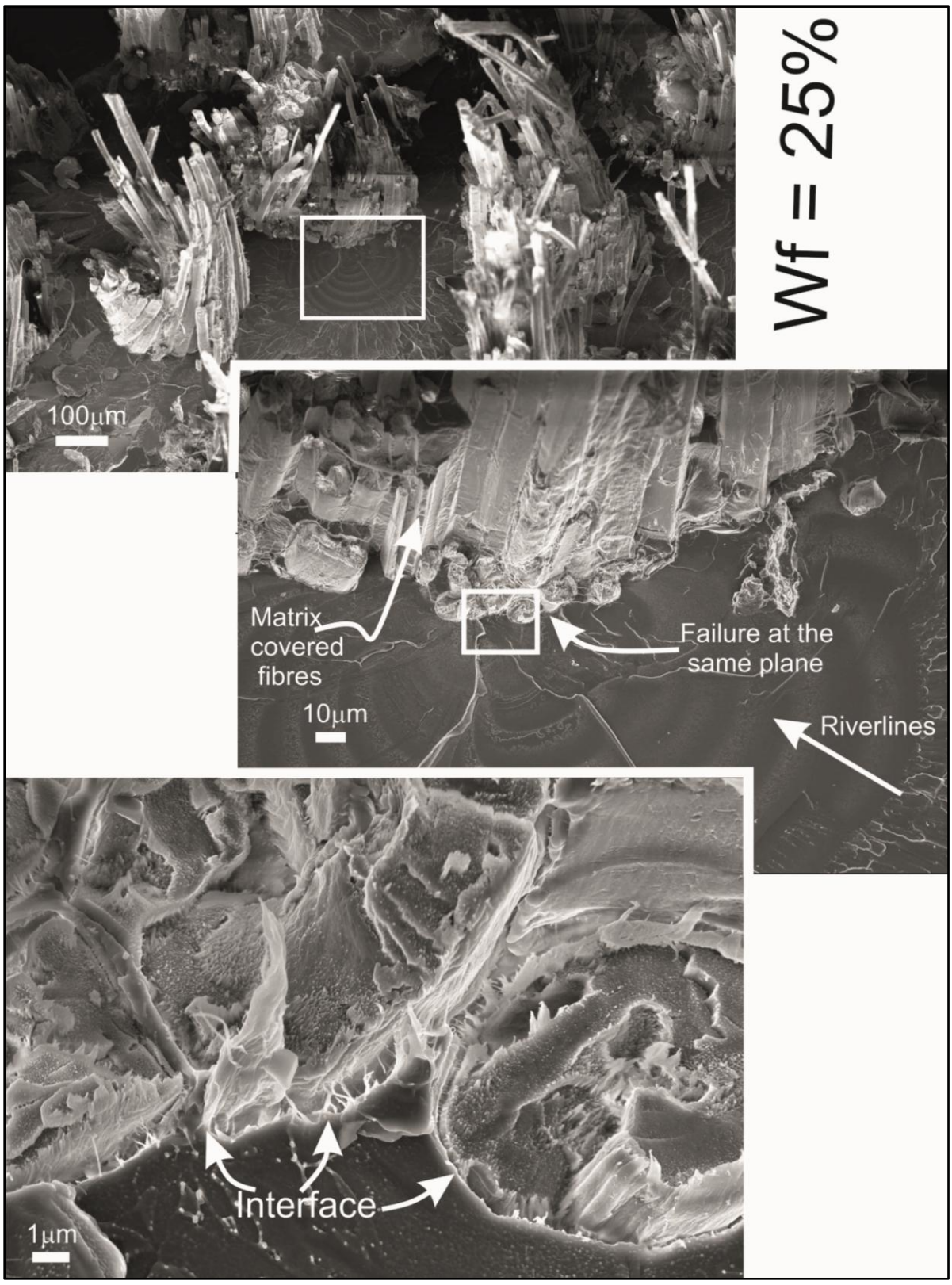

Figure 4.12a. Fracture surface of unidirectional flax/LPET composites with (a) a low, (b) a medium and (c) a high fibre weight fractions (W_f is equal to 0.25, 0.55 and 0.75, respectively).

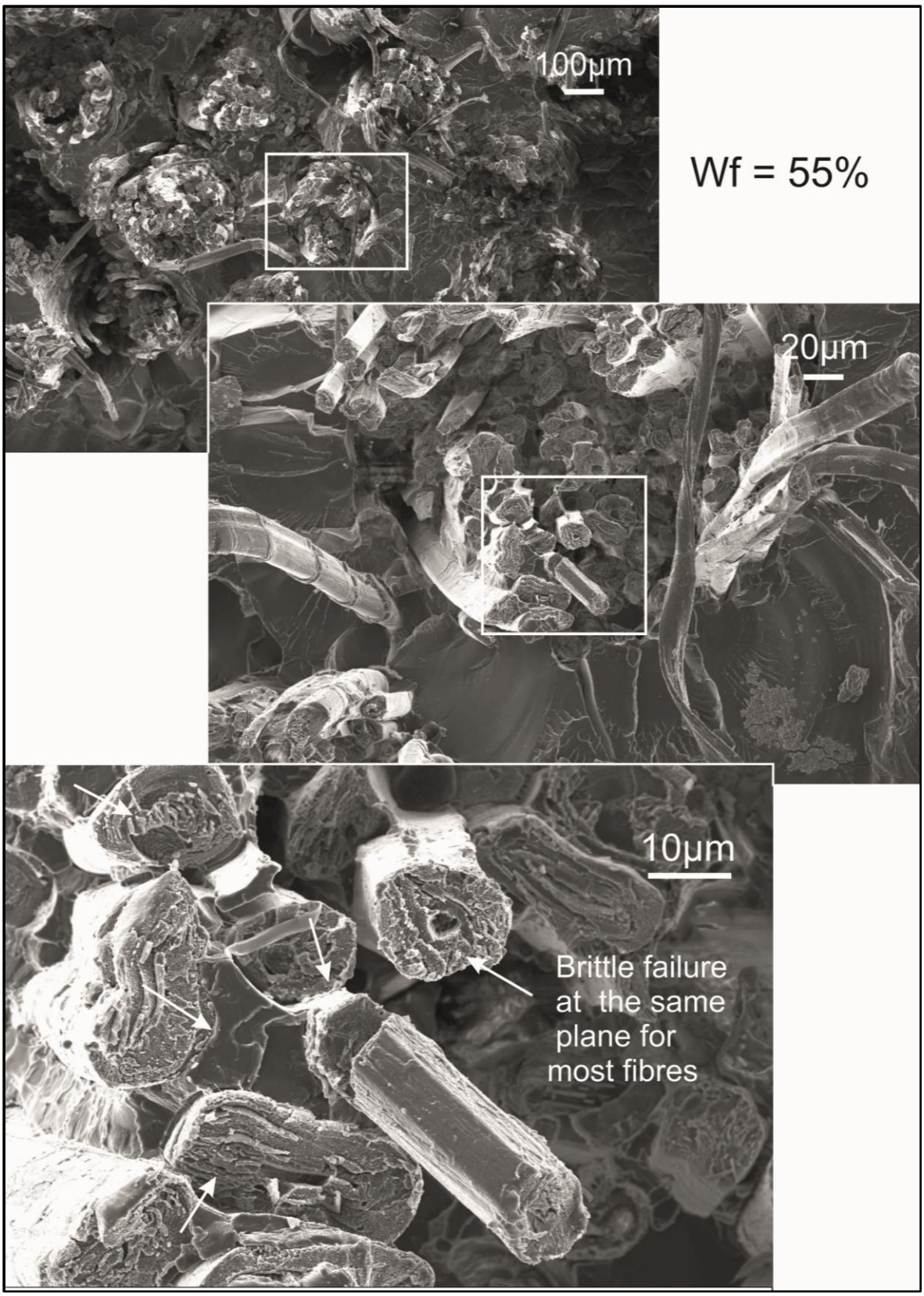

Figure 4.12b. Continued.

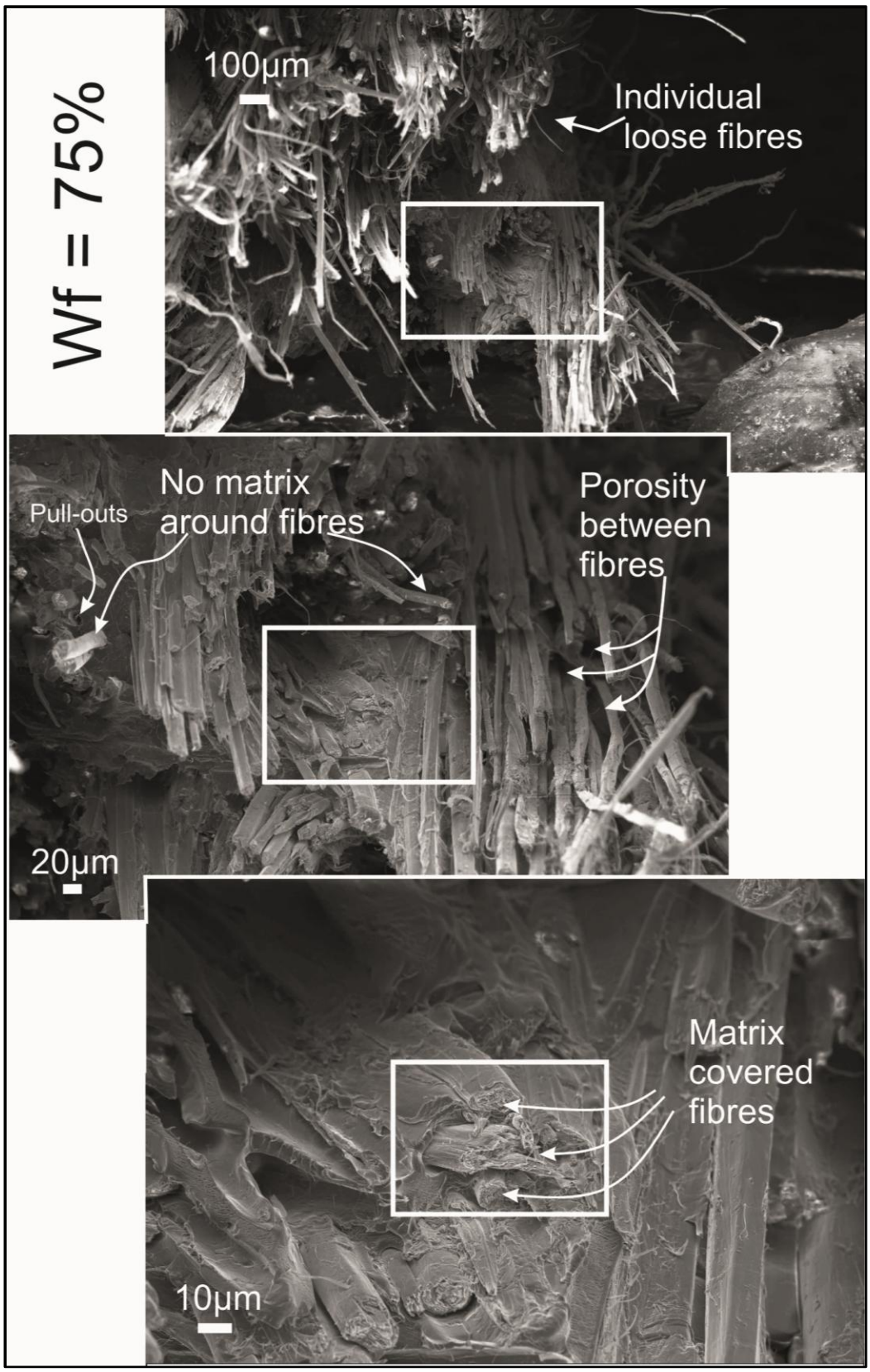

Figure 4.12c. Continued.

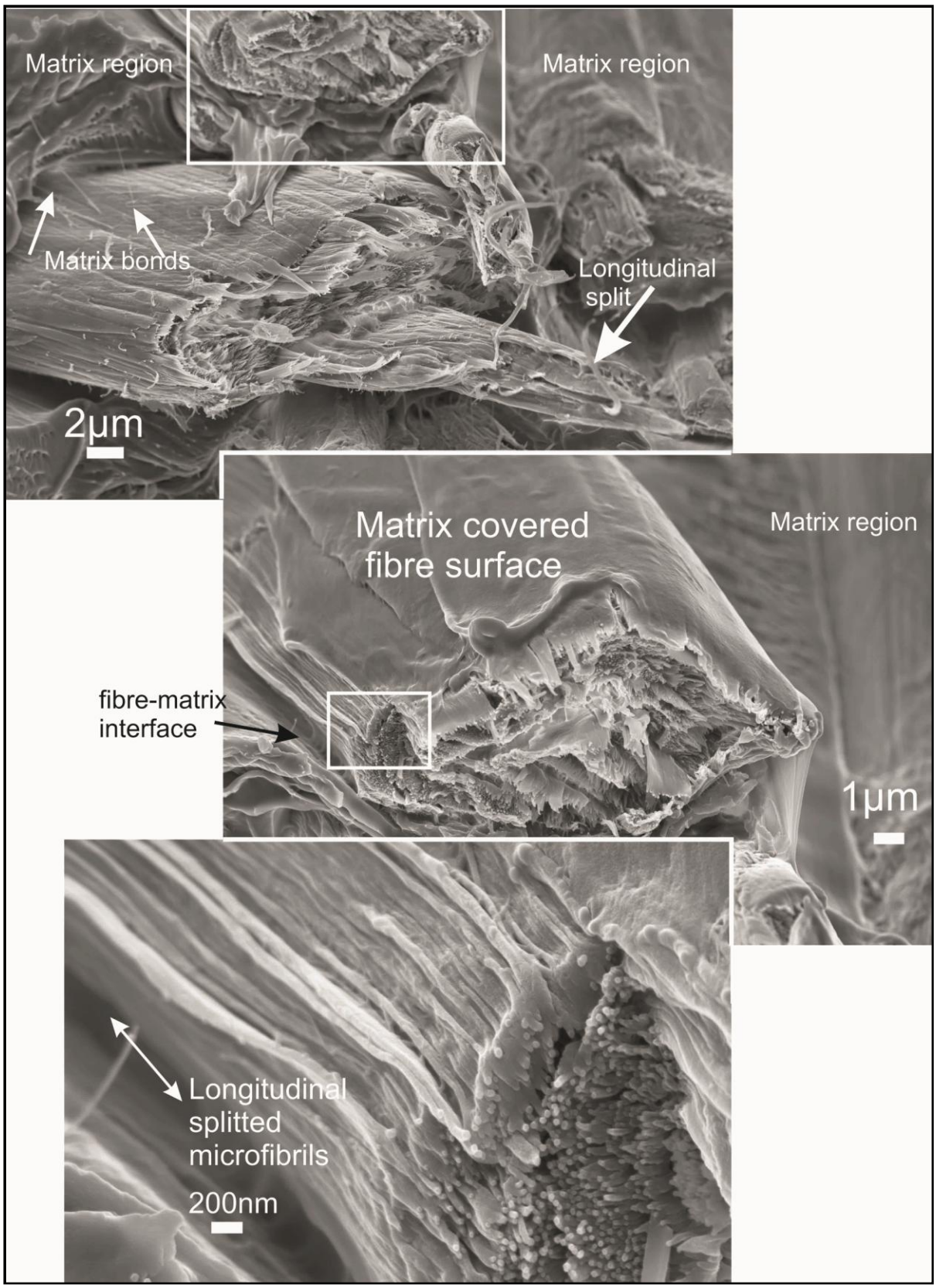

Figure 4.13a. Failure characteristic of single flax fibres in composites (high fibre weight fractions).

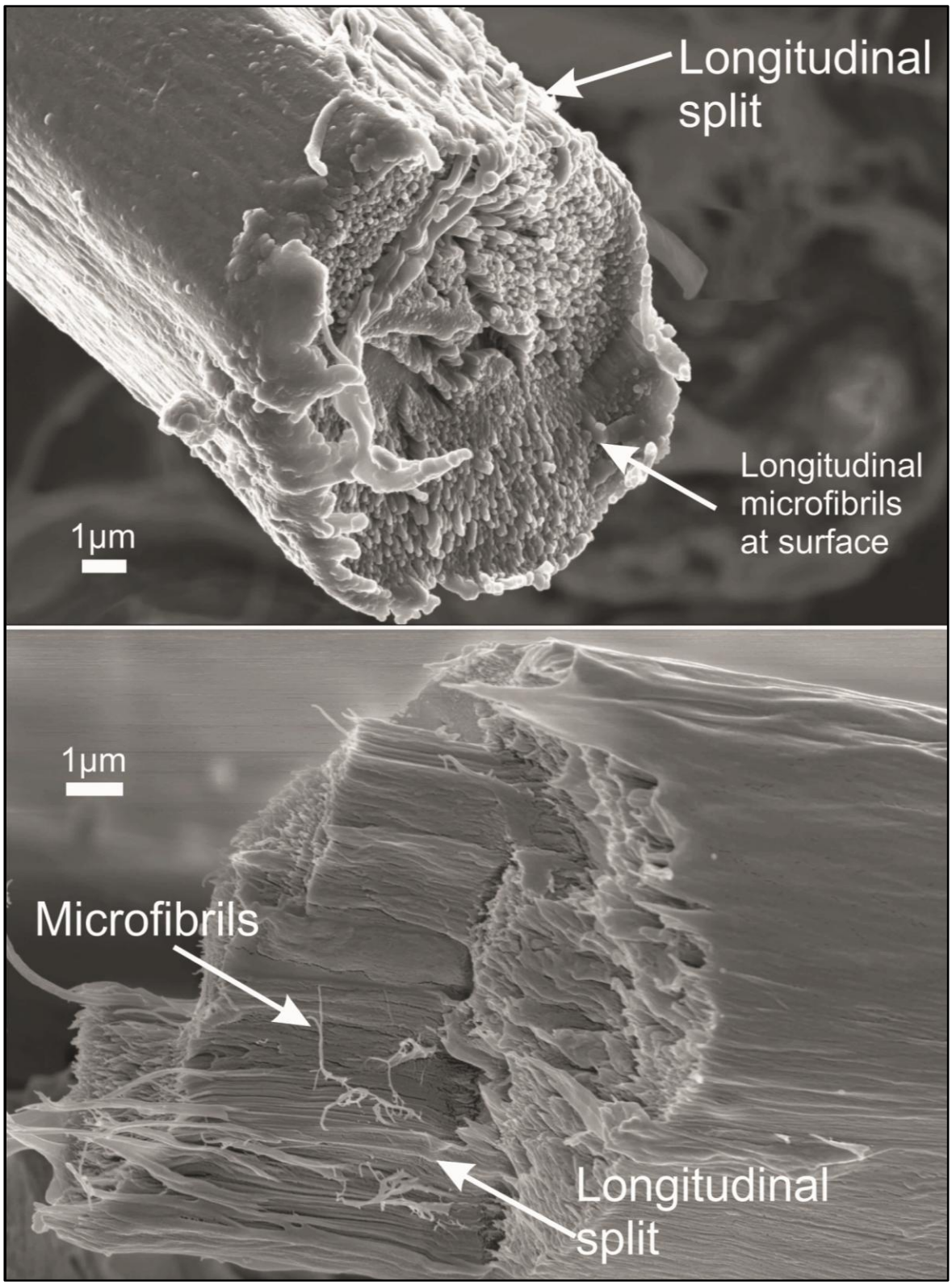

Figure 4.13b. Failure characteristic of single flax fibres in composites (low fibre weight fractions).

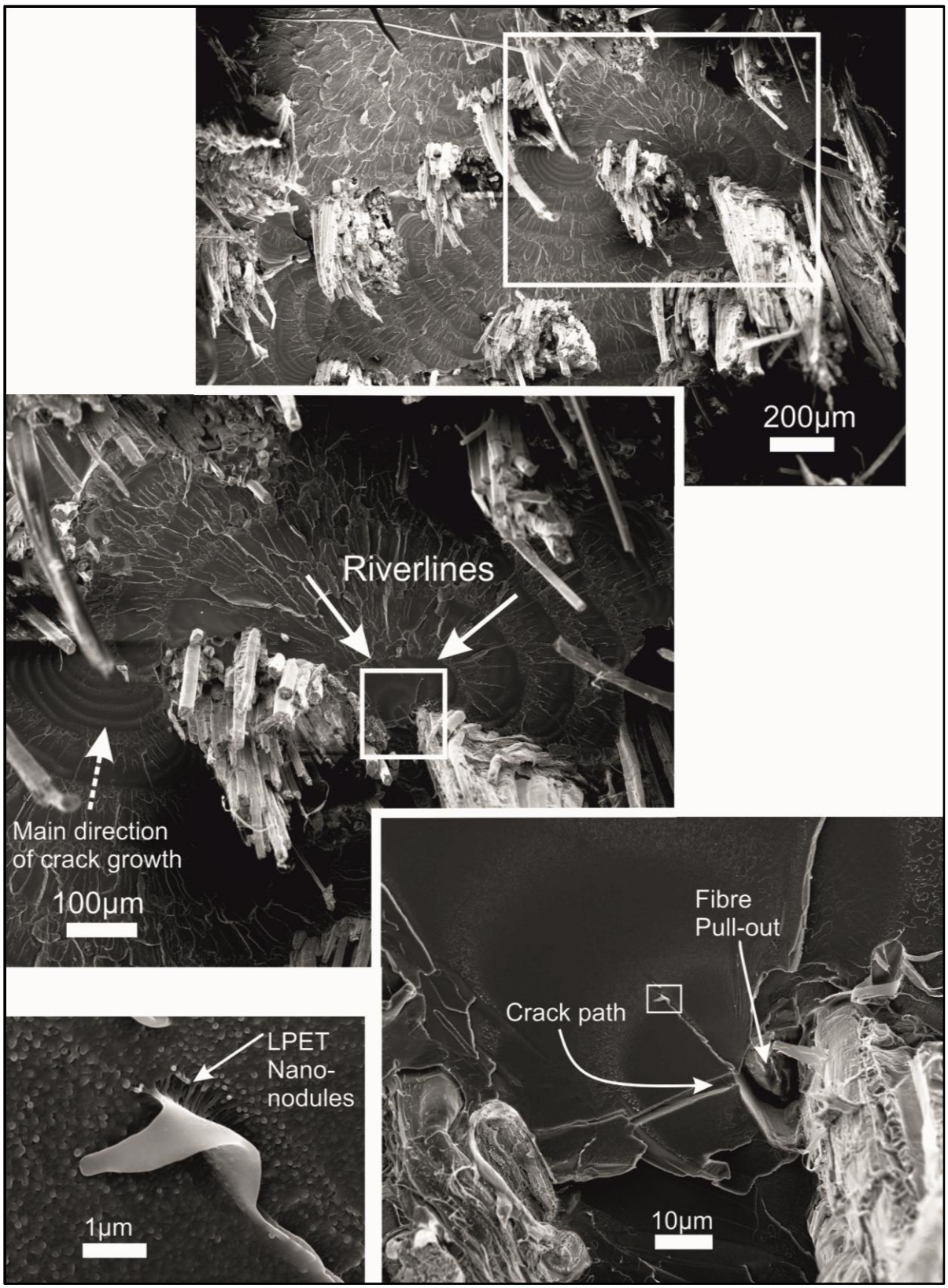

Figure 4.14. Failure characteristic of LPET matrix in the cross section of a composite.

4.2.4.4. A relation between tensile failure and fracture behaviour

It is likely that the river lines direction of these granular structures gives an indication of the crack growth direction. The Figure 4.14 shows a magnified view river lines has developed into granular structures and ended with a crack deflection in the boundary of fibre-matrix interface. (Hull, 1999). Since the strain to failure of the LPET matrix is lower than flax fibres (Table 4.2) the crack growth progress from matrix region to the interface between flax fibre and LPET matrix.

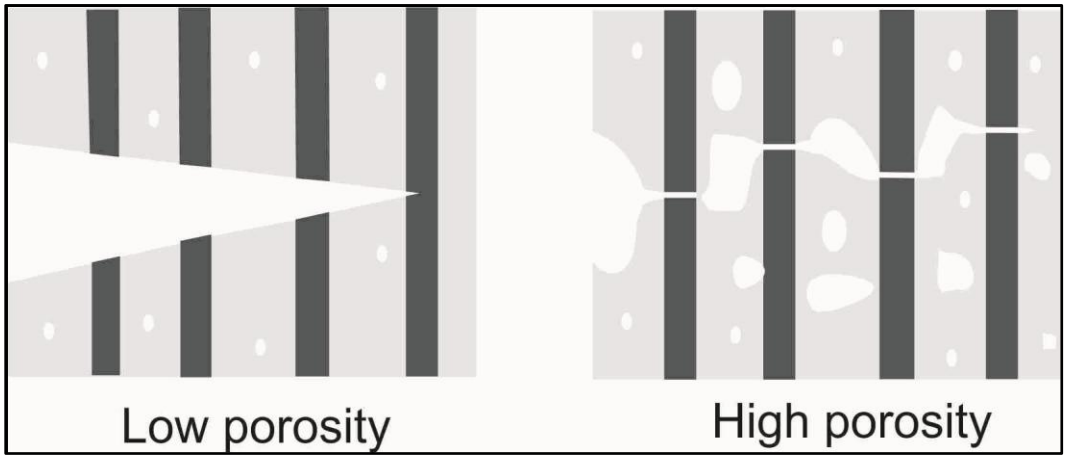

Figure 4.15. A sketch of load transfer mechanisms in low and high porous microstructure.

A sketch in Fig. 4.15 explains the effect of porosity on the fracture surface appearance. The presence of porosity should not affect the fibre/matrix interface, so that the failure mode should not change (LLS or GLS). Thus, at low and medium fibre weight fractions, a sharp matrix crack approaching a fibre is expected to induce fibre failure based on local load sharing mechanism. However, the presence of porosity changes the appearance of the fracture surface. For this reason, the fracture surfaces of the flax/LPET composites at high weight fractions ($Wf > 0.6$) can appear as though they are in global load sharing mechanism with different length of pull outs in porous regions.

Moreover, the composite failure results (Figure 4.14) show that the strength variation is higher and the average strength decrease for high fibre weight fractions ($Wf > 0.6$). Because, the presence of large porosity regions plays an active role in failure by growth of the cracks (Krstic, 1988). When fracture resistance of brittle fibre matrix composites is concern, the failure of the composites is controlled by critical flaws. Strength variability shows statically distribution based on flaw size (Freiman et al., 2012). The strength and flaw size of a homogeneous material is presented by Griffith fracture criterion (Broek, 1986) (Equation 4.3).

$$\sigma_c = \sqrt{\frac{G_c\, E}{\pi\, a}} \qquad (4.3)$$

where σ_c is the critical stress at fracture, G_c is critical energy release rate (fracture energy), a is critical flaw size and E is Young's modulus. According to the fracture criterion, the flax fibre /LPET composites have lower average strength for high weight fractions ($Wf > 0.6$) (Figure 4.8) due to increasing flaw size. In addition, the strength of composite is controlled by the largest flaw which varies from specimen to specimen. Therefore, the larger variation in the flaw size leads to the larger variation in tensile strength of the composites at high fibre weight fractions.

4.2.5. Modelling of unidirectional tensile test specimens by FEM

As shown in Figure 9, UD flax/LPET composites failed in the tab area during tensile testing. This is a general problem in testing of UD composites. Some earlier experimental and modelling studies (Adams and Harris, 1987; Cunningham et al., 1985) investigated the failure at the end of the tab based on the assumption of a stress concentration at the wedge of the tab and test material. Cunningham et al. (1985) showed that the thickness of the tab and adhesive materials had very little effect on the longitudinal stress concentration. Also, the wedge angle of the tab material and the stiffness of the tab material had a significant effect on the longitudinal stress of the test materials. Hojo et al. (1994) also found that both non-tapered square cut glass fibre reinforced composite (GFRP) tabs and tapered tabs with the same tab material showed failure in the gripping area. He also showed that test materials with rubber tabs failed in the gauge section but the same test materials with GFRP tabs failed in the grips in a tensile test. However, the problem was also expressed by Bogy (1971) who shows the stress state at the wedge tip can be singular. The solution was determined in terms of four elastic constants (Young's modulus and Poisson's ratio for each of the two material) for dissimilar elastic materials loaded with arbitrary boundary tractions. In two dimensions, stress singularity can be expressed as:

$$\sigma_{ij} \rightarrow r^{-p} \; for \quad r \rightarrow 0, \tag{4.4}$$

where σ_{ij} is the stress tensor, p is a singularity exponent and r is the radial distance from the wedge tip. The stresses approach infinity at the wedge tip ($\sigma_{ij} \rightarrow \infty \; for \; r \rightarrow 0$) when p has a positive real part ($0 < p < 1$). However, the stress at the wedge tip will be finite and the singularity vanishes when p has a non-positive real part ($p \leq 0$).

4.2.5.1. Problem definition

The purpose of this study is to develop a straight sided tensile test specimen geometry that fails in the gauge section by reducing the stress singularity at the vertex of the tab wedge. The singular stress field at the vertex of the tab and test material of the specimen can be expressed as [A4-5]:

$$\frac{\sigma_{ij}}{\bar{\sigma}} = A_{ij} \left(\frac{2r}{H}\right)^{-p} \qquad for \; r \rightarrow 0 \tag{4.5}$$

where $\bar{\sigma}$ is the applied stress in the gauge section, A_{ij} represent non-dimensional singularity functions and H is a characteristic dimension, here the thickness of the test material (isotropic and orthotropic) (see figure 4.16). Previous studies (Bogy, 1971; Bogy and Wang, 1971; Hein and Erdogan, 1971) showed that stress singularity exponents depends on the tab wedge geometry and the materials elastic properties but it is independent of external loading.

4.2.5.2. The model parameters

A schematic view of straight sided tensile specimen is shown in Figure 4.16a and b. The singularity problem at the tab end was analyzed in a two dimensional (plane strain) model in terms of the wedge angle, θ that was varied from 2.5° to 90°, tab/test material thicknesses, elastic properties of the isotropic tab and isotropic test materials, Σ from 0.005 to 10 [A4]. Also, the stress singularity was investigated for orthotropic tab and test materials by considering an orthotropic parameter using an orthotropic rescaling method since method allows reducing elastic parameters in the more complex stress field. For orthotropic materials, the stress field under prescribed surface tractions depends on two non-dimensional parameters λ and ρ defined as (Wang, 1991; Zhigang, 1990):

$$\lambda = \frac{E_{yy}}{E_{yy}} \qquad \rho = \frac{\sqrt{E_{xx}E_{yy}}}{2G_{xy}} - \sqrt{v_{xy}v_{yx}} \tag{4.6}$$

E_{xx} and E_{yy} denote Young's moduli in the of fibre and lateral directions for orthotropic materials, respectively. G_{xy} is shear modulus and v_{xy} and v_{yx} are the major and minor Poisson's ratios. For isotropic materials, $\lambda = \rho = 1$ and the stress field dependence of ρ is relatively weak (Zhigang, 1990).

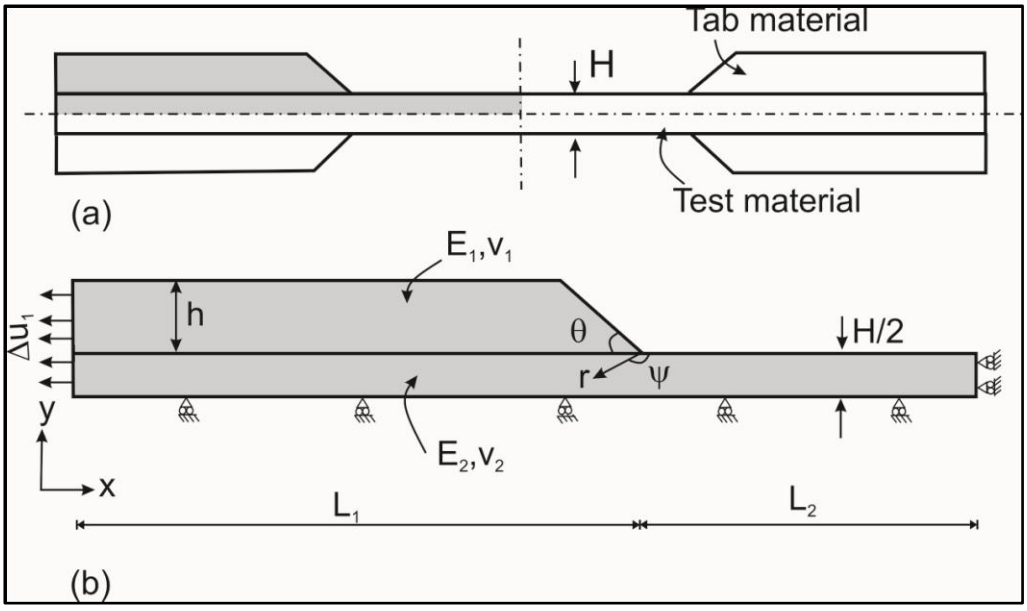

Figure 4.16. The straight sided tensile test specimen along the cross section (a) and modelled part of the quarter of tensile specimen (b) shown with defined boundary conditions.

The stress singularity exponents, *p*, were obtained by the slope of the log-log plot of the stress component σ_{xx} as a function of the distance to the wedge tip for a specific angular direction, $\psi = \pi$. The singularity exponent, *p* is obtained by the linear regression line when the data appear as straight lines as in the following equation.

$$\frac{\sigma_{xx}}{\bar{\sigma}} = A\left(\frac{2r}{H}\right)^{-p} \Rightarrow \log\left(\frac{\sigma_{xx}}{\bar{\sigma}}\right) = \log A - p\log\left(\frac{2r}{H}\right) \quad (4.7)$$

A finite element model was applied based on the relative displacement of the elemental nodes in the axial (x axis) direction (see figure 4.16). The meshes were prescribed as 2D triangular plane elements and smaller elements were used at the end of the tab material ($x = L_1$) (smaller than 10^{-5} H) since larger stress gradients are expected.

4.2.5.3. The stress distribution at the test material

Figure 4.17a shows the axial stress distribution, σ_{xx} (normalised with the applied stress, $\bar{\sigma}$) as a function of the distance from the wedge tip for $\psi = \pi$ in the case of no elastic mismatch ($\Sigma = 1$). The maximum stress in the test specimen having $\theta = 90°$ is much higher than the maximum stress of a specimen with $\theta = 15°$. This suggests that there is a singularity at the end of the tab and the value of the singularity exponent is higher for $\theta = 90°$ than that for $\theta = 15°$.

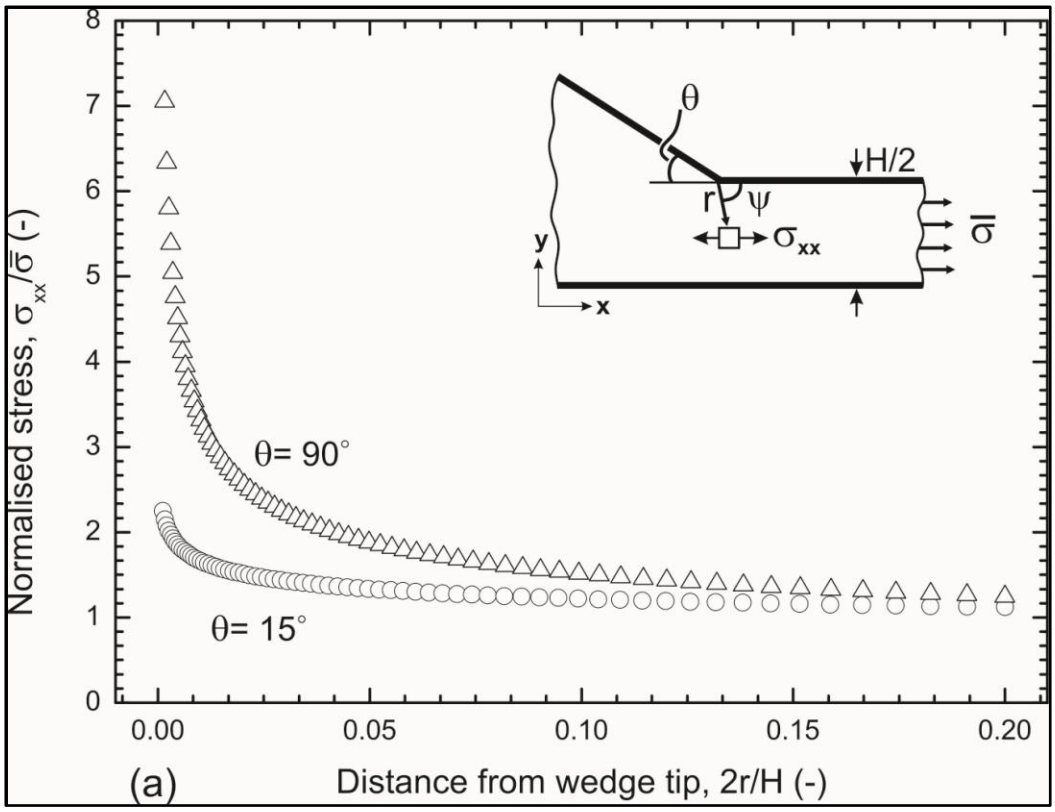

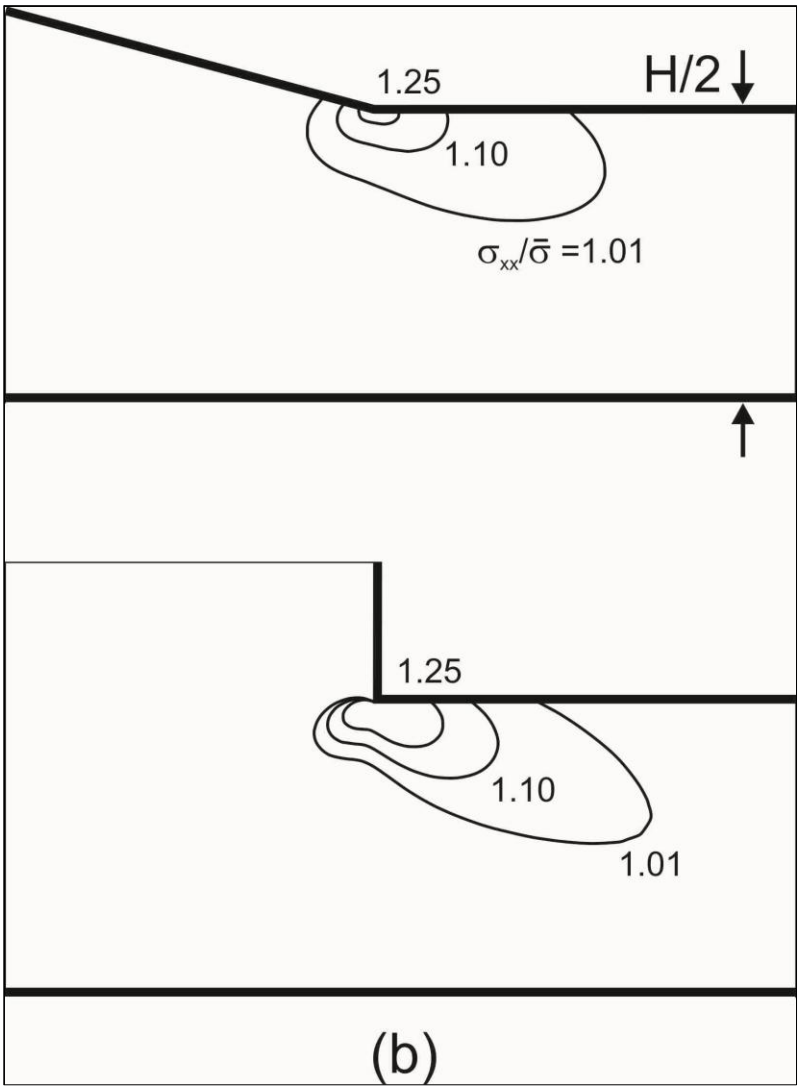

Figure 4.17. The stress distribution (a) as a function of the distance from the wedge tip of the tab and test material are presented with the axial stress σ_{xx} contours (b) for $\theta = 15°$ and $\theta = 90°$.

The contours of the axial stress distribution around the tab wedge are also presented in Figure 4.17b. The zones with a high normalized stress state are larger for specimens having a $\theta = 90°$ tab than for specimens having a $\theta = 15°$ tab [A4].

4.2.5.4. Stress singularity and singular zone for test materials

The stress singularity is shown as a function of stiffness ratio for different wedge angles for isotropic material in Figure 4.18a. The stress singularity for orthotropic test material joints was also solved as a function of an extensive stiffness ratio and wedge angles $\theta = 2.5°$ and $\theta = 10°$ for different orthotropic parameter values in Figure 4.18b. It is determined that the stress singularity values are between 0 to 0.5 for all wedge angles and stiffness ratios. Furthermore, the p value can

be reduced significantly by decreasing Σ and decreasing θ. It can be seen that the stress singularity is close to zero and changes an insignificant amount for θ=10° and $\Sigma<0.1$. It was noted that the stress singularity is relatively insensitive to elastic properties for wedge angles below $\theta = 15°$. However, the singularity exponent can not be removed completely for the tab wedge angle and material combination of the unidirectional test specimens. Therefore, it is important to discuss the practical implications of singular stress fields and the size of the singular zone. As can be seen from Fig. 4.17b the singular zone is rather small.

4.2.5.5. Practical implications of the singular zone

When the singular zone is small, comparable to a microstructural length scale, then strictly speaking the smeared out continuum approach should be replaced by an approach based on a microscale model. However, a closer approach is to consider that if the size of this singular zone of the continuum model is much smaller than one fibre diameter, the singular stress field is unlikely to initiate specimen failure. This judgement is based on the assumption that failure of a single layer of fibres would possibly not lead to specimen failure. On the other hand, in cases where the size of the singular zone is much larger than one fibre diameter, the singular wedge tip stress field is likely to initiate failure of many fibres, leading to premature specimen failure. Therefore, the following criterion is proposed for the avoidance of wedge tip failure: The tensile stress, σ_{xx}, may be 10% (or more) higher only within a radius, r from the wedge tip corresponding to one fibre diameter, d_f. Then, the criterion for gauge section failure can be written as [A4-10]:

$$\frac{\sigma_{xx}}{\bar{\sigma}}\left(r = d_f\right) \leq 1.10 \qquad (4.8)$$

The 10% limit is based on the engineering judgement that an error up to 10% in the failure strength is probably acceptable in most engineering situation. The proposed criterion can be used as follows. After the stiffness ratio, Σ and the orthotropic parameter λ are calculated, the maximum allowable wedge angle, θ_{max}, can be read off from Fig.4.19. The maximum allowable wedge angle can be estimated as listed in Table 4.3 for the various tab/test material combinations according to the failure criterion above. It can be seen from Table 4.3 that testing of glass/epoxy and flax/LPET composites is more challenging since they need much lower wedge angles than carbon-epoxy composites.

Table 4.3: Recommended wedge angle of tab specimen for material combinations.

Test material	**Tab material**	**Σ (-)**	**λ (-)**	**θ_{max} (°)**
Flax/LPET	Epoxy	0.12	0.1	5
Glass/Epoxy	Epoxy	0.10	0.2	10
HS-Carbon/Epoxy[1]	Epoxy	0.03	0.1	15
HM-Carbon/Epoxy [2]	Epoxy	0.01	0.02	45

1: High strength fibre, 2: High modulus fibre

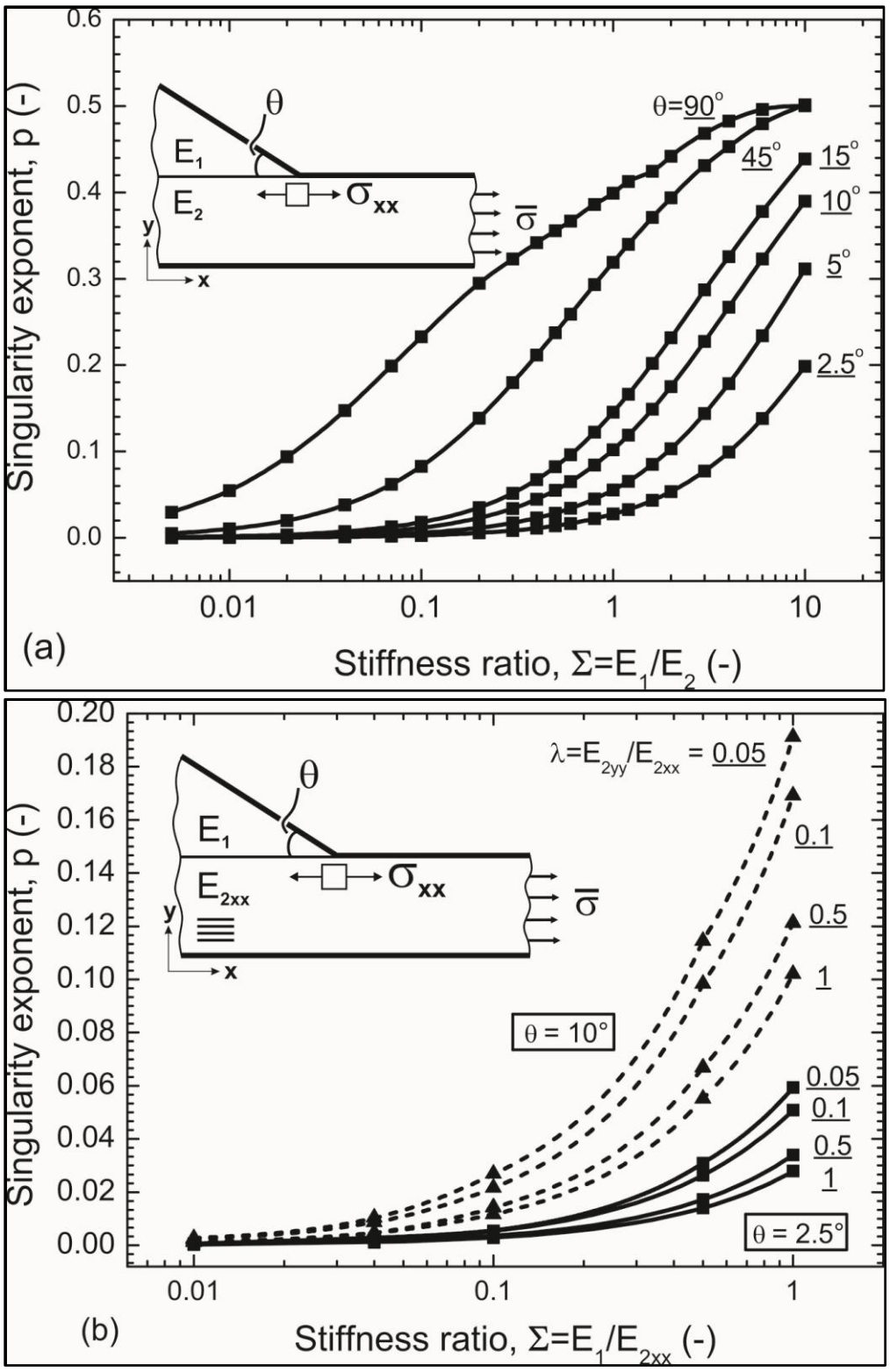

Figure 4.18. Singularity exponent as a function of the stiffness ratio for different wedge angles in isotropic (a) and orthotropic (b) materials.

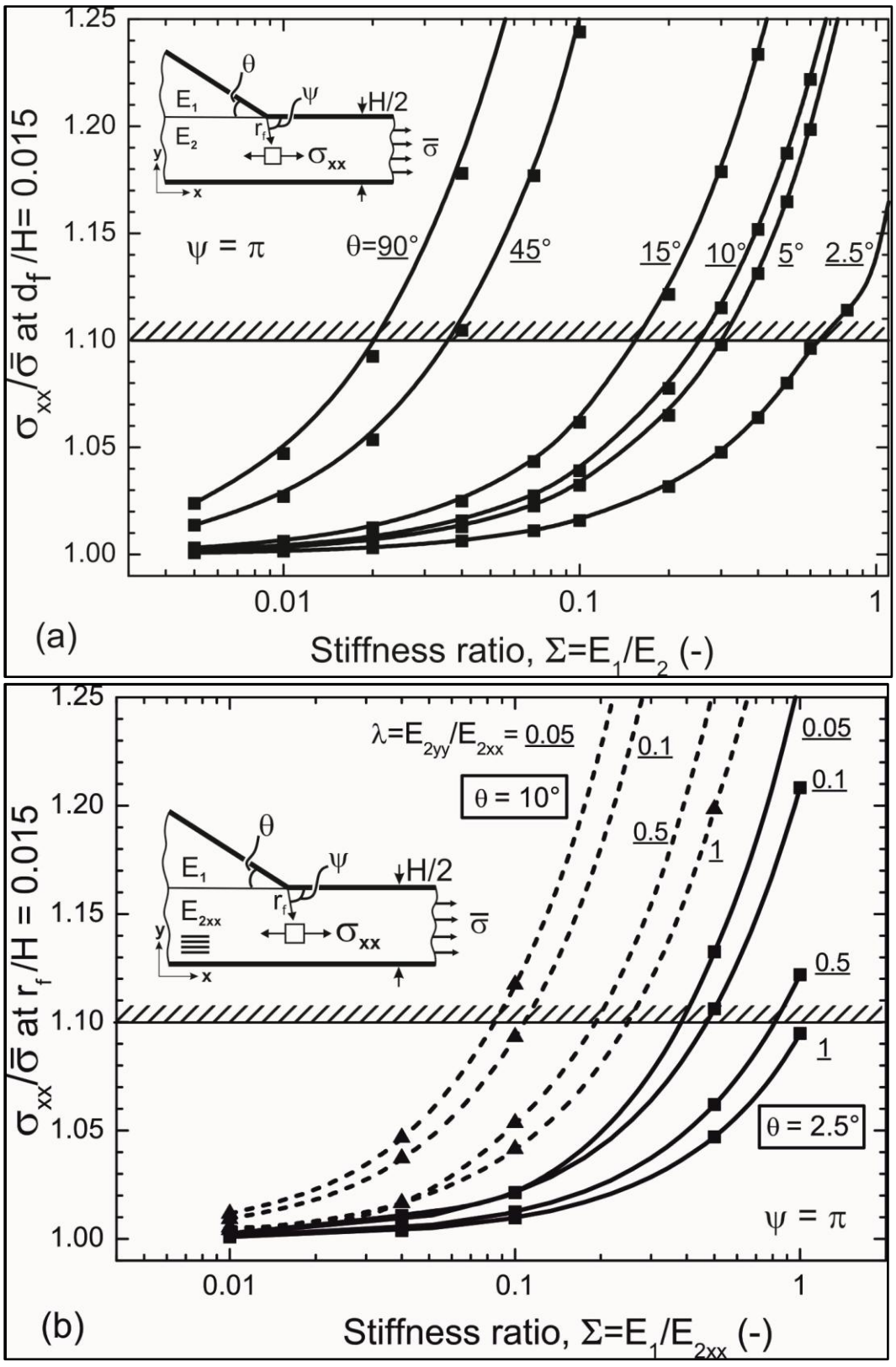

Figure 4.19. Stresses at *r/H =0.015* corresponding to one fibre diameter as a function of stiffness ratio, Σ for different wedge angles in isotropic (a) and orthotropic materials (b).

From a practical point of view, it is desirable not to use very small values of θ_{max}, This raises the question of what is the best way of the reducing wedge tip singularity while still having a reasonably specimen design. Also, a very soft tab material may not be useful from the point of view of gripping a specimen. This leads to a proposed specimen design in Fig. 4.20 where a very soft material is used as the wedge tip material (to decrease the wedge tip singularity) but a stiffer tab material is used for gripping. In a previous study, such an approach has experimentally been proposed by Wang et al. (Wang et al., 2006). They have tested YSZ - nickel oxide specimens with 90° aluminium tab specimens. Specimens with tabs but without wedge tip material failed in the grip section near the wedge tip. In order to decrease the singularity at the wedge tip, the aluminium tab material ends of the test specimens were modified by adding a wedge of a compliant wedge tip material (epoxy) (see Fig. 4.20). By this method, most specimens failed in the gauge section. Thus, the results of Wang's approach indirectly support our model predictions.

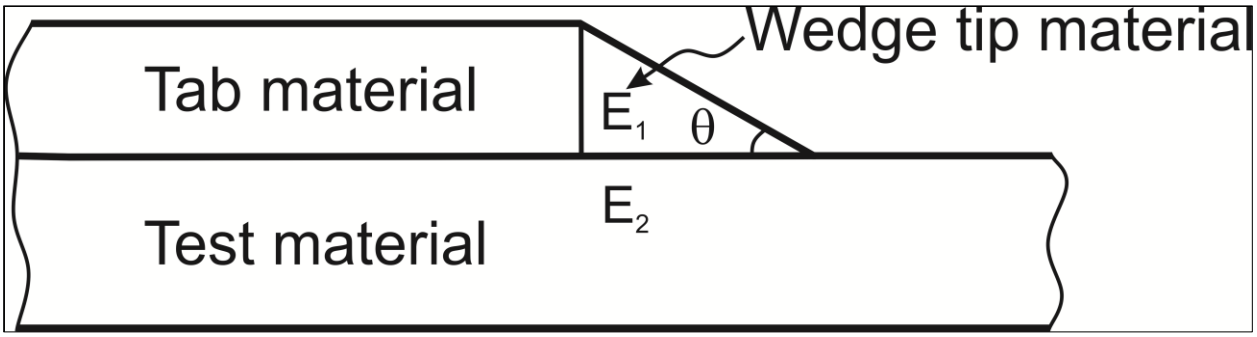

Figure 4.20. A suitable geometry of a test specimen combination with different materials for gauge section failure.

5. CONCLUSIONS

This study investigates the mechanical properties of single flax fibres and flax fibre composites.

The tensile behaviour of single flax fibres was examined together with microscopic observations. The fibre microstructure such as central voids (lumens) and fibre defects such as kink bands were observed along the fibre length and at the fracture surfaces by scanning electron microscopy and optical microscopy. Furthermore, the effect of the geometrical shape of the fibre cross sections on the tensile properties of the fibres was investigated. It is found that some of the variation of the fibre tensile properties can be attributed to the method of measuring the cross section of the fibres. Flax fibres have non-homogenous cross sections along the length of the fibre, and the variable aspect ratio of a fibre cross section is shown to significantly affect the variation of the calculated tensile properties, Also, the variable size of defects in the fibre cell wall leads to differences in the tensile behaviour of the fibres. Observations on the fracture surface of single fibres show that a large fracture area is formed in a non-brittle manner presumably due to cell wall defects, in addition to the anisotropy of the internal cell wall structures. This is in contrast to fracture mechanisms typically observed in brittle ceramic and glass fibres.

The effect of the applied consolidation pressure used to manufacture unidirectional flax/LPET fibre composites was studied using two different planar sizes of fibre assemblies consolidated under the same compression load. The effect of the different consolidation pressures on the volume fraction of the composite constituents was investigated, and this was related to the measured physical and mechanical properties of the composites. The model by Madsen et al. (2009) for volumetric composition, density and stiffness of plant fibre composites was used with the new experimental results and microscopic observations, leading to an improved understanding of the underlying mechanisms.

The maximum attainable fibre volume fraction (V_{fmax}) of the unidirectional flax/LPET composites was shown to be increased from 53 to 60% by increasing the consolidation pressure from 1.67 to 4.10 MPa. The higher consolidation pressure was shown to lead to a decrease in the porosity content from 11.3 to 8.6 %, and an increase in the maximum stiffness of the composites from 35 to 40 GPa. In addition, it was shown that after V_{fmax}, the porosity content of the composites was significantly increased (up to 32 %) causing a decrease in density and stiffness of the flax/LPET composites. Finally, it was shown that the fibre-correlated impregnation porosity and the structural porosity, caused by insufficient matrix, are important parameters for composite volumetric composition and tensile behaviour.

The fracture behaviour of the unidirectional flax/LPET composites was analysed for different fibre weight fractions (W_f). It was found that the fracture surfaces of the composites show evidence of a "local load transfer" process at low and intermediate fibre weight fractions ($W_f < 0.6$). The fracture surfaces show rather limited and short pull-out fibres in a brittle manner at lower fibre weight fractions. However, at high fibre weight fractions ($Wf > 0.6$), the fracture surfaces are rougher in

the higher fibre length. Even though the fracture surfaces are rougher and higher pull out fibres due to increasing porosity content between fibres, the composites are still controlled by “local load transfer” due to an indication of strong-matrix fibre adhesion at the fracture surfaces.

Furthermore, the general problem for tensile testing of unidirectional composites was investigated in the case of the unidirectional flax/LPET composites. The composites failed at the end of the tabs during tensile testing. A complicated stress field in the gripping area caused the specimens to fail prematurely, and thereby leading to an underestimation of the ultimate tensile strength. The premature failure in the gripping area of the tensile test specimens was assumed to be due to the presence of a stress singularity at the tab wedge tip. Failure at the gauge section can be achieved by reducing the stress singularity by selecting a suitable combination of the stiffness ratio of the tab and test materials and the wedge tip angle of the tab. This conclusion was established based on a finite element model developed which describes the decreasing stiffness ratio between tab and test materials, and a decreasing wedge angle leads to reduce the stress singularity. However, it is important to simplify the practical implications of a singular stress field and the size of the singular zone. It is proposed that if the size of this singular zone is much smaller than one fibre diameter, the singular stress field is unlikely to initiate specimen failure. This underlying idea is based on the assumption that failure of a single layer of fibres would probably not lead to specimen failure. A criterion is proposed for the occurrence of gauge section failure and the 10% limit is chosen since an uncertainty of 10% of the tensile strength value is considered to be the maximum allowable within a radius of the wedge tip corresponding to one fibre diameter.

Finally, a specimen suggested design using a tab material and wedge tip material is proposed for tensile testing of composite materials. The tab material should be stiff to facilitate a good gripping and load introduction and the wedge tip material should be rather compliant relative to the tested composite material.

6. FUTURE DEVELOPMENTS

The selection of fibres and procedures of the applied test methods are essential in the evaluation of the tensile test results. For this reason, the entire process should be well-controlled from plant harvesting to composite production in order to obtain the best possible reinforcement performance of the single fibres in composites. A test method providing that the correct cross sectional measurements, and defect quantification by X-ray microscopy should be carried out so that it can improve the determination of the tensile behaviour of single fibres. A development of a set-up for having controlled humidity conditions during testing of the single fibres might also improve the reliability of the results. The twisting effect of the fibre yarns and impregnation of the fibres certainly improve the understanding of the effect of single fibres in the composite mechanical properties. Furthermore, the FE results of the wedge tip singularity were applied for moulded homogenous tab and test materials. However, an adhesive layer should also be considered for modelling of the composite tensile specimens.

.

7. REFERENCES

Adams, R.D. and Harris, J.A., 1987. The influence of local geometry on the strength of adhesive joints. International Journal of Adhesion and Adhesives, 7(2): 69-80.

Andersons, J., Sparnins, E. and Joffe, R., 2009. Uniformity of filament strength within a flax fiber batch. Journal of Materials Science, 44(2): 685-687.

Astley, O.M. and Donald, A.M., 2001. A small-angle X-ray scattering study of the effect of hydration on the microstructure of flax fibers. Biomacromolecules, 2(3): 672-680.

Atalla, R.H., 1982. The structures of cellulose and their transformations. Abstracts of Papers of the American Chemical Society, 184(September): 33.

Baley, C., 2002. Analysis of the flax fibres tensile behaviour and analysis of the tensile stiffness increase. Composites Part a-Applied Science and Manufacturing, 33(7): 939-948.

Baley, C., 2004. Influence of kink bands on the tensile strength of flax fibers. Journal of Materials Science, 39(1): 331-334.

Baley, C., Morvan, C. and Grohans, Y., 2005. Influence of the absorbed water on the tensile strength of flax fibers. Macromolecular Symposia, 222: 195-201.

Barbero, E.J., 1999. Introduction to Composite Materials Design. Taylor & Francis.

Belingardi, G., Paolino, D.S. and Koricho, E.G., 2011. Investigation of influence of tab types on tensile strength of E-glass/epoxy fiber einforced composite materials. Procedia Engineering, 10: 3279-3284.

Biermann, C.J., 1996. Handbook of pulping and papermaking. Academic Press.

Bledzki, A.K. and Gassan, J., 1999. Composites reinforced with cellulose based fibres. Progress in Polymer Science, 24(2): 221-274.

Bledzki, A.K., Sperber, V.E. and Faruk, O., 2002. Natural and wood fibre reinforcement in polymers. Rapra Technology Ltd.

Bogy, D.B., 1971. Two edge-bonded elastic wedges of different materials and wedge angles under surface tranctions. Journal of Applied Mechanics, 38(2): 377-&.

Bogy, D.B. and Wang, K.C., 1971. Stress singularities at interface corners in bonded dissimilar isotropic elastic materials. Int J Solids Struct, 7(8): 993-1005.

Bos, H., Van Den Oever, M. and Peters, O., 2002. Tensile and compressive properties of flax fibres for natural fibre reinforced composites. Journal of Materials Science, 37(8): 1683-1692.

Bos, H.L. and Donald, A.M., 1999. In situ ESEM study of the deformation of elementary flax fibres. Journal of Materials Science, 34(13): 3029-3034.

Broek, D., 1986. Elementary Engineering Fracture Mechanics. Martinus Nijhoff.

Charlet, K. et al., 2007. Characteristics of Hermes flax fibres as a function of their location in the stem and properties of the derived unidirectional composites. Composites Part a-Applied Science and Manufacturing, 38(8): 1912-1921.

Charlet, K., Eve, S., Jernot, J.P., Gomina, M. and Breard, J., 2009. Tensile deformation of a flax fiber, Mesomechanics. Procedia Engineering, pp. 233-236.

Commission, E., 2009. Advisory group on flax and hemp. DG Agriculture and Rural Development, Belgium.

Commission, E., 2010. End of life veicle directive 1095. Department for Business Innovation&Skills, UK.

Cunningham, M., Schoultz, S. and Toth, J., 1985. Effect of end tab design on tension specimen stress concentrations, In recent advances in composites in the US and Japan, ASTM, pp.:253-62.

Curtin, W.A., Ahn, B.K. and Takeda, N., 1998. Modeling brittle and tough stress–strain behavior in unidirectional ceramic matrix composites. Acta Materialia, 46(10): 3409-3420.
Davies, G.C. and Bruce, D.M., 1998. Effect of environmental relative humidity and damage on the tensile properties of flax and nettle fibers. Textile Research Journal, 68(9): 623-629.
Davis, J.R., 2004. Tensile testing. ASM International.
Eichhorn, S.J. et al., 2001. Review: Current international research into cellulosic fibres and composites. Journal of Materials Science, 36(9): 2107-2131.
Fengel, D. and Wegener, G., 1989. Wood: Chemistry, Ultrastructure, Reactions. Walter de Gruyter.
Freiman, S., J., J. and Mecholsky, J., 2012. The Fracture of Brittle Materials: Testing and Analysis. John Wiley & Sons.
Gamstedt, E.K., Berglund, L.A. and Peijs, T., 1999. Fatigue mechanisms in unidirectional glass-fibre-reinforced polypropylene. Composites Science and Technology, 59(5): 759-768.
Garkhail, S.K., Heijenrath, R.W.H. and Peijs, T., 2000. Mechanical Properties of Natural-Fibre-Mat- Reinforced Thermoplastics based on Flax Fibres and Polypropylene. Applied Composite Materials, 7(5-6): 351-372.
Garrell, Shih, Lara, C. and Scattergood, 2003. Finite-element analysis of stress concentration in ASTM D 638 tension specimens. Journal of Testing and Evaluation, 31(1): 52-57.
Goutianos, S., Peijs, T., Nystrom, B. and Skrifvars, M., 2006. Development of Flax Fibre based Textile Reinforcements for Composite Applications. Applied Composite Materials, 13(4): 199-215.
Hamad, W., 2002. Cellulosic Materials: Fibers, Networks, and Composites. Kluwer Academic Publishers.
He, M.Y., Evans, A.G. and Curtin, W.A., 1993. The ultimate tensile strength of metal and ceramic-matrix composites. Acta Materialia, 41(3).
He, M.Y. and Hutchinson, J.W., 1989. Crack Deflection at an interface between dissimilar elastic-materials. International Journal of Solids and Structures, 25(9): 1053-1067.
Hein, V.L. and Erdogan, F., 1971. Stress singularities in a two-material wedge. International Journal of Fracture Mechanics, 7(3): 317-330.
Hojo, M., Sawada, Y. and Miyairi, H., 1994. Influence of clamping method on tensile properties of unidirectional CFRP in 0(degree) and 90(degree) directions--round robin activity for international standardization in Japan. Composites - Part A - Applied Science and Manufacturing, 25(8).
Hornsby, P.R., Hinrichsen, E. and Tarverdi, K., 1997. Preparation and properties of polypropylene composites reinforced with wheat and flax straw fibres: Part I Fibre characterization. Journal of Materials Science, 32(2): 443-449.
Hu, W., Ton-That, M.-T., Perrin-Sarazin, F. and Denault, J., 2010. An improved method for single fiber tensile test of natural fibers. Polymer Engineering & Science, 50(4): 819-825.
Hull, D., 1999. Fractography: Observing, Measuring, and Interpreting Fracture Surface Topography. Cambridge University Press.
Hull, D. and Clyne, T.W., 1996. An introduction to composite materials. Cambridge University Press.
Jiang, J., Wang, Z. and Chen, N., 2011. Natural fibre/polypropylene wrap spun yarns and preforms for structured thermoplastic composites. In: Y.J.D.Y. Tan (Editor), Advanced Material Science and Technology, Pts 1 and 2. Materials Science Forum, pp. 427-430.
Joffe, R., Andersons, J. and Wallstrom, L., 2003. Strength and adhesion characteristics of elementary flax fibres with different surface treatments. Composites Part A: Applied

Science and Manufacturing (Incorporating Composites and Composites Manufacturing), 34(7): 603-612.
Joyce, P.J., Violette, M.G. and Moon, T.J., 2002. Finite element analysis of unidirectional composite compression test specimens: A parametric study. Composite Materials: Testing, Design and Acceptance Criteria, 1416: 30-68.
Kim, J.K. and Pal, K., 2010. Recent Advances in the Processing of Wood-Plastic Composites. Springer.
Kolln, K. et al., 2005. Mechanical properties of cellulose fibres and wood. Orientational aspects in situ investigated with synchrotron radiation. Journal of Synchrotron Radiation, 12: 739-744.
Krstic, V.D., 1988. Porosity dependence of strength in brittle solids. Theoretical and Applied Fracture Mechanics, 10(3): 241-247.
Lamy, B. and Baley, C., 2000. Stiffness prediction of flax fibers-epoxy composite materials. Journal of Materials Science Letters, 19(11): 979-980.
Li, X., Tabil, L.G. and Panigrahi, S., 2007. Chemical treatments of natural fiber for use in natural fiber-reinforced composites: A review. Journal of Polymers and the Environment, 15(1): 25-33.
Lilholt, H. and Lawther, J., 2000. Natural organic fibres. Elsevier. In: A.a.Z. Kelly, C. (Editor), Comprehensive composite materials,. Elsevier, pp. 303-325.
Lubin, G. and Peters, S.T., 1998. Handbook of composites. Chapman & Hall.
Madsen, B., 2004. Properties of plant fibre yarn polymer composites – an experimental study, Technical University of Denmark
206 pp.
Madsen, B., Hoffmeyer, P. and Lilholt, H., 2007a. Hemp yarn reinforced composites - II. Tensile properties. Composites Part a-Applied Science and Manufacturing, 38(10): 2204-2215.
Madsen, B., Hoffmeyer, P., Thomsen, A.B. and Lilholt, H., 2007b. Hemp yarn reinforced composites - I. Yarn characteristics. Composites Part a-Applied Science and Manufacturing, 38(10): 2194-2203.
Madsen, B. and Lilholt, H., 2002. Compaction of plant fibre assemblies in relation to composite fabrication, 23. Risø international symposium on materials science, Roskilde, pp. 239-250.
Madsen, B. and Lilholt, H., 2003. Physical and mechanical properties of unidirectional plant fibre composites - an evaluation of the influence of porosity. Composites Science and Technology, 63(9): 1265-1272.
Madsen, B., Thygesen, A. and Lilholt, H., 2007c. Plant fibre composites - porosity and volumetric interaction. Composites Science and Technology, 67(7-8): 1584-1600.
Madsen, B., Thygesen, A. and Lilholt, H., 2009. Plant fibre composites - porosity and stiffness. Composites Science and Technology, 69(7-8): 1057-1069.
Malkapuram, R., Kumar, V. and Negi, Y.S., 2009. Recent Development in Natural Fiber Reinforced Polypropylene Composites. Journal of Reinforced Plastics and Composites, 28(10): 1169-1189.
Mehmood, S., 2009. Defect quantification of flax fibres. Risø DTU, Denmark.
Miao, M. and Shan, M., 2011. Highly aligned flax/polypropylene nonwoven preforms for thermoplastic composites. Composites Science and Technology, 71(15): 1713-1718.
Mieck, K.P., Lutzkendorf, R. and Reussmann, T., 1996. Needle-punched hybrid nonwovens of flax and PPFibers - Textile semiproducts for manufacturing of fiber composites. Polymer Composites, 17(6): 873-878.

Mohanty, A.K., Misra, M. and Hinrichsen, G., 2000. Biofibres, biodegradable polymers and biocomposites: An overview. Macromolecular Materials and Engineering, 276(3-4): 1-24.
Mott, L., Shaler, S. and Groom, L., 1996. A Technique to Measure Strain Distributions in Single Wood Pulp Fibers. Wood and Fiber Science, 28(4): 429-437.
Mukherjee, P.S. and Satyanarayana, K.G., 1986. An empirical evaluation of structure-property relationships in natural fibres and their fracture behaviour. Journal of Materials Science, 21(12): 4162-4168.
Müssig, J. and Stevens, C., 2010. Industrial Applications of Natural Fibres: Structure, Properties and Technical Applications. John Wiley & Sons.
Nattinen, K., Peltola, H., Madsen, B. and Joffe, R., 2011. Effects of process history on natural fibre properties in composites. Abstracts of Papers of the American Chemical Society, 241.
Neagu, R.C., Gamstedt, E.K. and Berthold, F., 2006. Stiffness Contribution of Various Wood Fibers to Composite Materials. Journal of Composite Materials, 40(8): 663-699.
Nevell, T.P. and Zeronian, S.H., 1985. Cellulose chemistry and its applications. E. Horwood.
Niu, H., Jiao, X., Wang, R. and Zhou, H., 2010. Direct manufacturing of flax fibers reinforced low melting point PET composites from nonwoven mats. Fibers and Polymers, 11(2): 218-222.
Nygard, P., Tanem, B.S., Karlsen, T., Brachet, P. and Leinsvang, B., 2008. Extrusion-based wood fibre-PP composites: Wood powder and pelletized wood fibres - a comparative study. Composites Science and Technology, 68(15-16): 3418-3424.
Okamoto, T., 2003. Recent developments in wood/plastic composites - Extrusion of wood-based materials. Mokuzai Gakkaishi, 49(6): 401-407.
Oksman, K., 2001. High quality flax fibre composites manufactured by the resin transfer moulding process. Journal of Reinforced Plastics and Composites, 20(7): 621-627.
Oksman, K., Skrifvars, M. and Selin, J.F., 2003. Natural fibres as reinforcement in polylactic acid (PLA) composites. Composites Science and Technology, 63(9): 1317-1324.
Page, D.H., 1969. A method for determining the fibrillar angle in wood tracheids. Journal of Microscopy, 90(2): 137-143.
Pickering, K.L., 2008. Properties and performance of natural fibre composites. Woodhead Publishing.
Pilato, L., 2010. Phenolic Resins: A Century of Progress. Springer.
Romhany, G., Karger-Kocsis, J. and Czigany, T., 2003. Tensile fracture and failure behavior of technical flax fibers. Journal of Applied Polymer Science, 90(13): 3638-3645.
Rong, M.Z., Zhang, M.Q., Liu, Y., Yang, G.C. and Zeng, H.M., 2001. The effect of fiber treatment on the mechanical properties of unidirectional sisal-reinforced epoxy composites. Composites Science and Technology, 61(10): 1437-1447.
Rowell, R.M., 2005. Handbook of wood chemistry and wood composites. CRC Press.
Saheb, D.N. and Jog, J.P., 1999. Natural fiber polymer composites: A review. Advances in Polymer Technology, 18(4): 351-363.
Sedighi-Gilani, M. and Navi, P., 2007. Experimental observations and micromechanical modeling of successive-damaging phenomenon in wood cells' tensile behavior. Wood Science and Technology, 41(1): 69-85.
Sridhar, M.K. and Basavarajappa, G., 1982. Indian Tex Res. J, 7(9): 87-89.
Staab, G.H., 1999. Laminar composites. Butterworth-Heinemann.
Sumere, V., 1992. Retting of flax with special reference to enzyme retting The biology and processing of Flax. CFM Publications, Belfast UK

Thomas, S. and Pothan, L., 2009. Natural fibre reinforced polymer composites: from macro to nanoscale. Éd. des Archives contemporaines.
Thouless, M.D. and Evans, A.G., 1988. Effects of pull-out on the mechanical properties of ceramic-matrix composites. Acta Metallurgica, 36(3): 517-522.
Thygesen, A., 2006. Properties of hemp fibre polymer composites - An optimisation of fibre properties using novel defibration methods and fibre characterisation. PhD thesis Thesis, Risø National Laboratory Roskilde.
Thygesen, A., Oddershede, J., Lilholt, H., Thomsen, A.B. and Ståhl, K., 2005a. On the determination of crystallinity and cellulose content in plant fibres. Cellulose, 12(6): 563-576.
Thygesen, L. and Asgharipour, M., 2008. The effects of growth and storage conditions on dislocations in hemp fibres. Journal of Materials Science, 43(10): 3670-3673.
Thygesen, L.G., Ander, P., Thygesen, L.G. and Ander, P., 2005b. Quantification of dislocations in spruce pulp and hemp fibres using polarized light microscopy and image analysis. Nordic Pulp and Paper Research Journal, 20(1): 64-71.
Thygesen, L.G., Eder, M. and Burgert, I., 2007. Dislocations in single hemp fibres-investigations into the relationship of structural distortions and tensile properties at the cell wall level. Journal of Materials Science, 42(2): 558-564.
Van de Velde, K. and Kiekens, P., 2001. Thermoplastic polymers: overview of several properties and their consequences in flax fibre reinforced composites. Polymer Testing, 20(8): 885-893.
Van de Velde, K. and Kiekens, P., 2003. Effect of Flax/PP panel process parameters on resulting composite properties. Journal of Thermoplastic Composite Materials, 16(5): 413-431.
Van de wejenberg I, I.J., Verpoest I, 2000. Proceedings of ECCM9, Bringhton.
Van de Weyenberg, I., Chi Truong, T., Vangrimde, B. and Verpoest, I., 2006. Improving the properties of UD flax fibre reinforced composites by applying an alkaline fibre treatment. Composites Part A: Applied Science and Manufacturing, 37(9): 1368-1376.
Vinson, J.R., Taya, M., Fibers, A.C.D.-o.H.M., Composites, T. and Fatigue, A.C.E.-o., 1985. Recent advances in composites in the United States and Japan: a symposium. ASTM.
Virk, A.S., Hall, W. and Summerscales, J., 2010. Failure strain as the key design criterion for fracture of natural fibre composites. Composites Science and Technology, 70(6): 995-999.
Wallenberger, F.T. and Weston, N.E., 2004. Natural fibers, plastics and composites. Kluwer Academic Publishers.
Wang, F., Toftegaard, H., Hendriksen, P.V. and Sørensen, B.F., 2006. Tensile mechanical properties of bi-layer structure for solid oxide fuel cells, CompTest Composites Testing and Model Identification, Portugal.
Wang, R., Guo, X. and Jiao, X., 2005. Method for fabricating non-woven fabric from flax and composite material. Univ Tianjin Polytechnic.
Wang, T.C., 1991. Orthotropy rescaling and implications for fracture in composites. International Journal of Solids and Structures, 28(2): 235-248.
Wolcott, M.P. and Englund, K., 1999. A technology review of wood-plastic composites. 33rd International Particleboard/Composite Materials Symposium, Proceedings. Washington State Univ Press, Pullman, 103-111 pp.
Wool, R.P. and Sun, X.S., 2005. Bio-Based Polymers and Composites. Materials & Mechanical. Academic Press, 1-640 pp.

Wool, R.P., Sun, X.S. and ScienceDirect, 2005. Bio-based polymers and composites [electronic resource]. Elsevier Academic Press, Amsterdam ; Boston :, 1-xix, 620 p pp.

Xia, Z. and Curtin, W.A., 2000. Tough-to-brittle transitions in ceramic-matrix composites with increasing interfacial shear stress. Acta Materialia, 48(20): 4879-4892.

Zafeiropoulos, N.E. and Baillie, C.A., 2007. A study of the effect of surface treatments on the tensile strength of flax fibres: Part II. Application of Weibull statistics. Composites Part a-Applied Science and Manufacturing, 38(2): 629-638.

Zafeiropoulos, N.E., Dijon, G.G. and Baillie, C.A., 2007. A study of the effect of surface treatments on the tensile strength of flax fibres: Part I. Application of Gaussian statistics. Composites Part a-Applied Science and Manufacturing, 38(2): 621-628.

Zhigang, S., 1990. Delamination specimens for orthotropic materials. Transactions of the ASME. Journal of Applied Mechanics, 57(3): 627-634.

APPENDIX:

Conference paper

[A1] Aslan, M., Mehmood, S., Madsen, B., Goutianos, S. The effect of processing on defects and tensile strength of single flax fibres, Proceedings of the 14th European Conference on Composite Materials (ECCM-14), 7-10 June 2010: Budapest, Hungary

Published paper

[A2] Aslan, M., Chinga-Carrasco, G., Sørensen, B.F. Madsen, B., (2011) Strength variability of single flax fibres, Journal of Materials Science 46:6344–6354. DOI: 10.1007/s10853-011-5581-x

Paper manuscript

[A3] Aslan M., Mehmood S., Madsen B., Effect of consolidation pressure on volumetric composition and stiffness of unidirectional flax fibre composites. (to be submitted to Composites Part A)

Submitted paper

[A4] Aslan, M., Sorensen, B.F., Tab design for uniaxial tensile test specimens of composite materials. (submitted to Composite Part A)

[A1]

Conference paper

Aslan, M., Mehmood, S., Madsen, B., Goutianos, S.

The effect of processing on defects and tensile strength of single flax fibres

Proceedings of the 14th European Conference on Composite Materials (ECCM-14), June 2010

14TH EUROPEAN CONFERENCE ON COMPOSITE MATERIALS
7-10 June 2010, Budapest, Hungary
Paper ID: 539-ECCM14

THE EFFECT OF PROCESSING ON DEFECTS AND TENSILE STRENGTH OF SINGLE FLAX FIBRES

M. Aslan*, S. Mehmood, B. Madsen, S. Goutianos

*Materials Research Division, Risø National Laboratory for Sustainable Energy, Technical University of Denmark,**
**muas@risoe.dtu.dk*

ABSTRACT

Natural fibres have received increasing attention as reinforcement in composite applications. However, the fibre strength shows a large variation due to variability in composite-like structure of fibre morphology and defects depending on the degree of the fibre processing. The fibre strength also affects the composites strength, limiting their application in load bearing structural components. In order to improve the composite properties, novel methods for fibre processing from the natural plants are required.

Single flax fibres were extracted from flax samples that were processed by two different processing steps. The numbers and sizes of defects were quantified from images by polarized optical microscope and fibre fracture surfaces were examined under environmental scanning electron microscope. Single fibre tensile tests were performed to measure tensile strength, Young's modulus and failure strain.

It is shown that the tensile strength and Young's modulus of the fibres depend critically on defects in the fibres, which may either be induced naturally during growth of the plant or be induced during processing of the fibres. It was found that increasing processing steps leads to an increasing number of defects and larger defect sizes, thereby decreasing tensile strength and Young's modulus of the fibres.

1. Introduction

Natural fibres have great variability in the morphological structure due to variation in environment, maturity of the plant as well as the adopted retting and decortication processes [1]. Therefore, morphological characterization has to be done before fibres can be used as reinforcement in composite materials in order to assess their performance. Due to high variability in their mechanical properties they are often employed only in low graded applications [2]. In particular, it has been found that the strength of natural fibres is critically affected by the defects and damage inside or at surface of the fibres. These defects may either occur naturally or be induced during the processing stages [3].

Flax fibres are located in the outer part of the stem of the flax plant. The fibres are extracted from the plant by retting and a series of mechanical processes. Firstly, field retting is used as a defibration step to degrade the binding between the fibres in the outer layer of the stem and the shives in the middle of the stem. The retting process leads to great variability in the quality of the fibres dependent on the

uncontrollable weather conditions and the nature of attacking microorganisms. Secondly, the retted stems are mechanically decorticated to separate the fibre bundles (technical fibres). The decortication process has a negative influence on the fibre quality, and this is particularly critical for the production of fibres for high graded applications such as reinforcement in composite materials. Thus, milder and more effective defibration and decortication processes must be developed before natural fibres can compete with synthetic fibres [4].

The aim of this study is to investigate the influence of consecutive processing steps on the amount of defects and the mechanical properties (tensile strength, Young's modulus, failure strain) of single flax fibres.

2. Experimental

2.1. Material

The flax fibres in this study were supplied by Ekotex from Poland. Two different types of flax fibres are used and described below:
- Stem fibres: The fibre stems are field retted after harvesting. The fibres were not subjected to any kind of mechanical treatments.
- Noils fibres: Firstly, the field retted fibre stems are broken into smaller parts by passing them between rollers. Afterwards, the fibre bundles in the outer part of the stems were separated from the broken woody core parts by a scutching process where the stems are passed between rollers equipped with knives. In this process, the knives scrape along the fibre and they are thereby introducing defects to the fibres. The obtained long scutched fibre bundles are still relatively coarse. The coarse fibre bundles are cut and the fibre's ends are tore off in a hackling process in order to get straightened and thinner fibre bundles, and to purify them. After hackling of the long scutched fibres, the fibres are divided into long hackled fibres and short fibres. The short fibres are the so-called Noils fibres [5].

2.2. Sample preparation and experimental set-up for defect quantification

Individual fibres were carefully extracted by hand from the Stem and the Noils fibre bundles. The single fibres were subsequently cleaned by ultrasound in deionised water bath for approximately 10 minutes. It was necessary to clean the fibres in order to get rid of impurities: grease and other dust particles and also to make the defects visible. The cleaned fibres were then glued on both ends to glass plates using a double sided tape under an optical microscope to avoid uneven surface and twisting of the fibres. Since an optical microscope has a low depth of field, the fibres need to be straightened

The fibres were analysed by using a Leitz optical microscope equipped with polarisation filters. Cross polarised light was used to make the defects appear as bright or dark patterns in the fibres. Light intensity and fibre angle to the polarised filters is required to be constant in order to get reliable results for defect quantification [6]. Five fibre samples of each fibre type were analysed in order to quantify the total number of defects. For each sample, a length of approximately 6 mm was scanned under the microscope.

2.3. Sample preparation and experimental set-up for mechanical testing

Single fibres were separated manually from the fibre bundles. The fibres were too delicate for manual handling and a cardboard was used as a specimen holder to facilitate the testing. Firstly, a rectangular cardboard (10cm x 1cm) was punched with hole of 5 mm diameter at the centre. The fibre ends were then fixed to the cardboard using cyanocrylate adhesive in such a way that the middle part of the fibre was placed above the hole. The tensile test was performed with a constant cross head speed of 0.5 mm/min on an electromechanical test machine equipped with a 50 N load cell. The cardboard was gripped in the jaws of the tensile machine close to the places where the fibre was mounted. The cardboard was then cut on both sides of the hole so that the fibre was carrying the full load alone between jaws. Approximately 50 fibres were tested for each fibre type (Stem and Noils). All testing was conducted at an ambient temperature of about 23°C and a relative humidity of about 55%.

The fibre dimensions were measured with an optical microscope. Since it was impossible to determine the cross section shape of the fibres, all fibres were assumed to be perfectly circular in cross section. Fibre diameters were measured at 9 different positions along the fibre and an average diameter was calculated for each fibre. The stress (σ) was calculated by the ratio of the load to the cross sectional area of the fibre.

$$\sigma = \frac{F}{A} = \frac{4F}{\pi d^2}$$

2.4. Fibre Surface Characterisation and Fracture Surfaces

The fracture surfaces of the fibres were examined under an environmental scanning electron microscope (ESEM). An ESEM is well suited for the investigation of biological materials since biological samples can be investigated in wet state at high magnifications. In the present study, ESEM is also used for surface defect characterization of fibres in order to get images with a high depth of field and resolution

3. Results and discussions

3.1. Defects Quantification

The individual fibres were observed to have many defects along their lengths. The defects were counted and their size was measured. Figure 1 shows that the fibre defects are observed as different size of transversal patterns in the polarised micrographs.

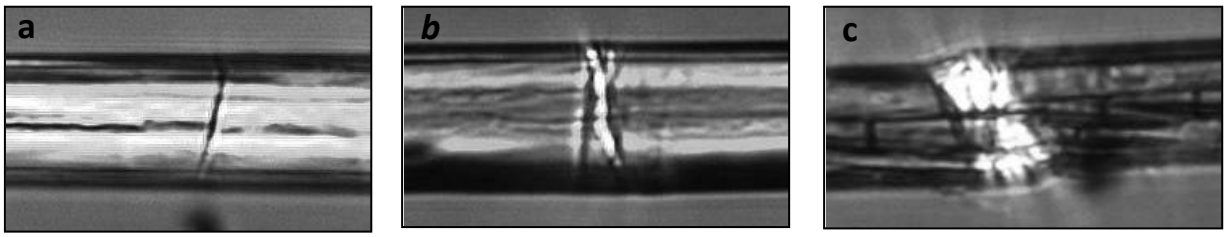

Figure 1: Defects on fibres observed by polarized optical microscope. Fibre diameters in all images are ca. 20µm

The defects that are seen as slightly bright or dark lines across the fibre (Figure 1a and 1b) are due to small changes in the angle of the cellulose microfibrils. These defects cannot be observed on the fibre surface with ESEM (results not shown). However, the larger defects (Figure 1c) denoted kink bands slip planes or compressed zones can be clearly observed with ESEM (see Figure 5).

Characteristic images from each differently processed fibre types obtained by using polarized optical microscope are reported in Figure 2. The Stem fibres seem to have a smooth surface with small defects whilst the Noils fibres have more and larger defects.

The number of defects was manually counted and is given in Table 1. It is seen from the results that the number of defects was increased by mechanical processing of fibres. Hence, the Noils fibres have higher number of defects per mm than the Stem fibres (28 vs. 20 defects per mm). In addition, a larger part of the fibre surface is covered by defects in the Noils fibres compared to the Stem fibres (a total width of defects of 0.37 vs. 0.20 mm per mm).

	Defect counts per mm	**Total width of defects per mm (mm/mm)**
Stem	20 ±10	0.20 ± 0.12
Noils	28 ± 6	0.37 ± 0.07

Table 1: Mean ± standard deviation values for defects counts and size in per mm of fibre length

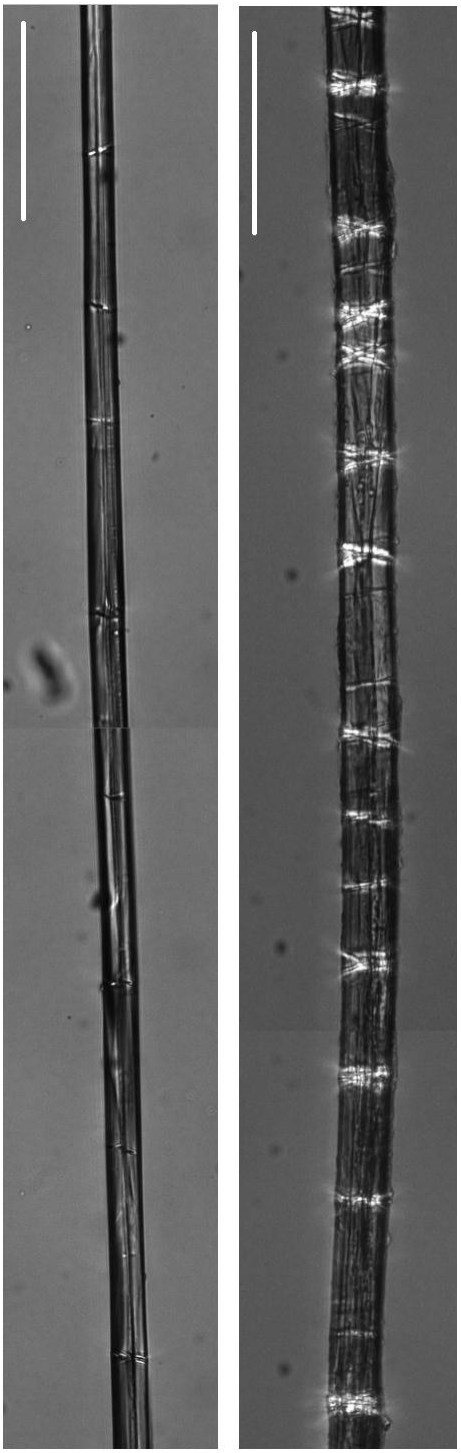

Figure 2: Representative images of the two types of flax fibres: Stem (left) and Noils (right) fibres. The defects can be seen as bright and dark lines across the fibres. The scale bars in both images are ca. 100µm.

3.2.Mechanical Properties of Single Fibres

Figure 3 shows typical curves of stress and strain for the Stem and the Noils fibres

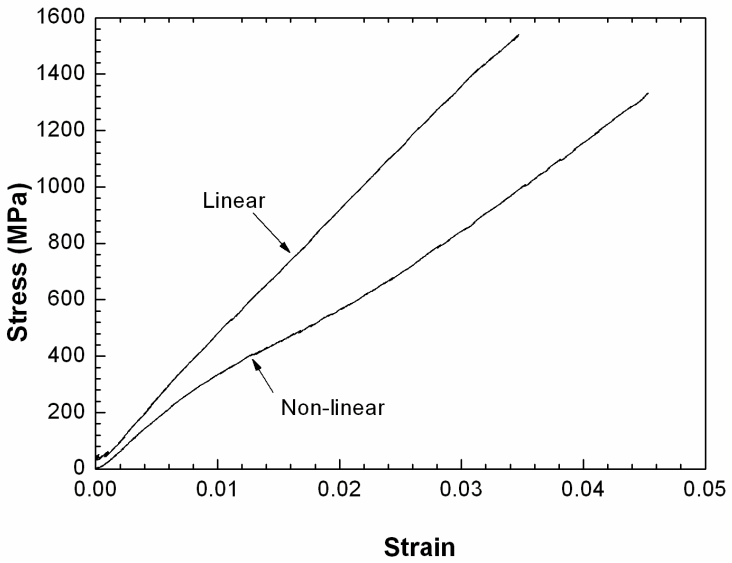

Figure 3. Representative stress-strain curves of single flax fibres.

The flax fibres showed some variation in their stress-strain behaviour. Some fibres showed essentially a linear stress-strain relationship. Other fibres showed a distinctive non-linear behaviour. Linear stress-strain behaviour was predominantly seen in the Stem fibres. The Noils fibres have much more non-linear stress-strain curves as shown in Table 2. The non-linear behaviour may be explained by an increased microfibril angle (above 10°) in the defect regions. It is known that the microfibril angle is higher in damaged regions than in defect free regions [7]. Since the mechanical processed Noils fibres have more defects than the Stem fibres, the non-linear stress-strain behaviour of the Noils fibres can be attributed to the presence of the defects.

	Fibre Diameter [µm]	**Tensile Strength [MPa]**	**Failure Strain [%]**	**Young's Modulus [GPa]**	**Number of Curve Types***	
					Linear	**Nonlinear**
Stem	16.3 ± 2.6	1445 ± 553	2.9 ± 0.6	52 ± 16	21	1
Noils	18.9 ± 3.6	812 ± 342	2.9 ± 0.9	30 ± 11	9	19

Table 2: Mean ± standard deviation values for diameter, tensile strength, failure strain, Young's modulus and number of typical stress-strain curve types of single flax fibres.

Mechanical properties of nearly 50 single flax fibres were acquired from tensile tests and they are summarised in Table 2. A trend of decreasing tensile strength and decreasing Young's modulus as a result of processing is observed. Hence, the Stem fibres had a higher tensile strength and Young's modulus than the Noils fibres. However, failure strain of the two fibre types were similar. As can be seen from the standard deviations, the Stem fibres exhibit a larger scatter in tensile strength and Young's modulus than the Noils fibres.

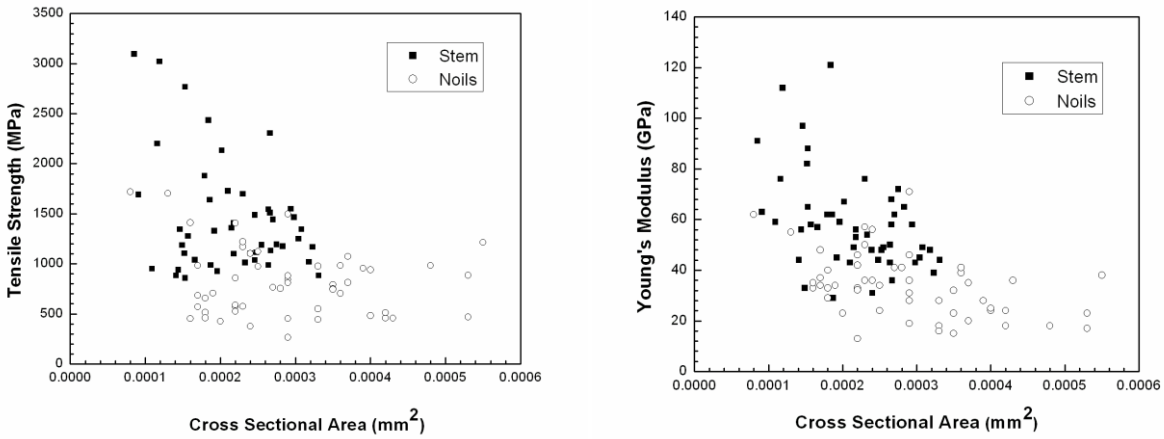

Figure 4. Tensile strength and Young's modulus as a function of cross sectional area for the two different types of single flax fibres.

The relationship between the mechanical properties (tensile strength and Young's modulus) and the cross sectional area of the fibres is shown Figure 4. Although the figure shows a large scatter in results, a major trend is that both the fibre strength and Young's modulus decrease when the cross sectional area of the fibres increases. It can be seen that the mechanically treated Noils fibres show lower scatter than the Stem fibres. Large scatter of mechanical properties may be due to non-circular cross-sectional area of the fibres. Both the tensile strength and Young's modulus for the Stem and the Noils fibres given in Table 2 are in good agreement with data from literature [1,8].

3.3.Morphological Analysis of Fibres

The appearance of defects sometimes depends on whether the fibre is investigated with optical microscope or environmental scanning electron microscope (ESEM). Figure 5 shows an example of the same defect observed by optical microscope and by ESEM. Since the fibre has some clear transverse marks on the surface (denoted kink bands, slip planes, buckling), it is possible to make observations with ESEM. However, small defects may not always be possible to see on fibre surface with ESEM, although they can be clearly seen with polarized optical microscope. Therefore, quantification of defects on flax fibres in the present study were done with polarized optical microscope where defects inside the fibres can be seen.

ESEM micrographs of fractured flax fibres are presented in Figure 6. The fibre surfaces are shown to be rough and a large amount of impurities are attached to surface. Fibre fracture occurred differently on outer surface and inside of the cell wall layers.

In addition to large transversal defects, which are most visible type of defects longitudinal defects can also be clearly seen on the surface (figure 6b). The crack propagation seems to be along the longitudinal defects. It appears from ESEM micrographs (Figure 6a) that transversal defects are points of crack initiation, and the fibre then continues to split along the longitudinal defects until faced with another transversal crack. Figure 6d shows an example of a fibre that has failed in a different way. The

surface layers show shear failure with fibrillation along the fibre direction. However, the inner layers show transversal failure. Similar results have been reported in the literature [8, 9].

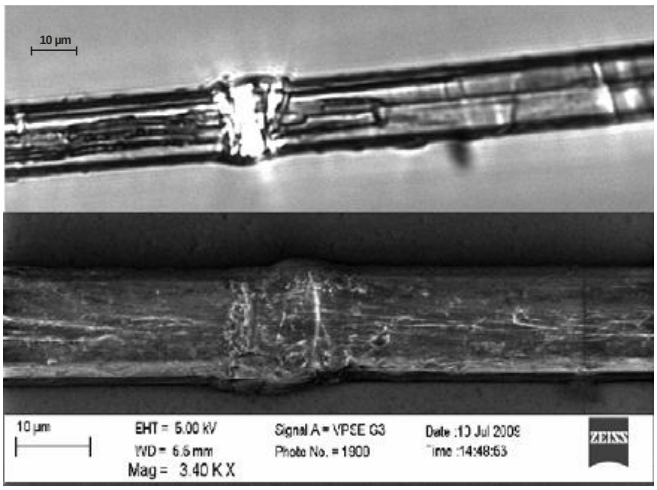

Figure 5: Comparison of the same large defect on the fibre observed by optical microscope (top) and ESEM (bottom).

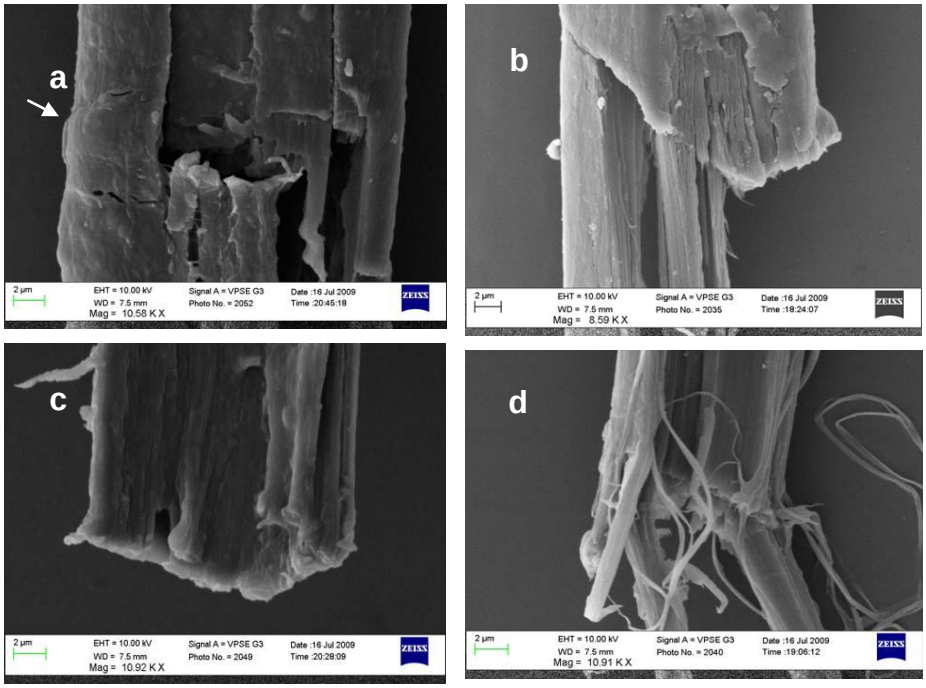

Figure 6. ESEM micrograph of flax fibres; a) The white arrows show transversal crack initiation on the flax fibre which is started at a fibre defect region, b) shows longitudinal cracks on the fibre along with micro fibrillar units on the fibre surface and inner layers, c) fracture surface with smooth and blunt ending, d) fracture surface with fibrillated fine structure and also surface layer with transversal crack path with smooth ending even though inner layers have longitudinal crack and fibrils.

4. Summary

The defect on flax fibres were quantified by polarised optical microscope and ESEM. The tensile test of single fibres was performed in order to show the effect of processing on: defect size, defect number and mechanical properties of flax fibres. The major results of the study are:

- Tensile strength and Young's modulus of flax fibres decreased as an effect of processing, but failure strain was unchanged.
- Increase in defect number and defect size was well correlated with a decrease in tensile strength and Young's modulus of the fibres.
- Fracture surfaces are followed on inner cell wall longitudinally and on outer cell wall transversely.

Acknowledgement

The authors thank Senior Scientist Bent F. Sørensen for valuable advices. The research has been partly funded by the European Community's Seventh Framework Programme (FP7/2007-2013) under grant agreement nº 214467 (NATEX) and WOODFIBRE3D

References

1. Charlet K., Baley C., Morvan C.: Characteristic of Hermes flax fibres as function of their location. Composites: Part A, **38**, 1912-1921 (2007).
2. Bleddzki K, Gassan SJ.: Composites reinforced with cellulose based fibres. Prog Polym Sci, **24**, 221–74 (1999).
3. Davies G. C., Bruce D. M.: Effect of environmental relative humidity and damage on the tensile properties of flax and nettle fibers. Textile Res J., **68**, 623–629 (1998).
4. Meijer, W.J.M., Vertregt, N., Rutgers, B., Van de Waart, M.: The pectin content as a measure of the retting and rettability of flax. Ind. Crops Prod. **4**, 273-284 (1995).
5. Cierpucha W., Kozlowski R., Mankowski R., Wasko J Mankowski T.: Applicability of flax and hemp as raw materials for production of cotton-like fibres and blended yarns in Poland. Fibres&textiles in eastern Europe, **12,** 3(47), 13-18 (2004).
6. Thygesen L.G., Jørgen B. B., Sørensen P. H.: Visualization of dislocations in hemp fibres: A comparison between scanning electron microscopy (SEM) and polarized light microscopy (PLM), Industrial Crops and Products **24**, 181–185 (2006).
7. Baley C.: Analysis of the flax fibres tensile behavior and analysis of the tensile stiffness increase Composites: Part A, **33**, 939–948 (2002).
8. Thygesen L.G., Eder M., Burgert I.: Dislocations in single hemp fibres-investigations into the relationship of structural distortions and tensile properties at the cell wall level. J. Mater Sci., **42**, 558-564 (2007).
9. Bos H.L., Donald M. A.: In situ ESEM study of the deformation of elementary flax fibres Journal of Materials science, **34** 3029-3034 (1999).

[A2]

Published paper

Aslan, M., Chinga-Carrasco, G., Sørensen, B.F. Madsen, B.

Strength variability of single flax fibres

Journal of Materials Science (2011) 46:6344–6354

J Mater Sci (2011) 46:6344–6354
DOI 10.1007/s10853-011-5581-x

Strength variability of single flax fibres

Mustafa Aslan · Gary Chinga-Carrasco · Bent F. Sørensen · Bo Madsen

Received: 3 March 2011 / Accepted: 20 April 2011 / Published online: 12 May 2011

Abstract Due to the typical large variability in the measured mechanical properties of flax fibres, they are often employed only in low grade composite applications. The present study aims to investigate the reasons for the variability in tensile properties of flax fibres. It is found that an inaccuracy in the determination of the cross-sectional area of the fibres is one major reason for the variability in properties. By applying a typical circular fibre area assumption, a considerable error is introduced into the calculated mechanical properties. Experimental data, together with a simple analytical model, are presented to show that the error is increased when the aspect ratio of the fibre cross-sectional shape is increased. A variability in properties due to the flax fibres themselves is found to originate from the distribution of defects along the fibres. Two distinctive types of stress–strain behaviours (linear and nonlinear) of the fibres are found to be correlated with the amount of defects. The linear stress–strain curves tend to show a higher tensile strength, a higher Young's modulus, and a lower strain to failure than the nonlinear curves. Finally, the fibres are found to fracture by a complex microscale failure mechanism. Large fracture zones are governed by both surface and internal defects; and these cause cracks to propagate in the transverse and longitudinal directions.

M. Aslan (✉) · B. F. Sørensen · B. Madsen
Materials Research Division, Risø National Laboratory for Sustainable Energy, Technical University of Denmark, Frederiksborgvej 399, 4000 Roskilde, Denmark
e-mail: muas@risoe.dtu.dk

G. Chinga-Carrasco
Paper and Fibre Research Institute, Høgskoleringen 6b, 7491 Trondheim, Norway

Introduction

The utilisation of renewable resources is of crucial importance for advancing towards a sustainable way of producing materials. Natural fibres are renewable resources that are used in a wide range of industrial applications such as textiles and increasingly in polymer composites, as an alternative to synthetic fibres. Flax fibres (*Linum usitatissimum*) are widely studied plant-based natural fibres for use as reinforcement in polymer matrix composites [1–7].

Flax fibres are known to show a large variability in their measured mechanical properties [2, 3]. Due to uncertainties about the reasons for the variability of fibre properties, and the influence of this variability on the final mechanical properties of the composites, flax fibres are often employed only in low grade composite applications [4]. The variability in fibre properties can be ascribed either to the variability introduced by the applied experimental characterisation method, or to the inherent variability of the flax fibres themselves. A typical approach of evaluating the cross-sectional area of the fibres as being circular, and to use the measured fibre 'diameter' to calculate the cross-sectional area is a rough approximation since the fibres have a polygonal shape [3, 5–8]. Furthermore, the fibres are known to vary in their cross-sectional area along the fibre length [9]. Altogether, any uncertain evaluation of the cross-sectional area brings a variation into the determined mechanical properties of the fibres [10]. In addition, flax fibres are delicate materials with cross-sectional dimensions in the order of micrometers, and a few millimeters in length; this enhances measurement errors during the mechanical testing of the fibres. Flax fibres themselves show variability in their cell wall structure due to variations in growth conditions, different levels of maturity of the fibres, as well as due to the non-uniformity of the retting

and decortication processes applied to extract the fibres from the plants. One type of structural characteristics in flax fibres are the so-called kink bands which are regions of the cell wall with a disordered organisation of the cellulose microfibrils in the matrix of hemicellulose and lignin. The kink bands are formed both naturally during growth, and artificially during fibre processing. The kink bands are presumed to act as defects influencing the mechanical behaviour of the fibres [2].

The aim of the present study is to investigate the various reasons for the variability in mechanical properties of single flax fibres. The experimental-based investigations include analyses of the applied method for determination of the cross-sectional area of the fibres, together with analyses of the different types of stress–strain behaviours, and fracture behaviours of the fibres. An attempt is made to correlate the latter two types of mechanical behaviours with the defect regions of the fibres.

Materials and methods

Materials

The flax fibres (*Linum usitatissimum*) were supplied by Ekotex, Poland. Two types of differently processed fibres were used. The two types of fibres were originating from different fields, and as such they are not coming from the same batch.

Green fibres

These fibres were obtained from plant stems that have been harvested with no further processing. Single fibres were carefully separated from the stems by hand.

Cottonized fibres

After the plant stems were harvested, they were kept in the field for retting. Afterwards, the fibre bundles in the outer part of the stems were separated from the broken shives in the core part by a decortication process where the stems were crushed and beaten by passing them between rotating wheels equipped with blunt knives. Next, the coarse fibre bundles were combed in a hackling process in order to get straightened fibres and thinner fibre bundles. Finally, to further disintegrate the fibre bundles into single fibres, they were cottonized by a mechanical process [11, 12]. Single fibres were separated carefully from the fibre bundles by hand.

Measurement of cross-sectional area of fibres

A precise determination of the cross-sectional area of the fibres is crucial for the calculation of the correct tensile stress values. Since the fibres have irregular polygonal shapes, errors can easily arise in the cross-sectional measurements. In the present study, the cross-sectional area of the fibres was measured with two different methods.

Method 1: circular fibre area measurements

An optical microscope (Aristomet, Leitz) equipped with polarised filters, and image analysis software (Image-Pro Plus 5.0) was used to measure the fibre width with an accuracy of ± 0.1 μm at 9 positions along the fibres within a gauge length of 5 mm (see Fig. 1). The cross-sectional area was calculated by assuming a circular cross-section.

Method 2: true fibre area measurements

The fibres were placed in a plastic holder to avoid tilted cross-sections, and to align the fibres. The fibres were then embedded in epoxy resin (EpoFix, Struers). The embedded fibre samples were ground and polished as described by Reme et al. [13]. A series of cross-sectional images were acquired at different locations using a Hitachi S-3000 variable pressure scanning electron microscope with a solid-state backscattered detector. The digital images were processed automatically with the PFI Fibre Cross-Section ImageJ plugin (version 3k). The images were thresholded. Touching fibres, fibre agglomerates and apparently misaligned fibres were removed by applying a combination of size, form factor and solidity shape measurements (see Fig. 2), as described by Chinga-Carrasco et al. [14].

Figure 3 shows a schematic drawing of the cross-sectional areas that were determined by the two different methods. A_{circ} is the circular fibre area determined by Method 1. A_{true} is the true fibre area and A_{lum} is the area of the lumen determined by Method 2. The cell-wall area is given by $A_{\text{cw}} = A_{\text{true}} - A_{\text{lum}}$. In addition, in Method 2, the shape of the fibre cross-sections was quantified by their aspect ratio, which is the ratio between the major and minor axis of a fitted ellipse with an area equivalent to the

Fig. 1 Optical microscope image of single flax fibre used for measurements of fibre width (Method 1)

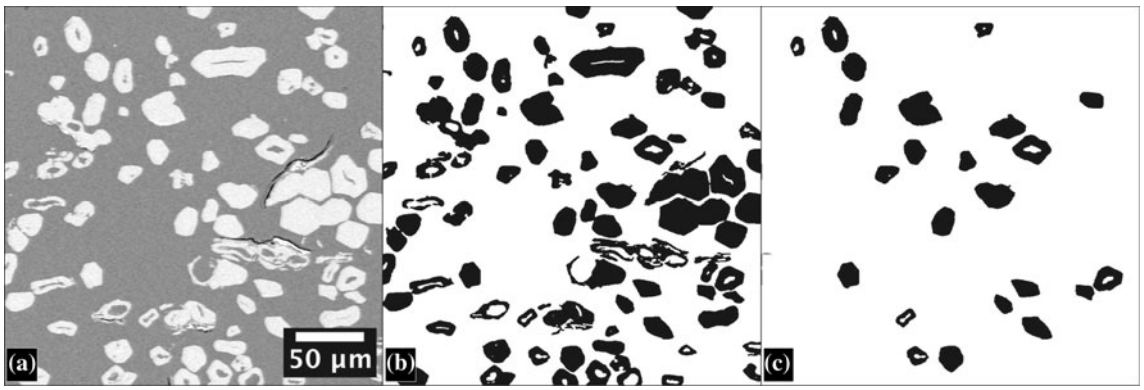

Fig. 2 Scanning electron microscope images of flax fibre cross-sections used for the measurements of fibre area (Method 2): **a** unprocessed image, **b** binary image, **c** processed image where fibres that were not suitable for measurements were automatically removed

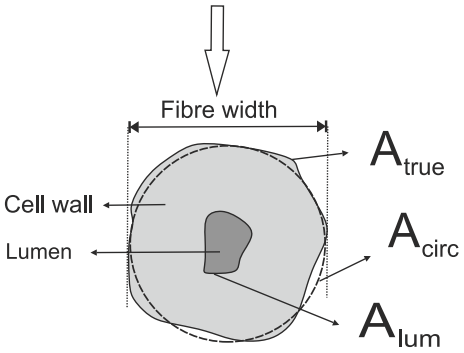

Fig. 3 Schematic drawing of the cross-sectional fibre areas that were determined by the two different methods (Methods 1 and 2)

fibre cross-sectional area, and with the same first and second degree moments (Image-Pro Plus 5.0). The aspect ratio is always ≥ 1.

Tensile testing of fibres

Single flax fibres were inspected with an optical microscope in order to exclude double fibres, and highly deformed and twisted fibres. Since the fibres are too delicate for manual handling, cardboard was used as a specimen holder to facilitate the testing. The fibre ends were fixed to the cardboard using cyanoacrylate glue. Prior to the tensile testing, using the optical microscope, the average fibre width was determined from 9 width measurements along the 5 mm gauge length, and the circular fibre area was calculated (Method 1). The cardboard was gripped in the plastic grips of the tensile test machine (ElectroPuls E3000, Instron) close to the places where the fibre was mounted. The cardboard was then cut on both sides of the central hole. The tensile tests were performed with a constant cross head speed of 0.5 mm/min. The load was measured using a 50 N load cell. The testing was done according to the ASTM D 3379 at an ambient temperature

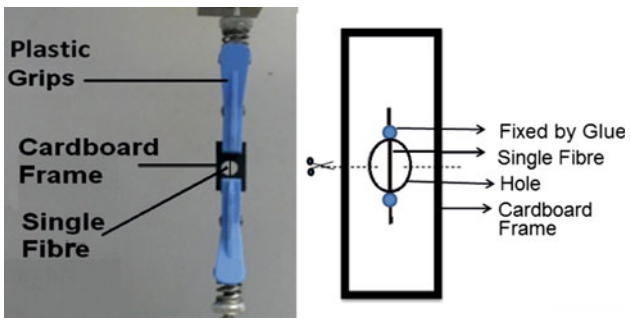

Fig. 4 Experimental setup for the tensile testing of single flax fibres

of about 23 °C and a relative humidity of about 55%. Figure 4 shows the testing configuration used. In total, 35 Green fibres, and 50 Cottonized fibres were successfully tested (15 Green fibre samples were discarded due to failure nearby the glue region).

Fracture surface of fibres

The fracture surfaces of the tensile tested fibres were examined in an environmental scanning electron microscope (ESEM, Zeiss). In addition, detailed surface images of intact fibres were acquired with an ultra field-emission SEM (FESEM, Zeiss) in the secondary electron mode.

Results

Cross-sectional area

Figure 5 shows the cross-sectional area distributions that were determined for single flax fibres (Cottonized fibres) using the two different measurement techniques, Method 1 and Method 2. The results obtained using the circular fibre area measurements (Method 1) are in the same range as the

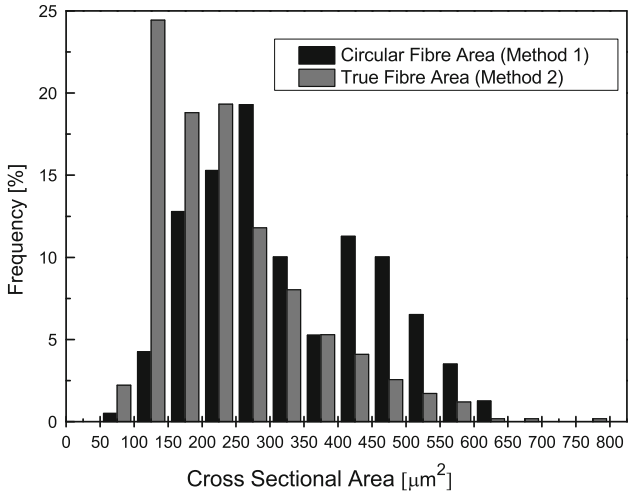

Fig. 5 Frequency distributions of fibre areas that were measured by the two different methods (Methods 1 and 2)

Table 1 Mean and standard deviation values of cross-sectional area and aspect ratio determined by Method 1 and Method 2 for two large groups of flax fibres (Cottonized fibres)

	Fibre counts	Mean ± SD
Circular fibre area, A_{circ} (μm^2) (Method 1)	399	327 ± 128
True fibre area, A_{true} (μm^2) (Method 2)	585	236 ± 115
Lumen content (%) (Method 2)	585	1.6
Aspect ratio (–) (Method 2)	585	1.42 ± 0.26

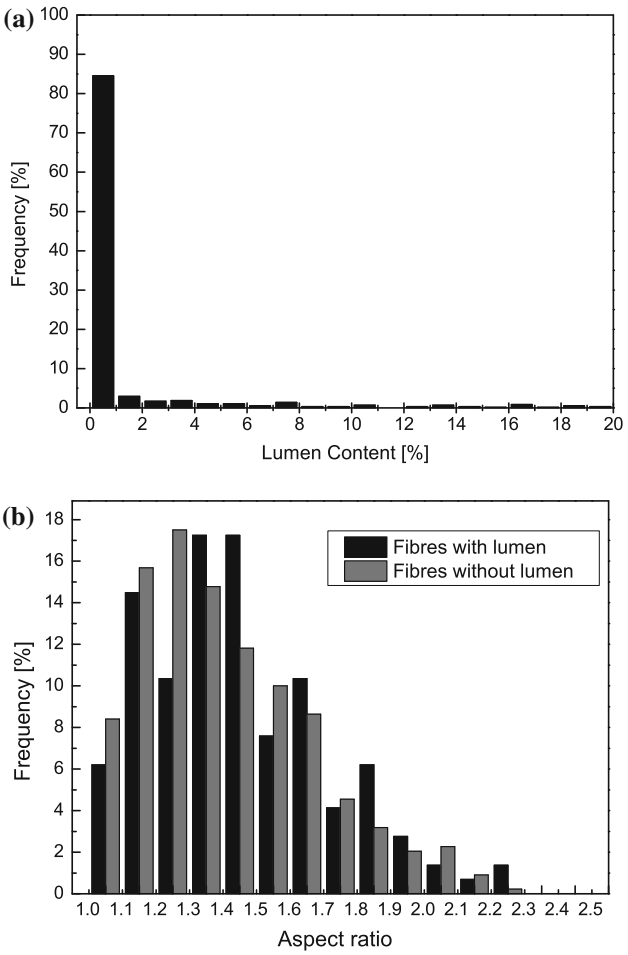

Fig. 6 Frequency distributions of the measured **a** lumen content and **b** aspect ratio of fibres (Method 2)

true fibre area measurements (Method 2). For both methods, 95% of fibres were distributed in the range of 100 to 650 μm^2. However, the distribution of Method 1 is shifted to the right of the distribution for Method 2 with mean ± SD fibre areas of 327 ± 128 and 236 ± 115 μm^2, respectively (Table 1). Thus, on an average basis, the area of fibres determined by Method 1 is 39% higher than the area determined by Method 2; see, however, the results below about the influence of the fibre shape.

Figure 6a shows that the lumen content (ratio of the lumen area to the true fibre area) of the fibres is typically very small although some large values of lumen content were found. Hence, it is found that 85% of all fibres show a lumen content below 1%. The mean lumen content is 1.6%.

The distribution of aspect ratios of the shape of fibre cross-sections is presented in Fig. 6b. Distributions are shown for fibres with lumen and without lumen. The aspect ratios are in the range of 1.0–2.3 and with means ± SD of 1.45 ± 0.27 and 1.40 ± 0.12, for fibres with lumen and without lumen, respectively. The grand mean ± SD aspect ratio of all fibres is 1.42 ± 0.26.

The results presented in Table 1 are for two large groups of fibres that did not consist of the exact same fibres. In order to compare the measurements of the exact same fibres, one group of 6 fibres was randomly selected. The circular area of each of the fibres was first determined by Method 1, and then the fibres were embedded in epoxy resin and the true area of each of the fibres was determined by Method 2 at several locations along the fibres. The measured cross-sectional areas and aspect ratios for these 6 fibres are shown in Table 2. It is seen that the percentage difference (in absolute values) in the area measurements between the two methods is consistently increased when the aspect ratio of the fibres is increased. For a low aspect ratio of 1.1, the area difference is only 3%, whereas the area difference is 37% for a high aspect ratio of 1.9. The results also point towards that the area determined by Method 1 is being overestimated for fibres with low aspect ratios, and it is being underestimated for fibres with high aspect ratios. The threshold aspect ratio is in the range of about 1.5–1.8.

Table 2 Mean and standard deviation values of cross-sectional area and aspect ratio determined by Method 1 and Method 2 for one group of 6 flax fibres (Cottonized fibres)

Fibre number	Circular fibre area, A_{circ} (Method 1) (μm^2)	True fibre area, A_{true} (Method 2) (μm^2)	Relative area difference, Δ_{area} (%)	Aspect ratio[a] (major axis/minor axis)
1	280 ± 30	273 ± 35	3	1.14 ± 0.04
2	280 ± 17	265 ± 40	6	1.41 ± 0.14
3	215 ± 25	194 ± 5	11	1.50 ± 0.15
4	240 ± 30	268 ± 30	−10	1.80 ± 0.19
5	316 ± 20	432 ± 31	−27	1.78 ± 0.17
6	224 ± 29	356 ± 15	−37	1.89 ± 0.13

[a] Aspect ratio of an ideal circular shape is equal to 1.0

Stress–strain behaviour

Initially, all the measured stress–strain curves were evaluated based on their curve shapes. The curves evaluated as being a result of experimental errors were excluded from further analysis. Figure 7 shows typical examples of such erratic curves. Several factors such as twisted fibres, double fibres, pre-loaded fibres and fibre slip from the glue are assumed to be the cause of these experimental errors. For the Cottonized fibres, 15 out of 50 stress–strain curves (30%) were excluded due to such experimental errors. For the Green fibres, 5 out of 35 stress–strain curves (14%) were excluded.

Besides the above-mentioned experimental error curves, it was found that the flax fibres show a distinctive variation in their stress–strain behaviour. Typical stress–strain curves for the Green and the Cottonized fibres are shown in Fig. 8. All the measured fibres were grouped based on the two distinctive stress–strain behaviours: (1) nearly linear stress–strain behaviour, and (2) nonlinear stress–strain behaviour. Interestingly, the linear stress–strain behaviour was the only curve type seen for the Green fibres, whereas both curve types were almost equally represented by the Cottonized fibres (see Table 3).

The values of tensile strength, Young's modulus and strain to failure were obtained from the stress–strain curves. The results are summarized in Table 3 by grouping

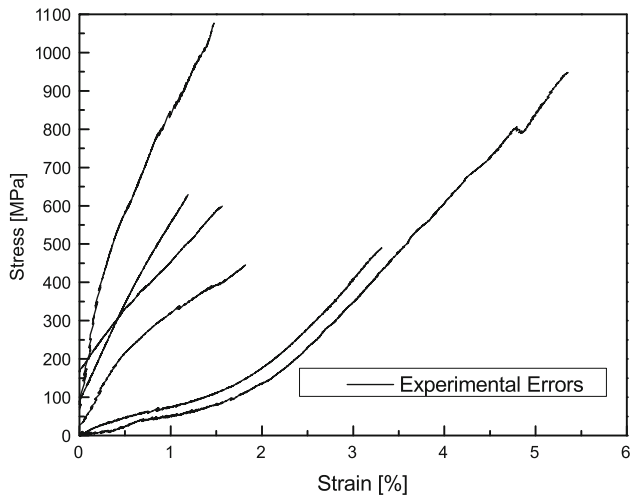

Fig. 7 Typical stress–strain curves of single flax fibres with experimental errors

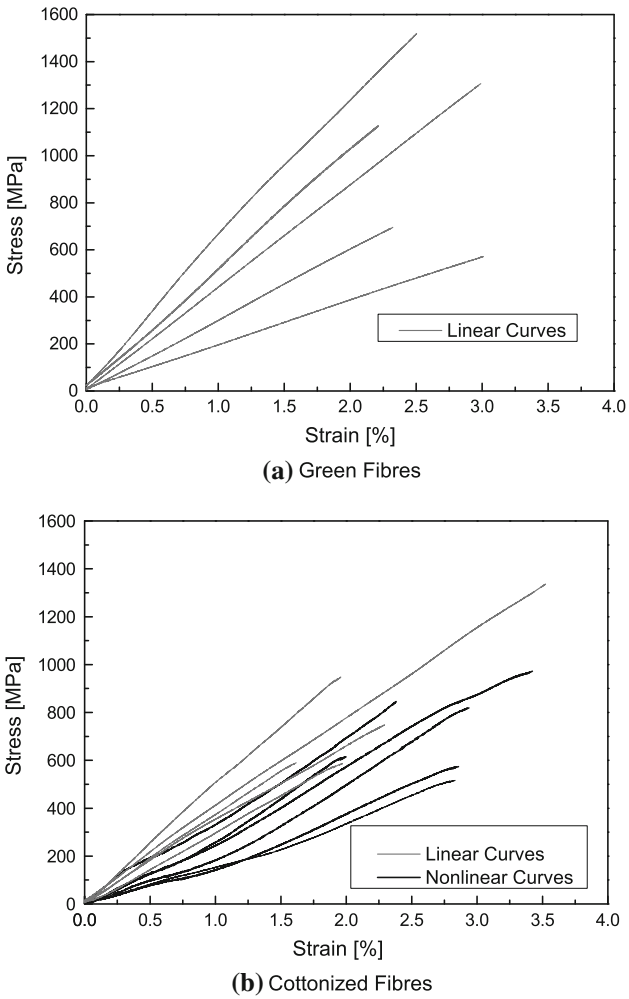

Fig. 8 Typical linear and nonlinear stress–strain curves of single flax fibres: **a** Green fibres, and **b** Cottonized fibres

Table 3 Mean and standard deviation values for diameter, tensile strength, Young's modulus and strain to failure for single flax fibres

Fibre type	Curve type	Number of curves	Fibre diameter[a] (μm)	Max load (N)	Tensile strength (MPa)	Young's modulus (GPa)	Strain to failure (%)
Green	Linear	30	18.9 ± 4.3	0.29 ± 0.13	974 ± 419	31.4 ± 16.2	3.00 ± 0.65
	Nonlinear	0	–	–	–	–	–
Cottonized	Linear	15	18.4 ± 3.0	0.19 ± 0.10	760 ± 392	33.1 ± 11.6	2.27 ± 0.63
	Nonlinear	20	19.8 ± 3.6	0.22 ± 0.11	641 ± 314	24.2 ± 10.7	2.50 ± 0.48

The results are grouped according to the fibre type and two types of stress–strain curves

[a] These values are the fibre widths measured by Method 1

them according to fibre type and stress–strain curve type. The following comparisons are made based on the mean values to show the trends of the results. For the Cottonized fibres, the nonlinear type of stress–strain curves exhibit a lower tensile strength (641 vs. 760 MPa), a lower Young's modulus (24.2 vs. 33.1 GPa), and a higher strain to failure (2.50 vs. 2.27%) than the linear type of curves. Based on the results from the linear curves, the Green fibres showed a higher tensile strength (974 vs. 760 MPa), and a higher strain to failure (3.00 vs. 2.27%) than Cottonized fibres. The relatively large variability of the measurements is shown by the large values of SD which gives coefficient of variations (CV = SD/mean) in the range of 20–50%.

Fracture behaviour

Figure 9 shows typical examples of the two types of defects seen on the surface of flax fibres: (i) transverse defects, which are the most visible type of defects and (ii) longitudinal defects. These two types of defects, which are introduced to the fibres both naturally during growth and artificially during processing, are found in the present study to control the fracture behaviour of the fibres.

On a macroscopic level, by observing the stress–strain curves of the fibres (see Fig. 8), it appears that the fibres fracture in a brittle manner. However, microscopic investigations have revealed that the fracture of the fibres occurs in a more ductile and complex manner by longitudinal splitting over a large area. Figure 10a shows an example of a flax fibre that was observed by optical microscope before and after a tensile test. Large surface transverse defects and small internal transverse defects were visible in the microscope before the test. Based on the observations of the fractured fibre ends (Fig. 10a), it is believed that the fibre starts to fracture at one (the largest)

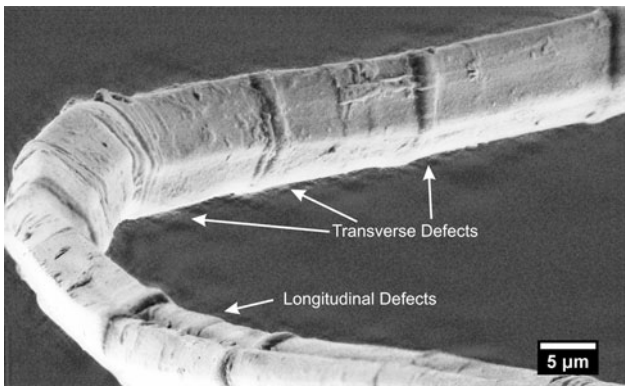

Fig. 9 Field-emission SEM image of a single flax fibre showing transverse defects and longitudinal defects

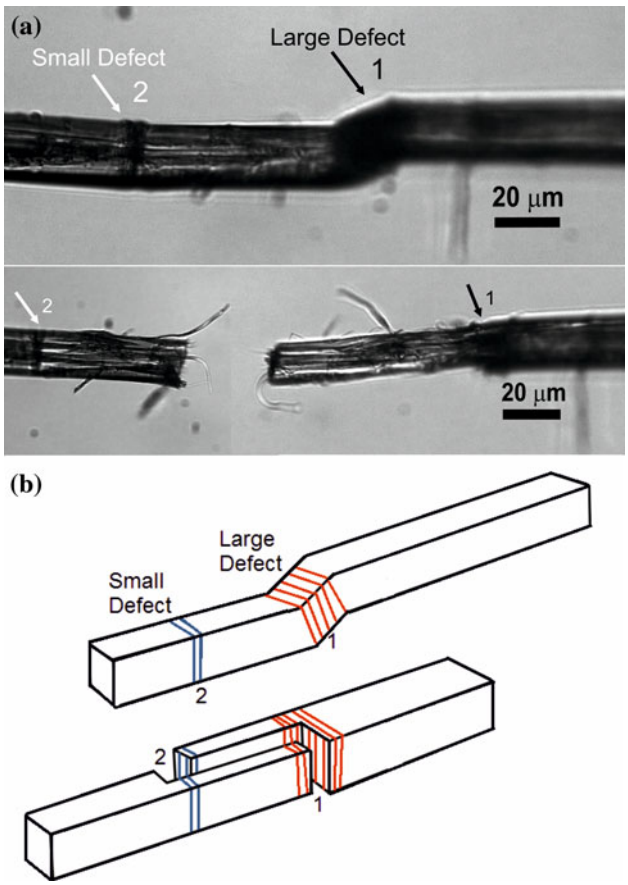

Fig. 10 Fracture behaviour of a flax fibre showed **a** by optical microscope images of a fibre before and after fracture and **b** in a schematic view. The locations of small and large transverse defects are indicated

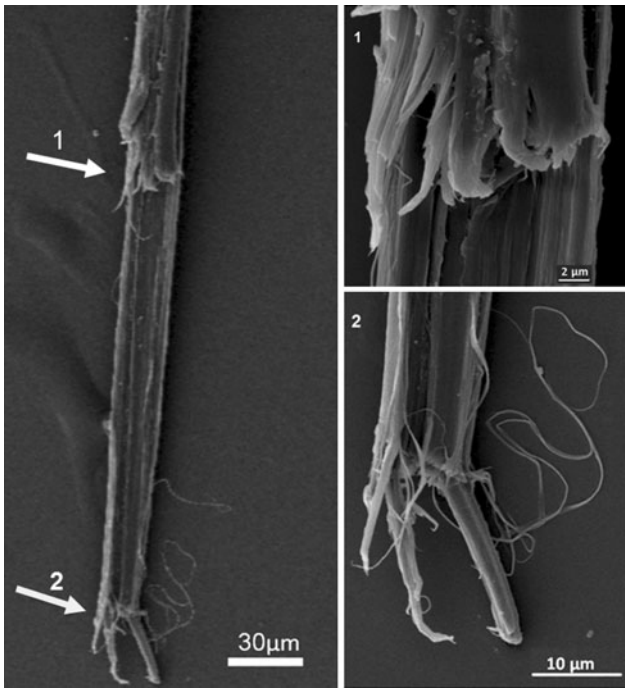

Fig. 11 Scanning electron microscope image of a large fracture zone in a single flax fibre. Magnified views (1 and 2) are presented to highlight the longitudinal cracks along the fibre, and the formed microfibrillar units at the inner layers at both fractured ends

defect and then it continues to split until faced with the next defect along the fibre length as shown by the schematic view in Fig. 10b.

Figure 11 shows an example of a fibre that has a large fracture zone. It is apparent that the fibre was split into smaller microfibrillar units at both fractured ends. It is believed that the fibre fracture started at the outer fibre surface in a transverse direction, and then it propagated in a longitudinal direction inside the cell-wall layers.

Discussion

Cross-sectional area

The results show that the cross-sectional areas measured by the two methods on two large groups of fibres are within the same range of area distribution (see Fig. 5). It can therefore be argued that the two groups of fibres are representative of identical and comparable sub-groups; i.e. the sampling of fibres in the two groups is unbiased. The difference between the mean values suggests that the circular fibre area measured by the Method 1 is overestimating the true fibre area by 39%. This value compares very well with the value of 42% found from similar measurements on bundles of jute fibres in the study by Virk [6]. Furthermore,

Table 4 Examples of cross-sectional shapes of flax fibres and their measured aspect ratios

Cross-sectional shape				
Aspect ratio	2.33	2.00	1.14	1.12

in a study of kenaf, bamboo, and curaua fibres, Teresaki et al. [15] demonstrated that the fibre area determined by the circular assumption is higher than the true fibre area, which was measured by laser scanning microscopy. The results in the present study, however, for the cross-sectional areas measured for the same fibres (Table 2), shows that the fibre area is only slightly overestimated by Method 1 for fibres having a low aspect ratio, and that the fibre area was much underestimated for fibres having an aspect ratio above a given threshold value. This is supported by the examples shown in Table 4 of different cross-sectional shapes of flax fibres and their measured aspect ratios. Altogether, it is demonstrated that the aspect ratio must be taken into account when considering the accuracy of the widely used Method 1. Similar considerations were made in the study by Thomason et al. [5].

As a consequence of the above considerations, it can be seen that the tensile strengths of the fibres, which were evaluated based on a circular assumption (Method 1), is likely to be either overestimated or underestimated depending on their aspect ratios. In general, the tensile strength will be determined with less accuracy for fibres having a high aspect ratio. The magnitude of the error can be estimated by approximating the cross-sectional shape of the fibres to be elliptical with dimensions of the minor and major axes a and b, respectively. Then, the true cross-sectional area is

$$A_{\text{true}} = \pi \tfrac{1}{4}\, a\, b \text{ for } (a \le b) \tag{1}$$

Then, at the point of maximum applied force, P, the true tensile strength, is

$$\sigma_{\text{true}} = \frac{P}{A_{\text{true}}} = \frac{P}{\pi\, \frac{1}{4} a\, b} \tag{2}$$

Assuming (incorrectly) that the fibre has a circular cross-section, and by measuring the fibre width, the cross-sectional area may be calculated wrongly. In the two most extreme cases, the cross-sectional area can be estimated from the minor axis, a, and the major axis, b, respectively. Then, the cross-sectional areas are calculated to be

$$A_{\min} = \pi\, \frac{1}{4}\, a^2 \text{ and } A_{\max} = \pi\, \frac{1}{4}\, b^2 \tag{3}$$

so that the tensile strength would be calculated as

$$\sigma_{\max} = \frac{P}{A_{\min}} = \frac{P}{\pi_4^1 a^2} \text{ and } \sigma_{\min} = \frac{P}{A_{\max}} = \frac{P}{\pi_4^1 b^2} \quad (4)$$

where the subscripts 'max' and 'min' refer to the maximum and minimum values, respectively. Combining Eqs. 2 and 4, the ratio between the strengths assuming a circular cross-section and the (true) elliptical cross-section can be calculated. The result is

$$\frac{\sigma_{\max}}{\sigma_{\text{true}}} = \frac{b}{a} \text{ and } \frac{\sigma_{\min}}{\sigma_{\text{true}}} = \frac{a}{b} \quad (5)$$

Figure 12 shows these upper and lower strength ratios as a function of the aspect ratio, *b*/*a*. The effect is quite significant. For instance, for a moderate aspect ratio of 1.25, the strength ratios are 0.8 and 1.25. Thus, the uncertainty in the strength value exceeds ±20%. For an aspect ratio of 2.3 (about the upper bound of aspect ratio found in the present study), the strength ratios are 0.43 and 2.3, respectively. For this situation, the calculated tensile strength value—obtained by assuming a circular cross-section—may be in error by more than 50%. If only an uncertainty of 10% is accepted then *b*/*a* must be below 1.10.

The results in Table 2 of measured fibre areas by Method 1 and 2 can be used to calculate the error of the experimental tensile strength values found in the present study. The relative area difference, Δ_{area}, between the two fibre areas is given by the equation

$$\Delta_{\text{area}} = \frac{A_{\text{circ}} - A_{\text{true}}}{A_{\text{true}}} = \frac{A_{\text{circ}}}{A_{\text{true}}} - 1 \quad (6)$$

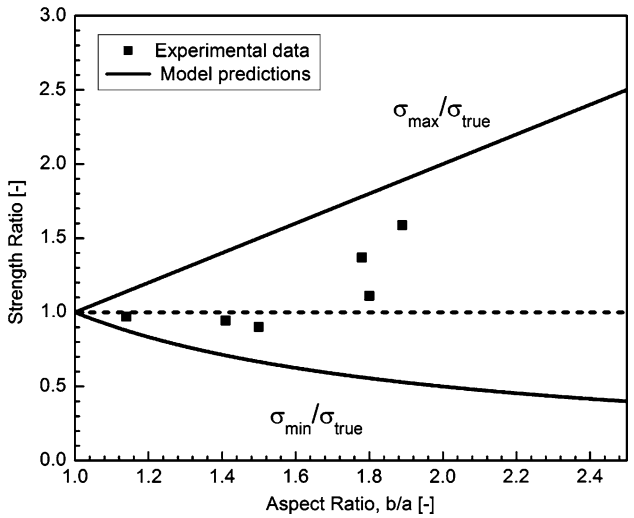

Fig. 12 Experimental data and model predictions of the ratio between the determined strengths of fibres using the assumed circular cross-sections and the measured true cross-sections, as a function of the aspect ratio of the cross-sectional shape of the fibres

An expression for the ratio between the experimental and true tensile strength can then be found

$$\frac{\sigma_{circ}}{\sigma_{true}} = \frac{A_{true}}{A_{circ}} = \frac{1}{\Delta_{area} + 1} \quad (7)$$

The equation is used to calculate the strength ratios ($\sigma_{\text{circ}}/\sigma_{\text{true}}$) of the 6 fibres in Table 2, and the results are shown as data points in Fig. 12. This demonstrates that the experimentally found errors in strength values are well located within the upper and lower bounds of the model lines.

In addition to the above considerations of fibre aspect ratio, it is also important to consider how the determined strength of the fibres is influenced by their lumen content. When the *apparent* fibre area is used to calculate the strength values, it necessarily means that in the case of fibres with a large variation in lumen content, the strength values will equally show a large variability. To avoid this, the *absolute* fibre area (i.e. the cell-wall area) should be used in the calculation of strength. However, this can only be done by direct methods such as the one used in Method 2. For the flax fibres in the present study, the lumen content was found to be very low with a mean of 1.6% although some fibres have large lumen contents, and where about 85% of all the fibres were found to have lumen content below 1%. In addition, it was found that the shape of the fibres, given by their aspect ratio, was not influenced by the fibres having a lumen. Hence, it can be stated that in the present study the variability of strength values is not influenced by the lumen content of the fibres. This is supported by a previous study by Charlet et al. [9] where it was shown that the lumen content of flax fibres rarely exceeds 8% and that the variation of mechanical properties is only slightly influenced by changes in the lumen content.

Stress–strain behaviour

The observed nonlinear stress–strain behaviour is likely to be the result of the re-arrangement of the cellulose microfibrils in the fibre cell wall during loading. Baley [7] recorded a similar nonlinear behaviour of flax fibres, and noted that the fibres started to show a linear behaviour after the first loading cycle, which was ascribed to a presumptive change of the microfibril angle during loading. Others have also reported that the stress–strain curves can be seen as having either a linear elastic behaviour or a nonlinear strain hardening behaviour [16, 17]. In the present study, the Cottonized fibres showed both linear and nonlinear stress–strain behaviours, whereas the Green fibres showed only a linear behaviour. This difference between the two fibre types might be explained by the previous finding that the highly processed Cottonized fibres have many more defects than the low-processed Green fibres [18] (see Fig. 13),

which possibly is caused by the stable growth of distributed damage. In other studies, it has been found that the microfibril angle is higher in defect regions than in non-defect regions [19–21], and this will lead to the hypothesis that more defective fibres will show more frequently a nonlinear stress–strain behaviour. This hypothesis is supported by the findings in the present study. Although, the proposed structure–property relationship needs more experimental verification, it is an interesting idea that the stress–strain behaviour of flax fibres can be used as a quantitative measure of their defect content. Furthermore, with the perspective of using flax fibres as reinforcement in composites, it can be mentioned that a similar nonlinear behaviour has been observed for the axial tensile stress–strain behaviour of unidirectional flax fibre/polyester resin composites [22]. As discussed earlier, the large scatter in mechanical properties can be attributed (partly) to the use of the circular fibre area; an error which is increased when the aspect ratio of the fibres is increased. In addition to this, the large scatter in mechanical properties is likely also to be attributed to the distribution of defects (or kink bands) along the fibres (see Fig. 13). Large defects lead to low mechanical properties, whereas smaller defects result in less reduced mechanical properties. A full quantitative understanding of the relationship between the size and number of defects and the mechanical properties of the fibres is still to be established, although a few studies have presented work on this [8, 23]. In the present study, despite the large scatter in mechanical properties, the results show as anticipated that the low-processed Green fibres tend to have a higher strength and a higher strain to failure than the highly processed Cottonized fibres.

The measured values of tensile strength, Young's modulus and strain to failure in the present study are generally in good agreement with data from the literature as shown in Table 5. It can be seen that the three parameters for mechanical properties of flax fibres show large variability both within studies and between studies. The variability in properties within studies can be quantified by the calculated coefficients of variation (CV). These CV values are in the range from 20 to 60%, in general for all three mechanical properties. The study by Baley [25] shows the lowest variability in properties with CVs between 27 and 36%. The observed variability in properties of flax fibres between studies is probably caused by differences in the origin of the fibres, fibre processing conditions, in addition to differences in the applied testing methods.

Fracture behaviour

It is obvious that the appearance of defects in an optical microscope (OM) image and in a scanning electron microscope (SEM) image (see Figs. 9, 10 and 13) is different. It is possible to identify fibre defects with the SEM when the defects are shown as clear transverse marks

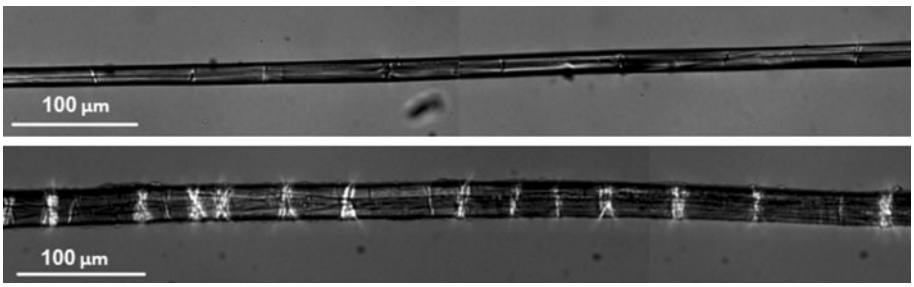

Fig. 13 Representative polarised optical microscope images of single flax fibres: Green fibres (*top*) and Cottonized fibres (*bottom*). Fibre defects can be seen as *bright* and *dark lines* across the fibres. Used with permission of Mehmood [18]

Table 5 Mechanical data from present and previous studies of single flax fibres

Tensile strength (MPa)		Young's modulus (GPa)		Strain to failure (%)		Reference
974 ± 419	(43%)	31 ± 16	(52%)	3.0 ± 0.7	(23%)	Present study
760 ± 392	(52%)	33 ± 12	(36%)	2.3 ± 0.6	(26%)	Present study
641 ± 314	(49%)	24 ± 11	(46%)	2.5 ± 0.5	(20%)	Present study
621 ± 295	(48%)	52 ± 18	(35%)	1.3 ± 0.6	(46%)	[8]
1,795 ± 1,127	(63%)	76 ± 40	(53%)	2.4 ± 0.7	(29%)	[9]
1,339 ± 486	(36%)	54 ± 15	(28%)	3.3 ± 0.9	(27%)	[25]
678 ± 216	(32%)	–	–	–		[24]
906 ± 246	(27%)	–	–	–		[24]
1,834 ± 900	(49%)	–	–	–		[2]

Shown are results (mean ± standard deviation, and coefficient of variation in brackets) of tensile strength, Young's modulus and strain to failure

(denoted kink bands) on the fibre surface. However, other types of defects are not visible on the fibre surface with the SEM, but they are clearly visible with the polarised OM. This suggests that these latter defects are located inside the fibres. Thus, a polarised OM is presently the most suitable imaging technique for investigating how the mechanisms of crack initiation and propagation are controlled by surface and/or internal defects.

It appears from the polarised OM micrographs that transverse defects can be sites of crack initiation. The observations of the fracture behaviour of the fibres suggest that they exhibit a brittle transverse failure in the outer surface, whilst the longitudinal microfibrillar splitting propagates inside the fibres. Previous studies have presented SEM micrographs of fracture surfaces [23, 26], but with no clear indication as to which type of defect caused the fibre fracture. However, based on the OM and SEM images in the present study, a mechanism is suggested to explain how both the surface and internal defects are controlling the fracture behaviour. The fact that the microscale failure mechanism is complex may explain why the strength variation of the flax fibres may not always follow a Weibull distribution [27]. The large fracture area formed in a complicated way is due to cell wall defects and anisotropy of internal fibre structures. This is in contrast to crack growth in brittle ceramics and glass fibres, which fail by unstable crack growth once a crack has initiated from a defect.

Conclusions

Single flax fibres were investigated to find the reasons for the large variability in their measured mechanical properties. The major reasons for the variability were found to be:

- Inaccuracy in the determination of the cross-sectional area of the fibres. By using the circular fibre area assumption, a considerable error is introduced into the calculated mechanical properties. Experimental data, together with a simple analytical model, are presented to show that the error is increased when the aspect ratio of the shape of fibre cross-sections is increased. Thus, the aspect ratio of the fibres must be taken into account to improve the accuracy (and to reduce the variability) of the mechanical properties.
- Two distinctive types of stress–strain behaviour (linear and nonlinear) of the fibres. The linear stress–strain curves were found to give a higher tensile strength, a higher Young's modulus, and a lower strain to failure than the nonlinear curves. It was suggested that the two types of stress–strain behaviour were correlated with the amount of defects; the low-processed Green fibres revealed only the linear behaviour whilst the highly processed Cottonized fibres show both the linear and the nonlinear behaviour.
- Complex fracture behaviour. The fibres were found to fracture by a complex microscale failure mechanism with large fracture zones governed by both surface and internal defects causing cracks to propagate in the transverse and longitudinal directions. A distribution in the size and number of defects along the fibres will lead to variability in the tensile strength obtained.

Altogether, it is recommended to furthermore investigate the correlation between the fibre defects and the mechanical performance of the fibres. It is believed that this will lead to an improved confidence in the use of flax fibres for reinforcement in polymer matrix composites.

Acknowledgements The authors gratefully acknowledge Stergios Goutianos and Hans Lilholt for helpful advices and Shahid Mehmood for technical assistance, and for valuable input on fibre defects. The research has been partly funded by the European Community's Seventh Framework Programme under grant agreement no 214467 (NATEX), and grant no 274-07-0300 (WoodFibre3D) by the Danish Agency for Science, Technology and Innovation.

References

1. Meijer WJM, Vertregt N, Rutgers B, Van de Waart M (1995) Ind Crops Prod 4:273
2. Bos HL, Van den Oever MJA, Peters OCJJ (2002) J Mater Sci 37:1683. doi:10.1023/A:1014925621252
3. Joffe R, Andersons J, Wallstrom L (2003) Composites A 34:603
4. Bledzki K, Gassan SJ (1999) Prog Polym Sci 24:221
5. Thomason JL, Carruthers J, Johnson KG (2011) Compos Sci Technol 71:1008
6. Virk AS (2010) PhD thesis, University of Plymouth, United Kingdom
7. Baley C (2002) Composites A 33:939
8. Davies GC, Bruce DM (1998) Textile Res J 68:623
9. Charlet K, Baley C, Morvan C (2007) Composites A 38:1912
10. Virk AS, Hall W, Summerscales J (2010) Compos Sci Technol 50:995
11. Cierpucha W, Kozlowski R, Mankowski R, Wasko J, Mankowski T (2004) Fibres Text East Eur 47:13
12. Harwood R, Nusenbaum V, Harwood J (2008) International Conference on Flax and Other Bast Plants Saskaaton Canada, p 118
13. Reme PA, Johnsen PO, Helle T (2002) J Pulp Pap Sci 28:122
14. Chinga-Carrasco G, Lenes M, Johnsen PO, Hult EL (2009) Micron 40:761
15. Terasaki Y, Noda J, Koichi G (2009) Adv Mat Res 79:235
16. Pickering KL, Beckermann GW, Alam SN, Foreman NJ (2007) Compos A 38:461
17. Andersons J, Sparnins E, Joffe R, Wallstrom L (2005) Compos Sci Technol 65:693
18. Mehmood S (2009) Unpublished results: Risø National Laboratory for Sustainable Energy. Technical University of Denmark, Denmark
19. Charlet K, Eve S, Jernot JP, Gomina M, Bread J (2009) Procedia Eng 1:233

20. Kölln K, Grotkopp I, Burghammer M, Roth SV, Funari SS, Dommach M, Muller M (2005) J Synchron Rad 12:739
21. Wang HH, Drummond JG, Reath SM, Hunt K, Watson PA (2001) Wood Sci Technol 34:493
22. Hill C, Hughes M (2010) J Biobased Mater Bioenergy 4:148
23. Thygesen LG, Eder M, Burgert I (2007) J Mater Sci 42:558. doi:10.1007/s10853-006-1113-5
24. Zafeiropoulos NE, Dijon GG, Baillie CA (2007) Composites A 38:621
25. Baley C (2004) J Mater Sci 39:331. doi:10.1023/B:JMSC.0000007768.63055.ae
26. Bos HL, Donald AM (1999) J Mater Sci 34:3029. doi:10.1023/A:1004650126890
27. Sparnins E, Andersons J (2009) J Mater Sci 44:5697. doi:10.1007/s10853-009-3785-0

[A3]

Paper manuscript

Aslan, M., Mehmood S., Madsen, B.

Effect of consolidation pressure on volumetric composition and stiffness of unidirectional flax fibre composites

(To be submitted to Composite Part A)

Effect of consolidation pressure on volumetric composition and stiffness of unidirectional flax fibre composites

Mustafa Aslan[1*], Shahid Mehmood[2], Bo Madsen[1],

[1] Materials Research Division, Risø National Laboratory for Sustainable Energy, Technical University of Denmark, Frederiksborgvej 399, DK-4000 Roskilde, Denmark*
Tel: 004546775800 E-mail: [*]muas@risoe.dtu.dk

Abstract

Unidirectional thermoplastic composites with flax fibres and LPET (Low melting Polyethylene terephthalate) matrix filaments were manufactured by a filament winding process followed by a vacuum assisted compression moulding process. The influence of applied pressure during compression moulding on fibre volume fraction, density, and axial stiffness of the manufactured composites is presented using a modified rule of mixture model and experimental results. The results show that attainable fibre volume fraction increases with applied pressure. In composites with higher volume fractions, it is observed that density and axial stiffness increases by increasing pressure due to decreasing composite porosity. The porosity is mostly results from impregnation problems at higher volume fractions. Microstructure of composite cross sections at different weight fractions shows a correlation between applied pressures, attainable fibre volume fraction and porosity distribution within composite structure. The results show an apparent correlation between the model and the composite constitutes for the samples tested. It is found that the higher consolidation pressure leads to decrease average porosity distribution of 10%, increase attainable volume fraction of 13% and a increase in the maximum stiffness of the composites from 35 to 40 GPa.

1. Introduction

Flax fibres have for long been considered as attractive raw materials in mainly the textile industry. However, they can be used as well as reinforcing fibres in composite materials for transport and construction applications [1]. Continuous textile yarns and fabrics with controlled yarn directions produced from short flax fibres are the key to the manufacturing of high performance flax fibre composites for structural applications[2].

High performance fibre composites present critical structural features needed for attaining maximum composite strength and stiffness [3]. The fibres should be long, well aligned in controlled directions, and they should be present at a high volume fraction Researchers have for long challenge to process flax fibre composites with such structural features [4-6]. Due to this challenge, it is typically argued that flax fibres should not be considered as reinforcement in

structural composites. Therefore, many studies of flax fibre composites are focused on non-aligned fibres at low volume fractions [7-11].

In general, the volume fraction of fibres in composites is a key parameter for the control of composite stiffness. The fibre volume fraction in unidirectional flax fibre composites is typically lower than the one in unidirectional glass fibre composites, as shown by Madsen and Lilholt (2004), since the flax fibre assemblies have lower compactibility than glass fibre assemblies due to their non-uniform cross sections [12]. However, the flax fibre composites can be comparable or even superior to glass fibre composites in terms of specific stiffness properties (stiffness per weight). Oksman (2001) shows that the specific stiffness of flax fibre composites (29 GPa/gcm^{-3}) is higher than the value of glass fibre composites (18 GPa/g cm^{-3}) at fibre volume fraction of 0.42.

The content of porosity in flax fibre composites should be kept to a minimum to obtain high performance composites. An analysing of the volumetric porosity content in the composites requires knowledge of porosity size, location and distribution [13]. The luminal cavity inside the fibre, the irregular shape of the fibre [14, 15]; the poor fibre/matrix interaction [16] and the un-optimised composite process parameters such as temperature and pressure lead typically to flax fibre composites with a large porosity content [17].

The objective of the present study is to investigate the effect of consolidation pressure on the attainable maximum fibre volume fraction (V_{fmax}) and the porosity content in order to have improved mechanical properties of flax fibre composites. Such investigations are needed before flax fibre composites can be used for structural applications. Model predictions are provided to determine the best volumetric composition of the composites, and the predictions are verified with the measured volumetric composition, density and stiffness of the composites. The experimental results and the model predictions are supported by microscopic observations of the morphology and the distribution of the composite constituents.

2. Theory

The microstructure of a composite shows a combination of three volumetric components: fibres, matrix and porosity. Knowledge of the volume fractions of fibres, matrix, and porosity are necessary to predict the physical and mechanical properties of composites.

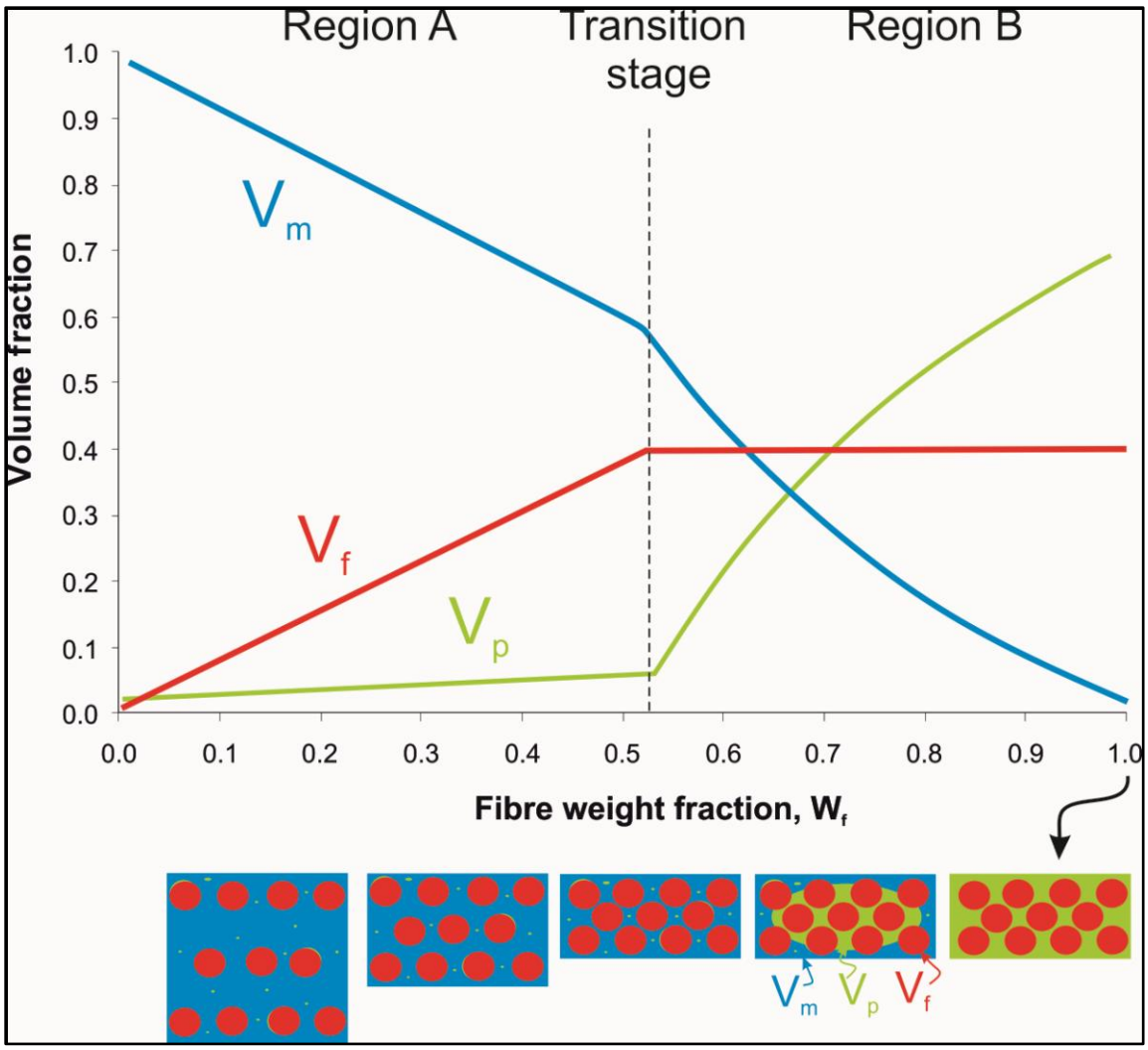

Figure 1: Model diagram of the interaction in composites between volume fractions of fibres, matrix and porosity as a function of the fibre weight fraction, shown together with schematized cross sections of composites.

Madsen et al. (2007) has showed that the volumetric composition in fibre composites can be depicted schematically as presented in Figure 1. The volumetric interaction of the constituents is separated by a transition stage between a Region A and a Region B. At the transition stage, the fibres are fully compacted to a minimum volume ($v_{c\ min}$), and the volume of matrix is only sufficient to fill the free space between the fibres.

In the Region A, (before the transition stage), the fibre assembly is not fully compacted ($v_c > v_{c\,min}$) and the volume of matrix is more than sufficient to fill the free space between the fibres. Different types of porosity can be indentified in the composites, e.g. interface porosity, and

matrix area porosity (as indicated in Figure 1), which are denoted processing porosity. The equations of volume fractions in Region A (Eq. 1,2,3) can be written as [13]:

$$V_f \equiv \frac{v_f}{v_c} = \frac{W_f \rho_m}{W_f \rho_m (1 + \sum \alpha_{pf}) + (1 - W_f)\rho_f (1 + \sum \alpha_{pm})} \quad (1)$$

$$V_m \equiv \frac{v_m}{v_c} = \frac{(1 - W_f)\rho_f}{W_f \rho_m (1 + \sum \alpha_{pf}) + (1 - W_f)\rho_f (1 + \sum \alpha_{pm})} \quad (2)$$

$$V_p \equiv \frac{v_p}{v_c} = \frac{W_f \rho_m \sum \alpha_{pf} + (1 - W_f)\rho_f \sum \alpha_{pm}}{W_f \rho_m (1 + \sum \alpha_{pf}) + (1 - W_f)\rho_f (1 + \sum \alpha_{pm})} \quad (3)$$

where V is volume fraction, W is weight fraction, ρ is density, α is porosity constant, and the subscripts f, m, and p are fibres, matrix and porosity, respectively. The fibre correlated and matrix correlated porosity constants, α_{pf} and α_{pm}, respectively, govern the content of processing porosity in the composites, as will be described later.

In the Region B, (after the transition stage), the fibre assembly is fully compacted ($v_c = v_{cmin}$) and the volume of matrix is insufficient to fill the free space between the fibres. The porosity caused by the remaining unfilled space between the fibres is denoted structural porosity. The equations of volume fractions in Region B (Eq. 4,5,6) can be written as [13]:

$$V_f \equiv \frac{v_f}{v_{c\,min}} = \frac{v_f}{\frac{v_f}{V_{f\,max}}} = V_{fmax} \quad (4)$$

$$V_m \equiv \frac{v_m}{v_{c\,min}} = \frac{v_m}{\frac{v_f}{V_{f\,max}}} = V_{f\,max} \frac{(1 - W_f)\rho_f}{W_f \rho_m} \quad (5)$$

$$V_p \equiv \frac{v_p}{v_{c\,min}} = \frac{(v_{c\,min} - v_f + v_m)}{v_{c\,min}} = 1 - V_{f\,max}\left(1 + \frac{(1 - W_f)\rho_f}{W_f \rho_m}\right) \quad (6)$$

where $V_{f\,max}$ is the maximum attainable fibre volume fraction.

The transition between the A and B regions corresponds to a volumetric composition of composites with a high fibre volume fraction and a low porosity content (see Figure 1), which results in composites with a high density and stiffness, and the transition stage gives therefore the optimum parameters for composite design. The optimum transition fibre weight fraction ($W_{f\,trans}$) can be calculated by Eq.7 [13].

$$W_{f\,trans} = \frac{V_{f\,max}\,\rho_f\,(1 + \alpha_{pm})}{V_{f\,max}\,\rho_f\,(1 + \alpha_{pm}) + V_{f\,max}\,\rho_m\,(1 + \alpha_{pf}) + \rho_m} \quad (7)$$

The density of composites with variable volumetric composition is calculated by the standard equation, which is valid for all multiphase materials:

$$\rho_c = V_f \rho_f + V_m \rho_m + V_p \rho_p \quad (8)$$

where the last porosity term equals zero (since $\rho_p \approx 0$). The density of the composites in Region A and Region B can be obtained by inserting Eqs. 1-3 and Eqs. 4-6 into Eq. 8, respectively. In the same way, the transition composite density ($\rho_{c\ trans}$) that represents the maximum attainable composite density, can be obtained by calculating the transition volume fractions of fibres, matrix and porosity by inserting Eq. 7 into Eqs. 1-3 (or Eqs. 4-6), and these volume fractions are then inserted into Eq. 8.

Micromechanical models of composites are derived based on the properties of the individual constituents and their arrangement. The simplest available model that can be used to predict elastic properties of composites is the rule of mixtures (ROM) model. This model works well for aligned and continues fibre composites where the basic assumption of equal strains in the two fibres and matrix constituents is correct. However, in composites with a more complex fibre arrangement, in terms of fibre geometry, fibre orientation, and fibre packing, in addition to having a non-negligible porosity content, a combined ROM model can be used (Madsen et al. 2009):

$$E_c = (\eta_o \, \eta_l \, E_f \, V_f + E_m \, V_m) \, (1 - V_p)^n \quad (9)$$

where n controls the effect of porosity to give stress concentrations in the composites, η_o is the fibre orientation factor (Krenchel 1964) and η_l is fibre length factor (Cox 1952). When the parameters V_f, V_m, and V_p for the Region A (Eqs, 1-3) and Region B (Eqs. 4-6) are known, the stiffness of the composites can be calculated by Eq. 9.

3. Experimental Methods

3.1. Materials

The composites were manufactured with flax fibre yarns (supplied by Extreme Materials, Italy) and with low melting temperature polyethylene terephthalate (LPET) filaments (supplied by Comfil, Denmark). The linear density was measured to be 88.9 ± 2.6 tex for the flax yarn and 56 ± 0.8 tex for the LPET filament.

3.2. Composite manufacturing

The unidirectional flax fibre reinforced LPET composites were manufactured by filament winding of flax yarns and LPET filaments followed by press consolidation. After the flax yarns

and the LPET filaments were wound on a frame, the fibre/matrix assembly was first dried under vacuum conditions (1 mbar, 23°C, and 16 hours) for moisture removal. Then, the fibre/matrix assembly was converted to a composite panel by a vacuum assisted hot pressing moulding method. The assembly was heated for 200°C for 15 minutes under vacuum before applying a compression moulding force of 200 kN for 1 minute, at 30 °C.

Composites were manufactured with different consolidation pressures (1.67 and 4.10 MPa) by using two different panel sizes. Small composite panels (120x400 mm) were consolidated under a pressure of 4.10 MPa, whereas large composite panels (300x400 mm) were consolidated under a pressure of 1.67 MPa. For both consolidation pressures, a series of composite panels were manufactured with fibre weight fractions in the range 0.24-0.83. In addition, one panel was manufactured with only LPET. For the composites, the fibre weight fraction of the wound fibre/matrix assembly, which is assumed identical to the fibre weight fraction (W_f) of the composite plate (Madsen 2004), was calculated from the measured linear density values of flax fibre yarns (tex_f) and LPET matrix filaments (tex_m) by using Eq. 10.

$$W_f = \frac{N_f\, tex_f}{N_f\, tex_f + N_m\, tex_m} \tag{10}$$

where N is the number of flax yarn and LPET filament bobbins used in the filament winding process.

3.3. Density

The density of the flax yarn fibres (ρ_f) and the LPET filaments (ρ_m) were measured according to the pycnometer method (ASTM 792) using water as the displacement medium. In this method, the luminal cavity of the flax fibres is assumed not to be included in the determined fibre density. The density of the composites (ρ_c) (and the neat LPET panel) was measured according to the buoyancy method (ASTM D792). For these measurements, four samples with dimensions 15x15x2 mm were cut from the central part of the composite panel.

3.4. Volumetric composition

Based on the measured materials densities (ρ_c, ρ_f and ρ_m) and fibre weight fractions (W_f), the volume fractions of fibres (V_f), matrix (V_m) and porosity (V_p) in the composites were calculated by the Eqs.11-13.

$$V_f \equiv \frac{v_f}{v_c} = \frac{m_f/\rho_f}{m_c/\rho_c} = \frac{m_f}{m_c}\frac{\rho_c}{\rho_f} = W_f\,\frac{\rho_c}{\rho_f} \tag{11}$$

$$V_m \equiv \frac{v_m}{v_c} = \frac{m_m/\rho_m}{m_c/\rho_c} = \frac{m_m}{w_c}\frac{\rho_c}{\rho_m} = W_m \frac{\rho_c}{\rho_m} = (1 - W_f)\frac{\rho_c}{\rho_m} \quad (12)$$

$$V_p = 1 - (V_f + V_m) \quad (13)$$

3.5. Microstructure

The polished cross-sections of the composites were observed under an optical microscope (Aristomet, Leica) to analyse the distribution of fibres, matrix and porosity. In addition, electron scanning microscopy (Supra, Zeiss) were used to measure the area and dimensions of the different types of porosities by using an image analyzer software (Image-Pro plus 5.0).

3.6. Tensile properties

Dumbbell shaped tensile specimens with outer rectangular dimensions of 180 x 25 mm and gauge section dimensions of 100 x 20 mm were cut from the composite panels. Thickness of the specimens varied in the range 2.0-2.5 mm. All specimens were initially conditioned in a climate chamber (temperature of 23°C and relative humidity of 50%) for 2 months until specimen weights were stable. Tensile tests were performed on an Instron universal testing machine according to ISO 527 at room temperature, with cross head speed of 2 mm/minute and load cell of 25 kN. Strain was measured on the two sides of the specimens using extensometers. For each composite panel, five specimens were tested.

4. Results and Discussion

4.1. Establishment of porosity parameters for the volumetric composition model

The fibre correlated porosity constant (α_{pf}), and the matrix correlated porosity constant (α_{pm}) in the volumetric composition model are linear proportionality constants of the assumed linear relation between the two types of porosities (V_{pf} and V_{pm}), and the fibre and matrix volume fractions (V_f and V_m):

$$V_{pf} = \alpha_{pf} V_f \quad (14)$$
$$V_{pm} = \alpha_{pm} V_m \quad (15)$$

The two types of porosities can be further divided into a number of sub-porosities that are controlled by their location in the composites: fibre lumen porosity ($V_{pf\ (1)}$), interface porosity ($V_{pf\ (2)}$), impregnation porosity ($V_{pf\ (3)}$), and matrix porosity ($V_{pm\ (1)}$), and each of these sub-porosities is assigned a porosity constant:

$$V_{pf} = V_{pf\,(1)} + V_{pf\,(2)} + V_{pf\,(3)} = \alpha_{pf\,(1)}\,V_f + \alpha_{pf\,(2)}\,V_f + \alpha_{pf\,(3)}\,V_f = \sum \alpha_{pf\,(i)}\;V_f$$
$$= \;\alpha_{pf}\,V_f \qquad (16)$$

$$V_{pm} = V_{pm\,(1)} = \alpha_{pm\,(1)}\,V_m = \sum \alpha_{pm\,(i)}\;V_m = \alpha_{pm}\;\;V_m \qquad (17)$$

Next, it will be described how the values of porosity constants were established based on the microstructure of the composites.

Figure 2 shows the three types of fibre correlated porosities in the flax/LPET composites. The fibre lumen porosity ($V_{pf\,(1)}$) is located in the lumen area (the central cavities) of the individual flax fibre cross sections. The interface porosity ($V_{pf\,(2)}$) is found at the flax fibre/LPET matrix interface. This kind of porosity is formed due to the non-perfect compatibility between fibre and matrix. The impregnation porosity ($V_{pf\,(3)}$) can be seen as free cavities in the interior of the flax fibre bundles. This is formed due to non-perfect matrix impregnation of the fibres.

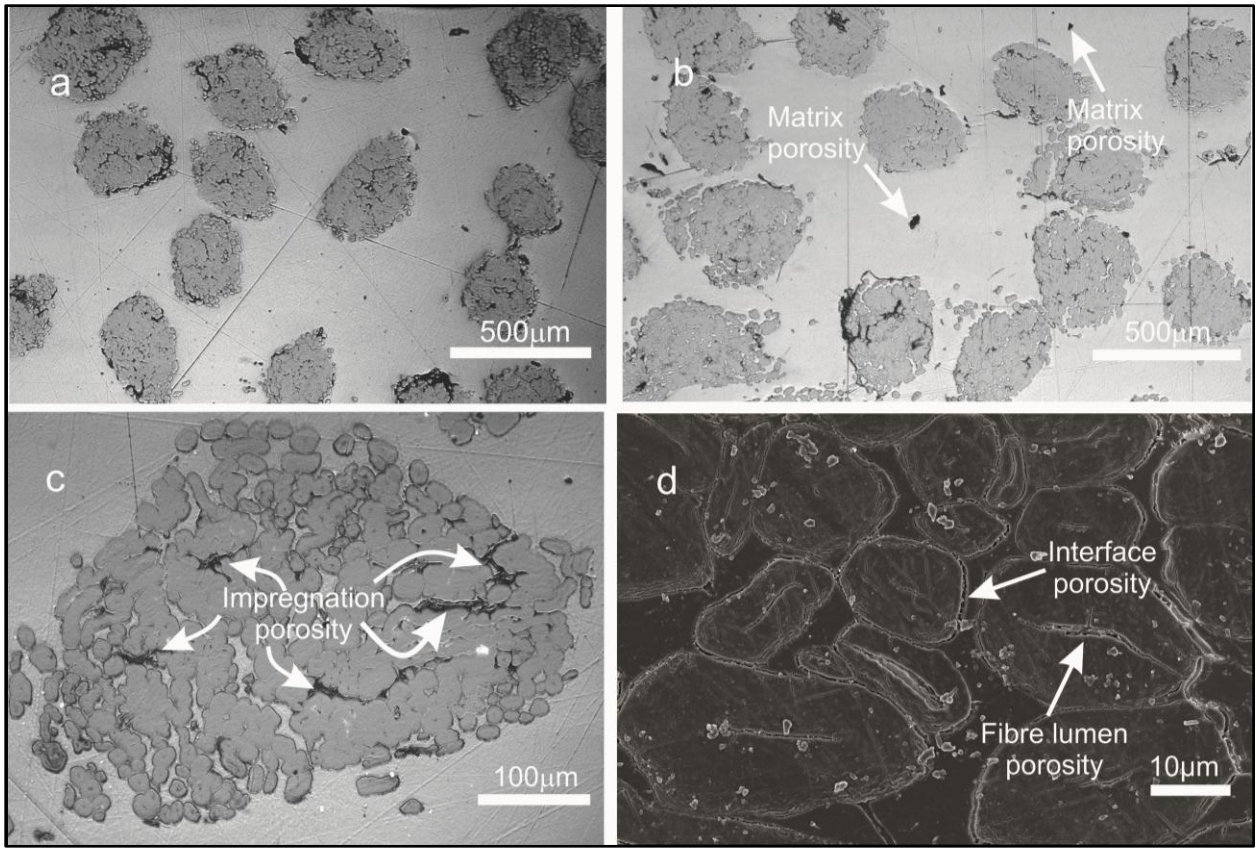

Figure 2: OM and SEM micrographs with increasing magnifications from a) to d) of polished cross sections of flax /LPET composites showing three types of fibre correlated porosities: fibre lumen porosity, interface porosity, impregnation porosity, in addition to one type of matrix correlated porosity: matrix area porosity.

The fibre lumen porosity and the interface porosity can be quantified by image analysis of polished composite cross sections. The fibre lumen porosity constant ($\alpha_{pf\,(1)}$) can be determined from the measured fibre lumen content (V_{lumen}) (Madsen et al. 2007):

$$\alpha_{pf\,(1)} = \frac{V_{lumen}}{1 - V_{lumen}} \tag{18}$$

The interface porosity constant $(\alpha_{pf\,(2)})$ can be determined from the measured dimensions of the debonded interface gap and the fibre cross sectional area (Madsen et al. 2007):

$$\alpha_{pf\,(2)} = \frac{b\beta C}{A}\frac{1}{1 - V_{lumen}} \tag{19}$$

where b is the width of the interface gap, β is the interface debonding fraction (β=1 for fully debonded fibres), A is the cross sectional area of the fibre, and C is the perimeter of the fibre cross-section.

Based on SEM micrographs of the flax/LPET composite cross sections (such as the one shown in Figure 2b), a large number of measurements were made of (i) the cross-sectional area of the fibres, (ii) the luminal area in the centre of the fibres, (iii) the perimeter of the fibre cross-sections, (iv) the width of the interface gaps, and (v) the interface debonding fraction. No systematic difference was found between composites with different fibre contents, and between composites processed by the two different consolidation pressures. The mean ± stdv. of the microstructural measurements are presented in Table 1. The mean fibre area and fibre luminal area was found to be 131 ± 57 μm^2 and 0.65 ± 0.48 μm^2 respectively, resulting in fibre lumen content (V_{lumen}) of 0.005. In a previous study of single flax fibres by Aslan et al. 2011, the fibre lumen content was determined to be 0.016. The measured values of the microstructural parameters presented in Table 1 were used to establish values of $\alpha_{pf\,(1)}$ and $\alpha_{pf\,(2)}$ on 0.005 and 0.006, respectively, by the use of Eqs. (18) and (19).

Table 1: Measurements of the microstructure of flax/LPET composites.

Microstructural parameters	**Value**
Fibre cross-sectional area (A) [μm^2]	131 ± 57
Fibre luminal area [μm^2]	0.65 ± 0.48
Fibre cross-sectional perimeter (C) [μm]	41.8 ± 10.1
Interface gap width (b) [μm]	0.09 ± 0.03
Interface debonding fraction (β)	0.20 ± 0.04
Fibre lumen content (V_{lumen})	0.005

The matrix porosity constant ($\alpha_{pm\,(1)}$) can be determined from the measured matrix porosity content (V_{matrix}) (Madsen et al. 2007):

$$\alpha_{pm\,(1)} = \frac{V_{matrix}}{1 - V_{matrix}} \tag{18}$$

In principle, V_{matrix} can be determined from composite cross sectional observations of neat matrix regions, but this presents some difficulties with respect to the definition of a matrix unit area (in analogy to a fibre unit area, which can be defined by a single fibre). Instead, V_{matrix} can be determined from the absolute matrix density (i.e. excluding porosities) ($\rho_{m\ abs}$), and the apparent matrix density (i.e. including porosities) ($\rho_{m\ app}$):

$$V_{matrix} = 1 - \frac{\rho_{m\,app}}{\rho_{m\,abs}} \tag{21}$$

The density of the LPET filaments was measured to be 1.357 g/cm^3, and this is assumed to represent the absolute matrix density ($\rho_{m\ abs}$). The density of the neat LPET plates made by compression moulding was measured to be 1.337 g/cm^3, and this is assumed to represent the apparent matrix density ($\rho_{m\ app}$). Based on these two measured density values, V_{matrix} is calculated to be 0.015, which means that the pure matrix regions in the composite contain 1.5 % porosity. This is in accordance with the microstructural observations showing only a few occurrences of porosities in the matrix (see Figure 2c). By the use of Eq. (21), the value of $\alpha_{pm\,(1)}$ was established to be 0.015.

The final porosity parameter in the volumetric composition model, the impregnation porosity constant ($\alpha_{pf\,(3)}$) is not straightforward to quantify directly from cross sectional images of composites, since it cannot be measured independently due to overlap with the other types of porosities (see Figure 2). Instead, this porosity constant can be determined from the slope of a linear regression line of the relation between experimental values of porosity (V_p) and fibre volume fraction (V_f) of the composites (Madsen et al. 2008):

$$V_p = \frac{\alpha_{pf\,(1)} + \alpha_{pf\,(2)} + \alpha_{pf\,(3)} - \alpha_{pm\,(1)}}{1 + \alpha_{pm\,(1)}}\, V_f + \frac{\alpha_{pm\,(1)}}{1 + \alpha_{pm\,(1)}} \tag{22}$$

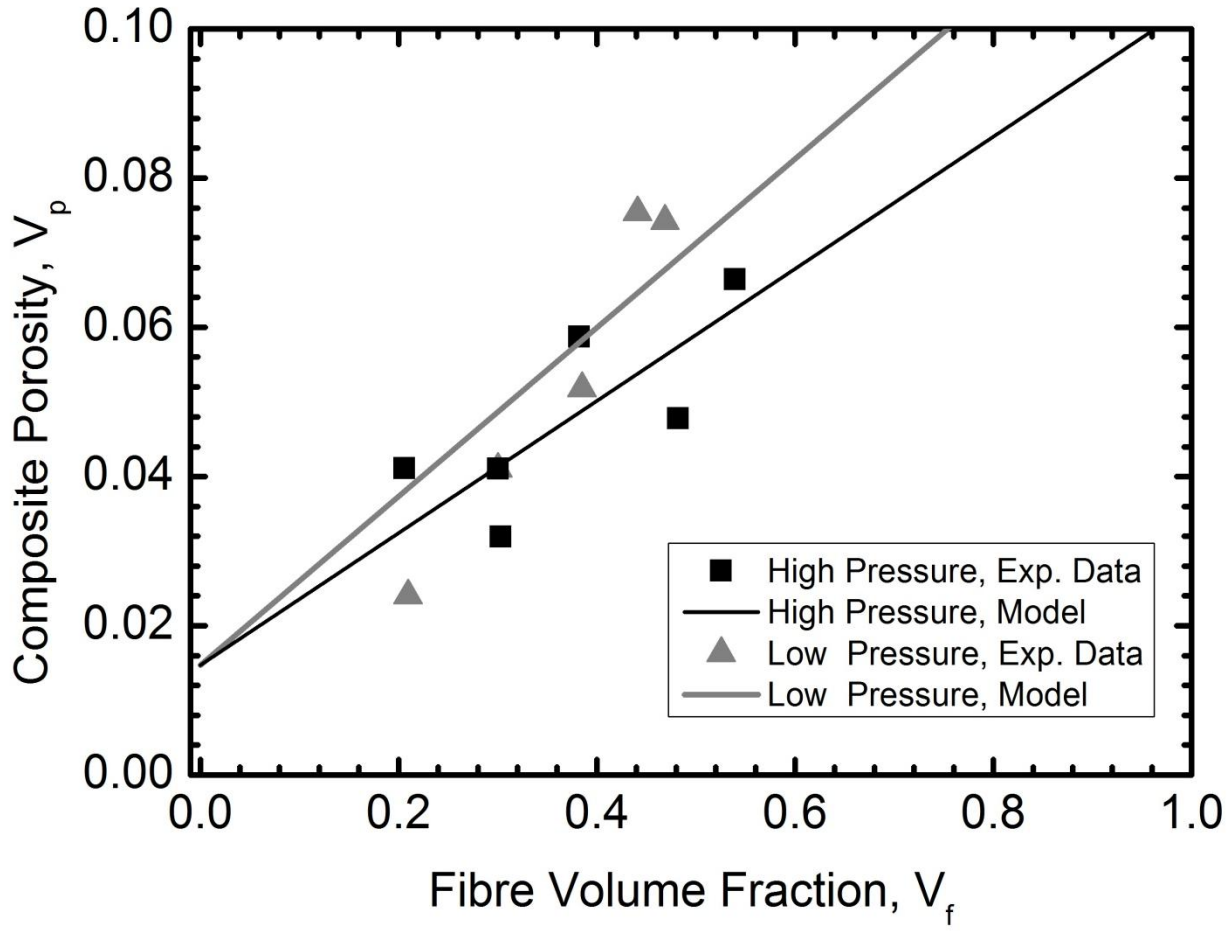

Figure 4: Porosity of flax/LPET composites as a function of fibre volume fraction. Shown are experimental data and model predictions for composites manufactured with low and high consolidation pressures.

Figure 4 shows the experimental values of porosity as a function of fibre volume fraction for the flax/LPET composites manufactured with the low and high consolidation pressures. It can be observed that the experimental data form approximate linear relationships, as foreseen by Eq. (22). The two regression lines are made with a fixed intercept of 0.015 ($= \alpha_{pm\,(1)}/1 + \alpha_{pm\,(1)}$) at $V_f = 0$, which is in accordance with Eq. (22). Based on the slopes of the regression lines, and by knowledge of the values of the three other porosity constants, $\alpha_{pf\,(3)}$ is determined to be 0.119 and 0.094 for composites made with the low and high consolidation pressure, respectively. Thus, the experimental data and the model analysis support the expected trend that the higher consolidation pressure leads to a slight reduction in the amount of impregnation porosity.

Table 2: Model parameters for the modelling of the volumetric composition of flax/LPET composites manufactured by low and high consolidation pressure.

Model Parameters		**Low Pressure Composites**	**High Pressure Composites**
Fibre density [g/cm^3]	ρ_f	1.589	1.589
Matrix density [g/cm^3]	ρ_m	1.357	1.357
Fibre lumen porosity constant	$\alpha_{pf\,(1)}$	0.005	0.005
Interface porosity constant	$\alpha_{pf\,(2)}$	0.006	0.006
Impregnation porosity constant	$\alpha_{pf\,(3)}$	0.119	0.094
Fibre correlated porosity constant	α_{pf}	0.130	0.105
Matrix area porosity constant	$\alpha_{pm\,(1)}$	0.015	0.015
Matrix correlated porosity constant	α_{pm}	0.015	0.015
Maximum fibre volume fraction	$V_{f\,max}$	0.530	0.597
Transition fibre weight fraction	$W_{f\,trans}$	0.611	0.676

Table 2 shows the established values of the porosity constants to be used for the modelling of the volumetric composition of the flax/LPET composites. It shows that the fibre correlated porosity (i.e. the sum of the sub-porosities) is higher for the low pressure composites compared to the high pressure composites with values of 0.130 and 0.105, respectively. This difference is due to the difference in impregnation porosity between the composites. It can also be noted that the impregnation porosity is the pre-dominant type of porosity in the composites, which also can be evaluated from the micrograph in Figures 2d.

4.2. Volumetric composition of composites

The values of the model parameters determined for predicting the volumetric composition of the flax/LPET composites are given in Table 2. The measured values of ρ_f and ρ_m are 1.589 g/cm^3 and 1.357 g/cm^3 respectively. As described above, α_{pf} is measured to be 0.130 and 0.105 for the low and high pressure composites, respectively, and α_{pm} is measured to be 0.015, with an assumed no difference between the two composites. The maximum attainable fibre volume fraction, $V_{f\,max}$, is determined by the average of measured fibre volume fractions in the Region B (see Figure 1). As shown in Table 2, $V_{f\,max}$ is determined to be 0.530 and 0.597 for the low and high pressure composites, respectively. By the use of Eq. (7), the transition fibre weight fraction, $W_{f\,trans}$, is calculated to be 0.611 and 0.676 for the two composites, respectively. This is the value of fibre weight fraction that gives optimum volumetric composition, and thereby optimum mechanical properties of the composites.

Figure 5 shows the experimental data together with model predictions of the volume fractions of fibres, matrix and porosity in the low and high pressure flax/LPET composites as a function of the fibre weight fraction. As can be observed, there is a good agreement between experimental data and model predictions. At low fibre weight fractions, below the transition stage, the volume fractions of fibres, matrix and porosity changes monotonically with the fibre weight fraction. At

high fibre weight fractions, above the transition stage, the fibre volume fraction shows a constant level, (= $V_{f\,max}$), the matrix volume fractions show a non-linear decreasing trend, and the porosity starts to increase rapidly.

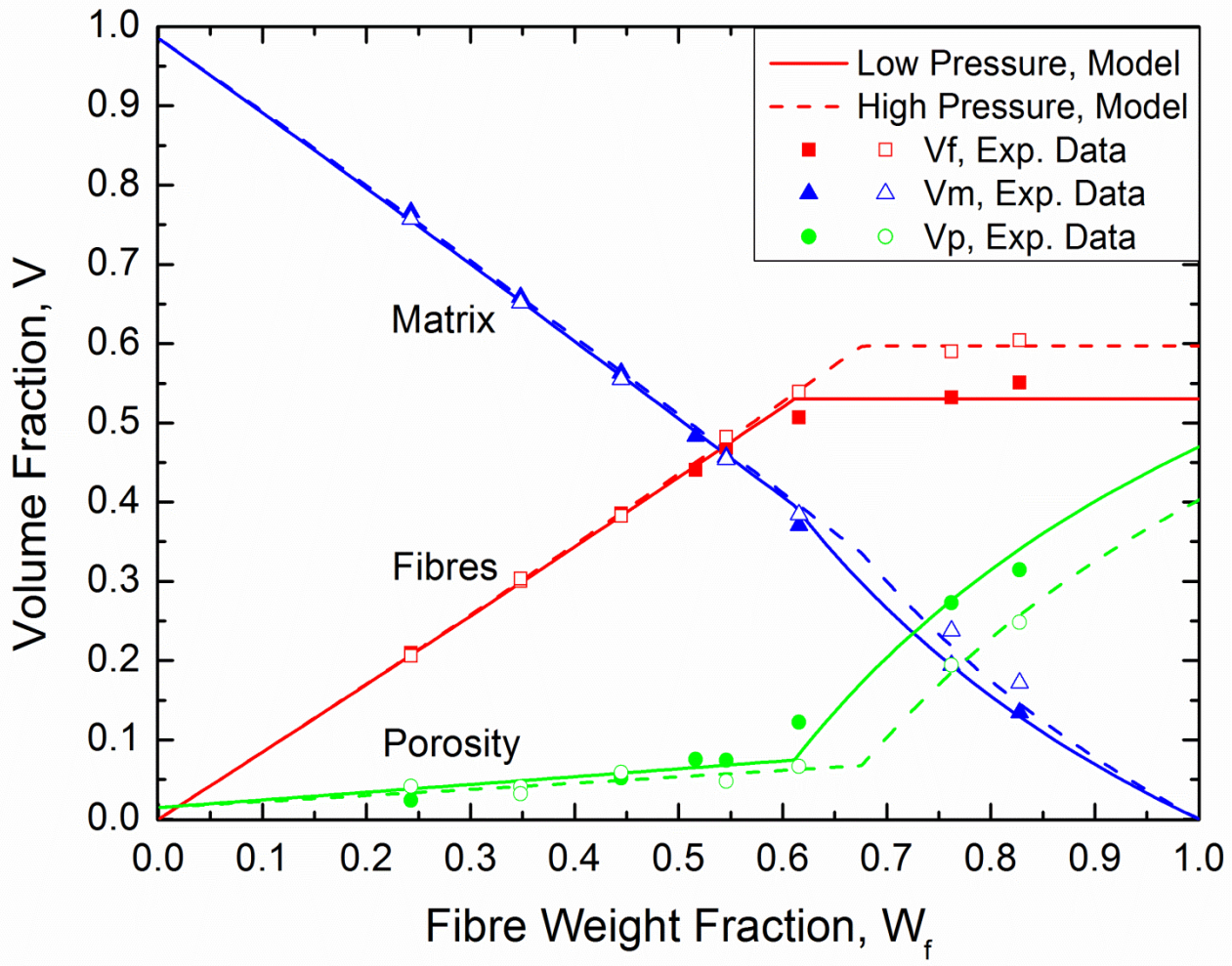

Figure 5: Volume fractions of fibres, matrix and porosity as a function of fibre weight fraction for flax/LPET composites manufactured by low and high consolidation pressure. Shown are experimental data and model predictions. Filled and open experimental data points are for low and high pressure composites, respectively.

As shown in Figure 5, the low and high pressure composites show almost similar trends in Region A, before the transition stage. In this region, the small observable difference in porosity between the composites is due to the small difference in the fibre correlated porosity constant with values of 0.13 and 0.11 for the two composites, respectively. As noted above, the main part of this porosity is assigned to impregnation porosity. In Region A, the small differences in the fibre and matrix volume fractions between the two composites are not easily observable. The fibre weight fraction at the transition stage between Region A and B is however clearly different between the low and high pressure composites with values of 0.61 and 0.68, respectively. Thus,

the fibre weight fraction can be increased to a higher level for the composites manufactured with the high consolidation pressure, before the maximum fibre volume fraction is attained (= $V_{f\ max}$). In other words, the higher consolidation pressure leads to the situation of a fibre assembly than can be more closely packed, and a higher fibre volume fraction can therefore be obtained in Region B. The difference in $V_{f\ max}$ between the low and high pressure composites is 7 % point, and as will be shown later, this leads to a marked difference in optimum properties between the composites. When the fibre weight fraction is increased further in Region B, the dramatic increase of porosity is caused by that the available matrix volume is not sufficient to fill the free space between the maximum packed fibres. The difference in $V_{f\ max}$ between the low and high pressure composites leads to a shift in the onset of the increase in porosity.

4.2.1. Microstructure of composites

Figure 6 shows optical microscope images of polished cross sections of flax/LPET composites with three different levels of fibre weight fractions ($W_f < W_{f\ trans}$, $W_f \cong W_{f\ trans}$, $W_f > W_{f\ trans}$), and manufactured with two different consolidation pressures (low and high). Thus, the effect of fibre content and consolidation pressure on the microstructure of the composites can be observed, and here follows qualitative descriptions:

- The spatial distribution of fibre bundles, i.e. fibre yarns, is affected by the fibre content. As expected, it is clearly shown that the yarns are increasingly being packed more closely together when the fibre content is increased. Below $W_{f\ trans}$, the yarns are more or less non-uniformly distributed with large matrix-rich areas between the yarns. When the fibre content is increased, the yarns are more regular arranged with small confined areas of matrix between the yarns. At fibre contents above $W_{f\ trans}$, the yarns are arranged in a closely packed configuration. No effect of the change in consolidation pressure can be observed on the spatial distribution of yarns at the three levels of fibre content.

- For composites with a low fibre content before the transition stage ($W_f < W_{f\ trans}$), no difference can be observed for the porosity content of the low and high pressure composites (as evaluated by the extent of black areas in the cross sections). This is consistent with the almost identical model lines for porosity in Region A, for the two composites, as shown in Figure 5. The porosity can be seen to consist mostly of impregnation porosity (i.e. black areas within the yarns), which also was shown by the above quantitative analysis (see Table 2).

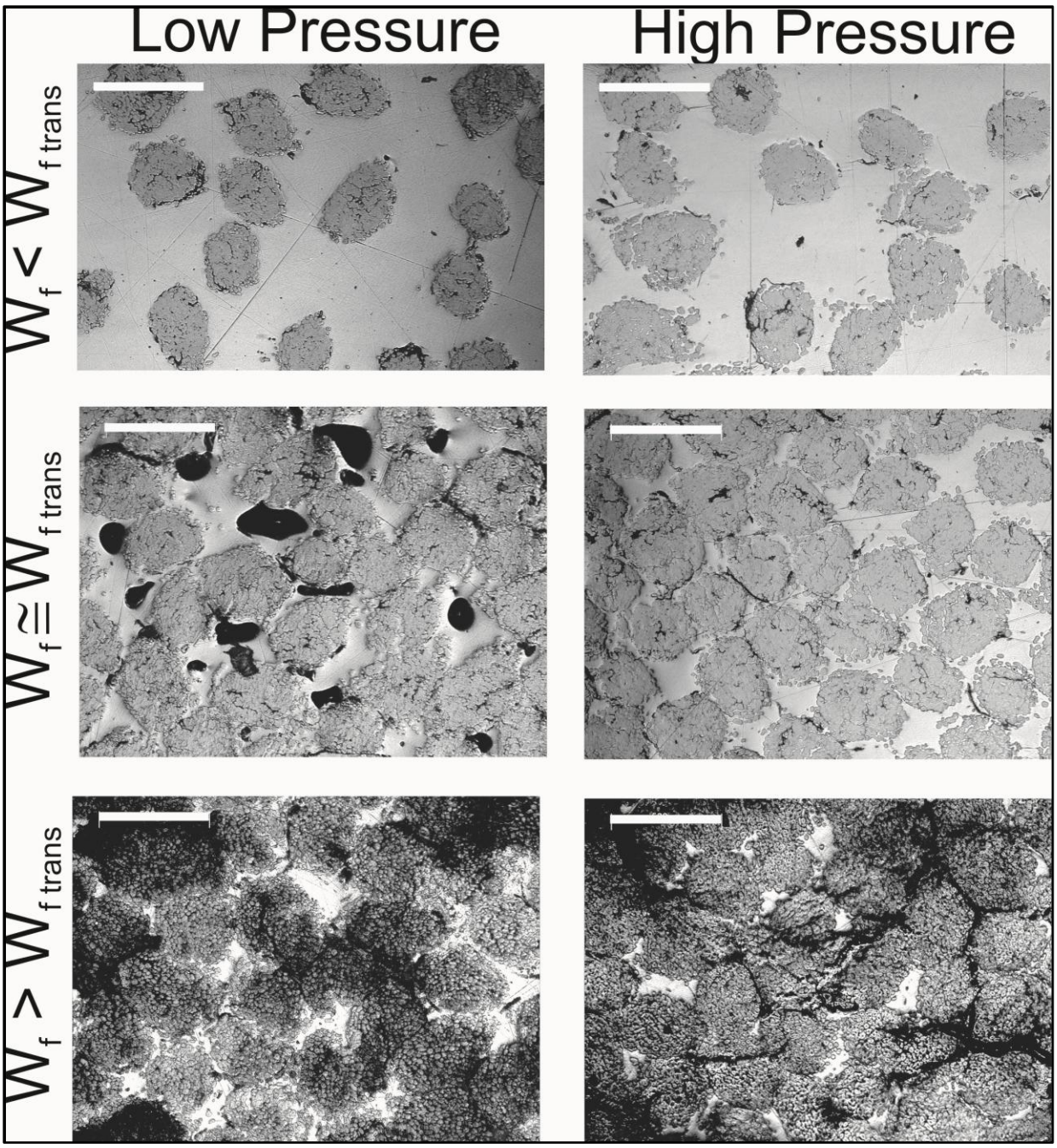

Figure 6: Optical microscope micrographs showing the microstructure of flax /LPET composites with three different levels of fibre weight fractions (W_f), with respect to the transition fibre weight fraction ($W_{f\,trans}$), and manufactured with two different consolidation pressures, low and high. Values of W_f are 0.24, 0.55 and 0.76 for both the low and high pressure composites. Scale bar is 200 µm.

- For composites nearby the transition stage ($W_f \cong W_{f\ trans}$), a characteristic microstructural feature can be observed, as shown by the middle image in Figure 6 for the low pressure composites. Large and confined areas of porosity are seen to be developed in the matrix-rich areas between the yarns. These are thought to be local occurrences of structural porosity due to an insufficient volume of matrix to fill the free space between the (almost) fully compacted fibres. Based on the microstructural observations, it is indicated that nearby the transition stage, there a preferable filling by the matrix of the space between the fibres in the yarns, and there is then not enough matrix to fill the space between the yarns, giving rise to structural porosity Other examples of these local structural porosities is shown in Figure 7. They were found to be non-uniformly distributed across the cross sections given rise to a very heterogeneous microstructure (which will be shown later to be correlated to an increase of the scatter of the measured properties). Interestingly, the occurrence of local structural porosity was observed only for the composites manufactured with the low consolidation pressure.

- For composites with high fibre content after the transition stage ($W_f > W_{f\ trans}$), the porosity takes up a dominating part of the materials, as shown by the micrographs in Figure 6. This is also consistent with the results of the quantitative analysis (see Figure 5) where the porosity content is determined to be in the range of 10-45% of the total composite volume. The major part of the porosity consists of structural porosity, which is almost uniformly distributed in the composite cross sections, but with a tendency to be located mostly within the yarns (in contrast to the above observation of local structural porosity). It is therefore indicated that in this case, there is a preferable filling by the matrix of the space between the yarns, and there is then not enough matrix to fill the free space within the yarns. It should however be noted that the high porosity content of these composites and the related low quality of the micrographs, impede a detailed evaluation of the microstructure.

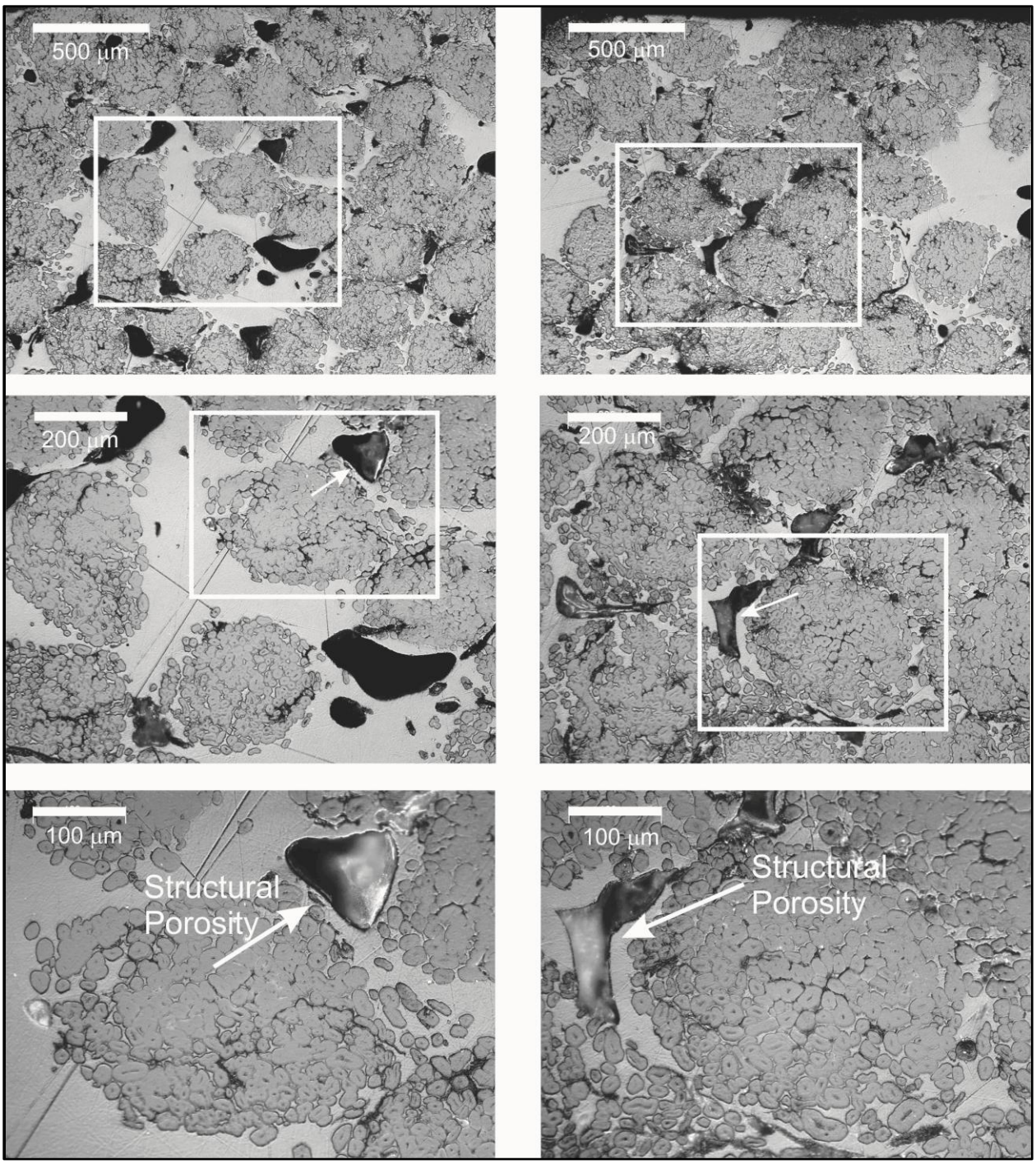

Figure 7: Optical microscope micrographs flax/LPET composites showing occurrences of local structural porosity.

4.2.2. Compaction behaviour of fibres

Many researchers have experimentally investigated the compaction behaviour of fibre assemblies, and have found that it can be simulated by a power law function ($V_f = a\ P^{b}$), where the fibre volume fraction (V_f) is calculated as a function of the compaction pressure (P) [12, 18, 19]. It has been shown that the compaction behaviour is controlled by the configuration of the fibre assemblies, such as fibre orientation, and fibre morphology. For unidirectional flax yarn assemblies, the values of the fitting constants, a and b, were established by Madsen and Lilholt (2002) to be 0.5 and 0.1, respectively.

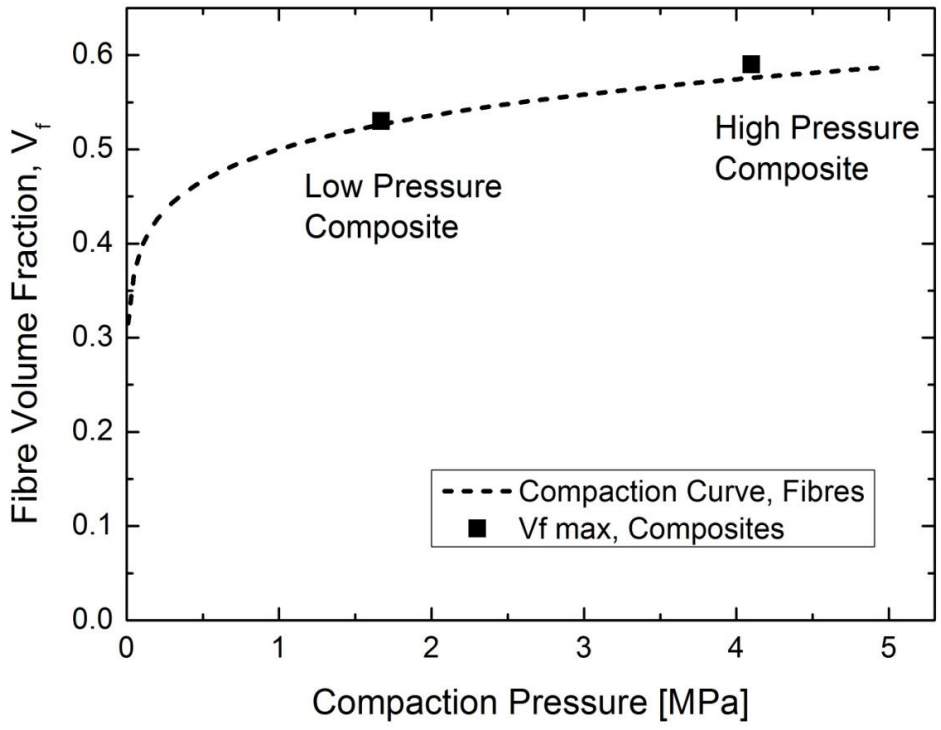

Figure 8: Compaction curve for unidirectional flax yarn assemblies together with values of $V_{f\,max}$ for the unidirectional flax/PET composites manufactured with two different consolidation pressures.

A textile flax yarn with a linear density of 64 tex was used, and this is in the same range as the one used in the present study with a linear density of 89 tex. Figure 8 shows the compaction curve for unidirectional flax fibres. The curve starts with a V_f of about 0.30 at zero compaction pressure, which means that the volume of flax fibres in the un-compacted assembly is 30% compared to the total volume (and the remaining 70% of volume is air). When the fibre assembly is compacted by increasing the compacting pressure, the fibre volume fraction is increased following a power law relationship. It can be anticipated that there is a correlation between the compacting behaviour of fibre assemblies, and the maximum fibre volume fraction that can be attained in the related composites. The two flax yarn composites of the present study were

consolidated with pressures of 1.67 and 4.10 MPa giving rise to values of $V_{f\ max}$ on 0.530 and 0.597, respectively. These two data points are shown together with the compaction curve in Figure 8.

It is seen that low and high pressure levels are well correlated with mathematical model (Madsen et al, 2007). The difference between the data from present study and those of Madsen and Lilholt (2002) was less than 0.02. Similar results has been found for hemp fibre composites (Madsen and Lilholt 2002).

4.3. Physical and mechanical properties of the composites

4.3.1. Density of the composites

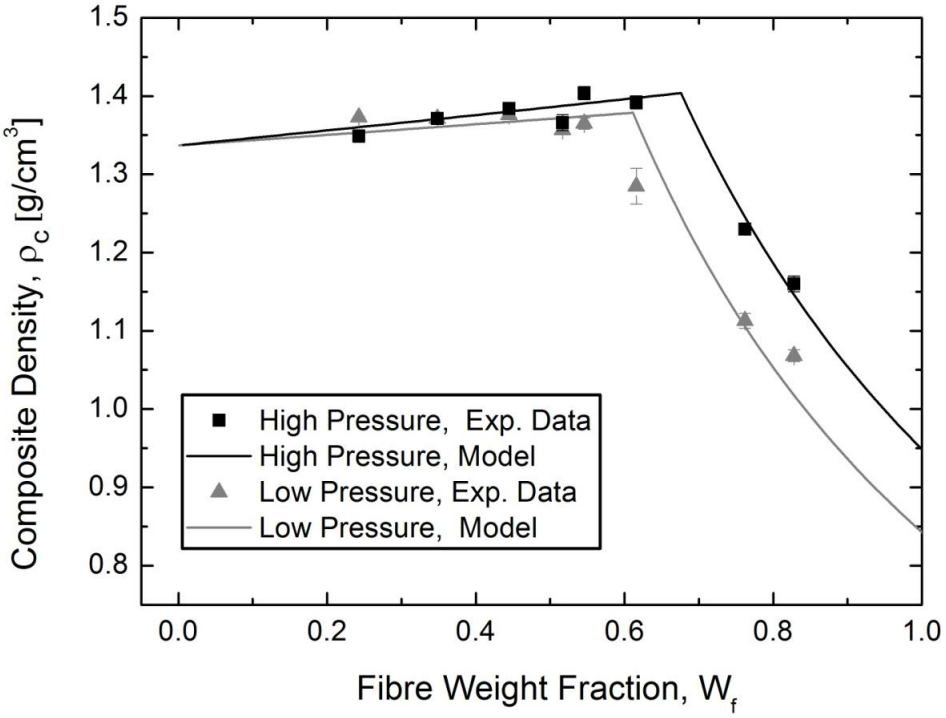

Figure 9: Composite densities as a function of fibre weight fraction for low and high pressure composites

Figure 9 shows that density (ρ_c) of low and high pressure composites increases as fibre weight fraction increase until the transition fibre weight fraction between region A and B which is determined by setting Eq.4 and then decreases with increase in fibre weight fraction. When composites are produced with higher pressure they show lower porosity fractions. At low weight fraction there is little difference in the density of composites for low pressure composites and high pressure composites. But at higher weight fractions density of low pressure composites is less due to larger porosity fractions. The model predictions also show good agreement with experimental density data.

4.3.2. Stiffness of the composites

The experimental data points of stiffness and model lines for low and high pressure Flax/LPET composites are shown Figure 10. The model predictions and experimental values of stiffness show almost the same increasing trend by increasing fibre weight fraction at low weight fractions (region A) for both low and high pressure composites. After transition region (region B) at high weight fractions, the stiffness starts to decrease by increasing weight fraction and significantly decreases for low pressure composites. The model lines are well correlated with experimental data points at low weight fractions but they are not consistent at high weight fractions due to increasing deviation of porosity fractions as an effect of pressure. Experimental data points show large scatter at higher weight fractions (transition region and region B). The stiffness of composites in axial direction is controlled by fibre volume fractions. The higher scatter results from higher porosity are due to structural porosities resulting from insufficient matrix and poor impregnation at higher fibre volume fractions.

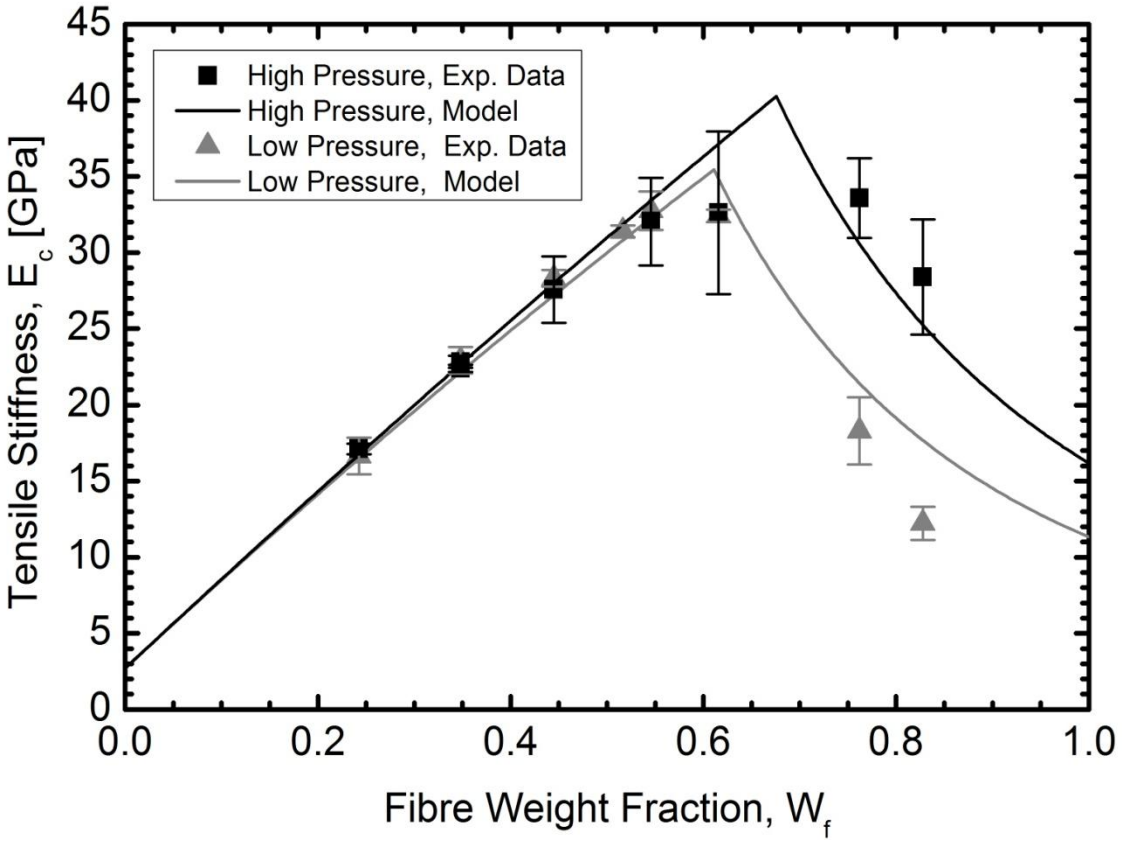

Figure 10: Composite stiffness as a function of fibre weight fraction for low and high pressure composite

Table3: Model parameters for the composite stiffness.

Model Parameters	**Low Pressure Flax/LPET**	**High Pressure Flax LPET**
E_f [GPa]	76.3	76.3
E_m [GPa]	2.83	2.83
n	2	2
η_0	1	1
η_1	1	1
E_{ctrans} [GPa]	35.5	40.3

The model parameters to predict the stiffness of composite are shown in Table 3. Measuring fibre stiffness (E_f) is necessary for selection of fibre reinforcement in unidirectional composites. The axial stiffness of the flax fibres calculated to be76.3 GPa using Eq.11. Accuracy of the fibre stiffness value has strong effect on the true value of maximum composite stiffness (E_{ctrans}). Stiffness of single flax fibres shows large variability between 13-116 GPa due to structural, processing defects and measurements errors [14].The matrix stiffness (E_m) is measured to be 2.8 GPa from the tensile stress-strain curves of 10 samples produced from pure LPET panel. Madsen (2004) found that the porosity efficiency exponent (n) is assumed equal to 2 since it gives a good fit to the experimental data for plant fibre composites [12]. Both fibre orientation factor (η_0) and fibre length efficiency factor (η_1) are calculated to be 1 for unidirectional composites. According to measured and nominal parameters, maximum attainable composite axial stiffness (E_{ctrans}) is calculated to be 35.5 and 40.3 MPa for low and high pressure composites, respectively. The model prediction results were found slightly higher than measured stiffness values to be 33-34 GPa at higher volume fractions.

5. Conclusion

In the present paper, the effect of panel size which induced different pressure levels on volume fraction of the composite constitutes has been investigated in terms of physical and mechanical properties. The following new findings for volume fraction model, density and stiffness model with validated experimental values in flax fibre/LPET composites are presented.

This effect was confirmed by compaction factor of the fibre assemblies before consolidation.

- Pressure difference makes decreasing effect on porosity at higher volume fractions and a large part of the porosity is caused by structural porosities (W_{ps}) at higher volumes which formed during processing in comparison to small part of fibre related porosities.
- A higher pressure certainly improves attainable maximum fibre volume fraction, the density and the stiffness properties of the flax fibre composites.
- Flax/LPET composites can be produced up to optimum 60% of volume fractions for unidirectional composites, which is the highest level until now.

6.REFERENCES

[1] K.L. Pickering, Properties and performance of natural fibre composites, Woodhead Publishing, 2008.

[2] J. Müssig, C. Stevens, Industrial Applications of Natural Fibres: Structure, Properties and Technical Applications, John Wiley & Sons, 2010.

[3] B. Madsen, H. Lilholt, Composites Science and Technology, 63 (2003) 1265-1272.

[4] S. Goutianos, T. Peijs, B. Nystrom, M. Skrifvars, Applied Composite Materials, 13 (2006) 199-215.

[5] K. Charlet, J.P. Jernot, S. Eve, M. Gomina, J. Bréard, Carbohydrate Polymers, 82 (2010) 54-61.

[6] J. Gassan, A.K. Bledzki, Journal of Applied Polymer Science, 82 (2001) 1417-1422.

[7] H. Toftegaard, in: Risø Report, Risø DTU, 2002.

[8] K. Van de Velde, P. Kiekens, Journal of Thermoplastic Composite Materials, 15 (2002) 281-300.

[9] K.P. Mieck, R. Lutzkendorf, T. Reussmann, Polymer Composites, 17 (1996) 873-878.

[10] T. Peijs, S. Garkhail, R. Heijenrath, M. Van Den Oever, H. Bos, Macromolecular Symposia, 127 (1998) 193-203.

[11] H.L. Bos, J. Müssig, M.J.A. van den Oever, Composites Part A: Applied Science and Manufacturing, 37 (2006) 1591-1604.

[12] B. Madsen, in: Department of Civil Engineering, Technical University of Denmark
2004, pp. 206.

[13] B. Madsen, A. Thygesen, H. Lilholt, Composites Science and Technology, 67 (2007) 1584-1600.

[14] M. Aslan, G. Chinga-Carrasco, B.F. Sorensen, B. Madsen, Journal of Materials Science, 46 (2011) 6344-6354.

[15] K. Charlet, C. Baley, C. Morvan, J.P. Jernot, M. Gomina, J. Breard, Composites Part a-Applied Science and Manufacturing, 38 (2007) 1912-1921.

[16] D.N. Saheb, J.P. Jog, Adv. Polym. Technol., 18 (1999) 351-363.

[17] B. Madsen, P. Hoffmeyer, H. Lilholt, Composites Part a-Applied Science and Manufacturing, 38 (2007) 2204-2215.

[18] S. Toll, Polymer Engineering & Science, 38 (1998) 1337-1350.

[19] Gutowski, Morigaki, Cai, Journal of Composite Materials, 21 (1987) 172-188.

[A4]

Submitted paper

Aslan, M., Sørensen, B.F.

Tab design for uniaxial tensile test specimens of composite materials

(Submitted to Composite Part A)

Tab design for uniaxial tensile test specimens of composite materials

Mustafa Aslan*, Bent F. Sørensen

Materials Research Division, Risø National Laboratory for Sustainable Energy,
Technical University of Denmark, Frederiksborgvej 399, DK-4000 Roskilde, Denmark*
Tel: 004546775800 E-mail: *muas@risoe.dtu.dk

Abstract

Although test standards give guidelines for specimen design for gauge section failure in order to determine the ultimate tensile strength correctly, unidirectional test specimens often show premature failure due to the presence of a stress singularity in the gripping section. In the present paper, a parameter study is performed to determine the effect of specimen geometry and elastic properties of tab and test materials (isotropic or orthotropic) on the stress singularity. The results showed that the singularity in the vertex of dissimilar material wedges can not be eliminated completely, but it can be reduced significantly. Softer tabs and low wedge angles decrease the stress singularity. There is no effect of thickness ratio of the tab/test material on the order of stress singularity. A simple criterion is proposed for the assessment of the severity of the stress singularity. For typical composite materials, gauge section failures should be achievable by selecting a suitable tab material and test material combinations with small wedge angles in the range of 5° and 10° depending on the stiffness ratio. The results suggest that the effect of stiffness ratio between the tab and test materials is not fully taken into account in the current standards.

Keywords: Stress singularity, Elasticity, Mechanical testing, Finite element model (FEM)

1. Introduction

Tensile testing of unidirectional composites is not straightforward. It is difficult to obtain a valid gauge section failure, i.e., failure located away from the specimen ends where the load is applied and the stress state is multiaxial and non-uniform. The occurrence of failure away from the gauge section thus leads to erroneous strength determination, denoted premature failure. As an example, Figure 1 shows a unidirectional Flax-LPET (Linear Polyethylene terephthalate) composite specimen with square cut GFRP (glass fibre reinforced plastic) tabs after uniaxial tensile testing according to the ISO 527 [1] standard. As can be seen from the Fig. 1, the test specimen failed at the end of tab.

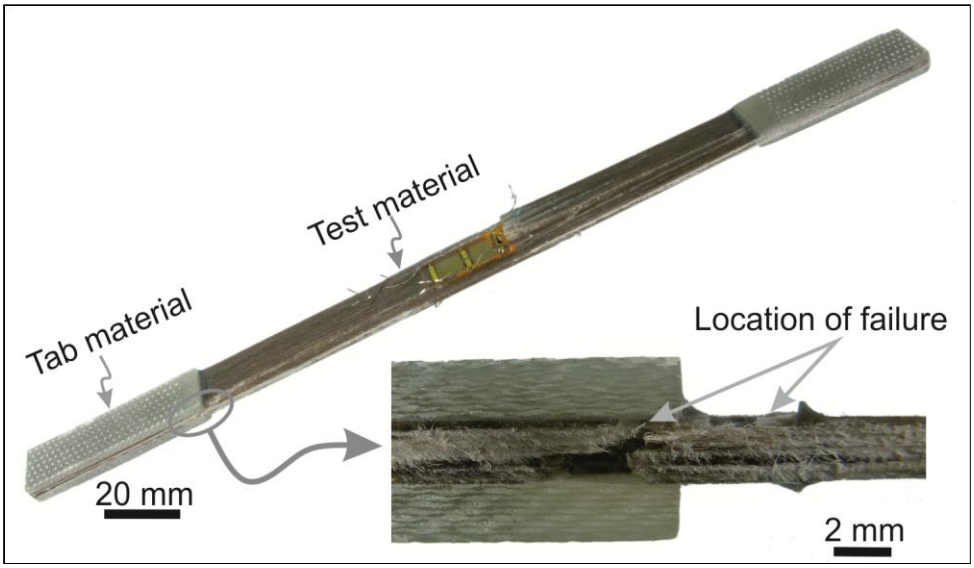

Fig. 1: Unidirectional flax / LPET composite tensile specimen (ISO 527) which failed in the vertex of tab-specimen edge.

The desired uniform, uniaxial stress state in the gauge section can be obtained by the application of a tension force through shear tractions along the surfaces at the specimen ends. In practice, the shear forces are applied using grips and friction. The grips clamp the specimen surfaces at each side by high normal forces. The grips themselves can cause damage to the surfaces of the test material in the gripping area. Such damage will likely lead to premature failure at the grips. Then, the strength of the test material will be under estimated. Therefore, tabs are usually bonded onto the test material in order to protect the test material from damage in the gripping area. The tabs protect the test material and introduce the load into the specimen but induce a complicated stress field at the end of the tab.

The standards differ in terms of the design of the specimen geometry, fixturing, gripping and displacement measurement method. The ASTM and JIS standards use tapered GFRP tabs while and ISO 527 standards allow the use of square cut tabs. Moreover, the ASTM D 3039 [2] standard suggests a large range of tab wedge angle ($\theta = 5 - 90°$) and a longer specimen than

the ISO 527 standard. In many cases, however, unidirectional straight sided specimens still fail prematurely from the tab ends [3]. For the width tapered specimen geometry, specimens show failure by cracking parallel to the fibre orientation (splitting cracks) from the wedge tip in both specimen sides during loading [4].

The effects of tab design and gripping conditions on the tensile properties were investigated experimentally by Hojo et al. [5]. They observed that the use of square cut GFRP tabs ($\theta = 90°$) and tapered GFRP tabs ($\theta = 10°$) did not result in significantly different tensile strengths. Many of the specimens (65 - 85%), both tapered and non-tapered, broke inside the tabs near to the wedge tip. For tension testing perpendicular to the fibre direction, specimens with GFRP tabs having a wedge angle of 90° broke at the end of the tabs and had a lower strength than specimens with rubber tabs which broke within the gauge section.

Wisnom and Maheri [6] presented experimental results of the uniaxial tensile strength of unidirectional carbon fibre-epoxy composites made from prepregs. The plies were placed in a stepped way in order to produce a tapered section of plates. The tensile strength of specimens with a wedge angle of 0.7° was found to be 14% higher than the strength of straight-sided specimens. This difference was considered to be statistically significant.

Belingardi [7] found that the gripping pressure, specimen geometry, tab material and manufacturing procedure affect the tensile strength of unidirectional tensile specimens under test conditions in accordance with the ASTM D 3039 standard. They found a significantly lower tensile strength for specimens having tabs molded to the test materials during production. The difference was attributed to residual stresses originating from the molding. Moreover, they suggested the use of a lower gripping pressure, lower wedge angle and softer tab material with adhesive bonding to avoid tab failure.

Most of the studies on the stress state of various tab configurations for a tensile test only consider a few specific geometric factors. However, the stress state depends on both the geometry and elastic properties. It is therefore difficult to make general recommendations from a few specific cases. This may be the reason for all the different type of materials and configurations proposed in the standards.

Some earlier studies investigated the stress state in terms of a stress concentration at the wedge of the tab/test material by finite element modelling (FEM). They found that both the tab geometry and the tab material type had a large effect on the stress distribution. The stress distribution was calculated with the aim of minimisation of the stress concentration at the end of the tab-test material interface [8]. Adams and Adams [10] investigated specimens with different tab configurations involving tab thickness, the tab length, tab wedge angle, and stiffness of the tab material by FEM. They stated that the tab thickness does not have any influence but a tab length of at least 40 mm was recommended for the minimization of the stress concentration.

The model results above were based on the assumption of a stress concentration (i.e. a finite stress) at the end of the tab. However, detailed linear elastic stress analyses reveal that the stress state at a wedge tip can be singular [11]. The general problem of two dimensional bonded half planes of dissimilar isotropic elastic materials loaded with arbitrary boundary tractions was first analysed by Bogy [11]. The solution was found with three non-dimensional combinations of four elastic constants (a Young's modulus and a Poisson's ratio for each of the two materials). However, Bogy [12] later expressed the stress fields for wedges of arbitrary angles in terms of the two non-dimensional elastic Dundurs' parameters α and β [13]. The Dundurs' parameters α and β are defined in plane strain condition as

$$\alpha = \frac{\Sigma - 1}{\Sigma + 1}, \qquad \text{with} \qquad \Sigma = \frac{E_1}{E_2}\frac{(1 - {v_2}^2)}{(1 - {v_1}^2)} \tag{1}$$

$$\beta = \frac{1}{2}\frac{G_1(1 - 2v_2) - G_2(1 - 2v_1)}{G_1(1 - v_2) + G_2(1 - v_1)}, \quad where \quad G_j = \frac{E_j}{2(1 + v_j)} \tag{2}$$

where E_j is the Young's modulus, Σ is the stiffness ratio, G_j is the shear modulus and v_j is the Poisson's ratio of material number $j = 1,2$. The first Dundurs' parameter α is a measure of the Young moduli difference across the interface. When material #1 is extremely stiff in comparison with material #2, α approaches +1. When material #1 is extremely compliant, α approaches -1. For most material combinations, β lies between $\beta = 0$ and $\beta = \alpha/4$ [14]. As seen from eq. (1), material combinations can also be defined in terms of the stiffness ratio, Σ, instead of α.

The order of the wedge tip stress singularity depends on the geometry of the tab and material elastic properties but is independent of external loading. In two dimensions, the stress singularity can be written as [12]

$$\sigma_{ij} \rightarrow r^{-p} \quad for \quad r \rightarrow 0, \tag{3}$$

where σ_{ij} is the stress tensor, p is a singularity exponent and r is the radial distance from the wedge tip. The parameter p is a complex number that consists of real and imaginary parts. The stresses approach infinity at the wedge tip ($\sigma_{ij} \rightarrow \infty \; for \; r \rightarrow 0$) when p has a positive real part ($0 < p < 1$). However, the stress at the wedge tip will be finite and the singularity varnishes when p has a non-positive real part ($p \leq 0$). Bogy also showed that a half plane bonded to a quarter plane (i.e., wedge angle of 90°) possesses a singularity for most applicable material combinations. For a high wedge angle, the imaginary part becomes non-zero, resulting in oscillatory stress behaviour.

Hein and Erdogan [15] presented numerical solutions for the stress singularity at the vertex of two elastically dissimilar half spaces. They found that high wedge angles lead to complex singularity values (i.e., non-zero imaginary part) and higher values of the real part singularity

exponent, so that singularity increases and becomes significant even for small values of stiffness ratio, Σ.

Xu et al. [16] investigated the stress state for straight-sided and convex bimaterial butt joints. They demonstrated experimentally that the final failure strength is higher for specimens having a convex corner joint than for specimens having a straight edged joint. They also showed numerically that a smaller corner angle gave a lower stress singularity and resulted in a relatively uniform interfacial stress distribution and higher tensile strength for convex corners.

The stress state of tensile specimen made of an orthotropic material is more complicated than specimens made of isotropic materials since the stress state depends on more elastic parameters. However, under certain restrictions, orthotropic composite materials can be analysed as being an isotropic specimen by the orthotropy rescaling technique [17]. The method allows reduction of the complexity of the stress field in composite materials.

For orthotropic materials, the stress field under prescribed surface tractions depends on two non-dimensional parameters λ and ρ defined as [17, 18]

$$\lambda = \frac{\mathrm{E_{yy}}}{\mathrm{E_{yy}}} \qquad \rho = \frac{\sqrt{\mathrm{E_{xx}E_{yy}}}}{2\mathrm{G_{xy}}} - \sqrt{v_{xy}v_{yx}} \tag{4}$$

where E_{xx} and E_{yy} denote the Young moduli in the direction of the x- and y-axis, respectively, v_{xy} and v_{yx} are the major and minor Poisson's ratios and G_{xy} is the shear modulus. For isotropic materials, $\lambda = \rho = 1$. In many cases, the stress field dependence of ρ is relative weak [18].

For the present problem, the stress distribution at the vertex of the tab and test material of the specimen can be expressed as follows

$$\frac{\sigma_{ij}}{\bar{\sigma}} = A_{ij}\,(\frac{2r}{H})^{-p} \quad for\ r \to 0 \tag{5}$$

where $\bar{\sigma}$ is the applied stress in the gauge section, A_{ij} represent non-dimensional singularity functions and H is a characteristic dimension, here the thickness of the test material.

The aim of the present study is to develop a tensile test specimen geometry that creates valid failures within the central gauge section of the test material by minimising or eliminating the stress singularity at the vertex of the tab wedge. The analysis includes both isotropic and orthotropic test materials.

The paper is organised as follows: first, a two dimensional model of a tensile test specimen is defined. A finite element model, used for analysing the problem is then described. Next, results for an isotropic bimaterial specimen are presented in terms of singularity exponents and functions for different wedge angles and elastic constants. Results for orthotropic material cases

are presented using the orthotropic parameter λ with $\rho = 1$. Then follows a discussion leading to proposals for practical test specimen design. Finally, the major results are summarised.

2. Problem Statement

A problem of interest is a straight-sided tensile specimen with an end-tab as shown schematically in Figure 2. The problem is analysed as a 2-dimensional problem since it is assumed that there is no variation of stress distribution along the *z*-direction (width).

The geometry of the test specimen is described in terms of the tab material thickness, *h*, the tab material length along the interface to the wedge tip, L_1, the gauge length of the test material, L_2, and the test material thickness, *H*. They are fixed as $L_1/L_2 = 2$, $h/L_1 = 0.025$ and $H/L_1 = 0.0125$ in the present study.

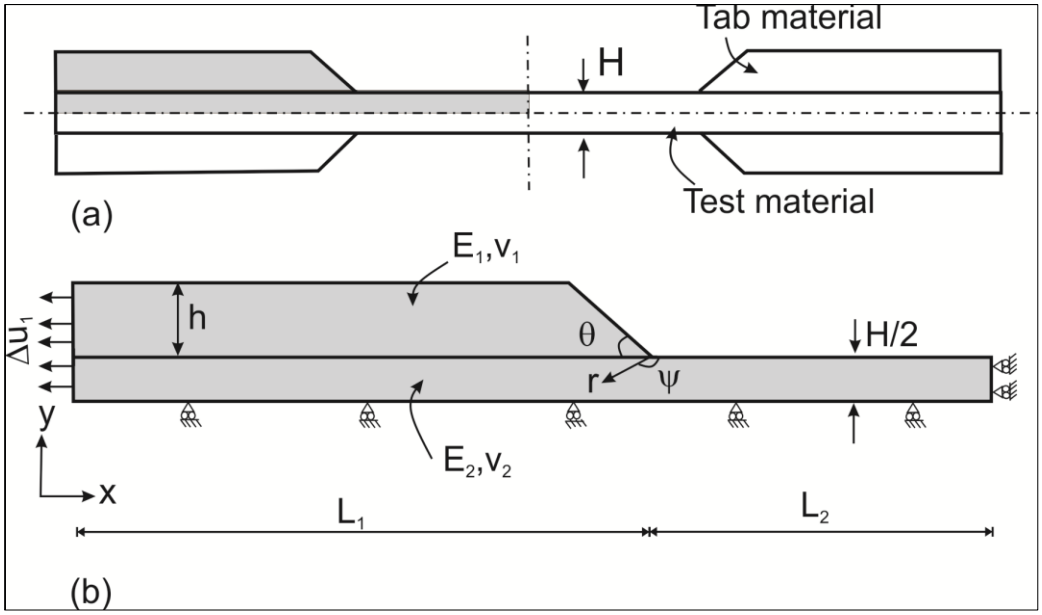

Fig 2: Schematic view of the 2D test specimen

The tensile test specimen will be analysed as a two dimensional (plane strain) problem. Owing to symmetry conditions, only one quarter of the specimen geometry needs to be considered in the model. For an isotropic and orthotropic wedge tip problem, the non-dimensional singularity exponent, *p* and singularity functions, A_{ij} take the form

$$p = f\left(\alpha, \beta, \lambda, \rho, \frac{h}{H}, \theta\right) \tag{6}$$

$$A_{ij} = f\left(\alpha, \beta, \lambda, \rho, \frac{h}{H}, \theta, \psi\right) \tag{7}$$

where α and β are given by (1), λ and ρ by (4), while θ is the wedge angle and ψ is an angular direction for stress components around the wedge tip. In the present study, the wedge angle, θ, was varied in values of 90, 45, 15, 10, 5, and 2.5°. The elastic properties of the tab material were varied in 20 different values of Σ (or α) from very compliant (Σ = 0.005) to very stiff (Σ = 10). The parameter β was varied in values of 0, $\alpha/3$ and $\alpha/4$. The orthotropic parameter λ was varied in values of 0.005, 0.1, 0.5, 1 but ρ was always fixed as 1 in this study.

The stress singularity exponents, p, and the singularity function, A_{xx}, are obtained by the slope of the log-log plot of the stress component σ_{xx} as a function of the distance to the wedge ti for a specific angular direction, $\psi = \pi$. The estimation procedure is explained in detail in Appendix 1.

3. Finite element model

The straight sided specimen was modelled by the finite element (FE) method using the commercial code Abaqus version 6.10-1 [19]. The mesh consisted of six-node (triangular) 2D plane elements denoted CPE6. Plane strain conditions ($\varepsilon_z = \gamma_{xz} = \gamma_{yz} = 0$) were prescribed. A typical mesh is shown in Figure 3. Since the primary interest is the determination of the potential stress singularity at the end of the tab material ($x = L_1$), small elements (smaller than 10^{-5} H) were used near the wedge tip where larger stress gradients are expected.

The boundary conditions were prescribed as the relative displacement of nodes of the elements in the axial direction (x-axis). The nodes on the right end and bottom of the model (midplane of the sample) were constrained in the x- and y-directions, respectively. The tab material and the test material were modelled to have a perfect bonding along the interface (i.e., shared nodes).

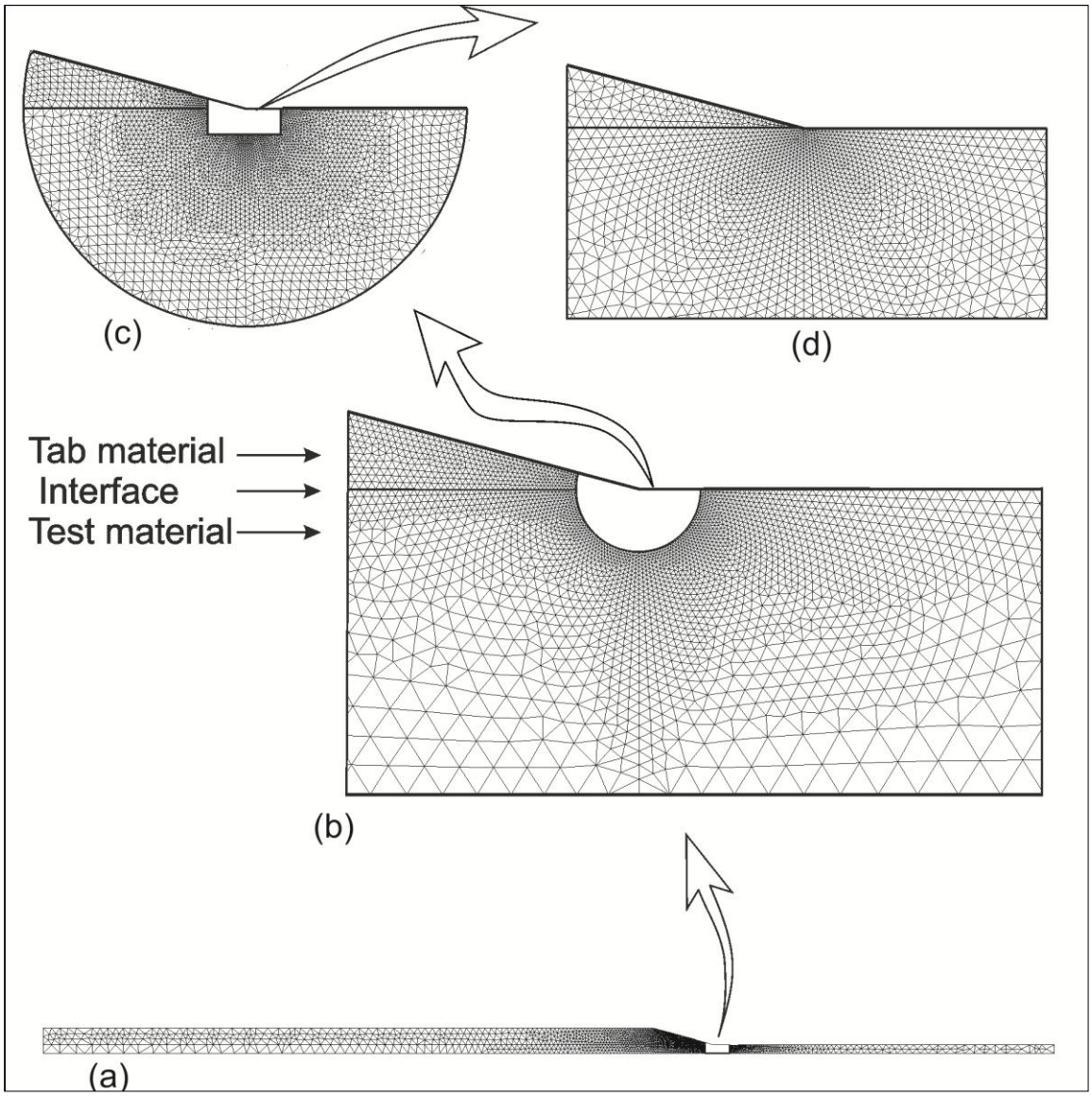

Fig. 3: A typical finite element mesh for the 2D problem

4. Results

4.1. Model Verification

Although the stress value at a singularity is in principle unbounded, a FE model will always give finite stresses. However, if the mesh is sufficiently refined around the singular point, the FE stress field will follow a singular field in a region near the singular point so that the effect of tab material type and geometry on the singularity can be determined correctly. More details about the mesh refinement close to the wedge tip are given in details in Appendix 2.

In order to determine the accuracy of the results and to check that the mesh is sufficiently refined near the wedge tip, p and A_{xx} were determined for different angular directions, ψ ($\pi/4$, $\pi/2$, $3\pi/4$ and π). The difference between the singularity values for these angular directions was found to be less than 0.001. This difference is considered to be insignificant (see Appendix 3).

Moreover, the results from the present model were checked with data from the literature. The stress singularity exponents of the present study were compared with values read off a graph from a study of Hein and Erdogan [15] (see Appendix 4). The difference between the data from present study and those of Hein and Erdogan [15] was less than 0.001.

4.2. Stress distribution at the wedge

Contours of the stress component σ_{xx} (normalised by the applied stress, $\bar{\sigma}$) in the wedge of the tab and test material are presented for $\theta = 15°$ and $\theta = 90°$ with $\Sigma = 1(\alpha = 0)$ in Figure 4. It is seen that the test specimen having $\theta = 90°$ has a larger region with high stresses near the wedge tip than the specimen with $\theta = 15°$. Figure 5 shows the axial stress, σ_{xx} (normalised with the applied stress, $\bar{\sigma}$) as a function of the distance from the wedge tip for the $\psi = \pi$ in the case of no elastic mismatch ($\Sigma = 1$). The maximum stress of the test specimen having $\theta = 90°$ is much higher than the maximum stress of a specimen with $\theta = 15°$. This indicates that the singularity is stronger for $\theta = 90°$ than $\theta = 15°$.

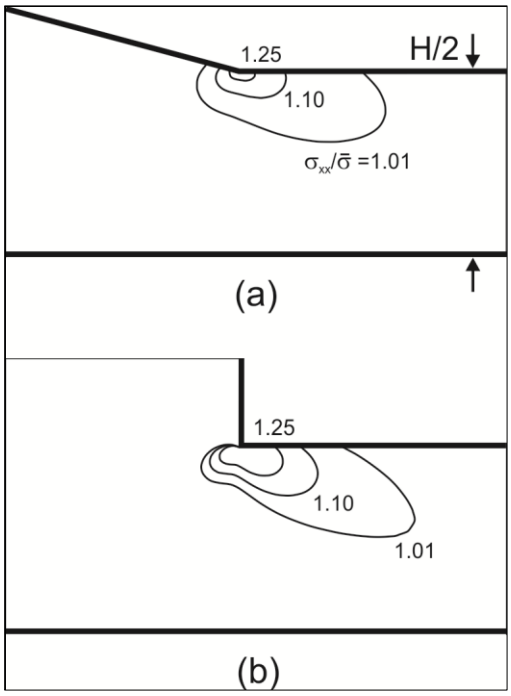

Fig. 4: Contours of the stress distribution ($\sigma_{xx}/\bar{\sigma}$) near the wedge of the test and tab material a) for $\theta = 15°$ and b) $\theta = 90°$

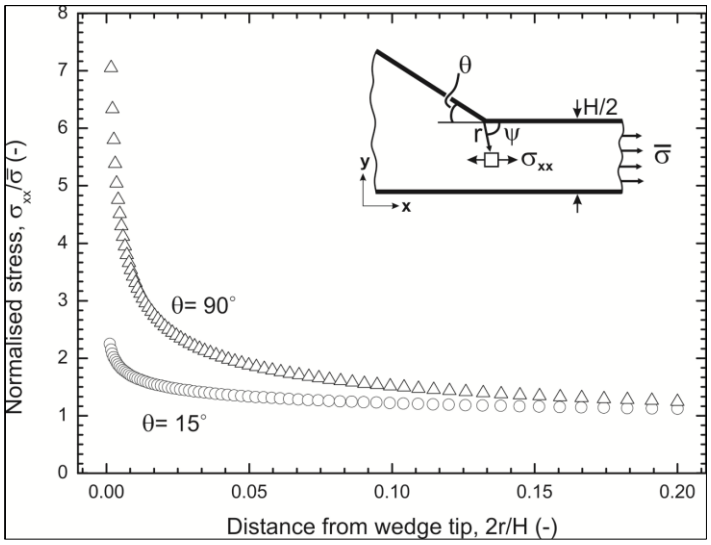

Fig. 5: Axial stress distribution as a function of position along the interface from the wedge tip for $\theta = 15°$ and $\theta = 90°$ for $\psi = \pi$

4.3. Stress singularity exponent and singularity function for isotropic materials

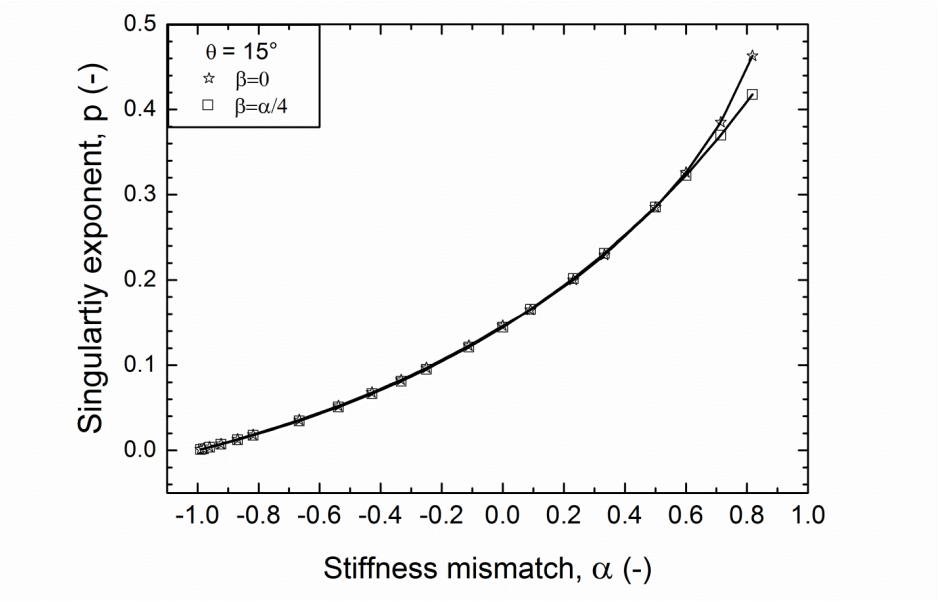

Fig. 6: Singularity exponent as a function of Dundurs' parameters (α and β)

The stress singularity exponent, *p*, of the stress field around the vertex are shown for $\theta = 15°$ in Figure 6 for isotropic materials in terms of the Dundurs' parameters, α and β. The major trend is that p increases with increasing α. It is seen that the singularity exponent takes the same value for different β values except for α very close to unity. Assuming that the effect of β is generally small, only material combinations with $\beta = \alpha/4$ will be investigated in the remainder of the study.

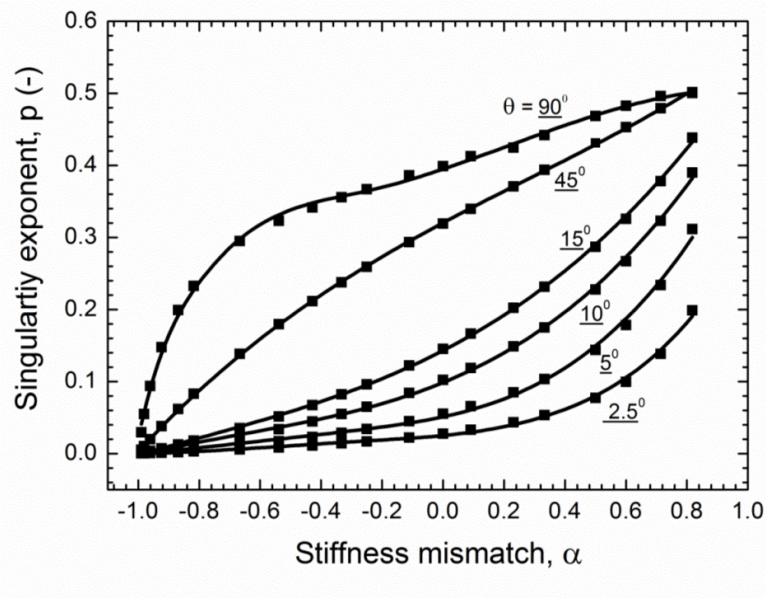

Fig 7: Singularity exponent (a) and constant (b) as a function of stiffness mismatch for different wedge angles

Fig. 7 shows p as a function of θ and α with $\beta = \alpha/4$. The results show that the p is between 0 and 0.5 for the entire range of Dundurs' parameters and different wedge angles. For a fixed θ, p decreases with decreasing α. For a fixed α, p decreases with decreasing θ. For $\theta \leq 15°$ and $\alpha < 0$, p is relatively insensitive to α. In contrast, for $\theta > 45°$, p varies rather strongly for $\alpha < 0$. However, for $\alpha \to -1$ ($E_1 \ll E_2$), it is convenient to show the singularity exponents in terms of the stiffness ratio Σ instead of α. The values of p and A_{xx} are re-plotted as a function of Σ in Figure 8a and b, respectively. It is instructive to compare results for different values of θ. For instance, the value of p for the test specimen having a $\Sigma = 0.01$ and $\theta = 90°$ is equivalent to the p value for a $\Sigma = 2$ and $\theta = 2.5°$.

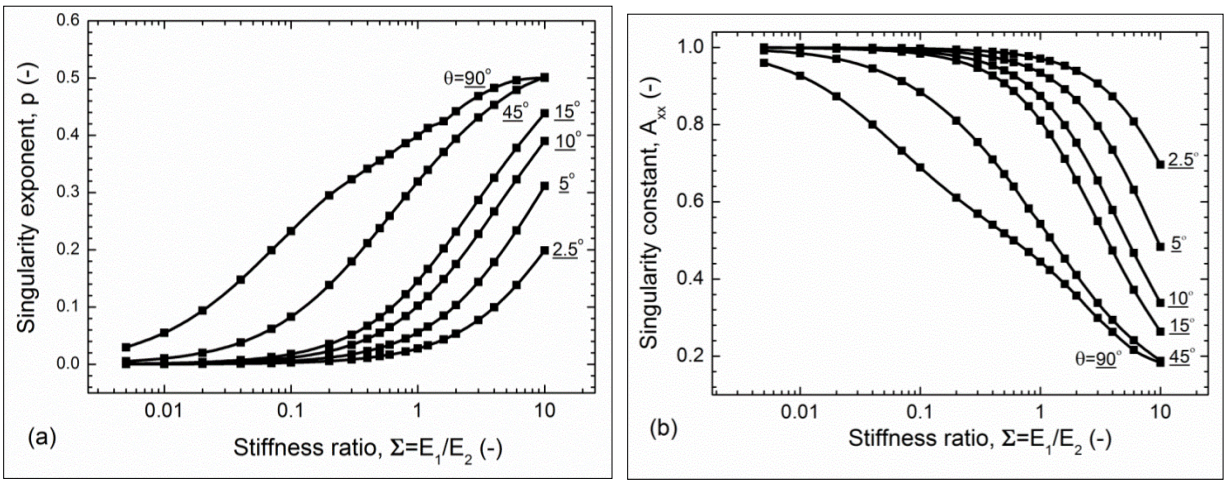

Fig. 8: Singularity exponent as a function of stiffness ratio for different wedge angles

Fig 9 shows the data of the lower left corner of Fig. 8 in greater detail. Note that for $\Sigma < 0.1$ and $\theta < 10°$, p is close to zero and depends only weakly on Σ and θ. For $\Sigma < 0.01$ and $\theta \leq 15°$, the effect of θ is small. Although the stress singularity exponent approaches zero for $\Sigma \rightarrow 0$, it does not varnish completely for any material combinations and wedge angles.

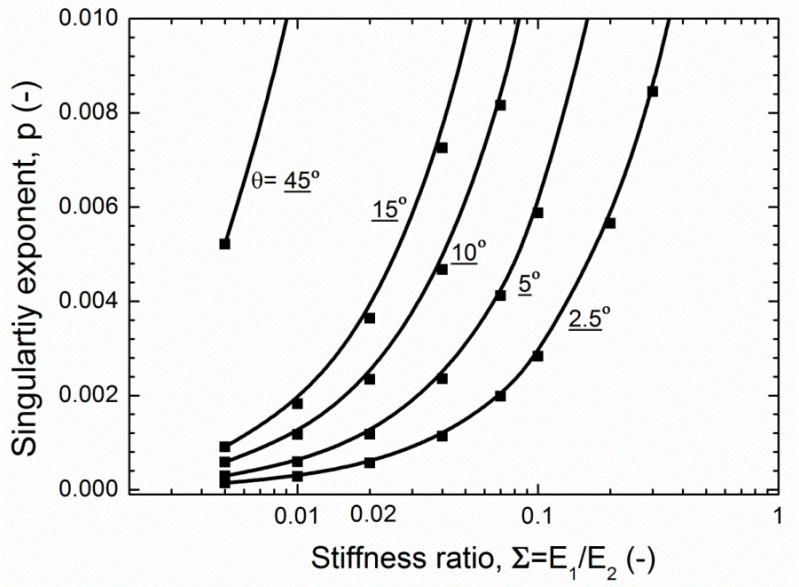

Fig. 9: The singularity exponent as a function of lower stiffness ratio, Σ and wedge angles, θ

The singularity exponent was determined for different thickness ratios of tab/test materials ($h/H = 0.25, 0.5, 1$). Specimens with a larger thickness ratio were found to have a slightly lower stress singularity exponent. However, the difference between singularity exponents was less than 0.001 which is considered to be insignificant.

4.4. Orthotropy rescaling (identical tab and test materials)

The orthotropy rescaling technique by *Suo et al*. [17] was used to analyse orthotropic problems. This approach can be used when the tab material has the same orthotropic elastic properties as the test material ($\alpha = \beta = 0$). As mentioned in the introduction, for $\rho = 1$, the stress field can be obtained exactly from an isotropic problem by the use of the orthotropy rescaling technique [17, 20]. This implies that the mathematical equations for the stress field of an orthotropic specimen (Fig.10a) are the same as for a rescaled isotropic specimen (Fig. 10b). Then, the singularity exponent of the wedge tip stress field of an orthotropic problem with a wedge angle, θ, is identical to the singularity exponent of the wedge tip stress field of an isotropic problem with a wedge angle θ^*. Using the orthotropy rescaling technique, the relationship between the two wedge angles is obtained as:

$$\theta^* = \tan^{-1}\left(\lambda^{-1/4} \tan\theta\right) \tag{8}$$

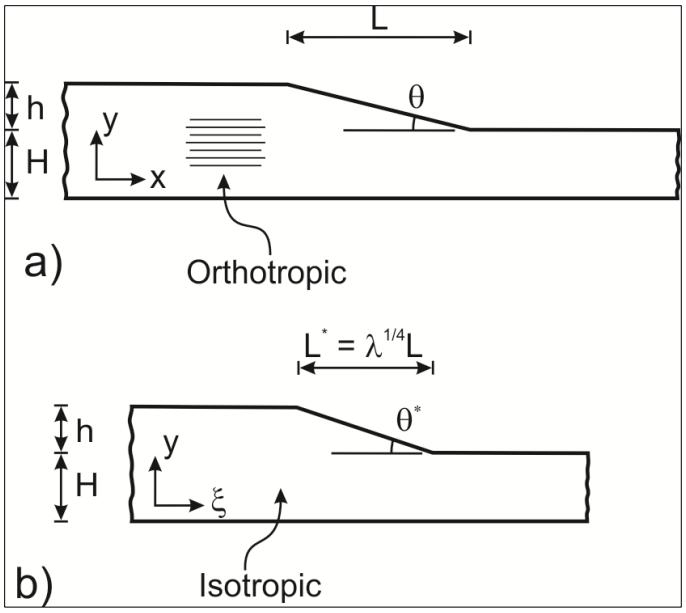

Fig 10: Orthotropic rescaling of a specimen for different material combinations in the *x*-*y* coordinate system

This corresponds to a shortening of the specimen, as indicated in Fig. 10b. This effect has been called $\lambda^{1/4}$ contraction [17]. Fig. 11 shows θ^* as a function of θ for various values of λ. The figure should be understood as follows. Each point on the curves represents the connection between θ and θ^* where the wedge tips stress singularity exponents of the two problems are identical. Note from the figure that $\theta < \theta^*$ for a composite that is stiffer in the *x*-direction than in the *y*-direction ($\lambda < 1$). Conversely, if we wish to choose a wedge angle, θ, of an orthotropic composite specimen such that the singular exponent is equal to the singular exponent, *p*, of an isotropic specimen with a given wedge angle, θ^*, for ($\lambda < 1$) the orthotropic wedge angle has to be smaller than the associated isotropic one. For instance, for $\lambda = 1/10$ (approximate the value for a unidirectional carbon fibre/epoxy composite), a wedge angle, $\theta^* = 5°$ of the isotropic problem corresponds to $\theta = 2.81°$ for the orthotropic problem. For small values of θ, a Taylor expansion, retaining only one term, gives (in radians):

$$\theta^* \approx \lambda^{1/4}\theta \tag{9}$$

From this equation it is immediately apparent that $\theta^* > \theta$ for $\lambda < 1$ (as also shown in Fig. 11 using Eq. 8, since then $\lambda^{1/4} > 1$.

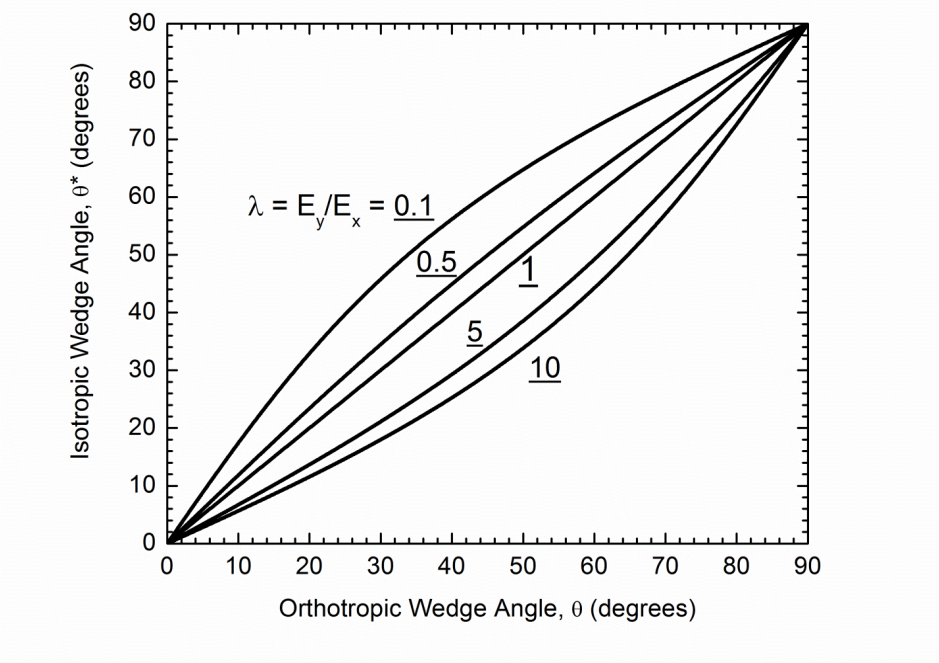

Fig 11: The rescaled isotropic wedge angles as a function of the orthotropic wedge angle, θ for different values of the orthotropy parameter, λ

In summary, orthotropic rescaling shows that tensile testing of orthotropic composites being stiffer in the *x*-direction requires a smaller wedge angle than an isotropic material in order to obtain the same singularity exponent, *p*. Equation (9) can be used to choose an approximate angle θ for an orthotropic material using the data of Fig. 8a for $\Sigma = 1$.

FE simulations were made to check the validity of Eq. (8). First, the singularity exponent, *p* was determined for a given wedge angle, θ, of an orthotropic problem. Next, the wedge angle, θ^*, of the equivalent rescaled isotropic problem was determined from Eq. (8), and the singularity exponent was determined by the FE model for this problem. As mentioned in connection with Eqs. 4 and 9, only when $\rho = 1$, the wedge angles of the orthotropic materials can be rescaled and transformed to isotropic materials. $\rho = 1$ was obtained by adjusting the shear modulus G_{xy} in accordance with Eq. (4). The singularity exponents were obtained for five different angular directions from $\psi = \pi/4$ to π for the orthotropic and the rescaled isotropic problems. Singularity exponents ± standard deviations obtained for the five angular directions are listed in Table 1.

Table 1: Singularity exponents for rescaled isotropic and orthotropic materials

Rescaled isotropic material	Angle	5°	10°	15°	45°
	Singularity	0.052±0.002	0.097±0.003	0.139±0.003	0.308±0.005
Orthotropic material	Angle	2.81°	5.61°	8.44°	25.31°
	Singularity	0.051±0.001	0.096±0.002	0.136±0.002	0.298±0.008

The differences between the two p values are within the uncertainty, confirming the validity of the orthotropy rescaling technique. For instance, in comparison to the orthotropic problem with $\theta = 2.81°$ has a singularity exponent ± standard deviation, $p = 0.051 \pm 0.001$ while for the rescaled isotropic material with $\theta = 5°$ has $p = 0.052 \pm 0.002$..

4.5. Stress singularity exponent and singularity function for orthotropic tab and test materials

A complete parametric study for orthotropic tab and orthotropic test materials becomes extensive. In order to find the major trends, some problems for a pair of orthotropic test material joints were solved by the FE method. The stress singularity of orthotropic test material with isotropic tab material (Fig. 12) and orthotropic tab material (Fig. 13) were investigated as a functions of material parameters Σ and λ with $\rho = 1$. The wedge angles were $\theta = 2.5°$ and θ = 10° for isotropic tab materials and $\theta = 2.5°$ for orthotropic tab materials, respectively. Singularity exponents and singularity functions are shown as a function of the stiffness ratio of the combination of isotropic tab material and orthotropic test material for different values of λ in Fig. 12. While p increases with increasing Σ and increasing λ, A_{xx} decreases with increasing Σ and increasing λ for $\psi = \pi$. Also, as for the isotropic materials (Fig. 8), material combinations involving tab materials with $\theta = 10°$ have a higher p value than those of tab materials with $\theta = 2.5°$.

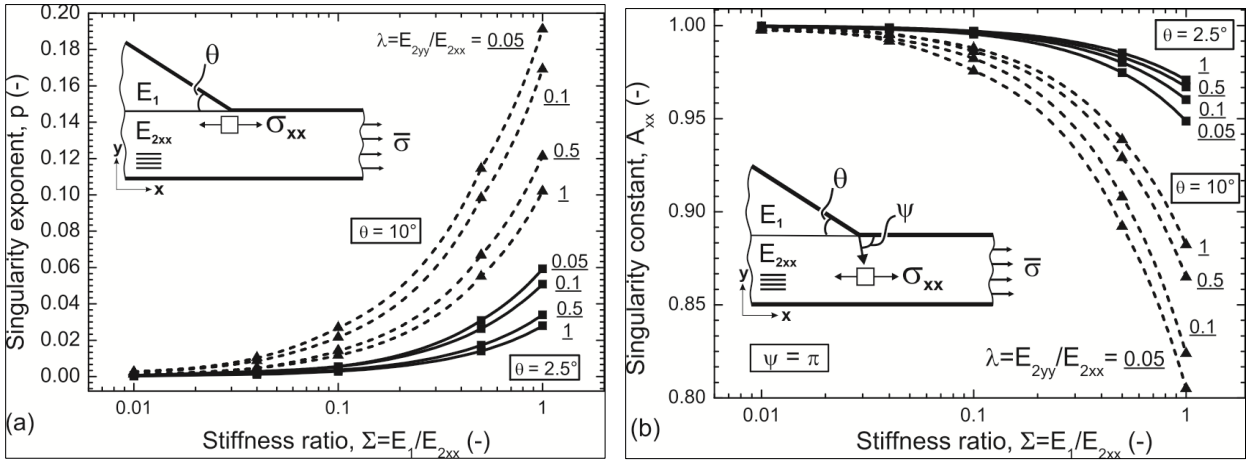

Fig 12: Stress singularity exponent (p) and constant (A) as a function of the stiffness ratio, Σ for different orthotropy parameters, λ in isotropy - orthotropy material combination

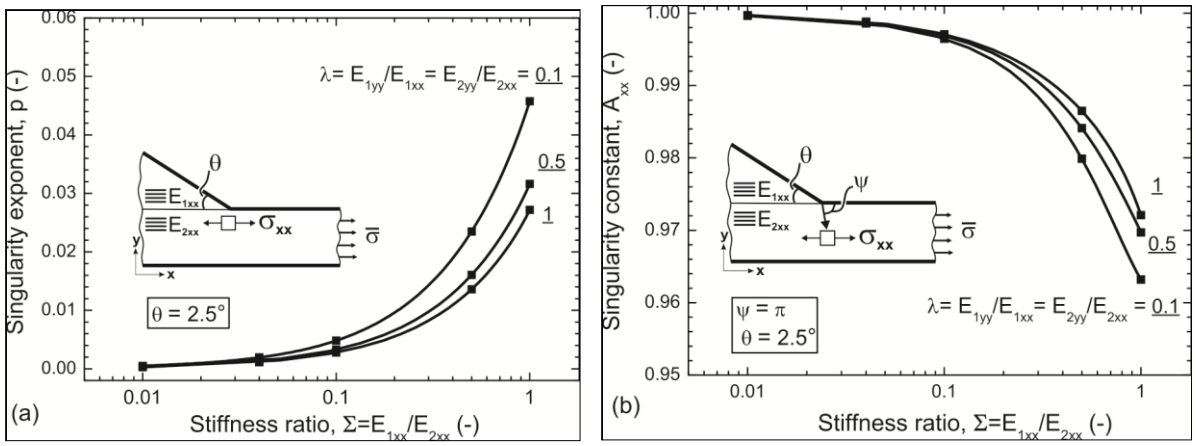

Fig 13: Stress singularity exponent (p) and constant (A) as a function of the stiffness ratio, Σ for different orthotropy parameters, λ in orthotropy – orthotropy material combination

Figure 13a and 13b show p and A_{xx} as a function of Σ for combinations of orthotropic tab materials combined with orthotropic test materials having the same orthotropy factor, $\lambda \leq 1$. The values of p for the orthotropic tab material are slightly lower than those for the isotropic tab material (Fig. 13a). Overall, for an orthotropic-orthotropic material combination (Fig. 13a), p shows the same trend as for isotropic-orthotropic material combinations (Fig. 12a).

5. Discussion

5.1. Practical implications of a singular zone near to the wedge tip

The results in Figs. 8-9 and Figs. 12-13 show that the wedge tip singularity can not be completely eliminated. Therefore, it is relevant to discuss the practical implications of a singular stress field and the size of the singular zone. It is obvious from Fig. 4 that the size of the singular zone is rather small. Recall also that the present analysis considers the composite test material as a smeared-out orthotropic material. However, when the size of the singular zone is comparable to microstructural length scales, the smeared-out continuum approach should be replaced by a microscale model that consists of discrete fibres embedded in a matrix material. Alternatively, we can consider what the singular stress field actually implies. Define, somewhat arbitrarily, a singular zone size by the radius from the wedge tip at which σ_{xx} exceeds the applied stress by 10% (The 10% limit is chosen since an uncertainty of 10% of the strength value is considered to be the maximum allowable). Now if the size of this singular zone is much smaller than one fibre diameter, the singular stress field is unlikely to initiate specimen failure. This underlying principle is based on the assumption that failure of a single layer of fibres would probably lead to specimen failure. Conversely, if the size of the singular zone is much larger than the fibre diameter, the singular wedge tip stress field is likely to initiate failure of many fibres, leading to

premature specimen failure. Therefore, in the following we propose to design the test specimen on the basis that the tensile stress, σ_{xx}, may be 10% (or more) higher only within a radius, r from the wedge tip corresponding to one fibre diameter, d_f. Then, the criterion for gauge section failure can be written as:

$$\frac{\sigma_{xx}}{\bar{\sigma}}\left(r = d_f\right) \leq 1.10 \qquad (10)$$

The approach can be used as follows. First, for a given combination of θ, Σ and λ, values of p and A_{xx} are read off from Figures 12 and 13. Then, it becomes possible to determine the stresses, σ_{xx} at $r = d_f$ if d_f is known, using Eq. 2. In this manner, the stresses can be calculated as a function of θ, Σ and λ as shown in Figure 14. In such a plot, the criterion (10) can be imposed as a straight, horizontal line. Wedge tip failure is predicted for points lying above the line and gauge section failure is predicted for points lying below the line.

As an example, consider a glass/epoxy composite test material. The fibre diameter, d_f, is $15\mu m$ and specimen thickness $H = 1$ mm gives $d_f/H = 0.015$. The singularity exponent, $p = 0.008$ and singularity function, $A_{xx} = 0.99$ can be read off from Fig. 13 for $\Sigma = 0.3$ ($E_{xx} = 39$ GPa, $E_{yy} = 9$ GPa, see Table 2), $\lambda = 0.25$ and $\rho = 1$. The values are used in Eq. 5 in order to calculate the stress for one fibre diameter, $r/H = 0.015$. Results are plotted in Fig. 14. Similar plots can be made for other values of d_f using the same approach.

Table 2: Elastic properties of various composite test and tab materials

Material	**E_{xx} [GPa]**	**E_{yy} [GPa]**	**Reference**
Flax/LPET	35	4	22
Glass/Epoxy	39	9	23
HS-Carbon/Epoxy[1]	142	11	23
HM-Carbon/Epoxy[2]	294	6	23
Epoxy	4	4	23

1: High strength fibre, 2: High modulus fibre

The normalised stress for $r/H = 0.015$, analysed for isotropic tab/test material combinations, is shown in Fig. 14a. The stress increases with increasing Σ and increasing θ. The 10% failure limit criterion, eq. (10), is fulfilled for all wedge angles up to 90° when the stiffness ratio is lower than 0.02. For θ = 15°, a much more moderate stiffness mismatch, Σ = 0.1 is allowable. Also, in the case of θ = 2.5°, stiffness ratios up to 0.5 can be chosen; this enables a large range of tab materials. Results for isotropic tab and orthotropic test material combinations are shown in Figure 14b. Imposing the 10% failure criterion, allowable stiffness ratios of $\Sigma = 0.3$ and $\Sigma = 0.1$ with $\lambda = 0.05$ are obtained respectively for $\theta = 2.5°$ and $\theta = 10°$.

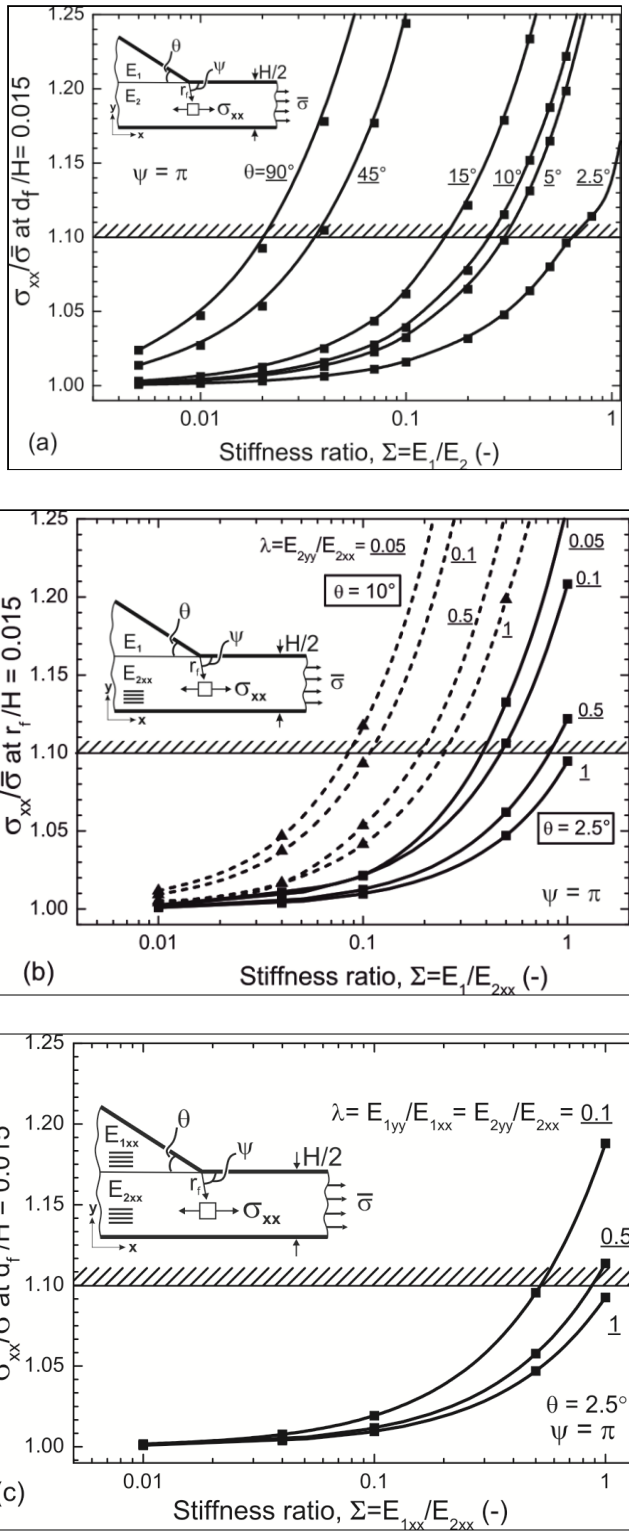

Fig 14: Stresses at *r/H =0.015* corresponding to one fibre diameter for $\theta = 2.5$ as a function of stiffness ratio, Σ and orthotropy parameter, λ for different material combinations a) isotropy-isotropy, b) isotropy-orthotropy c) orthotropy – orthotropy.

Stresses at $r/H = 0.015$ for θ = 2.5° are shown in Figure 14c for orthotropic tab materials and orthotropic test materials. The stresses are seen to increase with increasing Σ and decreasing λ as for isotropic material combinations (Fig. 14a). For instance, for $\lambda = 0.1$, the stresses are lower than the failure limit criterion, eq. 10, when Σ is smaller than 0.5. The stresses are slightly lower for an orthotropic tab material (Fig. 14c) than an isotropic tab material (Fig. 14b). Furthermore, from Fig. 14a, the p value of orthotropic materials for other wedge angles can be approximately obtained with the λ-effect estimated from Fig. 14 (Fig. 14b also includes those of isotropic materials for $\lambda = 1$ and $\rho = 1$). Since the stress for the orthotropic problems ($\lambda < 1$) are higher than for the isotropic problem, ($\lambda = 1$), the use of the isotropic data for orthotropic problems with $\lambda < 1$ is not conservative and should be used with care.

5.2. Comparison with literature results

It is tempting to test the proposed approach against the experimental results cited in the introduction. Oplinger [4] found that decreasing the wedge angle from 90° to 10° did not prevent tab failure for the same tab and test material (E-glass/epoxy composite). From Fig. 14a and Fig. 14c, it can be seen that for Σ = 1 and λ = 0.2, $\sigma_{xx}/\bar{\sigma}$ exceeds the failure criterion of 1.10, eq. (10), for both θ = 90° and θ = 10°. The experimental results of Oplinger [4] are thus consistent with our prediction.

Belingardi et al. [7] presented experimental results of unidirectional glass/epoxy composites for θ = 90° and θ = 30°. Specimens using aluminium tabs and steel tabs did not result in a gauge section failure. From Fig. 14a and b it can be seen that for $\Sigma > 1$ (the case for both tab material aluminium and steel), θ = 30° shows a normalised stress at $r/H = 0.015$ that is much higher than 1.25, exceeding the failure criterion Eq. (10). The experimental results (grip failures) are consistent with our predictions.

Hojo et al. [5] found experimentally that square cut tabs ($\theta = 90°$) and tapered tabs ($\theta = 10°$) with the same tab material (carbon/epoxy composite) showed tab failure. This is consistent with our predictions ($\lambda = 0.05$, Fig. 14c) since for $\sigma_{xx}/\bar{\sigma} > 1.10$, $\Sigma = 1$ for both wedge angles. Hojo et al. [5] also compared two different types of tab material (rubber and GFRP) for testing GFRP test materials in tension perpendicular to the fibre direction. Specimens with rubber tabs failed in the gauge section but specimens with the GFRP tabs failed in the grips. From Fig. 14a, we find that when the rubber-GFRP specimens are used ($\Sigma < 0.01$, $\theta = 90°$ for $\lambda > 1$, testing perpendicular to the fibre direction), the normalised stress is lower than 1.05 suggesting gauge section failure. However, for a GFRP tab/test specimen ($\Sigma = 1$ and $\theta = 90°$ for $\lambda > 1$) the stress values are higher than the failure criterion, eq. 10, predicting tab failure. Again, our criterion (10) gives predictions that are in agreement with the experimental results. It is encouraging that all the experimental results are consistent with the simple criterion (Eq. 10).

5.3. Design of practical applications

Table 2 shows typical elastic properties of unidirectional composites as test material. Values of epoxy as a tab material are also given.

Table 3 includes a list of different test materials (from Table 2) combined with a softer tab material (epoxy), as well as the appropriate values of Σ, λ and the maximum allowable (according to eq. 10) wedge angle, θ_{max}. Σ and λ are calculated from Eq. 1 and Eq. 4, respectively. Then, the stress values are read off from Fig. 14. The maximum allowable wedge angle, θ_{max}, can be estimated as listed in Table 3 for the various tab/test material combinations according to the failure criterion, eq. 10.

Table 3: Recommended wedge angle of tab specimen for common material combinations

Test material	**Tab material**	**Σ (-)**	**λ (-)**	**θ_{max} (°)**
Flax/LPET	Epoxy	0.12	0.1	5
Glass/Epoxy	Epoxy	0.10	0.2	10
HS-Carbon/Epoxy[1]	Epoxy	0.03	0.1	15
HM-Carbon/Epoxy [2]	Epoxy	0.01	0.02	45

1: High strength fibre, 2: High modulus fibre

It follows from Table 3 that testing of glass/epoxy and flax/LPET composites is more challenging to test since they need much lower wedge angles than carbon-epoxy composites. Referring the recommendations of the test standards, it is perhaps not surprising that they do not suggest a specific wedge angle for gauge section failure.

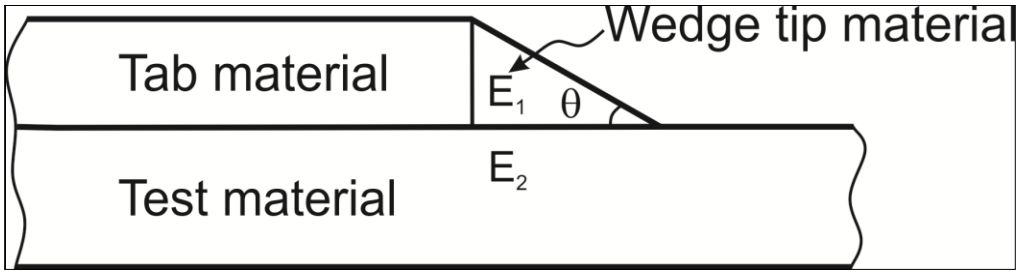

Fig 15: Geometry of test material and tab material modified with compliant wedge tip material.

In a study by Wang et al. [21], a tab material should be as stiff as possible and a wedge tip material should be as compliant as possible depending on the tested material, so that the loads transfer from the grips to gauge section without losing strength as shown in Fig 15. They showed that YSZ - nickel oxide specimens ($E_x = E_y = 200$ GPa) were first tested with 90° aluminium tab specimens. They all failed in the grip section near the wedge tip. Afterwards, in a subsequent

test series, the aluminium tab material ends of the test specimens were modified by adding a wedge of a compliant wedge tip material (epoxy) with $\theta = 20 - 30°$ (see Fig. 15) in order to decrease the singularity at the wedge tip. For these specimens, about 70-80% failed in the gauge section. The stiffer square tab material and softer wedge tip material as a combination of two materials appears to protect the test material from high grip forces and reduces the wedge tip singularity. The approach of Wang et al. [21], creating a lower wedge tab angle of a softer tab wedge tip material, should also be applicable to composite materials. Suitable wedge tip material angles are given in Table 3.

6. Summary

In the present study, the singularity exponent, p, and the singularity function, $A_{xx,}$ were determined as a function of the stiffness ratio, Σ, of the tab/test materials, the wedge angle, θ, of the tab material, and the orthotropy parameter, λ. The existence of a wedge tip singularity was taken into account in the numerical investigations and a fine FE mesh was used to determine p and A_{xx} accurately.

The results show that it is not possible to make the singularity at the end of tab material varnish. However, the value of p can be reduced significantly by decreasing Σ and decreasing θ. Since orthotropic tab materials with $\lambda < 1$ shows a lower singularity than isotropic tab materials, softer (isotropic) tab materials with low wedge angles should be used for testing. In practice, a design based on a stiff tab material and a soft wedge tip material (e.g., epoxy) with $\theta = 5°$ or $\theta = 10°$ can be used for glass and carbon fibre composite testing, respectively.

Acknowledgements

This work was supported by the European Community's Seventh Framework Programme in the project name of WoodFibre3D by the Danish Agency for Science, Technology and Innovation (Grant no 274-07-0300). The authors are grateful to Hans Lilholt, Erik Vogeley and Bo Madsen for valuable discussions.

Appendix 1: Determination of singularity exponent

The order of the singularity, p is obtained by the slope of the log-log plot of the stress distribution at near of the vertex. A representative figure is shown for the case of $\alpha = \beta = 0$ ($\Sigma = 1$ and $\nu_1 = \nu_2 = 0.33$) in the plane strain state. The stress component, $\sigma_{xx,}$ normalized by the applied external remote tension, $\bar{\sigma}$, is shown as a function of distance from the wedge tip, r, normalized by the test material thickness, H. As can be seen Fig. A-1, when the data is plotted

using logarithmic scales, the data appear as straight lines. The singularity exponent p and singularity function, A_{xx} are then obtained by linear regression as follows:

$$\frac{\sigma_{xx}}{\bar{\sigma}} = A\left(\frac{2r}{H}\right)^{-p} \quad \Rightarrow \log(\frac{\sigma_{xx}}{\bar{\sigma}}) = \log A - p\log(\frac{2r}{H}) \tag{11}$$

The singularity exponents of the present study are determined using Eq. 2. The stresses are determined in the range of r: $0.0001 \leq r/H \leq 0.20$. However, for $\theta \geq 45°$ and $\Sigma > 10$ the stresses are determined $0.002 \leq r/H \leq 0.20$ due to strong oscillatory behaviour.

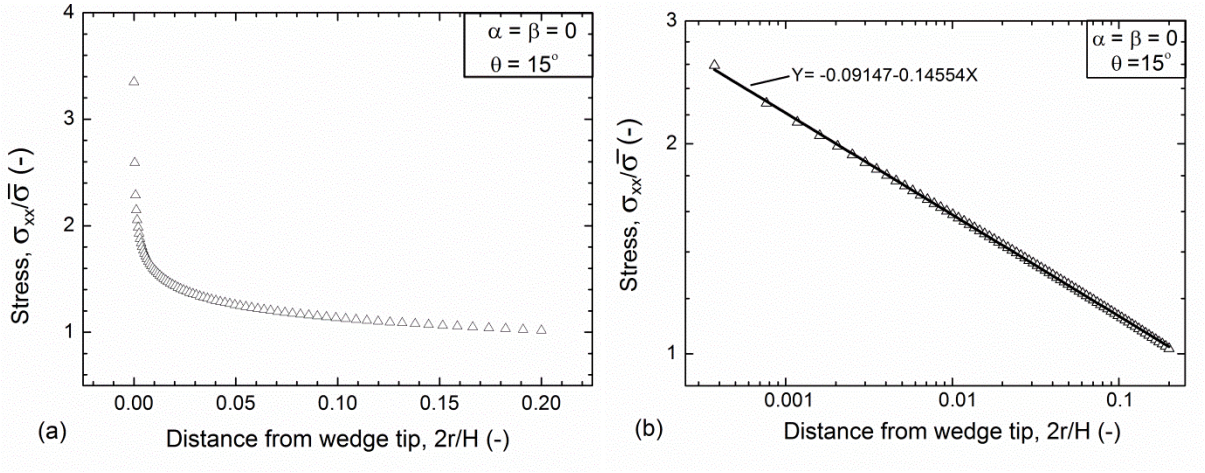

Fig A1: Determination of the stress singularity exponent and singularity constant. a) The distribution of average stresses against the distance, b) the distribution of the average stresses against distance in a logarithmic scale.

Appendix 2: Determination of singular stress field at wedge tip

The mesh refinement were analysed for the test specimen with a wedge angle, $\theta = 2.5°$. The stress components were shown as a function of distance from the wedge tip for $\Sigma = 1$ and $\Sigma = 0.01$ at $\theta = 2.5°$. Mesh sizes were applied by three different element sizes (fine, medium and coarse) in the certain distance from the wedge tip ($2r/H = 0.2$). The number of elements in the circular zone (Fig. 3c) for coarse, medium and fine element sizes is 563, 5407 and 19606, respectively. The fine mesh sizes were used to determine singularity exponents in the model (Fig. 3). The numbers of total elements of the entire model is 30197 (Fig. 3a).

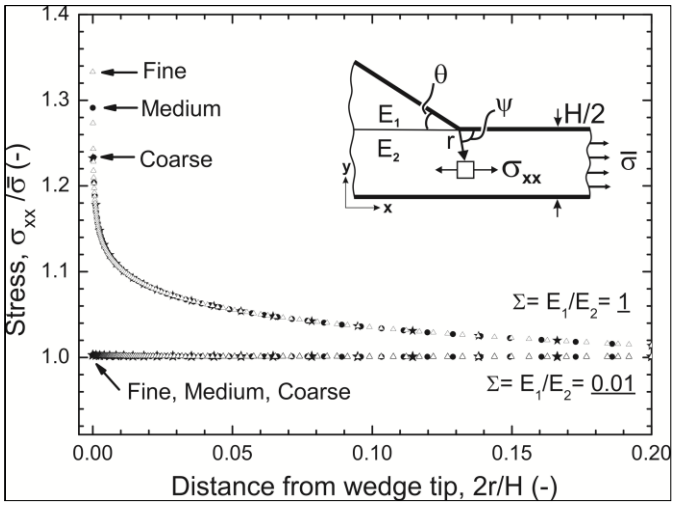

Fig A2: The normal stress distribution against the distance in terms of different mesh sizes for $\Sigma = 1$ and $\Sigma = 0.01$

In Figure A-2, it is seen that the peak value of the normal stresses for $\Sigma = 1$ clearly increases with increasing number of elements (finer mesh). The highest normal stresses for $\Sigma = 0.01$ remains at the same level by increasing the number of elements. Obviously, for $\Sigma = 0.01$ the stress singularity is weaker than that for $\Sigma = 1$.

Appendix 3: Accuracy of singularity exponent

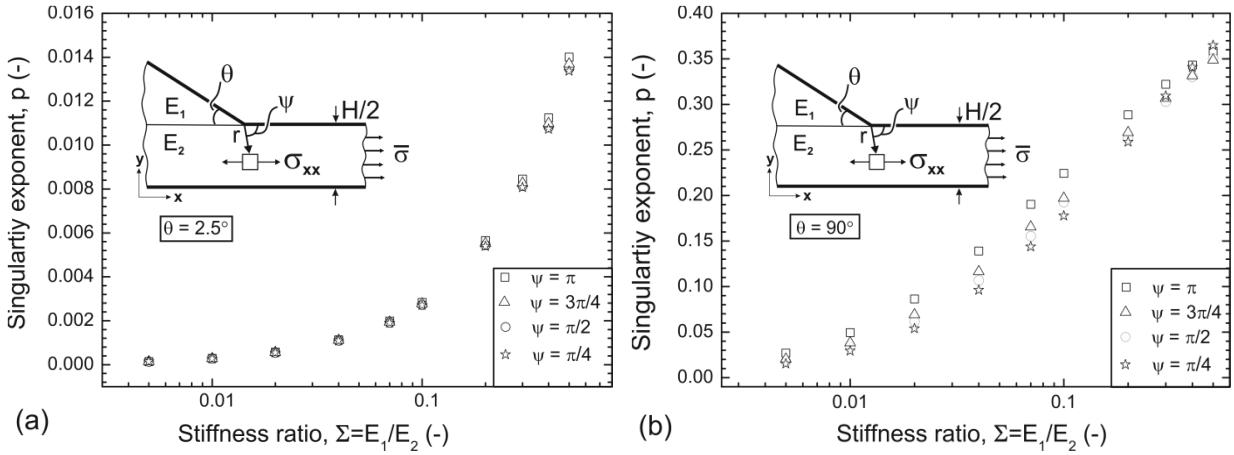

Fig. A3: The stress singularity exponents for the σ_{xx} stress component in ψ directions from $\pi/4$ to π as a function of Σ for a) $\theta = 2.5°$, b) $\theta = 90°$

In order to check the accuracy of the results, the singularity exponent, *p*, was determined for each of the stress components $\sigma_{xx}, \sigma_{yy}, \sigma_{xy}$ along four different directions, ψ from $\pi/4, \pi/2, 3\pi/4$ and π. The stress component in the loading direction, σ_{xx}, had a smaller difference in singularity exponents than the other stress components, σ_{yy}, σ_{xy}. For instance, the difference between of the

singularity exponents for stress components, $\sigma_{xx}, \sigma_{yy}, \sigma_{xy}$, for the different directions was found to be approximately $0.0006, 0.0011$ and 0.0115, respectively for $\theta = 2.5°$. Among the directions, $\psi = \pi$ shows the highest singularity values. In the body of the paper, values of p and A_{xx} are obtained in the $\psi = \pi$ direction since a particular attention will be given to the stress state at the end of the interface along the tab and test material at the wedge tip. Figure A-3 shows only the p values for the σ_{xx} stress component in ψ directions from $\pi/4$ to π as a function of Σ for $\theta = 90°$ and $\theta = 2.5°$. The difference between of singularity exponent for normal stresses, σ_{xx} is lower than 0.0007 for $\theta = 2.5°$ and lower than 0.047 for $\theta = 90°$.

Appendix 4: Model validation/ comparison with published results

Fig. A-4 shows the comparison the values of the singularity exponents between the present study and a literature study [15] as a function of Σ from 0.01 to 100 and $\theta = 15°$ for different material thicknesses. The singularity exponents determined by Hein and Erdogan [15] are read off from Fig 9 in their paper. The difference between p values of the present study and those of Hein and Erdogan [15] is less than 0.001. Some of this difference can be attributed to uncertainty of the read-off values. The results show that there are no significant differences between results of finite thickness and infinite thickness (two half spaces) of materials. This confirms that the singularity exponent is a independent property of layer thicknesses.

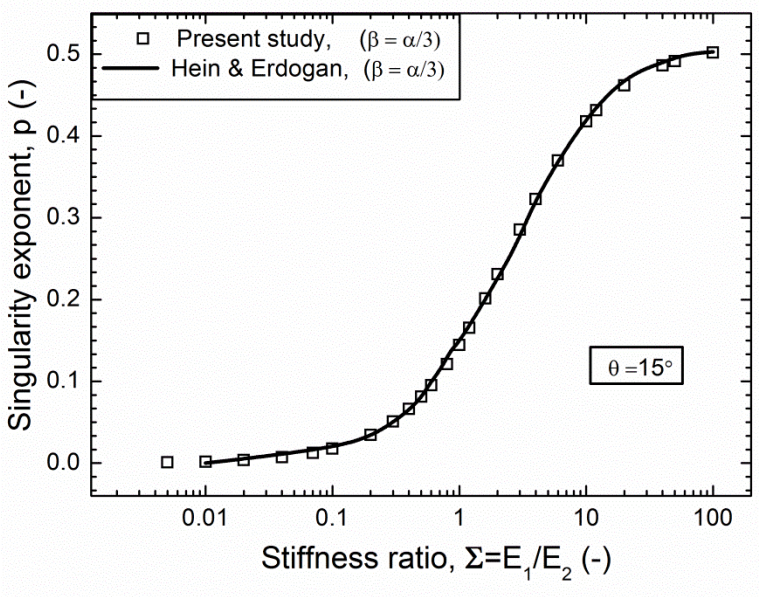

Fig. A4: A comparison of the values of the singularity exponents between the present study and a literature study [15] as a function of Σ from 0.01 to 100 and $\theta = 15°$ for different material thicknesses

References

1. ISO 527-1 Plastics, determination of tensile properties. Part 1: General principles Switzerland; 1993.
2. ASTM D 3039 Standard test method for tensile properties of polymer matrix composite materials 1993;99-109
3. Staab G. H. Mechanical test methods for lamina, Laminar composites ISBN 978-0-7506-7124-8 Elsevier 1999;102-41.
4. Oplinger, D. Studies of tensile test specimens for composite material Testing, TTCP Review, Ottawa, Canada; 1979.
5 Hojo M, Sawada Y. and Miyairi H. Influence of clamping method on tensile properties of unidirectional CFRP in 0 and 90 directions-round robin activity for internationsl dtandardization in Japan. Composites 1994;25(8):786-96.
6. Wisnom M.R. and Maheri M.R. Tensile strength of unidirectional carbon fibre epoxy from tapered specimens, Composites testing and standardisation, European conference on composites testing and standardisation, Hamburg Germany; 1994
7. Belingardi G., Paolino D. S., Koricho E. G Investigation of influence of tab types on tensile strength of E-glass/epoxy fiber reinforced composite materials Procedia Engineering,11th International Conference on the Mechanical Behavior of Materials (ICM11), Como; 2011.
8. Adams R.D. and Harris J.A. The influence of local geometry on the strength of adhesive joints. Int. J. Adhesion and adhesives 1987;7(2):69-80
9. Cunningham, ME Schoultz SV and Toth JM, Effect of end tab design on tension specimen stress concentrations, in recent advances in composites in the US and Japan, ASTM STP 1985;864:253-62.
10. Adams, O.D., and Adams D.F. Tabbing guide for composite test specimens. Federal Avitation Administration, Final report, Washington; 2002.
11. Bogy, D.B. Edge bonded dissimilar orthogonal elastic wedges under normal and shear loading, Journal of Applied Mechanics 1968;35:460-66
12. Bogy, D.B. Two edge-bonded elastic wedges of different materials and wedge angles under surface traction, Journal of Applied Mechanics 1971;38:377–86.
13. Dundurs, J. Discussion, ASME Journal of Applied Mechanics 1969;36:650–52.
14. Hutchinson J.W. and Suo Z. Mixed mode cracking in layered materials, Advances in applied mechanics volume 29 Academic Press Inc. California 1992;63-191
15. Hein, V.L. and Erdogan, F. Stress singularities in a two-material wedge, International Journal of Fracture Mechanics 1971;7:317–30.
16. Xu, L.R., Kuai, H. and Sengupta, S. Dissimilar material joints with and without free-edge stress singularities, Experimental Mechanics., 2004;44:608–615.
17. Suo, Z., Bao, G., Fan, B., and Wang, T. C. Orthotropy rescaling and implications for fracture in composites, Int. J. Solids Structures, 1991;28:235-48.
18. Suo, Z., 1990, Delamination specimens for orthotropic materials, Journal of Applied Mechanics,;57: 627-34.
19.ABAQUS users manual, version 6.10.1 Abaqus Inc., 2010.
20. Bao, G., Ho, S., Suo, Z., and Fan, B., 1992, "The role of material orthopy in fracture specimens for composites", *Int. J. Solids Structures*, Vol. 29, pp. 1105-16.
21. Wang, F H., Toftegaard, H. Hendriksen, P. V. and Sørensen B. F. Tensile mechanical properties of bi-layer structure for solid oxide fuel cells Conference: CompTest 2006 (Composites Testing and Model Identification), University of Porto, Portugal, 2006.

22. Aslan, M. Unpublished results: Risø DTU National Laboratory for Sustainable Energy, Technical University of Denmark, Denmark, 2011.
23. Bunsel A., Renard J. Fundamentals of fibre reinforced composite, Institute of Physics Publishing, Bristol, 2005.